Synthesis and Characterisation of Inorganic Trithiocarbonates, Perthiocarbonates and Related 1,1-Dithiolate Compounds

Inaugural–Dissertation

zur Erlangung des Doktorgrades

Doctor rerum naturalium

der Mathematisch-Naturwissenschaftlichen Fakultät

der Universität zu Köln

von

Christopher Martin James

aus Bad Homburg v. d. Höhe

2021

The work belonging to this dissertation was accomplished between April 2017 and October 2021 at the *Institute for Inorganic Chemistry* of the *University of Cologne* in the research group of *Prof. Dr. Mathias S. Wickleder*.

Principal reviewer and examiner:	Prof. Dr. Mathias S. Wickleder
Secondary reviewer and examiner:	Prof. Dr. Dr. (h.c.) Sanjay Mathur
Chairman of thesis defence committee:	Prof. Dr. Sandro Jahn
Secretary/minutes taker:	Dr. Corinna Hegemann

Date of submission: 04.10.2021

Date of confirmation of acceptance: 08.11.2021

Date of thesis defence: 10.12.2021

Dedicated to my family.

“I may be wrong, and you may be right,

and by an effort, together we may get nearer to the truth.”

Sir Karl Raimund Popper

Abstract

In the course of this work inorganic trithio- CS_3^{2-}, perthio- $CS_2(S_2)^{2-}$ and perthiodicarbonates $C_2S_6^{2-}$ as well as compounds having both trithio- and perthiocarbonate or other non-related anions incorporated were prepared and structurally elucidated. It was possible to extend the system by introduction of selenide for sulfide, yielding the new perselenodithiocarbonate anion $CS_2(Se_2)^{2-}$. The salts were crystallised with alkali metal and barium cations from solutions or under solvothermal conditions in sealed and evacuated glass ampoules. Substitution of the metal ions with ammonium led to crystals, including trithiocarbonate and dithiocarbamate anions $[S_2C(NH_2)]^-$ as determined from X-ray diffraction data.

At the interface of aqueous NH_3 and CS_2, the elusive $(N_2H_7)^+$ and CS_3^{2-} ions were stabilised in yellow crystals, which were identified as $(N_2H_7)_2CS_3$.

Reactions of alkali trithiocarbonate with transition metal salts were conducted under solvothermal conditions for the first time and crystalline specimen were obtained. Thus, a series of transition metal complexes with Ni^{2+}, Pd^{2+}, Pt^{2+} and Co^{3+}, as the central ion, could be crystallographically described in coordination with bidentate trithiocarbonato ligands. In the extension of the experimental series to lanthanoids, the treatment of $Eu(CH_3COO)_3$ with K_2CS_3 under solvothermal conditions in ethanol allowed to grow crystals of $K_9[Eu_2(CH_3COO)_9](CS_3)_3$.

The solvothermal route was also used for the treatment of $BaCS_3$ with Tl_2SO_4, but did not yield crystals of Tl_2CS_3, but Tl_2S_5.

Cu^{2+} was successfully incorporated in neutral $[Cu\{CS_2(S_2)\}]$ units forming a one-dimensional polymeric structure, which crystallised with ammonium and perthiocarbonate ions form a solution of CuCl in aqueous NH_3 and CS_2.

Among all structures the trithio-, perthiocarbonate and related 1,1-dithiolate anions could be described as planar for simplicity. The deviations from the ideal planarity and structural changes on the bond distances and angles, in particular comparing the free anions and when acting as a ligand for transition metals, is stressed throughout this work. Molecule vibrational spectroscopy is added consecutively to characterise these compounds.

Zusammenfassung

Diese Arbeit enthält die Präparation und strukturelle Aufklärung von Verbindungen die das Trithiocarbonat- $(CS_3)^{2-}$, das Perthiocarbonat- $[CS_2(S_2)]^{2-}$ oder das Perthiodicarbonat- $(C_2S_6)^{2-}$ Anion enthalten, sowie solchen, die sowohl Trithio- als auch Perthiocarbonat-Ionen enthalten oder andere Anionen. Die Salze wurden mit allen Alkalimetall- und Barium-Kationen aus der Lösung und/oder unter solvothermalen Bedingungen in evakuierten Glasampullen dargestellt und kristallisiert. Es war möglich auch Diselenid-Ionen an CS_2 zu binden und so in der Verbindung $K_5[S_2C(Se_2)]_{1,5}(CS_3) \cdot H_2O$ das Diselenodithiocarbonat-Dianion zu erhalten und erstmals strukturell zu beschreiben.

Mit Ammoniak als Edukt wurden die Metall Kationen mit Ammonium-Ionen substituiert und das Dithiocarbamat-Anion $[S_2C(NH_2)]^-$ in den Verbindungen $(NH_4)[S_2C(NH_2)]$ und $(NH_4)_5(CS_3)_2[S_2C(NH_2)]$ dargestellt und kristallographisch und spektroskopisch untersucht. An der Grenzfläche zwischen einer konzentrierten wässrigen Ammoniaklösung und CS_2 wuchsen Kristalle der Verbindung $(N_2H_7)_2CS_3$, welche ein Diamminhydrogen-Kation $(N_2H_7)^+$ enthält.

Unter solvothermalen Bedingungen in evakuierten Glasampullen gelang, mit der Bildung von Trithiocarbonato-Komplexen, auch die Reaktion von K_2CS_3 mit den Übergangsmetall-Kationen M^{n+} = Ni^{2+}, Pd^{2+}, Pt^{2+} und Co^{3+}. Erstmals konnten diese anionischen Komplexe $[M(CS_3)_n]^{n-}$ mit Kalium-Kationen stabilisiert werden. Die Aufklärung der Kristallstrukturen ist Teil dieser Arbeit. Das Trithiocarbonat-Anion tritt in diesen Komplexen als Chelat-Ligand auf.

Auf explorativem Weg wurde auch die Verbindung $K_9[Eu_2(CH_3COO)_9](CS_3)_3$ erhalten und kristallographisch aufgeklärt. Sie kann als Mischsalz von Europium(III)-acetat und Kalium Trithiocarbonat aufgefasst werden und ist die erste Lanthanoid(III)-Verbindung mit CS_3^{2-}-Ionen.

Aus der Reaktion von $BaCS_3$ mit Tl_2SO_4 unter solvothermalen Bedingungen wurden Kristalle mit der Summenformel $Tl_2(S_5)$ dargestellt. Das stabile Thallium(I)-Trithiocarbonat wurde so nicht in kristalliner Form erhalten.

Aus einer Lösung von CuCl in ammoniakalkalischer Lösung mit CS_2 bildeten sich neben CuS auch Kristalle der neuartigen Verbindung $(NH_4)_2[Cu\{S_2C(S_2)\}][S_2C(S_2)]$, welche neben Perthiocarbonat-Anionen auch neutrale eindimensionale $Cu[S_2C(S_2)]$-Ketten mit trigonal-planar koordinierten Cu^{2+}-Ionen enthielt.

Unter allen Kristallstrukturen konnten das Trithiocarbonat-, Perthiocarbonat und verwandte 1,1-Dithiolat-Anionen in den Grenzen der Genauigkeit als planare Molekülanionen aufgeklärt werden, was auch durch die Auswertung von Molekülschwingungsspektren

gestützt wurde. Strukturelle Besonderheiten wie Bindungslängen und Winkel, insbesondere beim Übergang vom freien Anion zum Liganden, werden diskutiert.

Table of contents

Table of abbreviations

a.k.a.	as known as
CCDC	Cambridge Crystallographic Data Centre
cf.	(latin: *conferatur*) – confer
CSD	Cambridge structural database
DMSO	dimethyl sulfoxide
DMF	dimethyl formamide
e.g.	(latin: *exempli gratia*) – for example
en	ethane-1,2-diamine
Et_2O	diethyl ether
EtOH	ethanol
EtO^-	ethoxide anion
eq.	equivalent
HMO	Hückel Molecular Orbital
HOMO/LUMO	highest occupied molecular orbital/lowest unoccupied molecular orbital
HSAB	hard and soft acids and bases
i.e.	(latin: *id est*) – that means
ICDD	International centre for diffraction data
ICSD	inorganic crystal structure data base (used version 4.6.0)
IR	infrared, near-infrared
LASER	light amplification by stimulated emission radiation
MeOH	methanol
n-buli	*n*-butyllithium
OAc	acetate anion/ acetato ligand
PDF-2	Powder diffraction file – 2 (2007)
Ph	phenyl
THF	tetrahydrofuran
UV-vis	ultraviolet-visible

Table of quantities and their units

E_N (atom)	electronegativity	E_N (atom)
m	mass	g or kg
M	molar mass	$g \cdot mol^{-1}$
n	amount of substance	mol
T	temperature	°C or K ($T_{[K]} = (273.15 + T_{[°C]} \cdot °C^{-1})$ K)
RT	room temperature	

1 Introduction

1.1 The discovery and elemental chemistry of CS_2

Trithiocarbonates, the derivatives of the trithiocarbonic acid, $(HS)_2CS$, belong to an interesting compound class. Research on these inorganic compounds, their organic derivatives and their differences towards the ubiquitous oxygen analogues enlivened scientists for two centuries to work in this field. Without any doubt, the development of the chemistry of thiocarbonates was dependent on the discovery of carbon disulfide, CS_2, 'the most important carbon-sulfur compound', by LAMPADIUS in 1796.[1] In the 19th century experiments were carried out by BERZELIUS, who was among the first to study the reaction of CS_2 with sulfides and hydrogen sulfides in aqueous solution.[2] Despite that early phase of well-founded scientific effort, BERZELIUS was able to draw an important conclusion, namely that of formation of sulfur analogues of the carbonates. Moreover, his preliminary work already covered the relative instability of solid products under ambient atmosphere as well as the formation of a red oil upon treatment of those solids with acid (cf. equation 1.1). Later, the identity of this red oil was revealed as $(HS)_2CS$, which under ambient condition is a red liquid, that behaves hydrophobically.[3–6] In this view, BERZELIUS can be taken as the explorer of (tri)thiocarbonates.

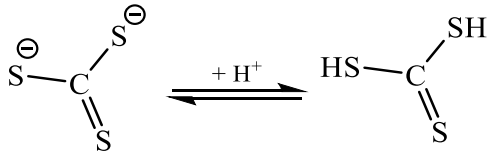

trithiocarbonate anion trithiocarbonic acid 1.1

Equation 1.1: Reaction to form trithiocarbonic acid by addition of protons to the trithiocarbonate anion.[7]

CS_2 was put into reaction with different other substances available at that time, for which reason the class of thiocarbonylthio or mercaptothiocarbonyl compounds, i.e., 1,1-

dithioacids and deriving 1,1-dithiolates were found. In this context it came to pass, that ZEISE, a contemporary of BERZELIUS, discovered *O*-alkyl dithioesters (HS)SC(OR) and dithiocarbamates $[S_2C(NR_2)]^-$ by treatment of CS_2 with alkoxides $(RO)^-$ or ammonia (NH_3), respectively, where R is a non-metal substituent.[8] He decided to name the former new compounds *xanthates*, after the Greek *xanthós*, meaning 'blond' or 'yellow'.[9] They played an important role in the evolution of sulfur chemistry. Moreover, ZEISE worked on alkylthiols as well, and the common term 'mercaptan', derived from Latin *corpus mercurio captum*, meaning 'capture mercury' originates from his work.[10]

Not last, existence of the related thioxanthates $[S_2C(SR)]^-$ and 1,1-dithiocarboxylates S_2CR^- shall not be unmentioned. The latter can be obtained by reaction of CS_2 with GRIGNARD reagent[i].[11] However, this work is not going to discuss this class of compounds further.

[i] Grignard reagents are typically organic magnesium compounds. Generic formula R−Mg−X, with R = alkyl/aryl moiety and X = halogenide. They are prominent to form new R−R* bonds by reaction with alkyl/aryl halogens R*−X.

1.2 The formation of 1,1-dithiolates

1.2.1 Fundamental concepts

Generally speaking, the formation of 1,1-dithiolates from CS_2, can be achieved by addition of a LEWIS-base into one of the double bonds in CS_2. In other words, a nucleophilic species (Nu^-) is demanded to build up an attractive interaction with the carbon atom, which simultaneously has to cancel one of the C=S double bonds, which is shown in equation 1.2.[12]

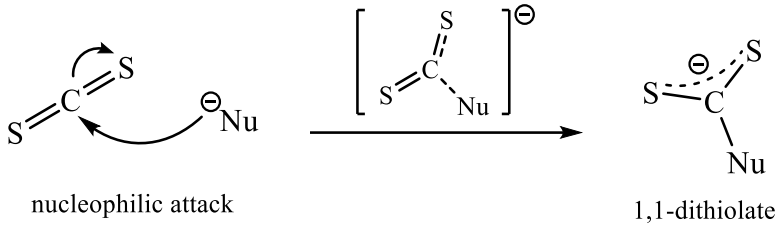

1.2

Figuratively, for the reactivity of CS_2, a comparison with the lighter homolog CO_2 can be stressed. CS_2 is a liquid at ambient conditions and is able to polymerise, which is a sulfur related property to show a lower tendency to form double bonds. CO_2 in turn is gaseous and under ambient pressure no liquid phase is known. Qualitatively speaking, the strong double bonds are formed easier, as the p-orbitals overlap is increased with the those of the central carbon atom, due to the smaller size of oxygen. Moreover, CO_2 is non-burning, non-toxic and exotherm, while endothermal CS_2 burns and is toxic.[13] CO_2 is readily soluble in water, stemming from a marked dipole moment due to the electronegativity difference of ~1.[14] CS_2 has no strong dipole ($\Delta EN = 0.06$) and only reacts with water at higher temperatures, yielding CO_2 and H_2S.[1]

It is important to introduce the fundamental principles that can be used to explain these reactions and there is a demand for definition of several terms concerning the reaction of CS_2 with nucleophiles as presented in equation 1.2. Covered by the concept of *Lewis acids and bases* (named after G. N. LEWIS [15]) as well as the concept of HSAB, the probability of a successful nucleophilic attack on the CS_2 molecule can be estimated. These theories describe the interactions of the reactants with similar outcome as the behaviour between nucleophiles and electrophiles.

Basically, a reaction is classified as Lewis acid and base reaction, if a localised lone pair of electrons (or a negative charge), that is not involved in the bonding of the Lewis base

molecule (often the HOMO), is donated to the unoccupied molecule orbital (LUMO) of a Lewis acid.[16] The energy level between of the HOMO and LUMO is defining whether the binding will be successful, i.e. if a net lower energy level of the newly formed molecular orbital between base and acid can be realised to be filled with electrons. It is important to note that in Lewis acid and base association reactions the donated electrons from the HOMO are only partially transferred by establishment of a *dative*, *polar* or *coordinative covalent* bond between the reagents.[13] Certainly, in most cases, including many transition metal-ligand coordinative bonds, a differentiation from a normal electron sharing bond is reasonable, as the electrons are far from being equally distributed within the range of the bond between the metal and the ligand.[17] However, in the case of the reaction of CS_2 with an electron donating nucleophile, the result will be better described as the formation of a covalent bond, i.e., the electrons will be equally shared. A useful, yet ambiguous, estimate for the probability of that reaction is given through the qualitative concept of HSAB characterisation. It was introduced by PEARSON in 1968 and the terms *soft* and *hard* refer to the polarisability of the electron cloud of the atom or molecule discussed in proportion to its size. For instance, the larger (smaller) and less (more) positively charged, the softer (harder) is the acid, and generally speaking soft acids favour soft bases over hard ones.[13,18] Practically, both the LEWIS and HSAB concepts offer ways to evaluate reaction possibilities in a thermodynamic view. This can in many cases be transferred to nucleo- and electrophilicity that are associated with a kinetic understanding of chemical reactions.

1.2.2 Basic reaction schemes for 1,1-dithiocarbonates

Introduction of a chalcogenide anion Ch^{2-} substituting the general monoanionic nucleophile in equation 1.2 (cf. above) makes thiocarbonates $(S_2C{-}Ch)^{2-}$ available. As shown in equations 1.3-1.5, this demands alkaline environment, and the formation can be understood as a stepwise reaction. Trithiocarbonates are unlikely to form in natural processes, because if the pH value is not maintained high enough, gaseous COS and H_2S are likely to form from the intermediates, shown in equation 1.6.

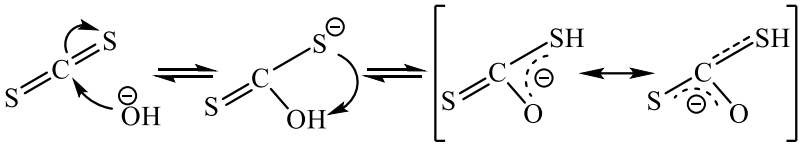

1.3

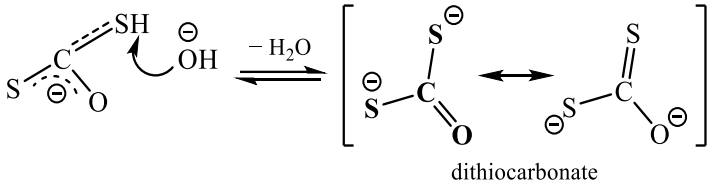

1.4

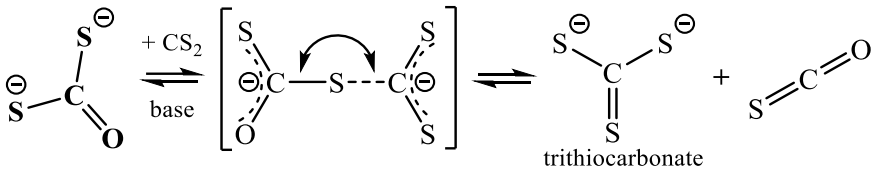

1.5

Equation 1.3-1.5: Three step reaction of CS_2 with hydroxide ions (aqueous alkaline media).[1]

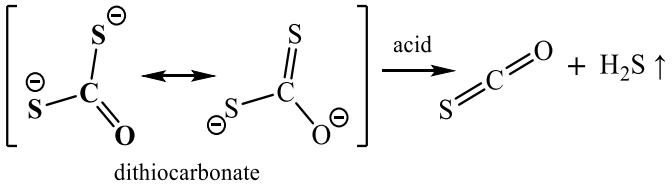

1.6

Equation 1.6: Abort of formation of trithiocarbonate at low pH values (aqueous medium).

Treating CS_2 with an alkaline species such as hydroxide ions can be used to form trithiocarbonates in three steps. First, as shown in equation 1.3, the nucleophilic addition occurs to from a monoanionic intermediate, where the proton of the introduced hydroxide ion is intramolecularly transferred to one of the sulfur atoms. In equation 1.4, another hydroxide ion removes that proton in a condensation reaction upon formation of a dithiocarbonate anion, which is relatively unstable and prone to either react with an additional CS_2 molecule or most likely decompose in the back reaction of equation 1.4 and 1.3. As shown in equation 1.5, the dianionic intermediate can react with CS_2 to form a trithiocarbonate anion and a carbon oxysulfide molecule. The stepwise reaction manner indicates, why dithiocarbonates could only be scarcely obtained in the solid state, as the alkaline media and excess of CS_2 forces the reaction to proceed towards the formation of trithiocarbonates. Only in 1991, the free dithiocarbonic acid $(HS)_2CO$ or (HS)(HO)CS, could be isolated.[1,19] The preparation of the hydroxy tautomer was included in patents for fluorosurfactants and cholesterol-lowering agents.[20]

If sulfides are added directly, tri- and perthiocarbonates[ii] are obtained more easily as the equilibria are shifted towards the desired products. In equation 1.7 and 1.8, the introduced nucleophilic hydroxide anions are exchanged for hydosulfide HS^- in alkaline media or for sulfide ions S^{2-}, respectively. In this context it should be mentioned that the reaction of weakly acidic H_2S with CS_2 does not form trithiocarbonic acid.[22] Polysulfide ions S_x^{2-} (x = 2, 3, 4, 5) form perthiocarbonate or perthiodicarbonate ions, which is written in equation 1.9.

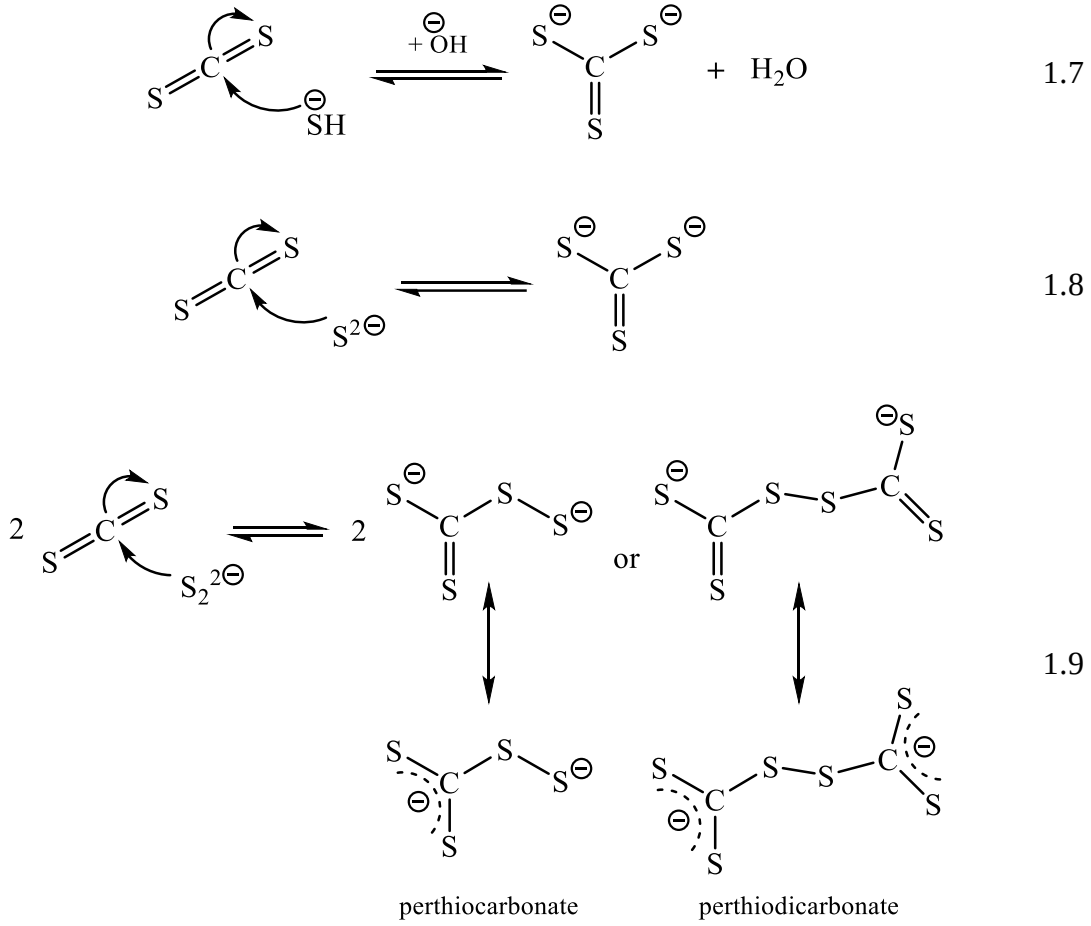

Equation 1.7-1.9: Reactions of sulfides with CS_2.

[ii] Note, that the term *tetrathiocarbonate* for $(CS_4)^{2-}$ is avoided for the sake of indication of the S−S single bond present in the molecule and prevent misinterpretation of the molecule shape of a tetrahedron. Because there also exist orthothiocarbonates, exhibiting a tetrahedral arrangement of C−S bonds on the central carbon.[21].

1.3 Common uses of CS_2 and dithio derivatives

About the end of the 19th century, by the time of industrial development of chemistry, a more complex variety of electron-donating groups, e.g., primary and secondary amines, phosphines, thiolates, etc, became available. As mentioned above, this persuaded scientists to react CS_2 with this growing number of available compounds. The products from these reactions became variable and research on their uses and applications increased. This was for two major reasons. On one hand, the improvement of rubber production and on the other, the demand for pesticides to control all sorts of plagues in agriculture. In both fields elemental sulfur had been used that far, which was successively replaced by tailored sulfur compounds.

Vulcanisation of rubbers

In the 20s of the last century, the vulcanisation of rubbers underwent reformation, as the crosslinking of the polymers with elemental sulfur was supported or even replaced by new additives. The industrial protocol of vulcanisation suffered from uneconomic reaction times and temperatures.[23] So called *accelerators* now offered the advanced control of sulfur concentration and chain length for the curing of polymers.[24] In short, the mode of action of the accelerator is the reaction of the released fragments with the polymer chain upon elevated temperatures. To control the kinetics and mechanisms of the multiple-step reaction, other additives can become necessary.[25] Derivatives of the dithiocarbamates and xanthates were applied in rubber making. Both compound classes are assigned to the group of fast to ultra-fast accelerators.[23,24] A great enhancement in particular was the intermixing of carbon into the material, that was only then realised, as under conditions without accelerators, the sulfur crosslinking was chemically hindered.[23] This emphasises the growing versatility of rubber compounds, as by the addition of carbon, the materials resistance and stiffness could be tuned.

Application as pesticide

Some compounds used in the improved vulcanisation protocols were also used in pesticides, where particularly (dithio)carbamates were common. For instance, *Thiodicarb*[iii], a derivative of the carbamates is used as a contact insecticide. *Larvin WP75* (*Bayer*), where

[iii] Chemical name: dimethyl *N*,*N*'-{thiobis-[(methylamino)carbonyloxy]}-bis(ethanimidothioate), Sum formula: $C_{10}H_{18}N_4O_4S_3$, CAS No. 59669-26-0

Thiodicarb is the main additive, is admitted outside the EU. The pesticidal activity, that is triggered upon hydrolysis, stems from the release of methomyl, that inhibits the acetylcholinesterase enzyme.[26] The compound has been abandoned from EU marketing in May 2007 as it was declared to be in suspicion to cause dietary risks.[27]

Reagents in RAFT polymerisation

Thiocarbonylthio compounds like dithiocarbamates, dithiolates, xanthates and trithiocarbonates are also used in *free radical polymerisation* (FRP) reactions. More closely, they are the agents, transferring the free electron of the radicals in so called *reversible addition-fragmentation chain transfer* (RAFT) polymerisation. In this context, they are referred to as *RAFT-agents*.[28] Syntheses and processing of polymers with all sorts of demands for properties have become a great pillar in the realm of chemical industry. Thus, a number of different preparation techniques are common, where free radical polymerisation plays an important role, due to its variability. There are three major steps in FRP: Chain initiation, propagation, termination and sometimes a fourth step can be considered as the chain transfer.[29] Within this specific field of polymer synthesis, RAFT polymerisation presents some advantages towards other synthesis protocols. By the intermediate chain transfer *via* the RAFT-agent, control of the chain growth is realised by means of concentrations of constituents, duration and temperature. The reaction in scheme 1 describes the key function of the thiocarbonylthio compound during polymerisation propagation.

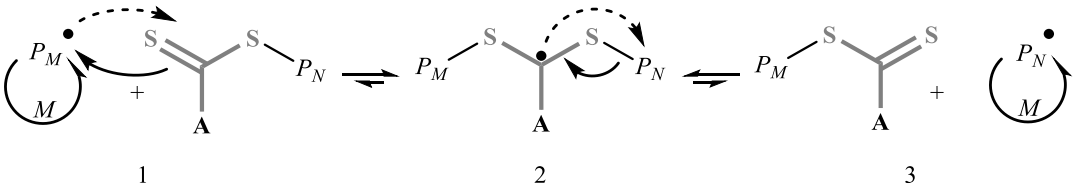

Scheme 1: Proposed mechanism of controlled polymerisation propagation via stabilizing thiocarbonylthio RAFT-agent (grey). Polymeric growth is formulated as the polymer molecules P_M and P_N are adding monomers M to their chain (cf. part 1 and 3). The middle reaction step 2 is the so called 'dormant species' as it is designed to be kinetically stabilised.[30,28]

FRP reactions are usually initiated by the formation of a radical, that can start the chain reaction with the monomer molecules, desired to form up a polymer structure. To avoid an accelerating uncontrolled growth and all kind of possible side reactions, that might be undesired, several parameters can be adjusted. The concentration of initiators is kept low,

so that only a low number of radicals with respect to the number of monomers are let loose. Next, to preserve the reaction running controlled, the formation of a kinetically stabilised radical, has to be favoured in comparison to possible side reactions. By the chemical design of the RAFT-agent the volatility of free radical electron to transfer back to the polymer chain seed, can be decreased. As proposed in scheme 1, the C=S double bond, or thiocarbonyl bond, precisely, the looser π-bond is cleaved to form a new bond to the polymer radical[iv] (cf. step 1). The radical electron is now trapped within the S−C−S fragment, probably occupying an orbital of the carbon atom as depicted (step 2). The substituent **A** acts as a setscrew for the stability of the new radical, as it can interact in terms of its inductive[v] and/or mesomeric[vi] effect. Depending on the type and reactivity of monomers and polymer radicals, **A** will be chosen to increase or decrease the probability of the radical electron to be transferred. Highly reactive polymer radicals, for instance, might be better controlled, with a more 'deactivating' substituent for **A**, at the RAFT-agent, like a phenyl group, where the radical electron can be distributed *via* the delocalised π-electron system (+M-effect). The term 'dormant' for the intermediate 2 in scheme 1 denotes this controlling key function of the RAFT-agent, which is written by disequilibrium arrows. The concentration of RAFT-agent in the reaction is set to a rather high value, which supports the stability of the dormant species. However, for propagation of the reaction, a certain rate of transfer of the radical electron back to the polymer chain 'held sleeping' is needed. In scheme 1, this process is described in step 3. From this moment on, the polymer radical P_N becomes active to grow by chain reaction with monomers M (cf. step 1 and 3).

In polymer synthesis often the mean molecular weight, or molecular dispersity, is of important significance. A narrow polydispersity (close to 1) categorises the polymerisation as controlled since the molecular mass of the product compound is then almost constant. In other words, the growth of the polymer molecules runs homogeneously, and termination of the growth starts only after all monomers available have been connected. This detail is responsible for another term used to describe this type of polymerisation: 'living'. It denotes, that if there are monomers available the chain growth proceeds, if not, termination is imminent.

[iv] At this point it is no more necessary to differentiate between a polymer seed or already advanced chain as the mechanism should in principle not be dependant of the polymer chain length. At least for a basic understanding, no differentiation is needed, although certain effects may not be neglected.

[v] An atom or molecule substituted for a hydrogen atom can act donating or withdrawing electron charge in the new electron bond that is formed upon substitution (+I-, −I-effect, respectively).

[vi] An atom or molecule withdrawing or supplying a delocalised π-electron system and/or free electron pairs to an already conjugated electron system (−M-, +M-effect, respectively).

If all parameters are well chosen, it is furthermore readily derived, that the polymer radicals P_M and P_N in scheme 1 are close in molecular weight, i.e., chain length and the polydispersity is close to the value of 1.
Notwithstanding, depending on the desired material properties, it is common practise to grant a certain polydispersity width (>1). This can for example lead to a softening, because shorter polymer chains are intermixed with longer ones. Again, by tuning of the substituent A and depending on the polymer desired, this can still be feasibly realised with RAFT polymerisation.[30,28,29]

There are far more than the described areas of application for thiocarbonylthio compounds. Particularly, trithiocarbonates are also viable in domain of medicine, pharmaceutics, fuel chemistry, ore froth flotation and synthetic chemistry.[31]

1.4 Aims and topics of this thesis

Having grasped the basic reaction patterns and theoretical background, generally, the aim was to prepare thiocarbonates in the solid state for crystallographic characterisation. This type of data is overall needed to grow knowledge on the chemical properties of compounds, their structural peculiarities and behaviour of elements in a broader sense.

Although inorganic thiocarbonates have been known for decades, only a couple of solid state structures were reviewed in *Topics in Sulfur Chemistry - Carbon Sulfides and Their Inorganic and Complex Chemistry*.[1] The work, written by GATTOW and BEHRENDT, covers knowledge on CS_2 and its 1,1-dithiolate derivatives up until 1977. Among the multitude of reports and publications referred to in said review, related to thiocarbonates are frequently unavailable, going way back to the 60s and 70s. In 1992 GATTOW reviewed progress on this topic, when still only a few more crystal structures were presented.[19]

Altogether, X-ray structure models of some basic inorganic compounds have up to today not been elucidated accurately. In spite the technology and applicability of structure determination techniques improved dramatically through the years, generally speaking, the number of solid-state structures still stands low when the trithio- or perthiocarbonate is a free dianion.

For instance, to the best of the authors knowledge, the only available crystal structure of the free perthiocarbonate anion is given by that of potassium perthiocarbonate methanol solvate $K_2[CS_2(S_2)] \cdot MeOH$.[32] For trithiocarbonates free of solvent molecules, so far, only crystal structures of the α- and β-trithiocarbonic acid,[33,34] sodium and thallium trithiocarbonate (the latter from PXRD data) were registered in single crystal databases.[35,36]

Furthermore, the LEWIS-basic property of the trithiocarbonate anion makes thiocarbonates a ligand capable of donating electrons to LEWIS-acids, which can be exploited to prepare anionic transition metal trithiocarbonato complexes. Likewise, the purely ionic compounds, only a few trithiocarbonato complexes of transition and main group metals are known and not all have been determined crystallographically. No purely inorganic compounds have been described crystallographically.

Finally, mixed thioselenocarbonates are structurally uncharted, which justifies to step ahead towards structural investigation of these hetero chalcogencarbonates. *In status solidi* inorganic dithiomonoselenocarbonates CS_2Se^{2-} of only sodium, potassium and barium are known.

To gain access to compounds with thiocarbonate anions and to overcome drawbacks due to their known sensitivity towards oxidants and long-term instability under moist atmosphere, inert preparation and analysis is needed.

As thiocarbonates are prone to release gaseous decomposition products, reactions of the educts in closed systems were realised using evacuated ampoules. At elevated temperatures solvothermal conditions increase the solubility of solids, which on cooling down start to crystallise. In particular, this was reported successful to grow crystals of sodium trithiocarbonate which persuaded to explore this method to prepare thiocarbonates further. The introduced starting compound CS_2 is fortunately both solvent and reactant. As it constitutes an nonpolar and relatively inert molecule towards ionic compounds, to enhance its reactivity, it is mixed with a minor amount of alcohol.

Another rather traditional method of preparation found in the literature, like the precipitation of group I and II salts from saturated solutions of $M^{I}HS$ or $M^{II}(HS)_2$ with CS_2 in ethanol and water, respectively, were acquired. Worked up, the crude products can be recrystallised under solvothermal conditions, again exploiting the better solubility at higher temperatures in a closed system. This poses another way to obtain products suitable for structure determination routines. Needless to say, X-ray structure analysis is in this regard of major importance, a powerful and to some extent unambiguous method to identify the structure and constituents of solids.

Additionally, IR and RAMAN spectroscopy were chosen, to investigate the compounds by means of their molecular vibrational properties. These complementary methods, together with the structure information give rise to the convenience of the compounds and offer to embed the results into the context of literature. Calculations based on the determined molecular geometries of the molecules on *density functional theory* DFT level provided support for the experimental spectra

2 Results and discussion

2.1 Sodium and potassium trithio- and perthiocarbonates

Starting to work on thiocarbonates, a useful entrance to this field was to prepare alkali trithiocarbonates, namely those, which were known since the first half of the 20th century. Based on the work by YEOMAN from 1921,[5] sodium, potassium and barium trithiocarbonate were precipitated as microcrystalline powder. However, to obtain products, suitable for X-ray structure determination, another approach was applied. The solvothermal treatment of alkali sulfide with CS_2 was first performed by HENSELER and JANSEN, who in this way obtained the single crystalline anhydrous sodium salt.[35] The reactions under solvothermal conditions were applied in a broader spectrum of starting materials. Among crystallisation and investigation of different new interesting compounds, it was successful to grow crystals of perthiocarbonates as well, which were not described in structure models free of solvate molecules. Substitution of the starting sulfide powder with selenide yield crystals featuring a new anion, the perselenodithiocarbonate, which could be described with SC-XRD structure modelling.

With a structure model, PXRD data of Na_2CS_3, K_2CS_3 and $BaCS_3$ could be identified. This further allowed to compare vibrational spectra of other alkali salts that could not be identified with SC-XRD, with those of the potassium and barium compound. With this trithiocarbonates of the series of alkali metals and barium were successfully prepared.

2.1.1 Sodium trithio- and perthiocarbonate salts

Sodium trithiocarbonate Na_2CS_3

Originally, the crystal structure of anhydrous Na_2CS_3 was first reported in the 60s by PHILIPPOT and RIBES, but neither the original work, nor data could be accessed.[37] Mentioned above, HENSELER and JANSEN (re-)discovered the crystal structure of anhydrous sodium salt in 1993, from a solvothermal reaction, confirming it to apply to the monoclinic crystal system with the space group *C*2/*c* (no. 15).[35] Their structure model was confirmed by analysis of the crystals of Na_2CS_3 **6** obtained in this work in using their route.

An earlier claimed high temperature phase transformation in the compound Na_2CS_3 was not pursued, as the original papers are unavailable, and more devotion was paid for the preparation and structural investigation of the other alkali trithiocarbonates (cf. below). Moreover, no indications of such a transformation was determined by HENSELER and JANSEN, who named the compound β-Na_2CS_3 for the low temperature phase.[35] In the review of GATTOW and BEHRENDT, a phase transformation in Na_2CS_3 is not communicated.[1]

The preparation of Na_2CS_3 **4**, following the work by YEOMAN,[5] was carried out as well, which usually yields a microcrystalline powder of that compound **4**. On one occasion a millimetre sized crystal agglomerate, which is depicted in figure 2.1, was obtained from the saturated alcoholic solution upon long standing. (It shall be noted that the numbering of the compound is related to the preparation, thus for instance, the crystals used to determine the structure of Na_2CS_3 **6** chemically mean the same compound as **4**, which in turn was powder.)

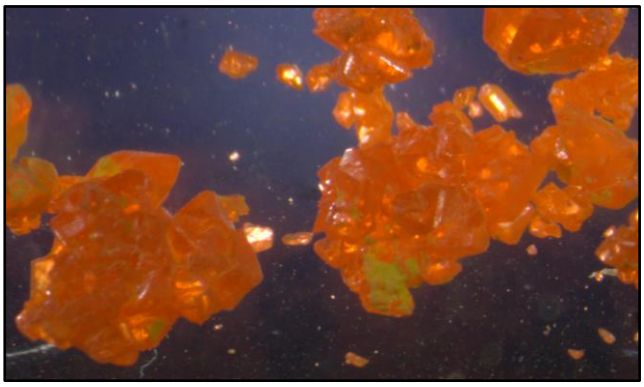

Figure 2.1: Photograph of a macroscopic polycrystalline agglomerate of polycrystals of Na_2CS_3, grown upon long standing from saturated alcoholic solution.

Crystal structure model

The unit cell is depicted in figure 2.2, with the origin at the inversion centre on the *c*-glide plane, and in table 2.1 a comparison of the determined cell parameters and residuals with those available in the database is given.

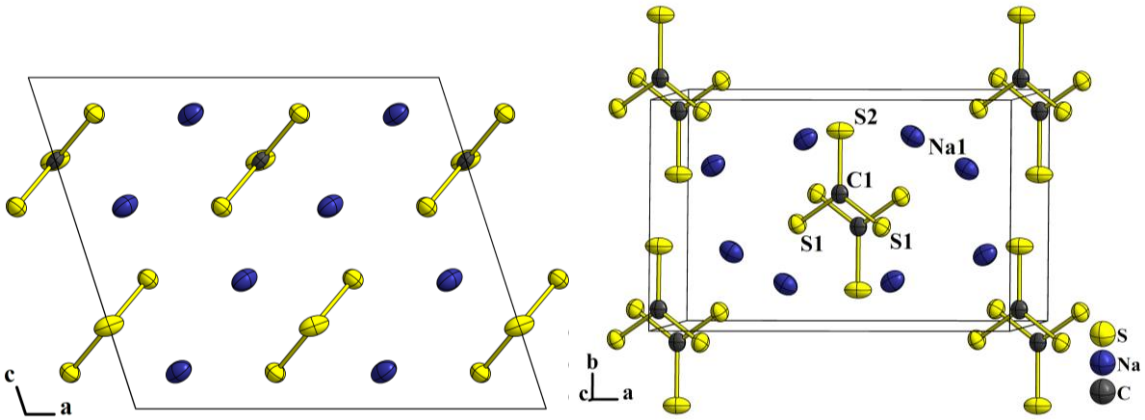

Figure 2.2: Depiction of the face centred monoclinic unit cell of Na_2CS_3 **6**. On the left, the parallel alignment of the trigonal anion is captured in view along the *b*-axis. On the right, the alternative orientation of the C1−S2 bond parallel to the *b*-axis is observed.

A detailed description of the structure can be found in the referred work by HENSELER and JANSEN. However, some interesting properties must not be left out.

The anisotropy ellipsoid of the S2 atom is tilted out of the trigonal trithiocarbonate anion plane, which, as stated earlier,[35] could indicate a symmetry lowering of the space group to *Cc*. As in the preceding work, the structure could not be solved in this lower symmetry. The sodium cation Na1 is surrounded by four nearest trithiocarbonate anions, which have two mono- and two bidentate ionic interactions *via* the negatively charged sulfur atoms, adding up to a coordination number of six. The Na−S distances range between 283.44(9) and 306.90(9) pm, where the mean value is 292.85 pm. In turn, each sulfur atom is coordinated by four sodium cations, very broadly forming a square around the central sulfur atom. Thereby, as described by HENSELER and JANSEN, a distorted anti-CaF_2 fashioned structure is set up, which is depicted in figure 2.3.

Table 2.1: Comparison of the data of the crystal structure model of Na_2CS_3.

Compound name (**No.**)	this work (**6**)	HENSELER, JANSEN 1993[35]
Temperature [K]	150(2)	RT
Crystal system	monoclinic	
Space group (No.)	*C*2/*c*	
a, *b*, *c* [pm]	998.5(1), 628.86(6), 846.42(8)	1003.6(1), 633.7(1), 855.5(1)
β[°]	107.955(7)	108.05(1)
V [nm^3]	0.50562(9)	0.5173(1)
Z		4
ρ_{calc} [g·cm^{-3}]	2.025	1.98
Absorption coef. μ [mm^{-1}]	1.455	1.307
Crystal size [mm^3]	0.12 × 0.07 × 0.05	–
X-radiation [nm]	Mo K_α	
Diffractometer	*STOE IPDS 2T*	*Enraf-Nonius CAD 4*
2θ range [°]	7.772 – 52.96	2 – 80
Index ranges	$-12 \le h \le 12$, $-7 \le k \le 7$, $-10 \le l \le 10$	$-18 \le h \le 18$, $-11 \le k \le 11$, $0 \le l \le 15$
Reflections collected	2594	9907
Independent reflections [R_{int}, R_σ]	529 [0.0666, 0.0373]	1582 [0.02, –]
restraints / parameters	0/29	0/29
Goodness-of-fit on F^2	1.105	–
R_1, wR_2 indexes [$I \ge 2\sigma(I)$]	0.0257, 0.0624	0.034, 0.033
R_1, wR_2 indexes [all data]	0.0283, 0.0633	
Residual electron density. peak/hole [e Å^{-3}]	0.58/-0.54	0.51
Flack parameter		
Absorption correction type	none*	–

*An absorption correction was abandoned, after the routine given in the chapter 4 could not improve the residuals for the crystal structure model.

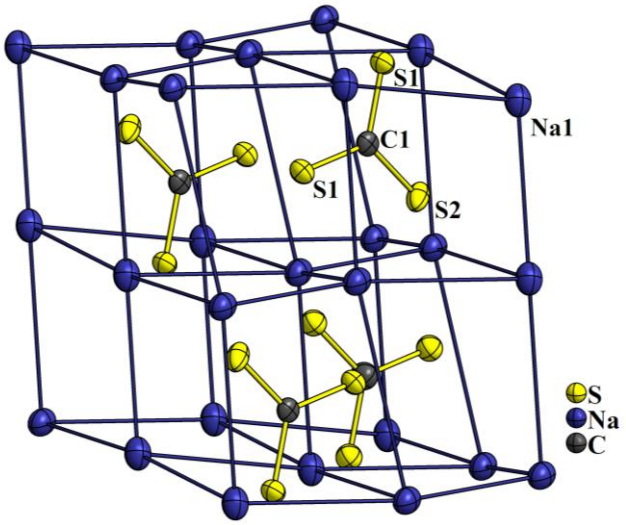

Figure 2.3: Anit-CaF_2 structure fashioned array of sodium ions, forming distorted cubes, of which half are inhabited by trithiocarbonate anions.

Despite the temperature difference of the measurements, the trithiocarbonate anion geometry is changed only marginally. In table 2.2 the crucial values are compiled. The ideal D_{3h} symmetry is broken, determining two non-equivalent C−S bonds. As C1 and S2 occupy the special site 4e, their position and bond coincide with the two-fold axis present in the space group symmetry. The molecule anion is thus constrained to C_{2v} symmetry, as the symmetry element forces the molecule to planarity (vertical mirror plane). S1 and Na1 possess regular lattice sites (8f).

Table 2.2: Geometry details of the trithiocarbonate anion in the structure model of Na_2CS_3.

distance / angle	150 K (this work)	RT[35]
C1−S1 [pm]	171.3(1)	171.51(7)
C1−S2 [pm]	172.2(3)	171.8(1)
S1−C1−S1 [°]	119.57(2)	119.35(7)
S1−C1−S2 [°]	120.21(1)	120,32(4)

X-ray powder diffraction

The powder obtained on the route of precipitation was identified as a mixed phase with major parts of Na_2CS_3 **4** with a fit of the PXRD data with the crystallographic phase information of the obtained Na_2CS_3 single crystal **6** (*C*2/*c*, own data) in a simple RIETVELD refinement (hydrogen atom sites were left out from the procedure). Some impurity with $Na_2CS_3 \cdot 2\ H_2O$, could be found due to additional intensities in the powder diffractogram, which is graphically summarised in figure 2.4. The dihydrate phase information was fitted

with a simple PAWLEY refinement (green line), neglecting to refine the atomic position in the impurity phase.

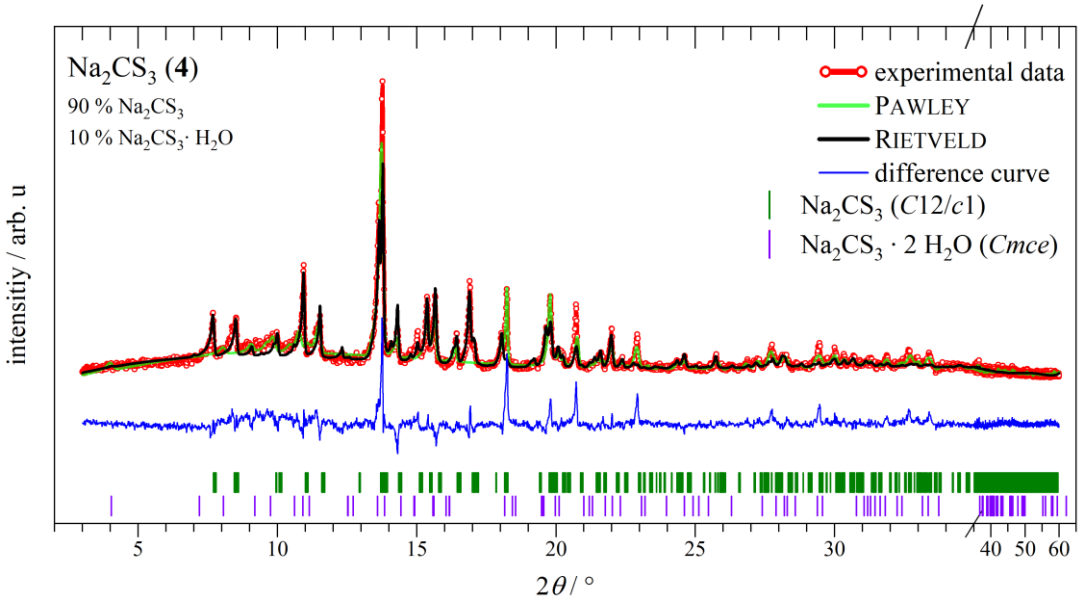

Figure 2.4: Graphical output of computational refinement of experimental PXRD data of Na_2CS_3 **4** (y_{exp} red curve). The RIETVELD and PAWLEY refinement curves are coloured black and light green, respectively, and the difference curve ($y_{exp} - y_{ref(black)}$) is blue. The symbols at the bottom mark the reflection angles simulated from the single crystal information on which basis the RIETVELD refinement was carried out. Some strong mismatches (indicated in the blue curve) could be fit in a PAWLEY refinement as drawn in light green.

From the blue difference curve, some misfits of the black curve and the experimental data is observed. Qualitatively, the reflection pattern is in accord with that of a mixed phase of majorly anhydrous Na_2CS_3. However, there are some peak ranges that clearly speak for additional phases or crystal phase misfits not covered by the refinement.

The reflection between 18 and 19° is either shifted to the right or contains further phase information, as it is too intensive to belong to the phase of Na_2CS_3, only. This particular intensity could be explained with impurity by the dihydrate phase, which is well simulated with a PAWLEY fit, using earlier reported cell parameters and space group of $Na_2CS_3 \cdot 2\ H_2O$. The green line representing the impurity also describes the intensities at 20 and 23° much better than the black line of the main product Na_2CS_3.

Qualitatively, one may assume that water molecules introduced *via* the moist atmosphere, due to the hygroscopic nature of the compound. They do not readily occupy the sites as determined in a $Na_2CS_3 \cdot 2\ H_2O$ crystal grown thermodynamically balanced including water of crystallisation. Rather, the migration of the water molecules into the lattice of the

formerly anhydrous Na_2CS_3 is accompanied with a successive change of the crystal lattice. As a result of the refinement technique, apparently this change includes the set-up of the orthorhombic system at an early stage of hydration. This constitutes that by hydration of Na_2CS_3 a higher order is successively established in the lattice, which explains the hygroscopic nature of the material structurally, since by increasing lattice order, the lattice energy increases. It shall be admitted after all that by the different refinement methods there are still intensities left in the experimental data that cannot be addressed by either one of the calculated lines.

Moreover, neither one of the phases of Na_2S (*Fm*$\bar{3}$*m*, ICSD no. 60436), Na_2S_2 (*P*$\bar{6}$2*m*, ICSD no. 73180), Na_2CO_3 (*C*2/*m*, ICSD no. 60311) or $Na[S_2COC_2H_5] \cdot 2\ H_2O$ (*P*$\bar{1}$, own data), all of which could be present from incomplete conversion, decomposition or oxidation, were useful to explain the origin of the unmatched intensities in figure 2.4.

Sodium trithiocarbonate dihydrate $Na_2CS_3 \cdot 2\ H_2O$

As explained in the experimental details the substitution of metallic sodium with sodium hydroxide as a precursor results in inclusion of H_2O in the crystal structure. As shown in figure 2.5 yellow, crystalline $Na_2CS_3 \cdot 2\ H_2O$ **5** could thus be precipitated from a saturated alcoholic solution of NaSH with addition of CS_2. The crystals were ground to a powder and a PXRD curve was recorded right after the preparation. At a later point in time, a suitable crystallite for SC-XRD analysis was used to record data for a structure model.

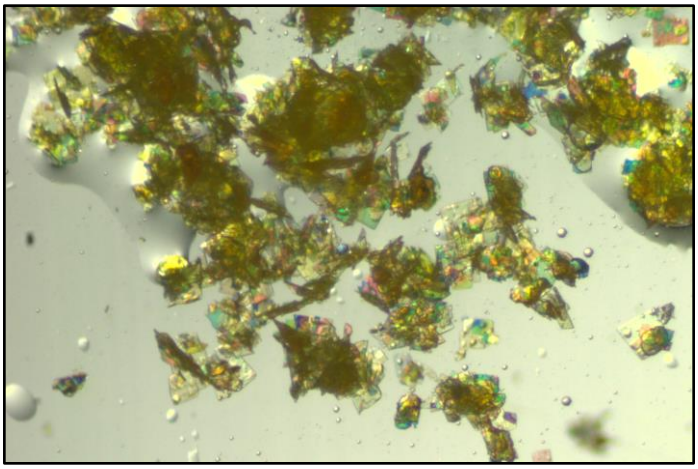

Figure 2.5: Photograph of yellow finely crystalline $Na_2CS_3 \cdot 2\ H_2O$ **5**.

Like the anhydrous compound, the crystal structure of $Na_2CS_3 \cdot 2\ H_2O$ was originally determined by PHILIPPOT and RIBES in 1969.[37] According to the original reference, reviewed by GATTOW and BEHRENDT, the space group *Ccmb*, using the formerly written

nomenclature had been determined, which was confirmed through analysis of modern SC-XRD data.

Crystal structure model

The orthorhombic space group *Cmca* (no.64) could be used for the description of the unit cell with eight formula units. The unit cell is depicted with two viewing angles in Figure 2.6. As a first impression, one can explain the structure as alternating layers, vertical to the elongated *a*-axis, that are filled with water and vacancies alternatively.

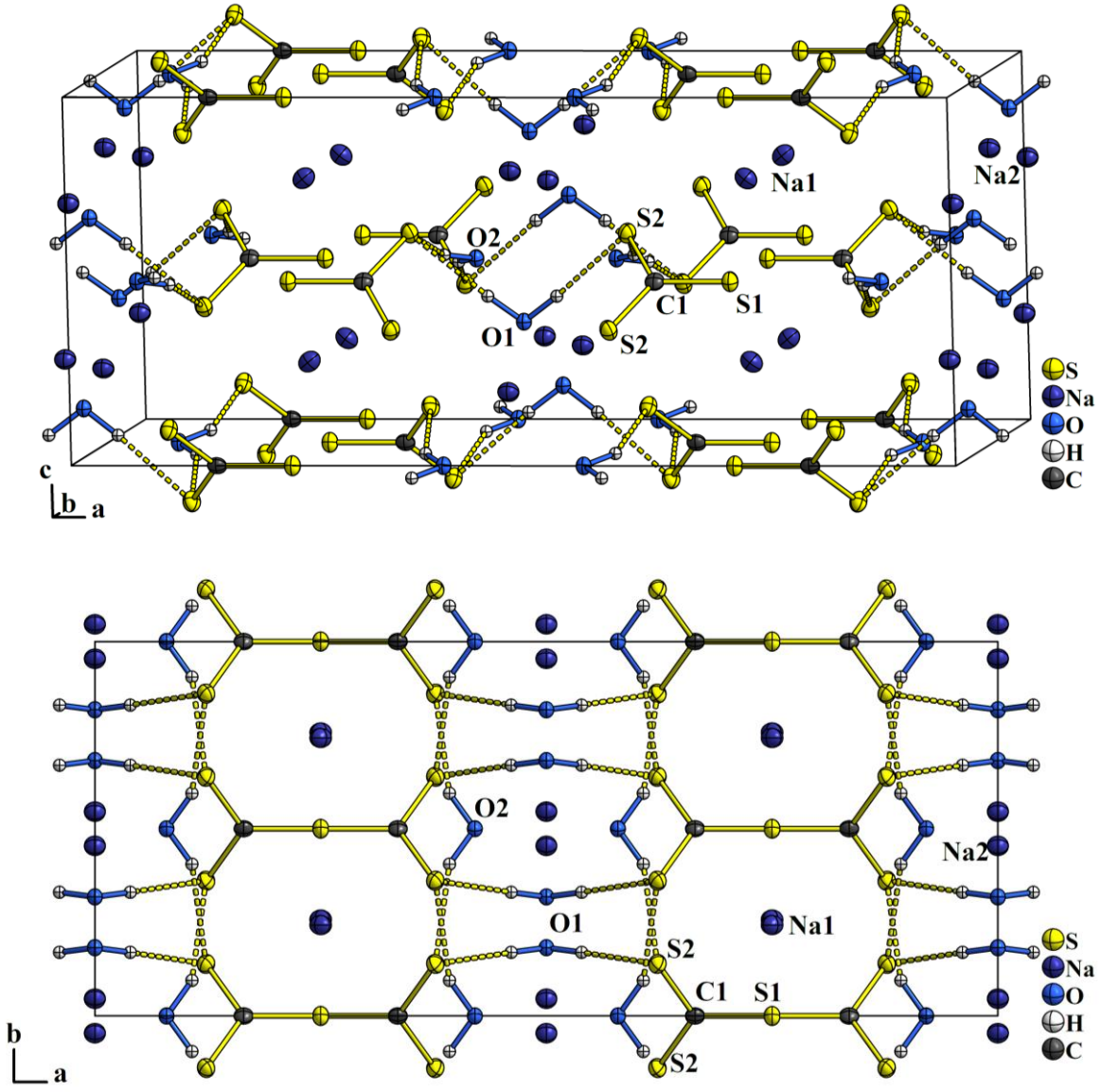

Figure 2.6: Depictions of the extended face-centred unit cell of $Na_2CS_3 \cdot 2\ H_2O$ **5**. All non-hydrogen displacement ellipsoids are drawn at 70 % probability. The dashed yellow connections indicate hydrogen bonds between the negatively charged sulfur atoms and the water molecules of crystallisation.

In the top drawing, the trithiocarbonate anions and water molecules set up a network *via* hydrogen bonds. The S2···O distances (S1 has no interaction with water) of 258.1(1) (O1) and 351.42(5) pm (O2), show that the H_2O molecules of crystallisation cannot be considered strongly hydrogen-bound.[38] This supports the fact that water could be carried off from the powder compound by drying. Some atoms occupy special sites in the present structure: The CS_3^{2-} possesses C_{2v} symmetry, as a two-fold axis parallel to the *a*-axis is coinciding with the C1−S1 bond (both atoms in site 8d). Due to that, the anion is forced to planarity and offers only two non-equivalent C−S distances for comparison. Expecting one of the bonds to exhibit double bond character by a decrease in length, cannot be discussed separately from the site symmetry. As the three C−S bonds differ only marginally (172.0(2) (S1) and 171.8(1) pm (S1)), the position of the double bond is not resolved from the X-ray structure model. In other words, the π-electron system is distributed homogenously over the molecule. The anion model describes hardly any difference compared to the model in the anhydrous compound (cf. above). Particularly, the CS_3^{2-} ions are likewise coordinated in the cation network, set up by two individual sodium atoms Na1 and Na2, describing a distorted cubical fashioned lattice. Their distinct positions are special (8e), with rows of Na1 coinciding with another two-fold axis parallel to *b* and Na2 located in the mirror plane (8f) in (011) and (½11), as shown in figure 2.6 (bottom). Interestingly, the earlier mentioned anti-CaF_2 fashioned structure, seen in the anhydrous compound, can thus again be recognised, which is shown in figure 2.7.

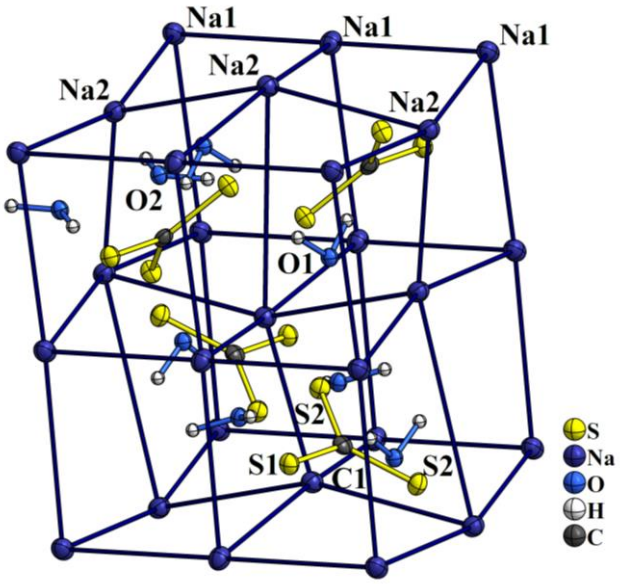

Figure 2.7: Drawing of the distorted primitive cationic framework in the crystal structure of $Na_2CS_3 \cdot 2\ H_2O$ **5**, where CS_3^{2-} anions occupy every second cuboid built by the sodium cations. This results in an anti-CaF_2 fashioned structure which is heavily distorted. Two water molecules of crystallisation per anion are included which are not considered in the comparison with the anti-CaF_2 like structure.

In this construction, S1 is coordinated by four Na1 ions, with an atomic distance of 290.05(5) and 298.57(6) pm, but as the primitive sodium ion lattice is not aligned with the unit cell dimensions, the C1−S1 bond is not orthogonal to the almost rectangular plane of the nearest Na1 ions. Below 400 pm, the S2 atom has only two ionic interactions with Na1 and Na2 in a distance of 292.72(5) and 299.76(6) pm, respectively.

Of course, compared to the anhydrous compound, additionally two water molecules are included for each anion. The O1 atom is found in the mirror plane, shifted away from the centre of the Na_4 trapezoid spanned by the nearest Na2 ions. The O2 water molecule is occupying the cation cuboids vacant from anion occupation, alternating with the neighboured anions in the cationic network. Dipole-cation interaction, i.e., hydration of the sodium ions, can be assumed and for O1 and O2, two Na2 ions are close (233.2(2) and 235.2(2) as well as symmetrically 237.2(1) pm). In order to compare, both the anti-CaF_2 fashioned structures in the anhydrous (cf. page 17) and the dihydrate compound a closer look at the atomic distances of the primitive sodium framework is used. This cation lattice in the anhydrous compound consists of smaller Na_8 cuboids, with the longest Na···Na distance to be 417.1(1) pm. Whereas, the longest Na···Na distance in the primitive framework is significantly longer in the dihydrate, reaching 565.48(6) pm, which is the distance between the planes inhabited by Na1 and Na2. Thus, inclusion of H_2O in the lattice

demands movement of the alternating planes of sodium cations away from each other. (Within the planes, the Na···Na distances are comparable to those in anhydrous Na_2CS_3 ~350 pm.) It may be stated that the trithiocarbonate anion holds the separated planes together. On one hand it coordinates towards the hydrated plane occupied with Na2, which are heterogeneously stabilised in their site by H_2O and negatively charged S2 with dipole−cation and ionic interaction, respectively. On the other hand, negative charge is brought to the plane of Na1 cations, because they are relatively well ordered symmetrically around S1. Thus, the Na1 plane is guided by a 2:1 ionic interaction between Na1 ions and negatively charged S1.

X-ray powder diffraction

The experimental PXRD data was treated with a RIETVELD analysis, which is graphically shown in figure 2.8, using the phases of anhydrous and the dihydrate of Na_2CS_3.

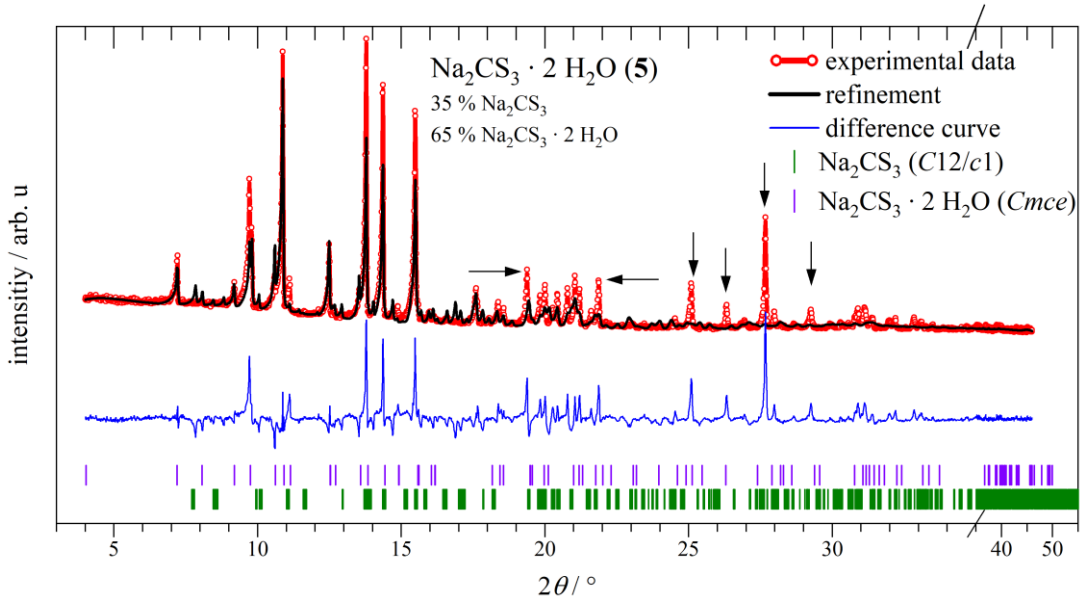

Figure 2.8: Graphical output of RIETVELD analysis of the PXRD data of $Na_2CS_3 \cdot 2\ H_2O$ **5** ground to a powder. Some strong mismatches of the refinement (black curve) can be observed from the peaks in the blue difference line ($y_{exp} - y_{ref}$). The arrows mark intensities of undefined additional phases.

Thus far, the atomic positions in the unit cell of $Na_2CS_3 \cdot 2\ H_2O$, were unknown, but with the crystal structure these positions could now be refined as well. However, some intensities could not be simulated with the crystal phase information of the dihydrate only. Because of the structural similarities described above, the anhydrous compound info was added as a second phase. This allowed to fit at least most of the strong peaks in the powder data,

identifying the powder as to consist majorly of these compounds. However, the intensity ratio of the experimental and refined peaks is not ideal, seen in the amplitudes of the difference curve above 2θ = 19°, shown in figure 2.8. Some additional intensities in the range of 2θ = 19 to 23° and 25 to 31° could not be described by the two main phases. The strongest reflections indicated by arrows clearly give rise to a third or even more phases in the powder mix, which could not be identified. It was tried to overcome these mismatches by a decrease of the space group symmetry of the dihydrate phase. Therefore, the single crystal data of $Na_2CS_3 \cdot 2\ H_2O$ **5** was solved in the primitice monoclinic group $P2_1/c$ (no. 14). This resulted in cancellation of the symmetry equivalent S2 site and enabled a third set of atomic *x*, *y*, *z*-parameters to be refined. This did not help to improve the RIETVELD refinement. Neither NaOH nor Na_2CS_3 could be identified as a third phase. Searching for the respective peak ranges of the refinement in the PDF-2 database did not uncover reasonable sub phases. After all, the strong mismatched peaks in the powder data cannot be identified properly.

Sodium perthiocarbonate $Na_2[CS_2(S_2)]$

According to the review of GATTOW and BEHRENDT,[1] X-ray structure investigations of sodium perthiocarbonate was reported earlier by SILBER and PELLOUX[39] but the original reference could not be enquired. In contrast to $Na_2CS_3 \cdot 2\ H_2O$ not even the review mentions single crystal structural data. An entry was obtained, searching for the original publication in the PDF-2 database, but it only features seven d_{hkl}-values of the compound covers no assignment of a space group.

Like the crystallisation of Na_2CS_3, the solvothermal route was successfully adopted to grow crystalline $Na_2[CS_2(S_2)]$. Beforehand, it was attempted to prepare the phases of sodium tri-, tetra- and pentasulfide as a starting material (cf. preparation of starting materials in section 0) as it was unclear which of those would be useful to obtain the desired product. Moreover, during the course of this work the question arose, if two CS_2 moieties can be connected with a sulfide chain, forming a $(S_2CS_xCS_2)^{2-}$ anion, with $x > 2$, i.e., a longer sulfur connection than in the perthiodicarbonate anion (cf. below).

Figure 2.9 shows a photograph of the obtained crystalline product that was suitable for an SC-XRD measurement.

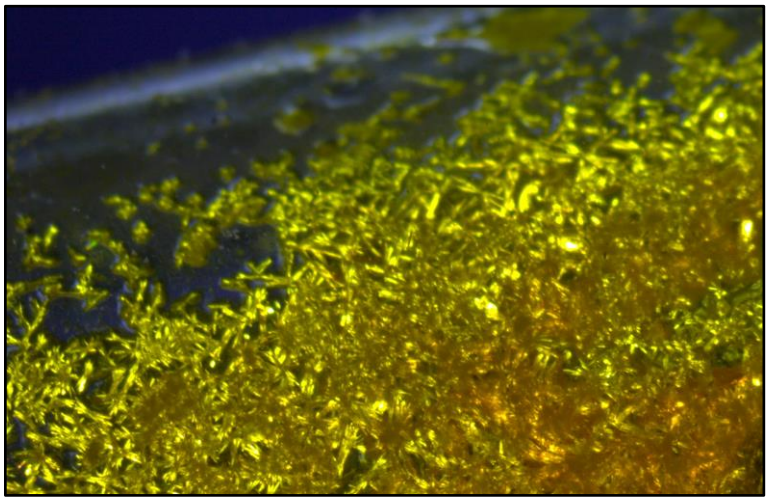

Figure 2.9: Yellow intergrown crystals of $Na_2[CS_2(S)_2]$ **28** covering the wall of the glass ampoule.

Several attempts were necessary to find a suitable specimen for measurement, because the structure models to describe the first data sets suffered from disorder. Eventually, a crystal was recovered quickly after finishing cool down from the solvothermal treatment. The structure was identified as anhydrous $Na_2[CS_2(S_2)]$ **28** which was free from disorder.

Crystal structure model

The structure contains four formula units per unit cell in the orthorhombic crystal system. The space group was determined to be *Pmna* (no. 53). Figure 2.10 shows the unit cell, set up by one unique $CS_2(S)_2^{2-}$ anion and two non-equivalent Na^+ cations.

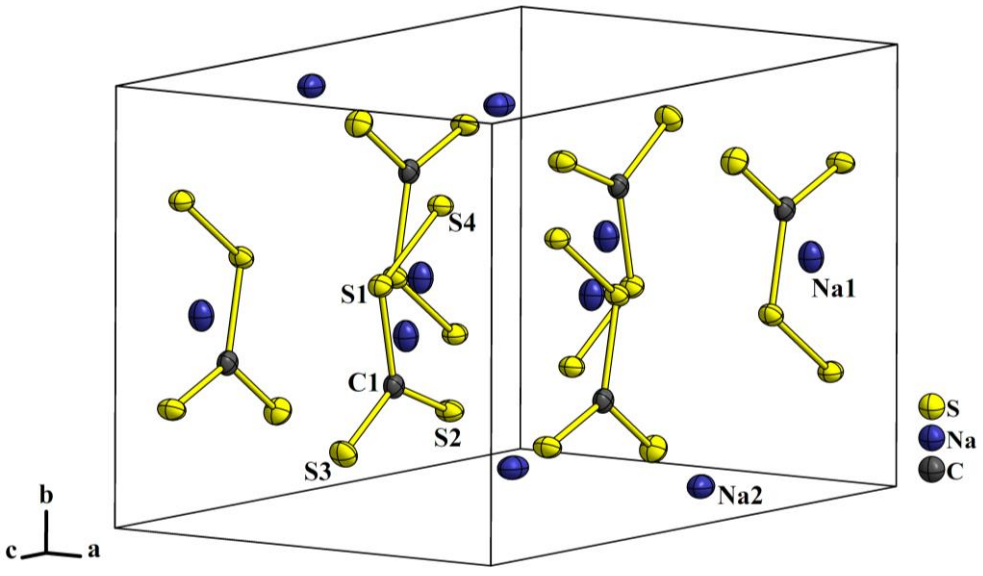

Figure 2.10: Unit cell of $Na_2[CS_2(S)_2]$ **28**. Displacement ellipsoids are drawn at 70 % probability.

The atoms of the molecular $CS_2(S)_2^{2-}$ anions are all occupying the WYCKOFF site 4h, which is in the mirror planes that are coinciding with the *a*-plane. Another parallel mirror plane at the centre of the unit cell is inhabited by $CS_2(S)_2^{2-}$ ions turned around as a consequence of the two-fold screw axes oriented in parallel, i.e., orthogonally with *a*, between the mirror planes. As all atoms are in the mirror plane, within the range of standard uncertainty, the molecule is forced into strict planarity, resulting in the molecule symmetry C_S.

The sodium ions Na1 and Na2 occupy the Wyckoff sites 4f and 4g, respectively. Both the sites own the symmetry element of a two-fold axis, directed parallel to the *a*-axis for Na1 and to the *b*-axis for Na2. The cations set up a primitive lattice of rhombic cuboids, drawn by Na···Na connections in figure 2.11 (left). These primitive distorted cuboids, which are alternatively vacant and filled by neighbouring $CS_2(S)_2^{2-}$ anions.

In 1970 $Na_2[CS_2(S_2)]$ was crystallised from an anhydrous solution containing argon. Apparently, 5 % argon (no further details) was captured in the crystalline sodium salt and even under reduced pressure was not released before decomposition.[40] Unfortunately, the original reference could not be accessed for further enquiry. However, seen in form of the vacant Na_8 polyhedrons in figure 2.11 (left), the room offered in the crystal structure accounts to about 0.76 nm^3. The volume of an argon atom based on its VAN DER WAALS radius is about 0.23 – 0.31 nm^3,[41] which should be sufficiently small to theoretically be located or even move in the vacant Na_8 polyhedron centres. In an ideal crystal, the vacant site would indeed form a tunnel in parallel direction along the *a*-axis, virtually allowing moieties of suitable size to move through the crystal lattice.

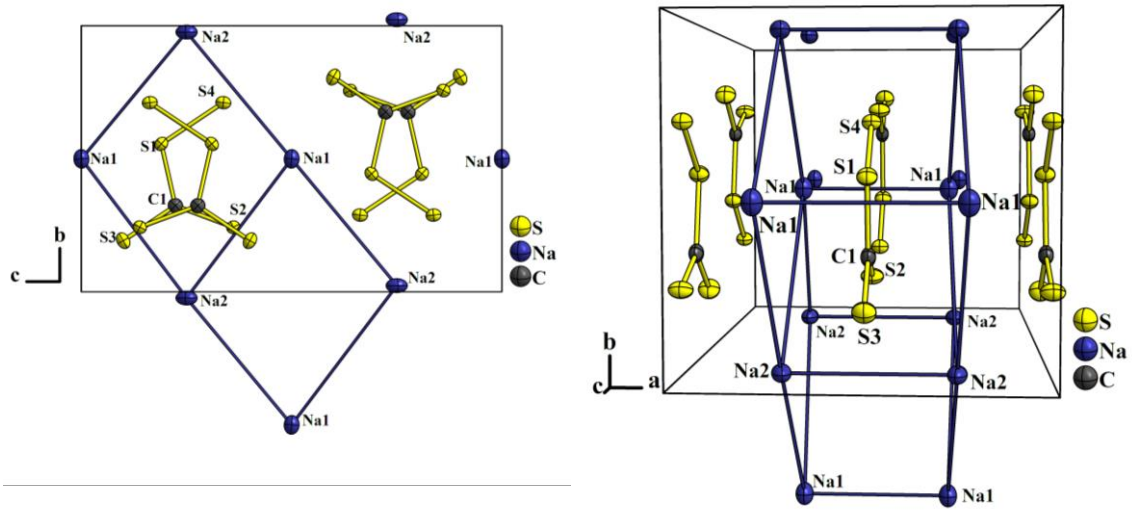

Figure 2.11: Parallel view along the *a*-axis of the unit cell of $Na_2[CS_2(S_2)]$ **28** with depiction of the rhombic base areas of the Na_8 cuboids. They are either filled with the alternatively oriented packing of perthiocarbonate anions or left vacant (left). The perspective side view towards the *c*-plane shows the sodium ions lined up in a non-ideal way, considering their tangency with the two-fold screw axis going parallel to the *c*-axis (right).

From the combination of symmetry elements, a two-fold screw axis occurs in parallel direction to the *c*-axis, which is depicted in figure 2.11 (right). In the view along this direction, one can observe, that the sodium atoms are just shifted a little from the ideal location, denying additional two-fold screw site symmetry. The rhombic polyhedron is therefore slightly distorted. Written in numbers, there are different distances of the Na1···Na1 polyhedron edge, namely 407.0(1) and 340.7(1) pm, naturally adding up to the lattice parameter $a \approx 747.7(1)$ pm.

The perthiocarbonate anion in the structure of $Na_2[CS_2(S_2)]$ **28** offers four distinct sulfur atoms, i.e., the covalent bonds in the molecule are free from symmetry dependence between each other. As expected, the S−S bond accounts to about 203.1 pm, which is in range of the atomic core distances found for polysulfide anions S_x^{2-} with x = 2, 3, 4, etc.[13] The C−S bonding is shorter with about 168.3 (C1−S2), 171.3 (C1−S3) and 173.7 pm (C1−S1) and does not markedly differ from those found in the trithiocarbonate anion. As the bonds are symmetrically non-equivalent, in this structure the delocalised π-double bond can be determined with increased weight at the C1−S2 connection (*cis* side), which is decreased compared to the C1−S3 and the C1−S1 bonds. The latter should have the smallest bond character at all, as it is the bridging sulfur atom.

2.1.2 Potassium trithio- and perthiocarbonate salts

Potassium trithiocarbonate K_2CS_3

Routes given in the literature to precipitate K_2CS_3 from alcoholic saturated solution upon addition of CS_2 were carried out. The anhydrous alkali trithiocarbonate was obtained as an intensely coloured pink powder **9**, shown in the photograph in figure 2.12 (right) and investigated with PXRD, IR and RAMAN spectroscopy.

Based on the strategy of growing single crystal specimen under solvothermal conditions, by reaction of alkali sulfide and CS_2, specimens for X-ray structure determination (photograph in figure 2.13) were obtained and the collected data was used to (re-)determine the crystal structure of K_2CS_3. Beforehand, the needed K_2S was prepared and qualified with a slight impurity of K_2S_2, which is graphically shown in figure 4.10 in the experimental sub-section 4.2.13.

The obtained K_2CS_3 powder **9** was also used as a starting material in solvothermal reactions with transition metal salts (cf. section 2.6). On many occasions, this procedure included recrystallisation of K_2CS_3 under these conditions and resulted in growth of K_2CS_3 **13** crystals, depicted in figure 2.14, that were measured with SC-XRD to enforce the structure model obtained in the first place.

Figure 2.12: Photographs of K_2CS_3 powder **9** after removal of the mother liquor and onset of drying step (left), and after drying (right).

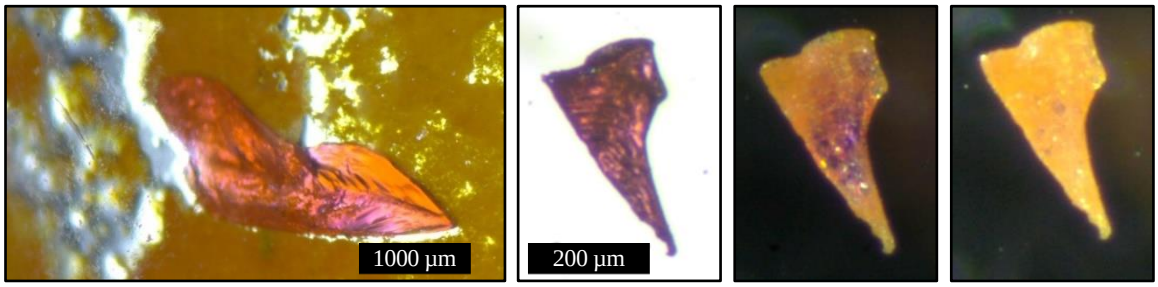

Figure 2.13: Photographs of the pink anhydrous K_2CS_3 crystal **12**. Crystal as obtained on the glass wall surrounded by yellow microcrystalline side product (left). Photos of the irregularly shaped crystallite of K_2CS_3 used for the SC-XRD experiment: The photos were taken after the measurement and show the clear crystal to weather and colour to change from pink to orange, although kept under inert oil. From middle to right, the progression of chemical weathering is displayed after one and three hours, respectively. (The polarisation filter in extinguishes background light.)

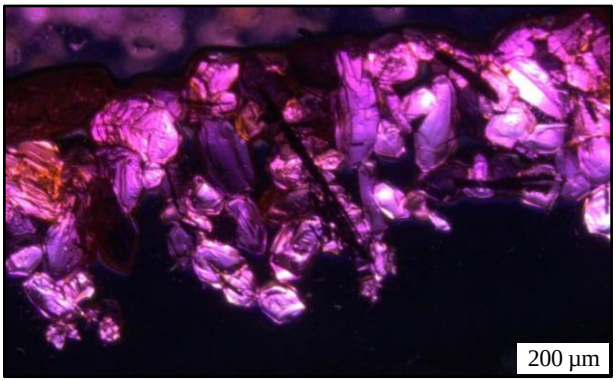

Figure 2.14: Opulent recrystallisation of K_2CS_3 **13** on the ampoule wall after a solvothermal treatment. The quality of the crystals was superior to those from reaction, leading to improved structure residuals.

The crystal structure of anhydrous K_2CS_3 cannot be found in the ICSD, and earlier reported crystallographic details go way back to the same untraceable reference of PHILIPPOT and RIBES that originally reported the structure of the sodium salt. However, taken form the mentioned review, one distinct space group has not been determined within the orthorhombic lattice.[1] Research through the PDF-2 database unfolded an entry (PDF no. 00-025-0687) of the authors, where anhydrous K_2CS_3 is assigned with the space group *Amam* (No. 63). A new set of collected X-ray structure data gave a different space group in this work. Nevertheless, as virtually the same lattice parameters are given in the PDF-2 entry and the review, it must be assumed that the authors may have struggled with disorder in their specimens. This can be understood, admitting that in the 1960s the operative requirements for crystals (e.g., size) used for structure determination were much higher.

Crystal structure model

In contrast to the lighter sodium compound (cf. above), the structure of K_2CS_3 **12** was solved with the space group $Cmc2_1$ (No. 36) with $Z = 12$ formula units. Table 2.3 contains the unit cell parameters of the obtained crystals in comparison with the reported values from PHILIPPOT and RIBES.

The structure consists of three non-equivalent trithiocarbonate anions and four different potassium cation sites. In figure 2.15, the extended unit cell is drawn in view along the *c*- and *a*-axis on the left and right, respectively.

Table 2.3: Comparison of unit cell parameters of K_2CS_3 reported in 1969 and obtained from the preparations in this work.

K_2CS_3 (no.) (details)	T / K	Crystal system	Space group (no.)	Cell parameters				V / nm^3	Z
				a / pm	b / pm	c / pm	α, β, γ / °		
this work **12**	150(2)	ortho.	$Cmc2_1$ (36)	999.7(2)	1565.0(3)	1208.9(2)	90	1.8916(7)	12
this work **13**	150(2)	ortho	$Cmc2_1$ (36)	999.4(1)	1564.9(1)	1209.50(9)	90	1.8917(3)	12
PHILIPPOT, RIBES 1969[37]	nA	ortho.	*Amam* (63)	1217.9	1573.9	1005.7	90	1.928	12

The anions of C1 and C2 are bisect by the mirror plane along their C1−S12 and C2−S22 bonds, respectively. The anion of C3 in turn is oriented differently. Its trigonal plane, i.e., all atoms of CS_3^{2-}, lies in that mirror plane, which coincides with the *a*-plane at $a = 0$ and ½. All atoms that coincide with the mirror plane are occupying the WYCKOFF site 4a. The trigonal planes of the CS_3^{2-} anions of C1 and C2 are not parallel to the *b*-plane of the unit cell, instead, they are tilted out of about 18 and 25°, respectively. This altogether makes the crystal structure of K_2CS_3 much more complex compared to its lighter sodium homologue, because there just one CS_3^{2-} anion per formula unit of asymmetry was determined in the structure.

Interestingly, none of the atoms in the structure of K_2CS_3 exhibit a two-fold screw symmetry at their position. By the mirror and the *c*-glide symmetry in the *a*- and *b*-plane, respectively, the two-fold screw axis is translated to multiple centres in the unit cell, all being parallel or even coincide with the crystallographic *c*-axis. Those screw axes lying in the *a*-plane are shown as dashed lines in figure 2.15 on the right. The atoms C2 and S33 are in the mirror plane and only close to tangency with that axis of symmetry.

Compared with the reported values for the C−S bond length in the trithiocarbonate anion, the situation here is inconspicuous. The possible oscillation of the negative charges between the sulfur atoms agrees with a C−S bond length shorter than a single bond, but longer than a double bond on all three covalent bindings. The planarity of the triangular arrangement of the sulfur atoms around the carbon atoms in the centre is only marginally different from the ideal angle of 120° between the bonds. Giving some numbers, the three non-equivalent CS_3^{2-} ions show X-ray C−S bond lengths of 171.7(2) and 172.6(4) (C1), 171.3(1) and 172.6(3) (C2) as well as 171.6(3), 171.5(4) and 172.8(3) (C3).

The potassium ions are distributed around the anions with respect to the symmetry of the point group. The ions K2 and K3 possess mirror symmetry in 4a site, where K1 and K4 occupy the general position 8a. The positively charged potassium ions connect with the trithiocarbonate anions in an ionic bonding network. However, no distorted lattice motifs as in Na_2CS_3 could be observed. More precisely K1, K2 and K3 are surrounded by a sphere of eight, K4 by seven nearest sulfur atoms that carry the negative charge of the anions, where the mean K−S distance is 332.11 (K1), 331.48 (K2), 330.28 (K3) and 333.60 pm (K4). The shortest and longest coordination distances are 311.8(1) pm for K3−S22 and 364.96(9) pm for K1−S32, respectively. For K2 and K3 the eight nearest sulfur atoms are also the nearest of all atom types, but the situation for K1 is different. There, the closest atom is C3 (2.986(1) pm) and C1 (340.2(3) pm) lies closer than three farer sulfur atoms. The ions K2, K3 and K4 each dislocate (>350 pm distance) from the nearest carbon atom. However, short K···C distances should not add to the overall ionic bonding as the carbon atom is oxidised to +IV. Furthermore, the carbon orbitals should be screened by the adjacent sulfur atom orbitals, not rising assumption for actual interaction between potassium and carbon.

Adding up the number of K−S coordination within range of 400 pm, results in eight for K1, K2, K3 and K4, but only, if for K4 the range is extended to 404.3(1) pm, for a very long K4−S33 coordination.

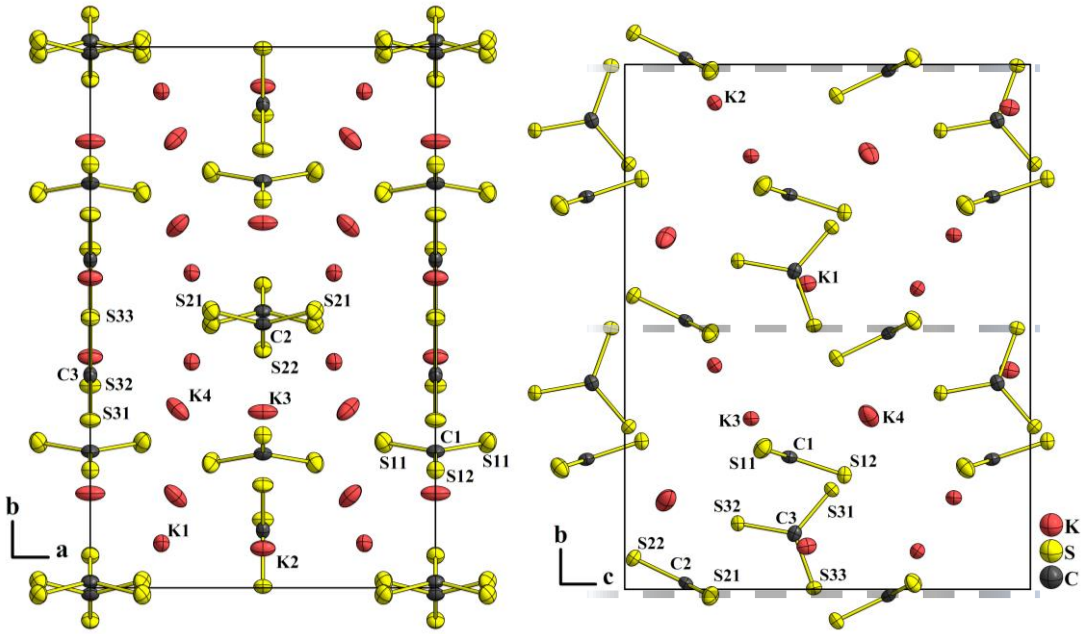

Figure 2.15: Extended *C*-centred unit cell of K_2CS_3 in *c*- and *a*-axis viewing direction on the left and right, respectively. The dashed lines on the right mark the two-fold screw axes coinciding with the mirror and *a*-plane.

As expected, the ionic network is designed with CS_3^{2-} performing both chelate and monodentate bonding of the cations. This is naturally possible, due to the delocalisation of negative charges to donate *via* the π-system of the anion. In view of the HSAB concept, as sulfide and potassium ions are of similar size and indeed possess the same electronic configuration, namely that of argon, they offer a relatively well-fitting *softness* in their electron cloud qualitatively improving their interaction, which contributes to the ionic network.

X-ray powder diffraction

As mentioned, knowledge of the crystallographic phase allowed to refine the PXRD data and identify the prepared pink salt with free from phase shift K_2CS_3. The PXRD data of the obtained K_2CS_3 **9** powder is displayed in figure 2.16, where the graphical result of a simple RIETVELD refinement is given. It is shown that the PXRD data fit the single crystal phase of K_2CS_3. The experimental data, refinement curve and difference curve are complemented with green line marks of the simulated PXRD from single crystal results. The refinement residuals are given in the appendix section 5.2. Stepwise, the experimental PXRD data was fit by refinement of the amorphous background, the cell parameters, the thermal displacement and the actual atom positions determined by SC-XRD. Results on the Raman and IR spectroscopic investigation of K_2CS_3 powder **9** is shifted to subsection 2.4.

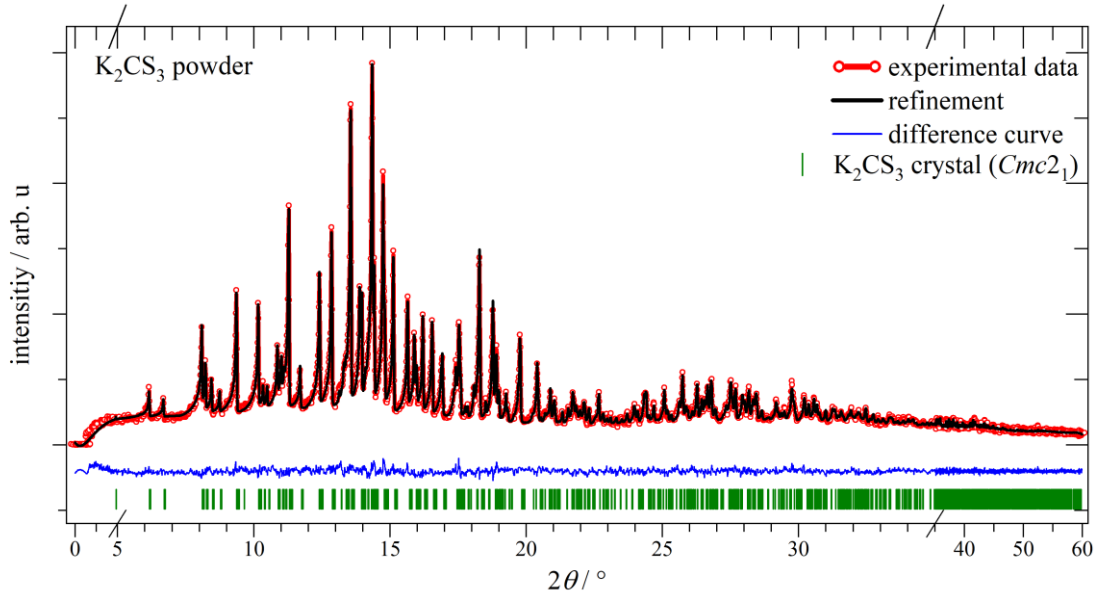

Figure 2.16: Simple RIETVELD diagram showing very good agreement (flat blue difference curve) between the experimental diffraction data of K_2CS_3 powder **9** (red) and the calculated curve (black) as a refinement of the experimental data with the single crystal information of K_2CS_3 **12**.

Potassium trithiocarbonate hydrate $K_2CS_3 \cdot H_2O$

In addition to the newly discovered structure of K_2CS_3, the crystal structure of potassium trithiocarbonate monohydrate, $K_2CS_3 \cdot H_2O$ **10** was (re-)determined from the SC-XRD data, too. A photo of the crystallites suitable for the measurement is found in figure 2.17. They were obtained from a batch of *K_2CS_3* which had been used for different purposes and thus exposed to moisture form atmosphere frequently. On the other hand, it is possible, that the powder has not been dried to the full extent in the first place after precipitation.

Crystal data of $K_2CS_3 \cdot H_2O$ **10** is available in the ICSD and was confirmed in this work. PHILIPPOT and LINDQVIST described this structure as the first ever to exhibit the free trithiocarbonate anion in an alkali salt.[42] Comparison of the newly collected data with that formerly published (table 2.4) shows marginal changes of the lattice parameters, note that the new structure has transformed the parameter *a* for *c* and vice versa. These can be explained to result from the temperature difference of 143 K during the measurements.

Table 2.4: Unit cell parameters of $K_2CS_3 \cdot H_2O$ **10** determined in this work and as reported by PHILIPPOT and LINDQVIST in 1970.

$K_2CS_3 \cdot H_2O$	this work (**10**)	PHILIPPOT, LINDQVIST, 1970[42]
T / K	150(2)	293
Crystal size / mm^3	0.16 · 0.15 · 0.12	0.48 · 0.16 · 0.16
Habit	pink-orange spheres	orange needles
Crystal system	monoclinic primitive	
Space group (No.)	$P2_1/n$ (no. 14)	
a, b, c / pm	637.78(1), 1689.7(3), 673.5(1)	675.9(5), 1706.6(4), 641.8(2)
β / °	95.09(1)	95.42(4)
V / nm^3	0.7229(2)	0.73700
Z	4	
No. of reflections (R*)	1945 (R_{int} = 0.0508, R_1[all data] = 0.0372)	1166 (0.067)
Device	STOE IPDS 2T	equi-inclination Weissenberg technique
Radiation	Mo k_α	Cu k_α

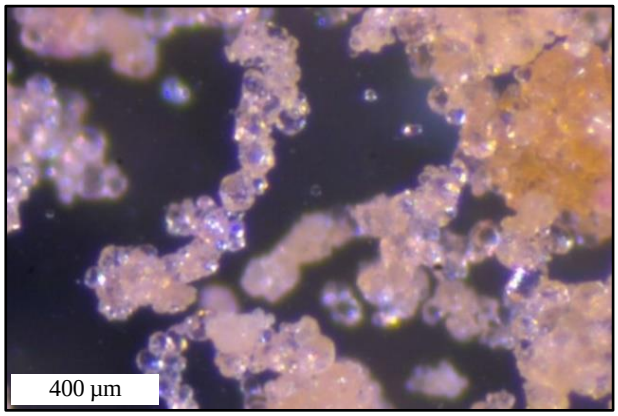

Figure 2.17: Photo of the crystallites of $K_2CS_3 \cdot H_2O$ **10** used for structure determination.

Crystal structure model

In the monoclinic lattice, one trithiocarbonate anion, two potassium cations and an oxygen atom were obtained after analysis of the X-ray structure data. All atoms occupy regular lattice sites 4e. Figure 2.18 and 2.19 depict the unit cell in view along the *a*- and *b*-axis, respectively. In the earlier publication the trithiocarbonate anion present in this structure was determined with C−S bond lengths of 170.2 to 172.7 pm and S−C−S angles of 120° within the range standard uncertainties. The same is found in this reinvestigation with the values given in the caption of figure 2.18.

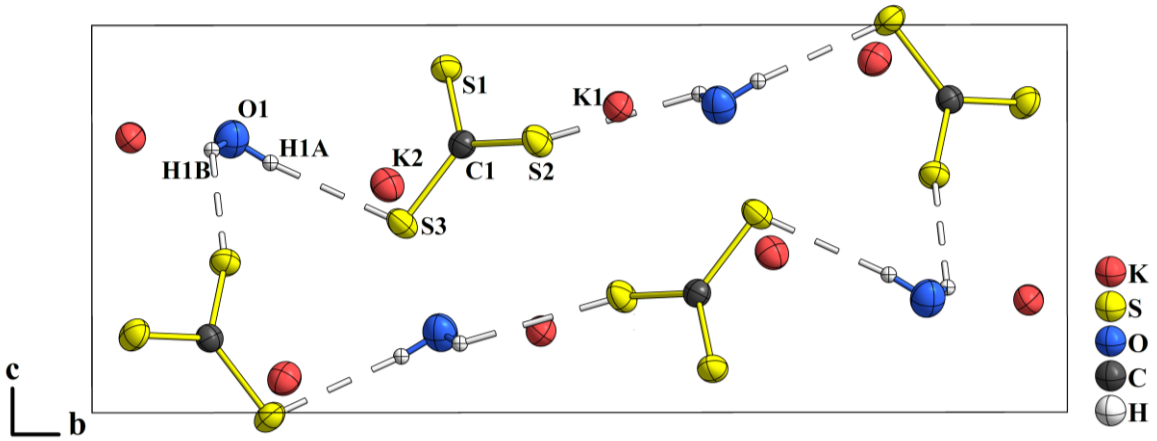

Figure 2.18: Unit cell of $K_2CS_3 \cdot H_2O$ **10** in the direction of the crystallographic *a*-axis. Considering the S···O distances, the indicated hydrogen bonds (dashed) can be classified weak. The C–S distances of the CS_3^{2-} anion are 172.3(1) (S1), 171.1(2) (S2) and 172.2(2) (S3) pm. All non-hydrogen atomic displacement ellipsoids are drawn at 70 % probability.

It can be confirmed that there are no hydrogen bonds between the water molecules of crystallisation. Moreover, they are arranged alternatively between the trithiocarbonate anions, most probably connected *via* the drawn O–H···S hydrogen bonds. The hydrogen atoms were added fixed to the residual electron density at the oxygen atom and afterwards they were refined freely, resulting in the distances and orientations as given. Their occupancy was fixed at 1. It is reasonable to draw simple O–H···S hydrogen bonds to emphasise the hydrophilic nature of alkali thiocarbonates. However, as X-ray structure data is in principle not suitable to exactly locate hydrogen in solid structures, the O···S distances (not drawn) can be stressed with more weighing. They are about 330 to 340 pm and, agreeing with STEINER, who suggested a geometrical ranking routine, can be assumed to include a weak hydrogen bonding only, amongst others considering the acceptor···donor distance.[38] As it was possible to dispose the water of crystallisation from $K_2CS_3 \cdot H_2O$ to obtain K_2CS_3 (cf. above), the weak hydrogen bonding is explained.

The potassium ions arrange roughly inside a diagonal plane perpendicular to the *b*-plane as seen in figure 2.19 . K1 and K2 are six- and seven-fold coordinated by sulfur donors, forming an ionic network. Additionally, the cations possess a shorter K–O distance, giving rise to the assumption of dipole interaction. These findings do not differ from those found in the reference.

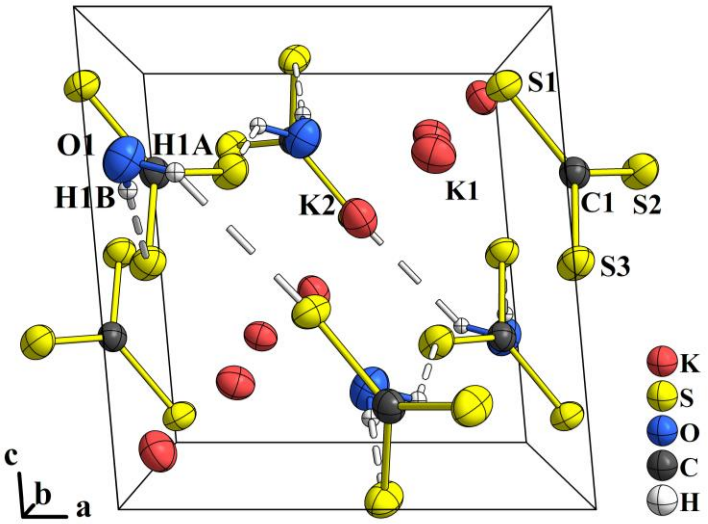

Figure 2.19: View along the *b*-axis of the unit cell of $K_2CS_3 \cdot H_2O$ **10**. All non-hydrogen atomic displacement ellipsoids are drawn at 70 % probability.

X-ray powder diffraction

Indeed, the crystals were obtained from a powder of K_2CS_3 that has not been stored under inert conditions and was prepared almost one whole year before. The PXRD data, collected shortly after the preparation, was analysed with respect to the probability, that the powder might not have been completely dried. Thus, as shown in figure 2.20 the diffractogram was successively fit with a phase mix of anhydrous and monohydrate K_2CS_3.

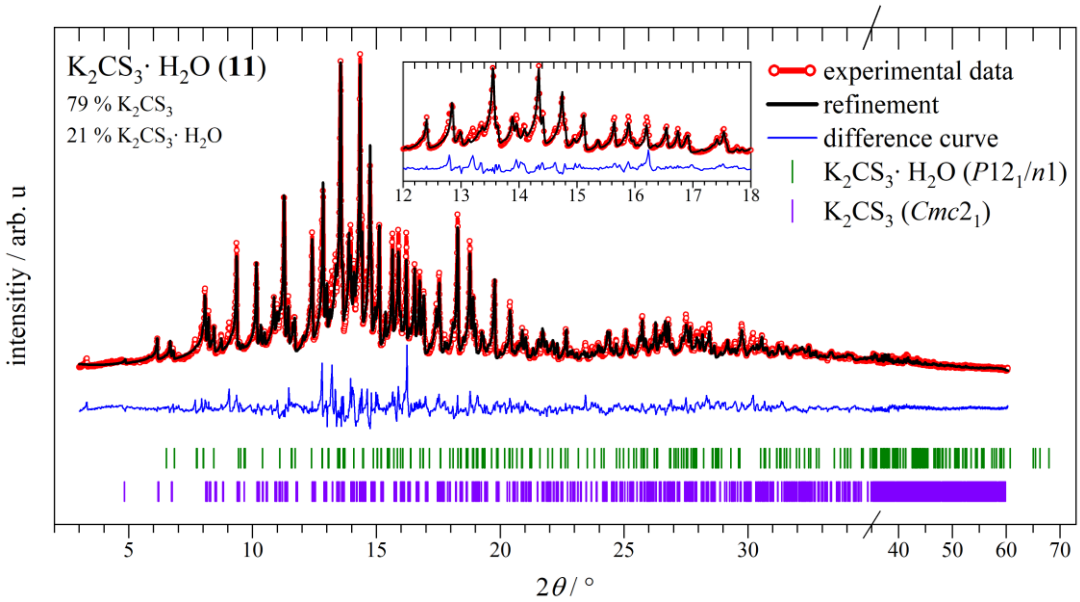

Figure 2.20: Experimental data and RIETVELD refinement of $K_2CS_3 \cdot H_2O$ powder **11**. Some small intensities do not fit well, as clearly described by the inconstancy of the blue difference line (see inset). However, the overall refinement based on the two main phases as given in the top left corner shows decent match of the data.

Potassium perthiocarbonate $K_2[CS_2(S_2)]$

Indeed, the crystal structure of anhydrous $K_2[CS_2(S_2)]$ **29** is the first to describe a solvent free perthiocarbonate. It was obtained from a solvothermal reaction of CS_2 with commercial *sulfurated potash*, German "Schwefelleber", which comes in brownish yellow lumps consisting mainly of K_2S (< 50 %). Repeatedly, single crystals of $K_2[CS_2(S_2)]$ were grown inside glass ampoules during the cool-down after the treatment at elevated temperatures. Figure 2.21 shows a microscope photograph of the grown crystallites that were usable for single crystal data collection.

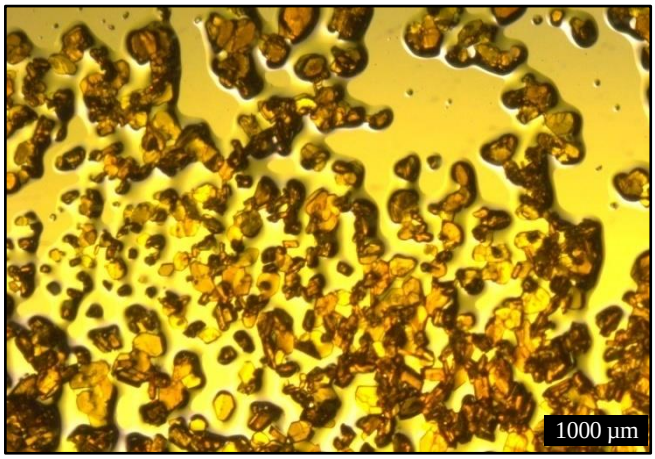

Figure 2.21: Crystals of $K_2[CS_2(S_2)]$ **29** grown on the ampoule wall. The yellow background stems from the excess liquid reactants.

No entries for $K_2[CS_2(S_2)]$ or its solvated derivatives are contained in the PDF-2 database and from the review of GATTOW and BEHRENDT, it is taken, that the compound has been prepared free of solvate molecules and investigated with X-ray methods before according an original reference published in 1974. Again no more details could be extracted as said reference could not be accessed and the review does not give any crystallographic details.[1,43]

Crystal structure model

Potassium perthiocarbonate $K_2[CS_2(S_2)]$ **29** crystallised in the monoclinic crystal system. Four formula units are distributed in the unit cell obeying the space group $P2_1/n$ (no. 14). All atoms occupy the regular site (4e) inheriting none of the symmetry elements found in the space group. Five non-equivalent potassium cations and three non-equivalent perthiocarbonate anions are determined. Neutrality in charge is maintained, as one of the $CS_2(S_2)^{2-}$ molecules was solved with a disorder of inversion. In figure 2.22 the unit cell in

view along the special *b*-axis is depicted, which gives a comprehensive overview of the atomic arrangement.

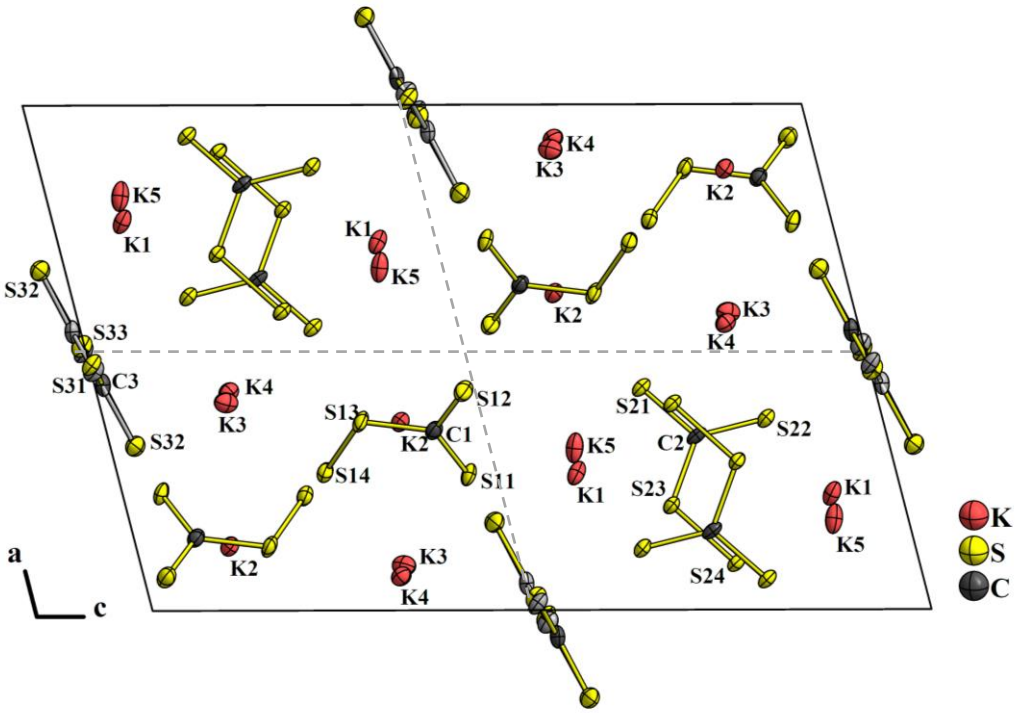

Figure 2.22: Depiction of the extended unit cell of $K_2[CS_2(S_2)]$ **29** in view along the *b*-axis. All atom ellipsoids are drawn with 70 % probability. The disordered $CS_2(S_2)^{2-}$ anion in the point of inversion centring *a*- and *c*-plane is shown with grey atoms, indicating the partial occupation.

The two-fold screw axes run in parallel with the *b*-axis and is located in the centres of the four areas separated by the dashed lines in figure 2.22. The lines also mark points of inversion at the centre of the cell edge, the cell corners and the centre of the unit cell.
The different perthiocarbonate anions labelled in the picture add up to twenty negative charges per unit cell: eight of those are contributed by four C1 anions; eight more negative charges are added by the C2 anions, and as the distorted C3 anion is located on both the cell edge and plane centre, it adds four negative charges. All potassium cations are located inside the cell and are counted plus one positive charge each, giving a total of twenty to achieve neutrality in the unit cell.
The distorted perthiocarbonate anion (C3 anion) is depicted for close examination in figure 2.23. It is disordered by the point of inversion occurring in the *a*- and *c*-plane centres.

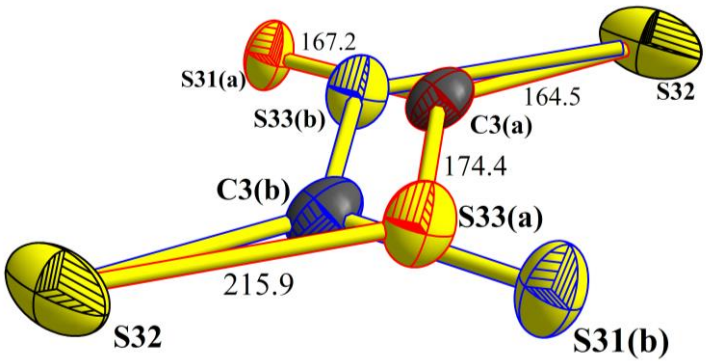

Figure 2.23: Disorder of the perthiocarbonate anion in $K_2[CS_2(S_2)]$ **29**. The numbers give the atomic distances in pm. All atomic displacement ellipsoids are drawn at 70 % probability.

The atoms C3, S31 and S33 are refined with a site occupation of ½. By the centre of inversion two orientations of the perthiocarbonate anion are possible, which are drawn with red (a) and blue (b) borders in the figure, respectively. Note, that S32 is coloured with the default border colour black, because it accounts to an occupancy of 1 and describes two different sulfur atoms. Crystallographically, the site named S32 unifies these chemically different atoms either bound to the C3 atom or to S33. This means, that drawing the anion in either one of the disordered orientations, the atom named S32 applies twice, namely as a thiocarbonyl sulfur and the terminal sulfur of disulfide. Indication that the position of S32 may be better described split into two very close but non-equivalent sulfur atoms (e.g., S32(a) and S32(b)) of only ½ occupancy is seen in the larger displacement ellipsoid compared to the other sulfur atoms. This is supported in consideration of the core distances to the covalent bonding partners C3 and S33, which is lower (164.5(7) pm) and higher (215.9(2) pm) compared to the non-disordered perthiocarbonate anions in the structure, respectively. Another way to decrease the size of the ellipsoid of S32 would be to assign it only ½ occupancy as well, resulting in a disordered trithiocarbonate anion instead. From a chemical view, the assumption of both tri- and perthiocarbonate anions to crystallise with potassium can neither be negated nor approved, because the precursor used in the reaction was mixed phase potassium sulfide, consisting of K_2S mostly. The monosulfide was proven to give K_2CS_3 upon treatment with CS_2 under solvothermal conditions (cf. above), thus a parallel formation of CS_3^{2-} and $CS_2(S_2)^{2-}$ can be assumed in first approximation. However, the data refinement residuals (cf. appendix table 5.3) increase dramatically when S32 becomes only half occupied and the displacement ellipsoids of S32 and C3 collapse to be *non positive definte*, simply meaning the thickness of the ellipsoids becoming negative, which is nonphysical. This justified to conclude the structure model with a 50 % inversion

disorder on the C3 perthiocarbonate anion and with the sulfur atom site S32 to be doubly present in each of the orientations.

All anions naturally stand in ionic interaction with the potassium cations. Recalling equation 1.9 on page 6, the two negative charges on the perthiocarbonate anion should reside majorly at the terminal sulfur atom of the disulfide group and delocalised between the 1,1-dithiocarbonyl sulfur atoms. Mono- and bidentate coordination of the cations is observed (cf. figure 2.24a and b as well as figure 2.25). As the electric charges are unlikely to reside at the bridging persulfide atom, the ionic interaction with cations, thus is considered weaker.

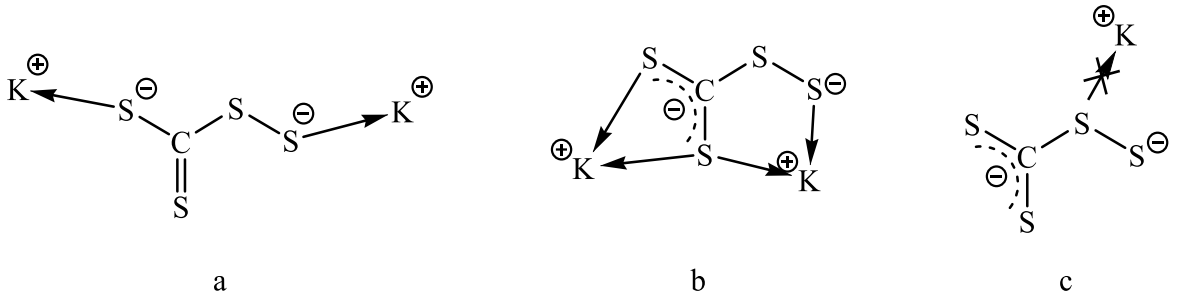

a b c

Figure 2.24: Coordination schemes of the perthiocarbonate anion on potassium cations.

Not exceeding 400 pm, the ions are in range with a number of seven (K2), eight (K1, K4) or nine (K3, K5) sulfur donors. Participation in ionic interaction of the bridging persulfide atoms S13, S23 and S33 as described in figure 2.24c was neglected for simplicity. (Still it is drawn as an orange contact in figure 2.25.) Depending on the orientation of the disordered $CS_2(S_2)^{2-}$ ion, the potassium ions are coordinated with six to seven (K1, K4, K5), seven (K2) or seven to eight (K3) sulfur atoms. Thus, the limits are given with the disordered sulfur atoms either counted one, or zero.

for instance as shown in figure 2.25, K1 is coordinated by three chelate donors and one monodentate perthiocarbonate anion (cf. figure 2.24b and a, respectively), where one chelate is the disordered $CS_2(S_2)^{2-}$ ion. For both orientations two attractive ionic interaction contacts can be observed, one being undisputed as it is the S32 atom and should carry a negative charge for ionic interaction either way.

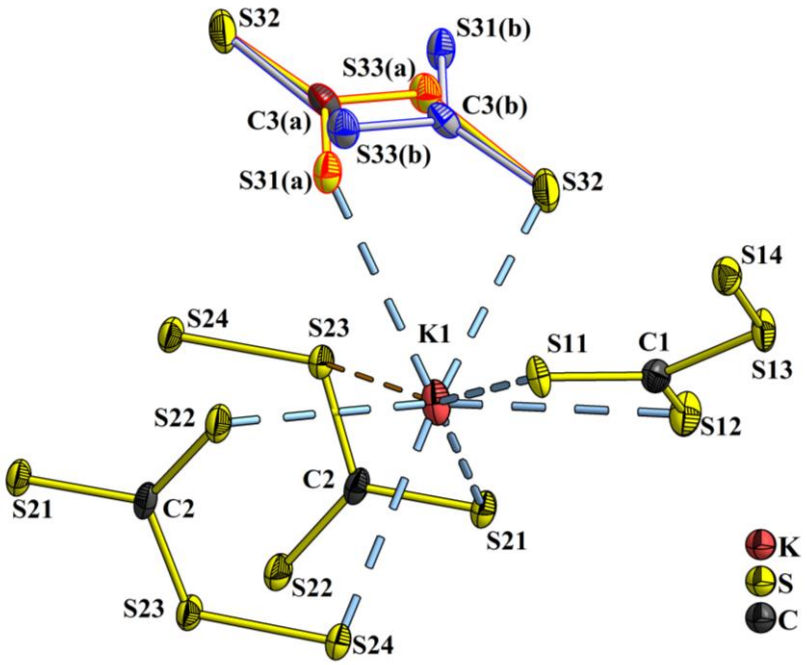

Figure 2.25: Coordination situation on the K1 site in the crystal structure of $K_2[CS_2(S_2)]$ **29**. The dashed K−S contacts indicate ionic interaction.

The second connection of K1 with that disordered anion is either K1−S31(a) or K1−S33(b), with 342.7(1) or 376.0(2) pm distance, respectively. The second negative charge of the anion, delocalised *via* the π-electron system is oscillating between S31 and S32, confirming S31 able to interact with the COULOMB field of K1. S33, in turn is the bridging sulfide, i.e., the persulfide, where the electronic charge density is unlikely to reside, minoring the strength of ionic bonding interaction with K1. Thus, two of six ionic interactions of K1 with near sulfur donors, namely those of the disordered anion should at least be considered less exactly or less accurately described. Similar coordination considerations can be guessed for K3, K4 and K5. Only K2 happens to have no interaction with the disordered perthiocarbonate anion.

The non-disordered perthiocarbonate anions are generally of the same geometry as seen in the crystal structure of $Na_2[CS_2(S_2)]$ **28** (cf. above). However, in the sodium compound the anions are lying in a mirror plane, which is not the case in the structure of K_2CS_3 **29**. This allows to inspect the nature of their geometry uncoupled from symmetry elements present in the crystal lattice.

Potassium trithiocarbonate chloride hydrate $K_7(CS_3)_3Cl \cdot H_2O$

The crystal structure of $K_7(CS_3)_3Cl \cdot H_2O$ **14**, a new compound, is part of this work. It was obtained as a crystalline side product with one molecule of water, possibly coming from *wet* ethanol, from the solvothermal reaction of K_2CS_3 9 with $CoCl_2$ as described in the idealised equation 2.1. The obtained cobalt complex will be discussed in subsection 2.6.1.

$$CoCl_2 \xrightarrow[\text{ethanol, 100 °C, 6d}\\ \text{sealed ampoule}]{K_2CS_3} K_7(CS_3)_3Cl + K_5[Co(CS_3)_3]CS_3 \qquad 2.1$$

As the products of the reaction were investigated with SC-XRD, and the collected data solved, the compound was identified unknown to the literature.

Intermixing of chloride anions in anionic thio-carbon compounds has not often been reported. In 1974 STEPHENSON et al. described new thiocarbonyl complexes of ruthenium ($[Ph_3P]_2RuCl_x(CS)_y$], where x/y = 4/2 or 5/1, Ph = phenyl). It can be learned that in these compounds, ruthenium chloride moieties are incorporated, which are coordinated with additional CS ligands. A rhodium *O*-ethyl xanthate complex ($[Me_2PPh]RhCl_2(S_2COR)$) with additional chloride ions has been reported by COLE-HAMILTON and STEPHENSON in the same year. Crystal structure models of these do not exist to date.[44]

Crystal structure model

The thiocarbonate chloride hydrate double salt crystallised in a primitive orthorhombic lattice with two formula units per unit cell. The structure is set up with space group *Pmmn* (No. 59(b)) with the cell origin at a centre of inversion ($\bar{1}$) and the structure model bares a 50% disorder of one of the trithiocarbonate anions, centred with C1. In figure 2.26 the disorder is displayed in the unit cell, drawn in grey. The water molecule of crystallisation, i.e., the oxygen atom suffers from a disorder of 50 %, too. Calculation for display of the hydrogen atoms was thus abandoned, as their localisation is anyway not precise by means of X-ray structure analysis.

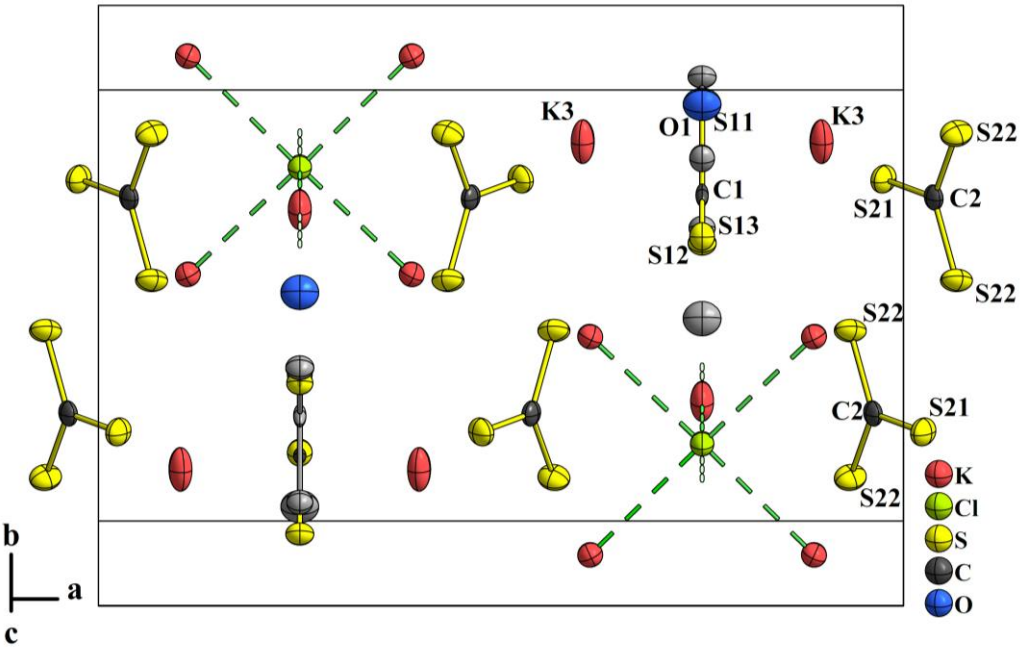

Figure 2.26: Unit cell display of $K_7(CS_3)_3Cl \cdot H_2O$ **14** in tilted view along the *c*-axis. Displacement ellipsoids are drawn at 70% probability.

Actually, O1 lies close to the disordered S13 atom, suggesting a S13−O1 bond of 175 pm distance, resulting in a $S_2C(SO)$ anion, i.e., a *1,1-dithioperthiooxocarbonate* (that was never reported so far). This option was abandoned, as under the applied reaction conditions, the formation of sulfur monoxide is very doubtful. In consideration of oxygen impending the reaction, more reasonable products would have been $S_2O_3^{2-}$, CS_2, and CO_2.[5] Thus, the O1 atom should stem from a water molecule, occupying the far position from the disordered trithiocarbonate anion, providing enough distance of > 315 pm, which cannot be mistaken for a covalent bond. The situation is graphically described in figure 2.27, where the disorder is demonstrated in a closer display. In other words, the red S13(a)−O1 bond can be considered unstable, thus it is assumed, that the disorder is fashioned in either one of the orientations using the far S···O distance, drawn as a dashed connection. The origin of water of crystallisation remained unclear, but as seen above, K_2CS_3 is hygroscopic, and a subtle amount of water could have been introduced by a partial amount of $K_2CS_3 \cdot H_2O$ in the powder. Furthermore, as a solvent, absolute ethanol was used as purchased and could have incorporated water from the atmosphere over time.

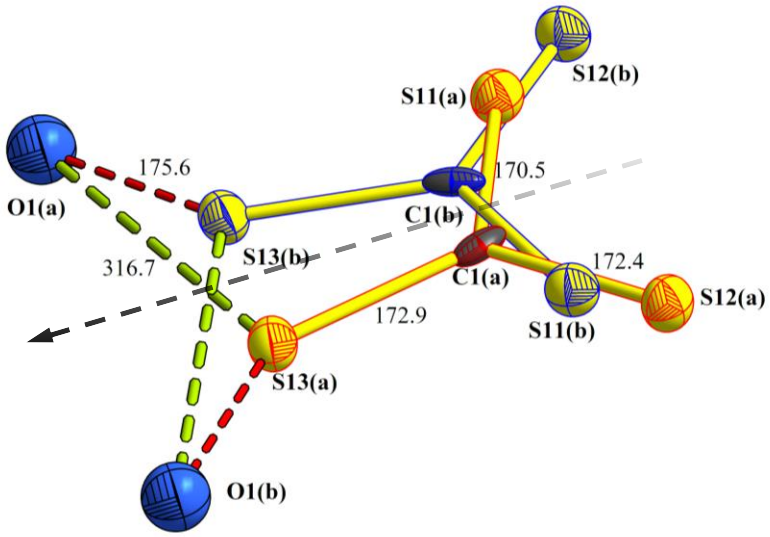

Figure 2.27: Demonstration of the disordered trithiocarbonate anion in the structure model of **14** centred by the two-fold rotation axis (black arrow). All atoms are displayed with a chemical occupancy of 50 %. The distance of S13···O1 must not be mistaken as a bond (red dashed). The green dashed line is of reasonable distance to conclude a water molecule of crystallisation. The numbers give atomic distances in pm.

The disordered atoms C1, S11, S12, S13 and O1 occupy the lattice position 4e, which is a site in the mirror plane perpendicular to the *a*-axis, i.e., the triangular plane of the C1 trithiocarbonate anion lies in the mirror plane, thus obtaining C_s point symmetry. The disorder can be described to stem from the two-fold axis located very close to the C1 atom, which is nevertheless shifted from the ideal two-fold axis position. The intersection of the two perpendicular mirror planes present in the space group *Pmmn*, defines that two-fold axis.

Alternating, the asymmetric area below and above the disordered anion and water molecule of crystallisation, the atoms K1 and Cl1 occupy the lattice site 2b, which exhibits the highest symmetry (*mm*2), as it contains all symmetry operations of the space group. Due to their ionisation, they indeed meet the same electron configuration of argon. With the K2 cation, residing in the regular site 8g, K1 and Cl1 form the motif of rock salt as a chain of K_6Cl octahedra translating the crystal one-dimensionally. The atoms K2 build up symmetric square planes not ideally centred by the chloride ion (distance Cl1 form square plane centre: 15.5(1) pm). This is as there is no mirror plane perpendicular to the *c*-axis, i.e., the axis of the one-dimensional K_6Cl chain. The rock salt like motif is demonstrated in figure 2.28.

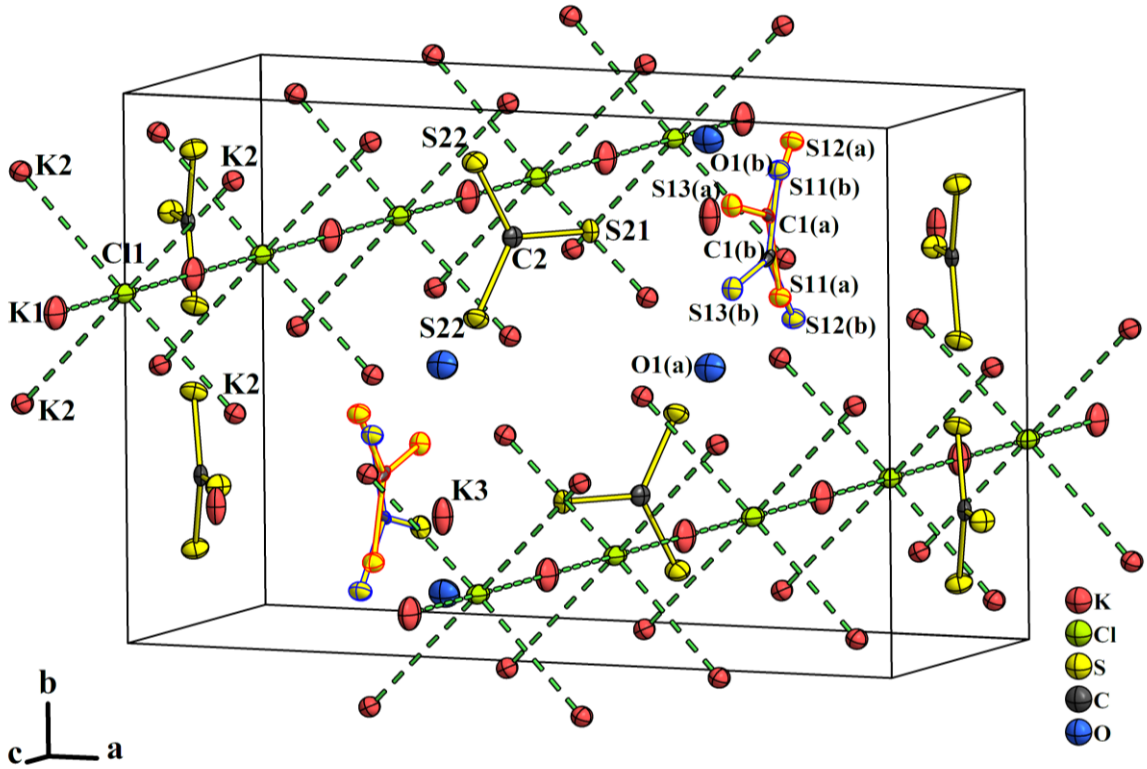

Figure 2.28: Depiction of the unit cell from side perspective, emphasising the unbroken rock salt K_6Cl chain extended along the two-fold axis in *c*-direction. The disordered C1 trithiocarbonate anions are again colour coded, with 50 % occupancy each.

In the structure of KCl, the ions are at a perfectly symmetric distance of K−Cl = 314.5 pm[vii], which almost reproduced in the structure of $K_7(CS_3)_3Cl \cdot H_2O$ **14**, with K1−Cl1 and K2−Cl1 of 319.4(2) and 313.30(5) pm, respectively. The divergence from the cubic structure indeed demands to use the term 'rock salt like' for description, as the K_6Cl octahedra are elongated along the two-fold axis, i.e., the ···K1−Cl1−K1··· row.

K3 lies in site 4f, the mirror plane perpendicular to the *b*-direction that also includes the atoms C2 and S21. The regular sited S22 atom attached to C2 is thus translated by the mirror symmetry. The ordered trithiocarbonate anion obtains C_{2v} symmetry with the C2−S21 bond being the two-fold axis of symmetry.

The interaction between the different species in the structure is considered of ionic type. The potassium cations K1 and K2 stabilise the Cl^- anion but also stand in attractive interaction with the negatively charged sulfur atoms, which is shown in figure 2.29, where the ionic K−S bonds are drawn limited to a distance below 400 pm (cf. K_2CS_3). The coordination is affected by the disorder, expressed by either a dipole interaction with the

[vii] KCl, ionic distance, ICSD entry 18014[45].

O1 atom or a sulfur coordination, valuing between 295.6 pm (O1−K2) and 377.1 pm (S12−K1). Leaving one K1 ion desolated with zero sulfur connections from one disordered anion affects the design of the next nearest cation K1'. Those interactive atomic distances were for simplicity counted half only. For K2, again depending on the orientation, either O1 and S12 or S13 and S11 offer close interaction distances.

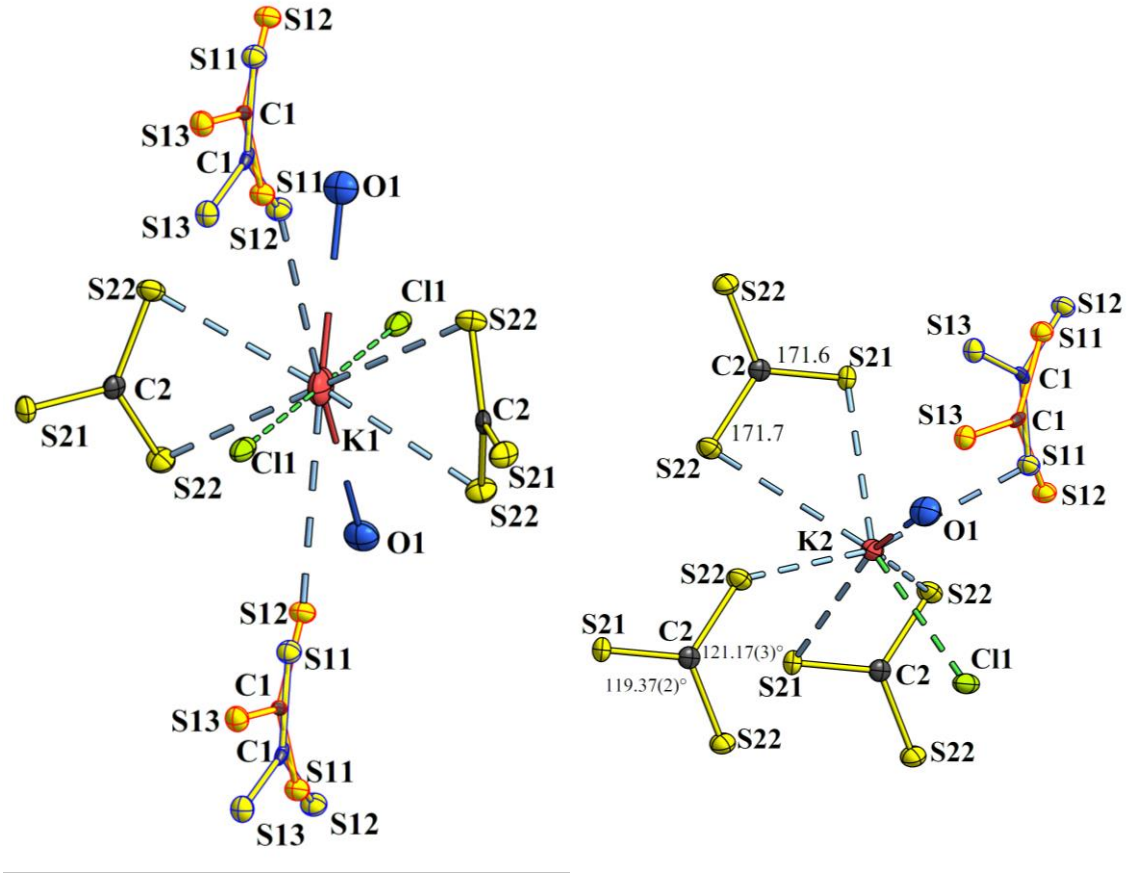

Figure 2.29: Arrangement of ionic and dipole interaction with the cations K1 and K2 in the structure of $K_7(CS_3)_3Cl \cdot H_2O$ **14** on the left and right, respectively. Anionic sulfur donor and chloride connection is drawn in dashed blue and green, while the dipole interaction with O1 is drawn as a two-coloured broken bond. The numbers given additionally on the right are bond lengths in pm and angles in ° of the ordered trithiocarbonate anion.

The ordered trithiocarbonate anion acts as a chelate ligand in symmetry equivalent distances of 328.4 pm (S22−K1) or mixed distances of 326.7 (S21−K2) and 350.0 pm (S22−K2). In total, K1 can be assigned with eight and K2 with seven heterogenous ionic (S, Cl) and/or dipole (O) interactions.

The mirror sited cation K3 has no interaction with Cl1 and belongs to the trithiocarbonate sub-structure. The cation is drawn in connection with the nearest groups in figure 2.30. It is six-fold surrounded by trithiocarbonate anions. In the mirror plane, from one side two disordered CS_3^{2-} moieties are in close range, offering a variable number and type of

connection partners depending on the local orientation. The mean value of two interactions (4·½) is counted, ranging between 321.9 (S12−K3) and 338.9 pm (O1−K3). In the mirror plane, two ordered trithiocarbonates cover the room opposite the disordered groups. One of them performs a tridentate coordination, the trigonal anion plane oriented almost perpendicularly to the virtual C2−K3 axis of 309.3 pm distance. The other anion offers a monodentate ionic K3−S21 interaction.

Finally, from top and bottom of the mirror plane, two more monodentate K−S bonds are found. In total K3 is coordinated by eight atoms with either ionic (S) or dipole interaction (O).

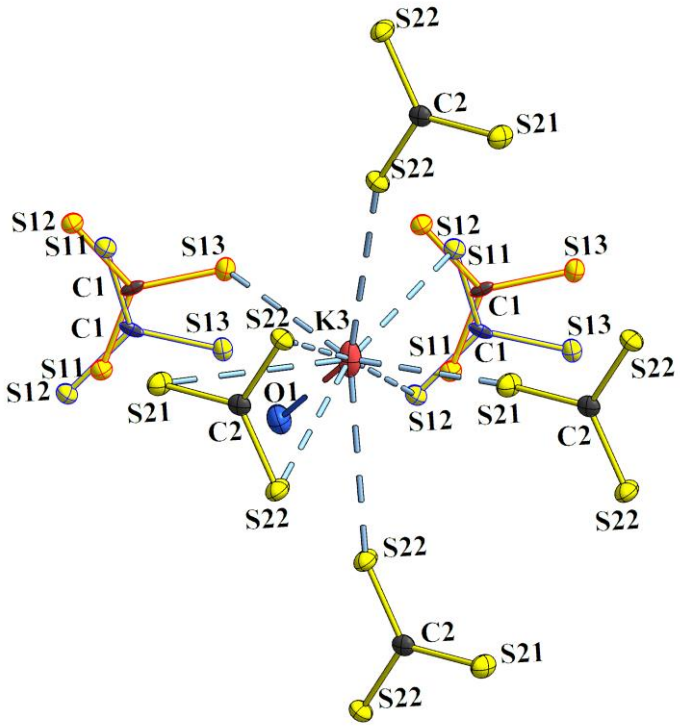

Figure 2.30: Depiction of the potassium trithiocarbonate sub-structure in the crystal structure of $K_7(CS_3)_3Cl \cdot H_2O$ **14**. The cation K3 connects only with trithiocarbonate anions by ionic interaction, drawn as blue dashed lines. One dipole interaction with the water molecule is probable.

It can finally be noticed that like in the structure of K_2CS_3, the geometry of the ordered CS_3^{2-} anions comprises all C−S bonds larger than 170 pm. Usually, one can expect one C−S bond to be decreased with some significance, proposing the favoured location of the double bond. In other words, in the solid-state, due to the site effect the geometry of the trigonal shaped anions should be influenced. However, as seen above no clear signs of such symmetry lowering effects were observed.

Potassium perselenodithiocarbonate trithiocarbonate hydrate $K_5[CS_2(Se_2)]_{1.5}(CS_3) \cdot H_2O$

No crystal structures are known when sulfur is substituted by selenium on the thiocarbonate anion. On analogous routs as shown in the equations 1.7 - 1.9 on page 6, selenides or hydrogen selenides can be converted to triselenocarbonates with CSe_2. Mixing selenides with CS_2, gives the interchalcogencarbonates CS_2Se^{2-} or $CSSe_2^{2-}$. In the 1960s different compounds belonging to this group have been prepared and investigated by means of their vibrational properties.[46] The conjugated dithiomonoselenocarbonic acid SC(SeH)(SH) is only known in its asymmetric state with one sulfur and the selenium atom to be protonated, i.e., the double bond favours to be situated between carbon and the other sulfur atom. Upon alkylation the both the symmetric and asymmetric ester can be obtained.[19] Monothiodiselenocarbonic acid $SC(SeH)_2$ is to the present unknown. In turn, some work on triselenocarbonic acid $SeC(SeH)_2$ characterising its dissociation, pH-value, decomposition in aqueous solution, conduction and size of the CSe_3^{2-} ion has been reported.[47]

Like the related trithiocarbonic acid, the dithomonoseleno and triselenocarbonic acids have been prepared by protonation of the anion in a suspension of the barium salt with hydrochloric acid. The preparation of triselenocarbonic acid was found to demand a certain degree of moisture, as in dry ether $BaCSe_3$ did not react upon treatment with HCl. Triselenocarbonic acid could thus be obtained below −10 °C as a dark red grease.[48]

Knowledge on the derived salts is limited to the dark violett $BaCSe_3$ and K_2CSe_3, as well as orange $Ba(CS_2Se)$ and orange-red $K_2(CS_2Se)$.[1,49] $BaCSe_3$was reported to be a stable compound that dissolves without decomposition in O_2-free water giving a green solution, in turn organic solvents except formamide afford decomposition.[48]

Herein the solvothermal reaction of CS_2 and K_2Se was carried out to find out if in analogy of the crystallisation of K_2CS_3 **12** (cf. above), the formation of CS_2Se^{2-} occurs. As stated, the aimed compound K_2CS_2Se was earlier reported by SEIDEL to be of orange-red colour, very hygroscopic and pronounced sensitive to oxidation.[49] It was prepared in analogy of the more investigated barium compound, which forms after reaction of BaSe or $Ba(SeH)_2$ with CS_2, but using ethanol as solvent.

Under solvothermal conditions orange-red crystals grew from the reaction mixture and a crystal suitable for SC-XRD, shown on the photograph in figure 2.31, was recovered from the ampoule. The collected data could be solved and identified with the chemical formula $K_5[S_2C(Se_2)]_{1.5}(CS_3) \cdot H_2O$ **15**, which contains the yet unknown perselenodithiocarbonate anion $CS_2(Se_2)^{2-}$.

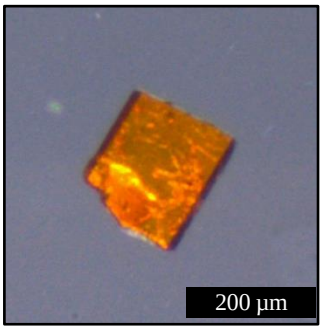

Figure 2.31: Photo of a crystal of $K_5[CS_2(Se_2)]_{1.5}(CS_3) \cdot H_2O$ **15** picked from the ampoule, in which K_2Se **50** was treated with CS_2.

Crystal structure model

The collected data was solved in a centred monoclinic space group *C*2/*c* with four formulas per unit cell. Two perselenodithiocarbonate anions are distinct from one another, as one is disordered by inversion. The disorder was handled by granting an occupation of 50 % of each atom. A tetraselenide anion (double tilted Se_4^{2-} chain) with Se31(a)–Se31(b) connection through the point of inversion was abandoned as an option for this anion site, as the resulting angles would need to be significantly larger than 90°,[13] which is not the case. An additional trithiocarbonate anion yield the best residuals during the refinement. However, it remains vague if the anion might in truth not be a dithiomonoselenocarbonate anion CS_2Se^{2-}, which could be disordered in three ways by rotation around the principal axis, making an absolute structure determination challenging. A µRaman spectrum was recorded of the same red crystals, which were kept sealed in another ampoule. The spectrum and results of this investigation is found in sub-section 2.4.2.

Some electron density was found left near the Se–Se moiety of the $CS_2(Se_2)^{2-}$ anions, that can be explained rising from the large electron density cloud of selenium. Figure 2.32 shows the unit cell in the view along the *b*-axis. In this, the disordered $CS_2(Se_2)^{2-}$ molecule plane is parallel to the viewing direction. A closer look at the elusive dianions is given in figure 2.33, where also the disordered anion is drawn in its two possible orientations (a) and (b) with red and blue borders, respectively.

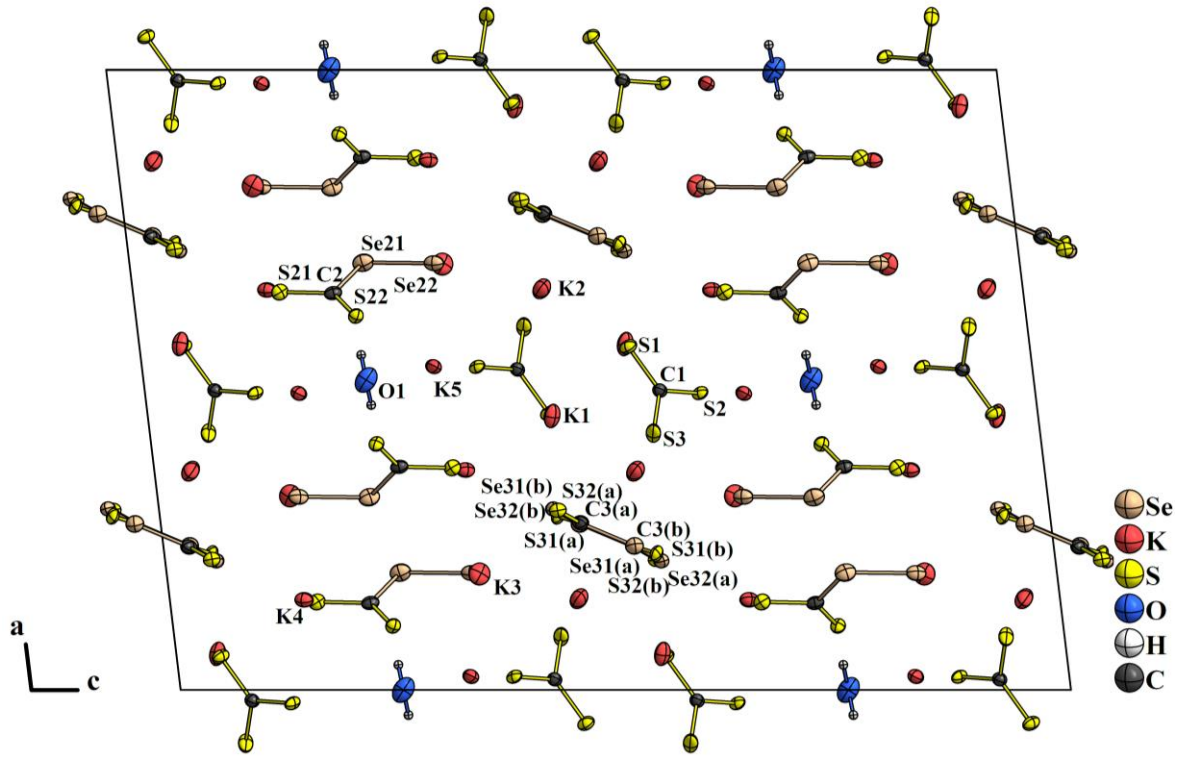

Figure 2.32: Depiction of the unit cell of $K_5[CS_2(Se_2)]_{1.5}(CS_3) \cdot H_2O$ **15**. The disordered $CS_2(Se_2)^{2-}$ ions are centred by points of inversion at ¼ *b* (shifted behind the paper plane). All non-hydrogen atomic displacement ellipsoids are drawn at 70 % probability.

On the perselenodithiocarbonate, the determined atomic distances and angles are of reasonable size. Altogether the geometry of perthiocarbonate is recognised. Likewise, in (HS)(HSe)CS, the double bond seems to have an increased probability at the C2−S22 and C3−S31 connection, for they are slightly decreased in length compared to C2−S21 and C3−S32, respectively. As the perselenide moiety, like in the perthiocarbonate anion (cf. above), is not capable to stabilise a double bond to the carbon atom, the π-electron system is therefore delocalised between the two attached sulfides. The chalcogen atoms arrange angles around the carbon atom that are comparable to those determined on the perthiocarbonate anion. The torsion angle about C−Se is 178.2(1) and 179.3(3)° for the ordered and disordered anion, respectively, allowing to call the anion planar for simplicity. The S−C−S angles are 126.2(3) and 126.0(5)°, which is not significantly increased compared to the related perthiocarbonate in $K_2[CS_2(S_2)]$ **29**. Also, the geometry towards the diselenide moiety substituting the perthio unit is similar, because the angles at the carbon atom are not symmetric with the *cis*-angle larger than the *trans*. The angular distribution can be considered to minimise the repulsion between the lone pairs at each chalcogen atom. The C−S distances are not varied from those seen in the structures without selenium.

The moiety C−Se−Se, with the terminal selenium atom non-bonded to other atoms than the bridging selenium, is unknown to the CSD. However, the determined distances between the atoms of this unit, given in figure 2.33 for the ordered anion in the structure, are within range of comparable structures, featuring bridging Se−Se moieties. For instance the structure of molecule crystals of dimethyl diselenide $(H_3C)_2Se_2$ show C−Se distances of 193.8 and 194.8 pm, and the bridging Se−Se measures 231.0 pm.[50] In selenocyanogen, or diselenium dicyanide $Se_2(CN)_2$, the respective distances are 185.5 and 186.7 pm for C−Se and 235.6 pm for Se−Se. Withdrawal of electron density from the C−Se−Se−C moiety by the cyanide groups, i.e., the nitrogen atoms, explains the shortening of the C−Se bond compared to dimethyl diselenide. It was shown that the C≡N triple bond is not changed upon substitution of selenium with sulfur, but that for the related disulfur compound the respective C−S bond is strengthened, due to an increased resonance probability of the π-electrons giving the $\cdots S^+{=}C{=}N^-$ fragment. At the same time the dichalcogen bond is only weakened slightly.[51] For the discussed structure of the new $CS_2(Se_2)^{2-}$ a strong inductive effect by sulfur, weakening the C−Se bond is not expected, as the electronegativities are only of marginal difference.[52] Due to that, interestingly, the C−Se distances in **15** are closer in agreement with the structure of diselenium dicyanide than dimethyl diselenide. Actually, the Se−Se bond is hardly affected from the moieties it is attached to, for in α-Se the similar distances are ranging between 232.7 and 234.6 pm.[53]

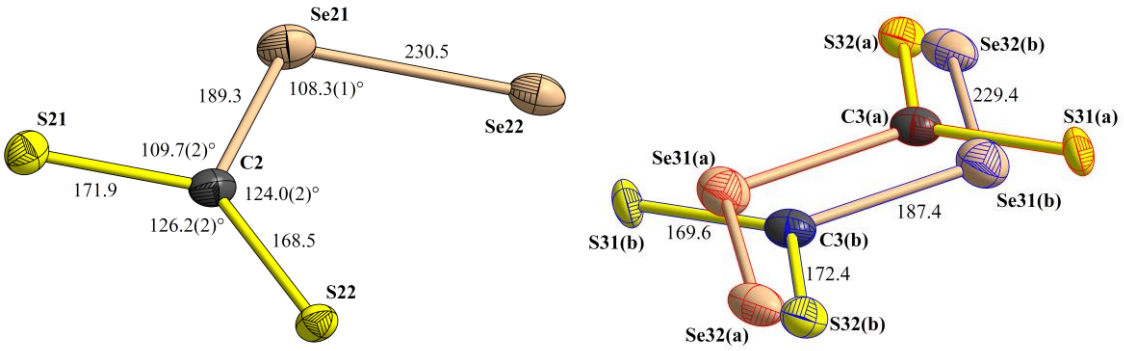

Figure 2.33: Zoomed drawing of the two non-equivalent $CS_2(Se_2)^{2-}$ anions in $K_5[CS_2(Se_2)]_{1.5}(CS_3) \cdot H_2O$ **15**. On the left, the non-disordered molecule anion is shown. On the right, the inversion disordered moiety is shown, solved by the occupation of 50 % of each atom. The numbers give the atomic distances in pm, angles are given in °, except for the disordered molecule. All displacement ellipsoids are drawn at 50 % probability.

The trithiocarbonate anion present in the structure gives rise for discussion. While two of the three C1−S bonds clearly have a reasonable distance of 171.5(4) (S1) and 171.9(4) pm

(S3), comparable with the already described structures, the C1−S2 bond is markedly larger, namely 175.4(4) pm. Of course, this value is much smaller than found for the C−Se single bond in the $CS_2(Se_2)^{2-}$ ion (cf. figure 2.33), but considering CS_3^{2-} to actually comprise a CS_2Se^{2-}, a certain double bond character will also be found at the C−Se bond, manipulating the distance to a lower value. The anisotropic displacement ellipsoid of S2 is moreover clearly smaller compared to S1 and S3, indicating a larger electron density than that of sulfur at the position of S2. These findings indicate one selenium atom to partially (if not totally) occupy one of the sulfur sites of this anion. As already indicated above, there is furthermore no reason for the formation of trithiocarbonate, as there was no sulfide present in the reactants, excluding a doubtful decomposition of CS_2. However, the crude product consisted not only of the crystals giving rise to the discussed structure. Granting the possibility of sulfur or sulfide impurities introduced either by CS_2 or formed upon the reaction on routes not yet clarified, the formation of trithiocarbonate might still occur. Overall, the CS_2Se^{2-} anion could be the true nature of the CS_3^{2-} molecule, since rotating this moiety about its principal three-fold axis, would disguise the position of selenium from the X-ray sensitivity. During the refinement a variety of disorders on the anion, namely partial (split) occupation of sulfur and selenium on all three positions (S1, S2 and S3) or only on sets of two, did not significantly change the refinement statistics. At last, a mixed occupation of the anion site with trithiocarbonate and dithiomonoselenocarbonate, could also not outnumber the residuals obtained by description of the data with CS_3^{2-}. Refinement of a shared S2 occupation with both sulfur and selenium, using the *ShelX* compatible constraint command EXYZ, yield a chemical occupancy ratio of sulfur to selenium of 4.9 to 1. Therefore, it was abandoned to refine selenium in this anion.

The only special site in the unit cell shown in figure 2.32 is occupied by the oxygen atom of the water molecule marking the two-fold axis parallel to *b*. The hydrogen atoms on the water molecule have been fixed by calculation within the *ShelX* program package.

Five non-equivalent potassium cations interact with the trithio- and perselenodithiocarbonates *via* ionic bonds. Dipole-cation interaction can be assumed only between the water molecule of crystallisation and K5, which is in 284.1(4) pm distance, i.e., much shorter than some of the dipole-cation interactions in $K_7(CS_3)_3Cl \cdot H_2O$ **14** (cf. above). The coordination of the $CS_2(Se_2)^{2-}$ and CS_3^{2-} ions by K^+ is depicted in figure 2.34. The atom S21 is pointing towards a pyramidal arrangement of potassium ions (K1, K3, K4 (2x), K5), which caps a primitive cuboid structure of K3, K4 and K5 encapsuling the ordered $CS_2(Se_2)^{2-}$ anion. At the other end of the anion the Se22 atom is similarly surrounded by

five potassium cations (K2, K3 (2x), K4, K5). More centred in the cuboid, the S22 and Se21 atoms stand in interaction with a lower number of cations. Four ionic interactions can be counted for S22, while the bridging Se21 only accounts to three, considering distances below 400 pm only. The latter can be explained, as the negative charge is less stabilised at the bridging Se21 (cf. perthiocarbonate), rising no need to arrange at that site for positively charged ions. Five potassium ions pose the counter charge for S1 below 340 pm, while S2 and S3 are in close range of six cations. Interestingly, S2 being in suspicion for a partial identity of selenium (cf. above) has its ionic contacts from 333.5(1) to 366.3(2) pm, while S3 has its longest distance to a potassium ion to be 331.9(1) pm, i.e., lower than the closest of S2. In cubic K_2Se, the ionic K−Se distance has been determined to value 333 pm.[54] This again poses another argument to assume S2 to partially incorporate selenium.

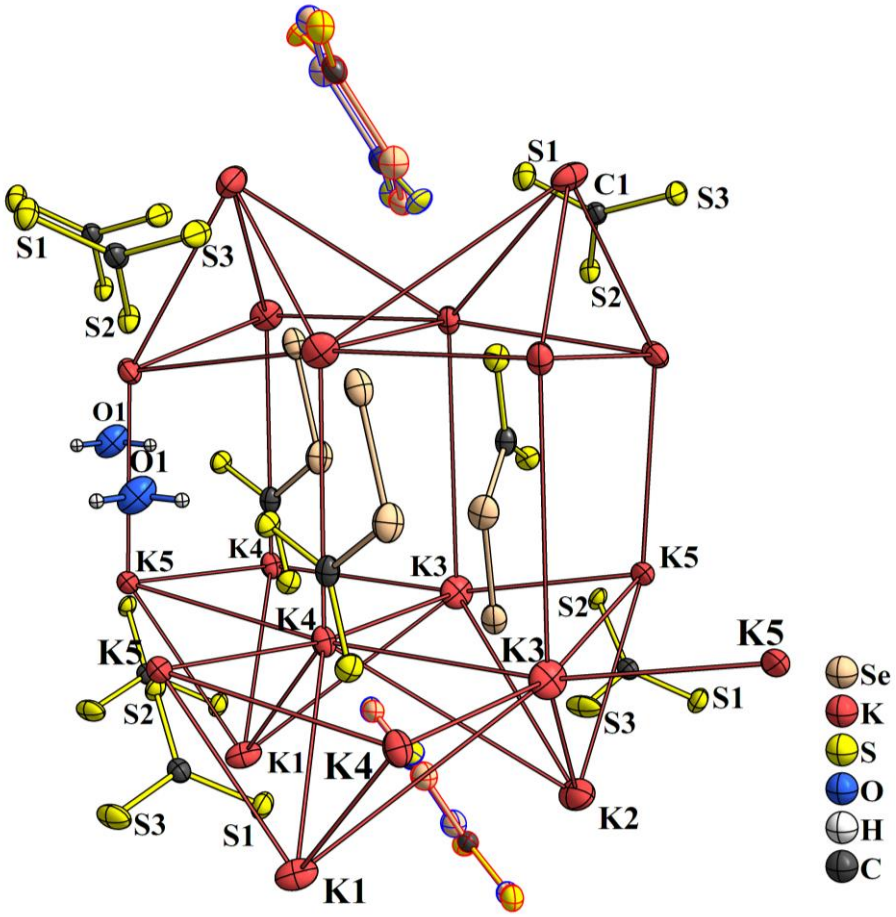

Figure 2.34: Demonstration of the cation framework arranged around $CS_2(Se_2)^{2-}$ (not labelled for clarity) and CS_3^{2-} anions and H_2O of crystallisation in $K_5[CS_2(Se_2)]_{1.5}(CS_3) \cdot H_2O$ **15**.

2.2 Barium trithiocarbonate

Crystallographically, $BaCS_3$ was first investigated by KREBS et al. in 1965[55] but an entry on the crystal structure is missing in the CSD. Back then, the crystals were slowly grown from diluted aqueous barium hydrosulfide solution, stored on CS_2 at RT. The absence of a crystal entry in the database arises most probably from the reason, that the authors could not differentiate one space group only, as the compound was found to crystallise in a chiral space group. They assigned the unit cell with either one of the primitive trigonal space groups $P3_121$ (152) or $P3_221$ (154), or one of the primitive hexagonal groups $P6_1$ (169) or $P6_5$ (170), as they discovered enantiomorphic twinning in their specimens.

A non-available publication on the crystal structure and therefore less convenient for the discussion of $BaCS_3$, by PHILIPPOT et al. is referred to in the review of GATTOW and BEHRENDT.[1,56]. The crystallographic results were found included in the PDF-2, where six *d*-values and assignment of the primitive trigonal space group $P3_112$ (no. 151) is given.

In this work $BaCS_3$ was recrystallised under solvothermal conditions for structure determination from precipitated powder on analogous routes mentioned before. As detailed in the experimental section, the major difference was that instead of ethanol, water was used as a solvent for $Ba(OH)_2$ to overcome the poor solubility in ethanol.

In figure 2.35 microscope photographs of the crystals used for X-ray structure determination are given alongside with a photo of the dried powder of $BaCS_3$.

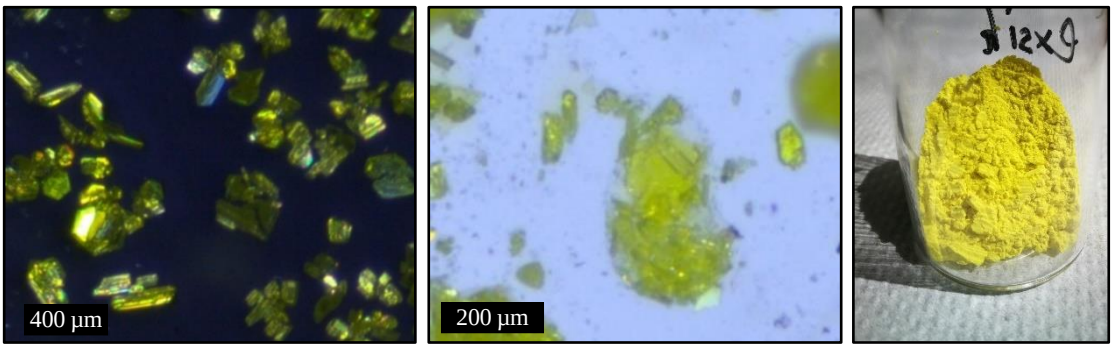

Figure 2.35: Photos of the bright yellow crystals of $BaCS_3$ **27** as obtained on the inside of the ampoule wall (left), and transferred to glass substrate, where the crystals were submerged in inert oil for sorting (middle). On the right: Photo of the fine yellow $BaCS_3$ **26** powder.

Crystal structure model

Essentially, the description by KREBS et al. could not be negated in course of the re-investigation of the crystal structure of $BaCS_3$. However, considering the newly determined

crystal symmetry, for the first time within almost 60 years, the structure is elucidated unambiguously.

A crystal was indexed with a primitive hexagonal lattice using the point groups 6 or 622. Both groups are enantiomorphic and twinning can occur, especially when crystals are grown from solution. However, as grown under solvothermal conditions, a much smaller crystallite was analysed with SC-XRD compared to that in 1965. It is therefore reasonable to assume that by the decreased size a single crystalline domain could be measured. Thus, the pseudo-symmetry 6/*mmm* claimed by KREBS et al., due to their twinned sample, was not offered as a suitable point group for the newly collected data. In short, solving the crystal data a 6_5-axis could be neglected from solving of the crystal data, as the *Flack parameter* close to 1 affirmed a 6_1-axis present in the crystal. It shall be said that the formation of crystals with 6_5-symmetry is not refused, in fact their parallel growth aside the crystals possessing 6_1-symmetry is taken for granted beyond dispute.

One could now understand the system with a higher symmetry or that postulated by the authors named above. With six formulas per unit cell, the chiral space groups $P6_122$ (no. 178) or $P6_1$ (no. 169) were found suitable for the structure model of $BaCS_3$. Essential crystallographic parameters reported by KREBS and co-workers are given in table 2.5 alongside the parameters found by the re-investigation.

Table 2.5: Crystallographic parameters and data of $BaCS_3$ **27** and comparison of residuals of the models in the different space groups. Where applicable reference values taken from KREBS et al. are added.

	$BaCS_3$ **27**, this work		KREBS et al.[55]
Empirical formula	C Ba S3		
Sum formula	$BaCS_3$		
Formula weight	245.53 g mol^{-1}		
Temperature	150(2) K		
Crystal system	primitive hexagonal		trigonal or hexagonal P
$a = b$ / pm	651.79(9)		654 ± 2
c / pm	1969.7(3)		1997 ± 4
c / a	3.022		3.054
V / nm^3	7.247(2)		
Z	6		
ρ_{calc} / g cm^{-3}	3.376		3.30
μ / mm^{-1}	9.321		
X-radiation (nm)	MoKα (λ = 0.071073)		CuKα (λ = 0.15418)
Crystal size / mm^3	0.08x0.08x0.08		0.5x0.1x0.1
Space group (no.)	$P6_122$ (178)	$P6_1$ (169)	$P6_1$ (169) or $P6_5$ (170) $P3_121$ (152) or $P3_221$ (154)
Independent reflections (R_{int}, R_σ)	504 (0.0672, 0.02)	1024 (0.0645, 0.0277)	
R_1 [all data, $I > 2\sigma(I)$]	0.0318, 0.0307	0.0339, 0.0316	
wR_2 [all data, $I > 2\sigma(I)$]	0.0590, 0.0587	0.0548, 0.0542	
Flack parameter	-0.01(3)	-0.01(4)	
Goof on F^2	1.336	1.195	
Largest diff. residual density peak/hole	0.97/-1.12 e/Å^3	1.07/-1.04 e/Å^3	
Colour	bright yellow		luminous yellow
SC-XRD device	*STOE IPDS 2T*		WEISSENBERG film

By looking at the structure model in space group $P6_1$ and compare it with that in $P6_122$ a chemical difference cannot be seen. In fact, increasing the space group symmetry adding two two-fold axes only changes two unambiguous sulfur atoms to become crystallographically equivalent. The atom S2 occupies the general lattice site 12c making it suitable to emphasise the differences of the obtained space group solutions. By different colourisation of the two symmetry-equivalent C−S2 bonds of the trithiocarbonate anion, this is visualised in figure 2.36 and 2.37. The 6_1-screw axis coinciding with the c-axis is thereby emphasised. In the figures the additional symmetries occurring in the space group

$P6_122$ are described by dashed lines. The two-fold axes in the *a*- and *b*-plane are intersecting with the *c*-axis at different positions, namely at 0 and ½ *c* in the *a*-plane and ⅓ and ⅔ *c* in the *b*-plane. The both rotate around the *c*-axis obeying the 6_1 screw-translation in the polar space group. As the refinement residuals do not clearly favour one of the solutions (cf. table 2.5), the higher symmetry was finally chosen. By the description of one less sulfur atom in the asymmetric unit, less parameters are needed to describe the collected data, compared to the model solution in $P6_1$.

If one considers the red and blue coloured S2 atom bonds to be non-equivalent, i.e., non-equivalent sulfur atoms, e.g., S2 and S3, both the two-fold axes symmetry operations were cancelled and the space group $P6_1$ would be obtained. In the consequence of the superior space group symmetry, the atoms Ba1, C1 and S1 occupy the special lattice site 6b, which possesses the symmetry of one of the two-fold axes. Consistently, in the formerly postulated space group $P6_1$ only the general site 6a occurs. Of course, this affords a different site symmetry of the trithiocarbonate ion, which is increased from C_s to C_{2v}, assuming all atoms to be planar. (In the range of uncertainty, the CS_3^{2-} anion is planar in this structure.)

As already mentioned, this symmetry detail is not influencing the chemical properties like e.g., vibration energies of covalent bonds. Therefore, a site effect on the molecular vibration cannot be expected in spectroscopic data, not to mention the influence of the different temperatures on these energies (150 K vs. RT).

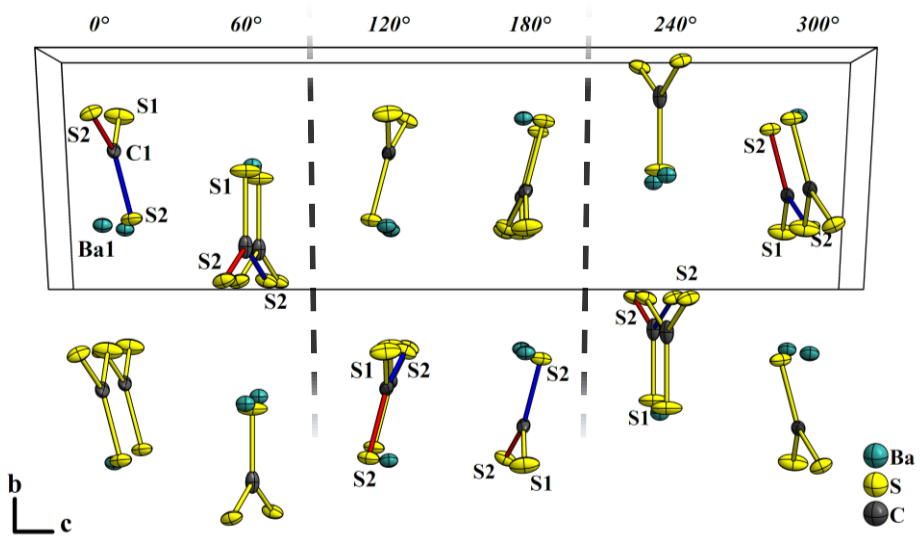

Figure 2.36: Crystal structure model of $BaCS_3$ **27** with perspective view along the *a*-axis. The steps of translation of 1/6 *c* and rotation of 60° by the 6_1-screw axis located in the bottom horizontal line is emphasised by the differently coloured but equivalent C1−S2 bonds. This view shows the two-fold axis, which is parallel to the *b*-plane at ⅓ and ⅔ *c* marked with the dashed lines. The atomic displacement ellipsoids are drawn at 70 % probability.

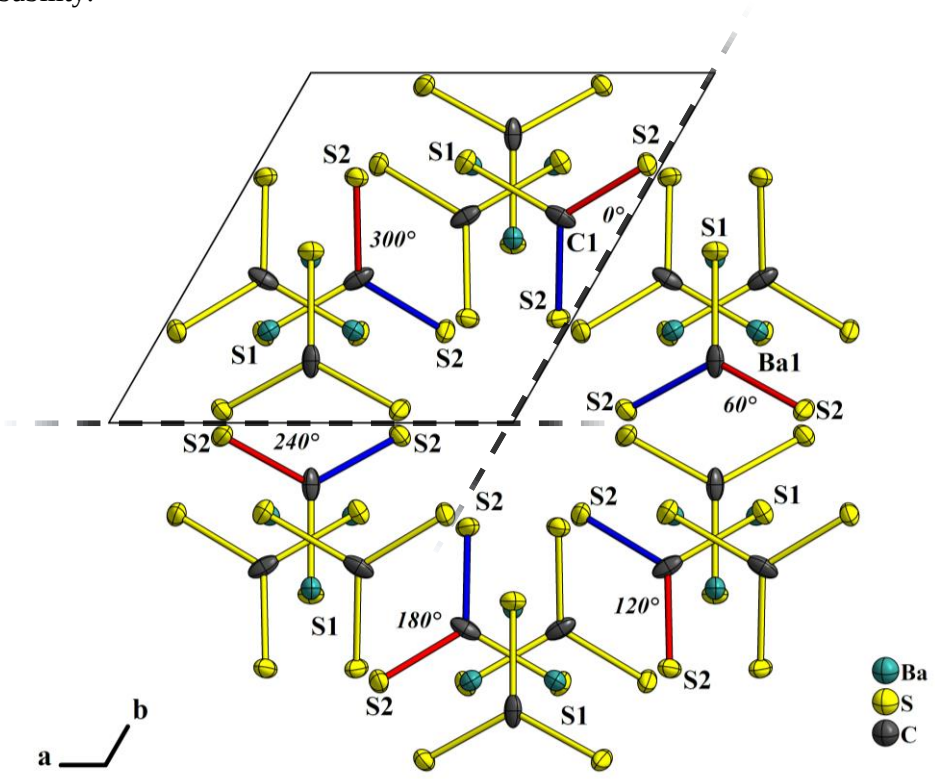

Figure 2.37: View along the 6_1-axis in the structure of $BaCS_3$ **27**. The dashed lines mark the two-fold rotation found in the *a*-axis at 0 *c* and in the *b*-plane at ⅓ *c*.

Like in the crystals of alkali thiocarbonates, in $BaCS_3$ attractive ionic bonding between the Ba^{2+} and CS_3^{2-} ions lead to the formation and stabilisation of the compound. The coordination of the barium cations is depicted in figure 2.38, where the two-fold symmetry axis conserved in the virtual line of S1, C1 and Ba1. Ionic interaction of the carbon atom in nearest distance with barium was neglected for coordination issues, as *true* ionic interaction should only occur between the atoms that carry electric charges.

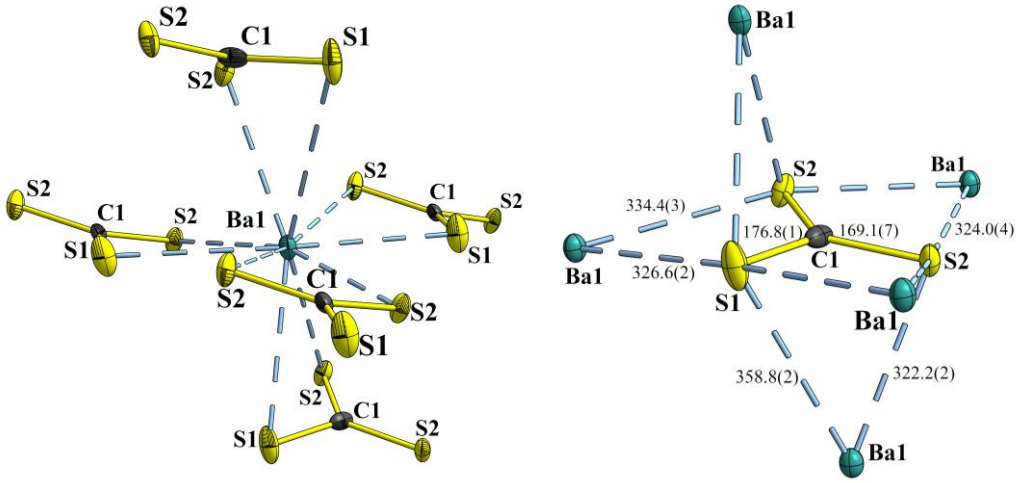

Figure 2.38: Ten-fold coordination by five trithiocarbonate anions of barium, centred in a trigonal bipyramid fashioned polyhedron (left). The trithiocarbonate anion is consistently performing bidentate coordination of the five nearest barium cations (right). The numbers give the bond lengths and atomic distances in pm. Displacement ellipsoids are drawn at 70 % probability.

Barium is thus coordinated by five trithiocarbonate anions that perform bidentate ionic bonds *via* sulfur atoms. The centres of the anions are positioned in the fashion of a distorted trigonal bipyramid. As visible in figure 2.37, the Ba1 site is shifted away from the 3_2-screw axis occurring in the intersection of three C1−S1 bonds. By that, the coordination polyhedron centred by the barium ion is distorted from an ideal trigonal bipyramid.

X-ray powder diffraction

As mentioned above, crystals could be obtained by recrystallisation of powder of $BaCS_3$ **26** under solvothermal conditions. The powder (depicted in figure 2.35 (right)) was investigated with PXRD and the data curve could be fitted based on the phase information of the single crystal structure. The graphical result is shown in figure 2.39. In contrast to the decent refinement of the powder data of e.g., K_2CS_3 (cf. above), in the case of $BaCS_3$ there are strong signals in the difference curve, indicating some mismatch. Both stronger

and weaker intensities in the experimental data could not ideally be represented with only the phase of $BaCS_3$ as obtained from the single crystal analysis. For the RIETVELD refinement, the background, the lattice parameters and atom positions as well as their thermal ellipsoids were allowed to alter from the single crystal lattice. As the intensity of the peaks in X-ray powder diffractograms are dependent on the multiplicity of the respective d_{hkl} lattice spacing, these stronger amplitudes in the difference curve do not necessarily lead to the conclusion of a second or impurity phase. Because at a closer look, there are only a few low intense signals in the experimental data that were not modelled with the refinement curve at all. Without success, phases of the starting material $Ba(OH)_2 \cdot 8\ H_2O$ as well as a possible side phase of BaS were used in an attempt to explain these inconsistencies. No reason for the misfit of the refinement with the data is the discussed chirality of the space group used to describe the structure, as the spatial information is lost in the powder and cannot be obtained from PXRD.[57]

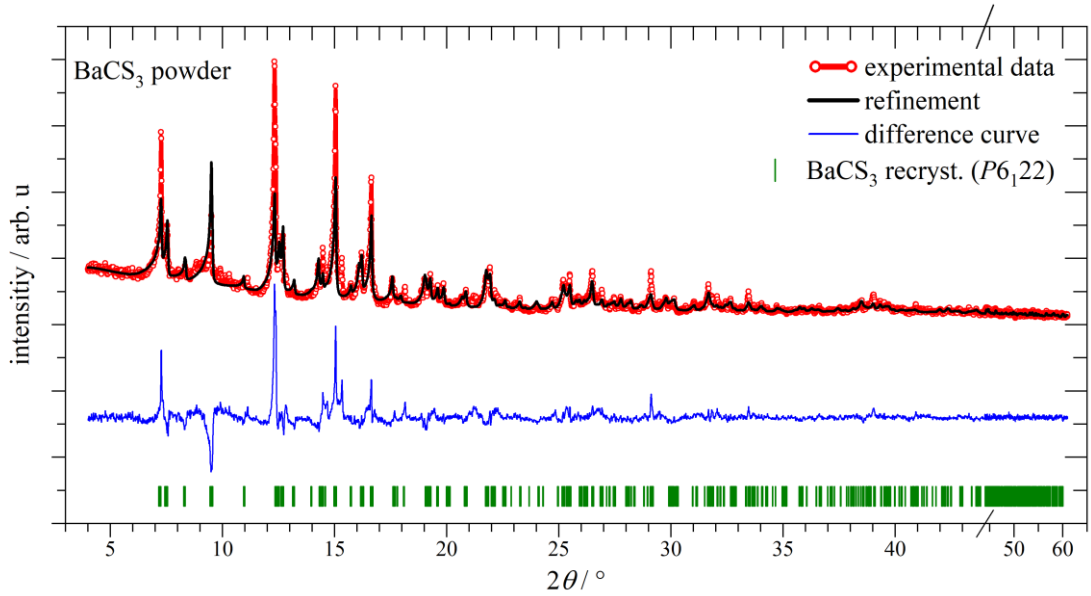

Figure 2.39: RIETVELD refinement of the $BaCS_3$ powder **26**.

Thermal analysis

The powder was also investigated on its thermal stability. A DTA curve was recorded during a heating cycle between RT to 700 °C. A strong endothermic signal at 416.5 °C indicated decomposition or melting of the compound. A weight curve was not included in the measurement. The residuals were analysed with PXRD, concluding the product of the thermal treatment to consist of BaS. A remarkable accuracy of the reflections in the diffractogram of the residuals was noticed. The data for these investigations are given in the appendix section 5.3.

2.3 Thiocarbonates of lithium, rubidium and caesium

2.3.1 Lithium salts

The lithium salt of the trithiocarbonic acid is probably the most neglected, because up to now only one reference from SEIDEL and MEYN was found and since then the compound was never mentioned anywhere. It was therefore attempted to prepare and characterise lithium trithiocarbonate by means of SC-XRD.

SEIDEL and MEYN reported that *n*-butyllithium reacted with trithiocarbonic acid, forming a fine yellow crystalline precipitate. It was characterised by elemental analysis and IR spectroscopy, identifying the compound to be Li_2CS_3.[58]

Treatment of $(HS)_2CS$ with *n*-butyllithium

Following the above, a yellow and highly deliquescent powder **2** was obtained, which could not be identified with the sum formula Li_2CS_3 beyond doubt. A photograph of the obtained yellow material **2** after precipitation is given in figure 2.40. The product **2** could not be recrystallised as the other alkali trithiocarbonates but was subjected to PXRD and spectroscopy methods as obtained. Unfortunately, due to low signal-to-noise ratio, the PXRD data could not be used for indexing. Prolonged PXRD measurements to help for a better signal-to-noise ratio were discarded, because the compound decomposed even sealed in glass capillary. No satisfying reference entry matching with the weak diffraction intensities was found in the PDF-2 database too, thus the PXRD data did not suffice for identification of the material. The curve can be found in the appendix section 5.2 in figure 5.1 on page 253.

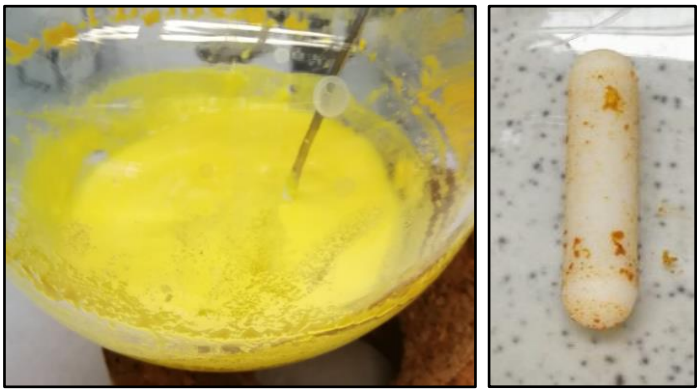

Figure 2.40: Yellow precipitate **2** from treatment of SC(SH)2 with *n*-butyllithium in toluene below 0 °C. under argon The inset shows orange red droplets on the magnetic stirrer bar immediately formed from residuals of the product upon exposure to ambient atmosphere.

The investigation with ATR-IR and RAMAN spectroscopy is shifted at this point and will be discussed in the context of other data below (cf. 2.4 from page 95). In short, some of the expected bands could be observed, suggesting the presence of a 1,1-dithiolate moiety. The decomposition upon exposition with air left orange red droplets on the stirrer bar for instance. This is another sign for a trithiocarbonate anion as the heavier homologues of alkali trithiocarbonates deliquesce under formation of red droplets too.[5]

Lithium trithiocarbonate hydrosulfide hydrate - $Li_4(CS_3)(HS)_2 \cdot 5\ H_2O$

Alternatively, preparation of Li_2CS_3 using traditional methods were tried, too. But, on the route that worked for other alkali trithiocarbonates, the experiments, where lithium metal was converted to the hydrosulfide and treated with CS_2 afforded an orange jelly substance. Consistently, no solid-state structure investigation could be undertaken.

On substitution of lithium metal with LiOH, as starting material, yellow crystals were finally obtained, which are displayed on the photos in figure 2.41. As they only formed in very low yield at the glass wall of the reaction vessel, analysis was limited to SC-XRD. Collection and solving of such data could identify the crystals as a trithiocarbonate hydrosulfide double salt, with the formula $Li_4(CS_3)(HS)_2\ 5\ H_2O$ **3**. An example for a double anionic trithiocarbonate hydrosulfide alkali salt has not been described before.

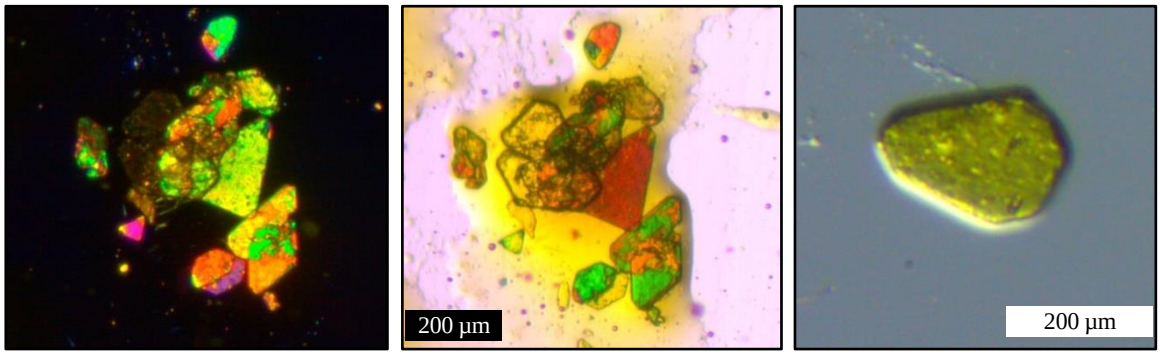

Figure 2.41: Overview of a group of obtained crystals of **3** with and without polarisation filter, respectively (left and middle). Photo of the crystallite used for structure determination measurements.

Crystal structure model

The setup of the unit cell structure is depicted in figure 2.42.

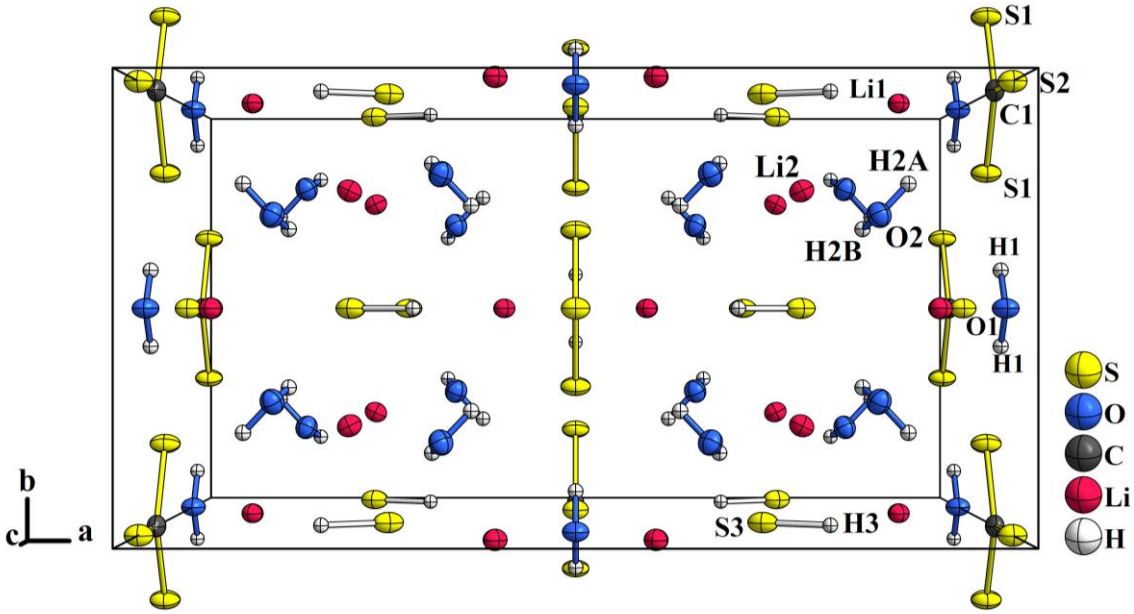

Figure 2.42: Unit cell of $Li_4(CS_3)(HS)_2$ 5 H_2O **3** viewing along the crystallographic *c*-axis coinciding with a 2-fold axis.

The space group *Fmm*2 belongs to the polar space groups, that do not possess a defined origin as there are more than two points in the lattice, that do not move upon symmetry operation. The atoms occupy numerous special lattice sites. All space group symmetries coincide in the WYCKOFF site 4a, which is occupied by the C1, S2 and O1 atom. They enqueue along the 2-fold axis, which coincides with the *c*-axis, (the viewing direction in figure 2.42), and identical with the mirror planes intersection. The group of atoms occupying sites of lower symmetry in either one of the mirror planes (100) and (010) are

S1 and H1 as well as S3, Li1 and H3, respectively. The Li2 cation is found in lattice site 8b, the two-fold screw axis centred at ¼,¼,0, lined up parallel to the *c*-axis, thus it has no occupation in the one of the mirror planes. The first water molecule of crystallisation is ordered along the *c*-axis in alternation with CS_3^{2-} anions. The second water molecule in the structure possesses no special site and is located around the straight virtual line defined by the Li2 cations, which coincides with a two-fold axis. Thus, with knowledge of the typical distances of S···H−O hydrogen bonds, one can define the structure with a ’Li(HS) · H_2O’ domain and a hydrated ‘Li_2CS_3’ network. The hydrogen atoms have been refined free, measuring O1−H1 = 84(3) and O2−H2A/B = 76(3)/79(3) pm, with water molecule angles of 109(4) and 105(3)°, respectively. The hydrosulfide molecule has an S−H distance of 131(8) pm, which is rather large compared among a number of 24 entries in a search and retrieve result of free hydrosulfide anions in the CCDC (none of them used neutron sources). From neutron diffraction study of Na(HS) an ICSD entry assigned the bond in the hydrosulfide anion with 124.1 pm. Stressing, that in neutron diffraction, hydrogen distances often are determined smaller compared to X-ray diffraction, allows to accept the obtained S−H distance.

The hydrosulfide anion is not donating a hydrogen bond with a near moiety (cf. figure 2.43). Indeed, grasped in figure 2.42 the hydrogen atom is pointed into the vacant space. Resulting in a one-dimensional connection of the coordination tetrahedra inhabited by Li2, the hydrosulfide anion in turn is accepting a water donated hydrogen bond, which is of acceptor-donator distance (S···O) of 323.6(1) pm. Literature data is sparse in this concern, underlining that sulfur has been observed both in the role as a possible strong hydrogen bond acceptor and to act inert towards such interaction. As there is actually a continuum of situations in this regard,[38] no clear evidence for an S···H−O bond is drawn from the structure model. At last, from the distance, it can be ranged rather weak in strength. Other S···H−O connections in the structure are present as the *Li_2CS_3* sub-structure is surrounded by water molecules. With S···O distances of 320.9(1) and 333.6(1) pm, again the hydrogen bonds can be considered weak in strength, but are comparable with a range of values determined earlier in this regard.[38]

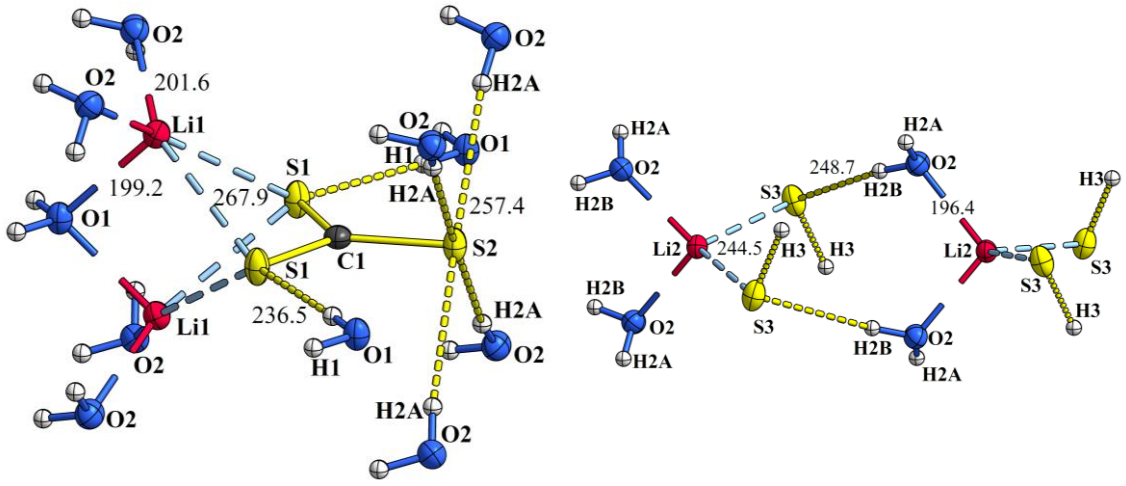

Figure 2.43: Inter atomic and molecular arrangement in $Li_4(CS_3)(SH)_2 \cdot 5\ H_2O$ **3**. All non-hydrogen atomic displacement ellipsoids are drawn at 70 % probability. The surrounding of the trithiocarbonate anion is depicted on the left. Contacts only with Li1 show a hydrated Li_2CS_3 sub-domain to be present in the lattice. The tetrahedral coordination of Li2 with two hydrosulfide and two water molecules is shown on the right. Numbers give the respective distances in pm.

Balance of the anionic charge of the trithiocarbonate is performed by neighbouring lithium cations, which coordination is depicted in figure 2.43. The trithiocarbonate anion lies within the *a*-plane of mirror symmetry and is bisect along the C1−S2 bond by the mirror *b*-plane. This forces the geometry of the molecule to be exactly planar and the only two geometric quantities that stay non-equivalent are the two different bond lengths C1−S1 = 171.2(2) and C1−S2 = 171.9(3) pm, which compared to other herein described structures are of close value, indicating an almost ideal delocalisation of the C=S double bond over all three of the C−S bonds. Different from that, the angles, determined at the anion, exhibit a markedly alternating value of the ideal 120°. Especially the ionically interacting S1 atoms differ with S1−C1−S1 = 117.05(2)° and S2 with no such interaction is close to ideal with S1−C1−S2 = 121.48(2)°. In consequence, the ideal D_{3h} symmetry is not obtained, but C_{2v}.

The structure overall cannot be described to be an entirely ionic network, as the two defined sub-structures are only connected *via* probable hydrogen bonds, as already stated. This is in line with the finding that the geometry of the trithiocarbonate anion is almost ideal with the isolated molecule. Because of the coordination of two symmetry-equivalent Li1 cations, the jolted angle <120° at the CS_3^{2-} ion of the involved sulfur atoms can be explained. At the other end of the CS_3^{2-} ion, the S2 atom has no Li^+ coordination at all and is only stabilised by four hydrogen bonds, performed by four water molecules, in a square-planar fashion. Overall, except the two Li1 interactions, there are only weak hydrogen bonds assumed,

giving rise to assume a less strong crystal field, explaining the homogenous geometry of the trithiocarbonate anion. Still the symmetry in the crystal model confines the anion to a strict geometry, but the residuals of the solution allow to take these considerations for granted.
In the *Li_2CS_3* sub-structure, the symmetry equivalent Li1 ions have a distance measuring 277.6(7) pm, which is significantly shorter, compared to the non-equivalent L1···Li2 distance of 321.5(4) pm. Distances below 300 pm in lithium salts are however not unusual, for instance, in Li_2S at 10 K the X-ray distance of Li···Li, with 284.5 pm, is almost as short.[59] Other than the symmetry-identical ionic sulfur interaction, it can be assumed that Li1 is obtaining three dipole-cation interactions with water molecules *via* orientation of their lone pairs. For reference, the O···Li distance of a coordinating water molecule of crystallisation, determined to 191.1 pm in the X-ray structure of $Li_2(SO_4) \cdot H_2O$ was retrieved.[60] In the crystal described here, the distances are of similar size ranging from O2···Li2 = 196.4(3) to O2···Li1 201.6(3) pm.

Concluding remarks

Neither anhydrous Li_2CS_3 nor its hydrate could be obtained in simple analogy to the heavier trithiocarbonate homologues.
As the solubility product of LiOH in ethanol is small compared to NaOH or KOH, concentration of the starting solution to a needed degree failed and the desired product did not simply precipitate upon addition of CS_2. Eventually, the forced crystallisation upon addition of ether, results in crystallisation of *all* specimen present in the H2O/EtOH solution as idealised in equation 2.2.

$$2\ SH^- + 4\ Li^+ + CS_3^{2-} \xrightarrow[+\ Et_2O]{H_2O/EtOH} Li_4(CS_3)(SH)_2 \cdot 5\ H_2O \downarrow \qquad 2.2$$

Regarding other attempts, where other alkali metals could be crystallised with the tri- and perthiocarbonate anion, only brown viscous liquids or jelly was obtained. This also holds for experiments under solvothermal condition. The treatment of Li_2S with CS_2 in an evacuated glass ampoule at 100 °C did not yield solid products solid products.
As the reactivity of *n*-butyllithium is beyond comparison to that of LiOH in anhydrous environment, it should be used in further work in the future. The introduction of the volatile trithiocarbonic acid to react with the organo-lithium may be refined in terms of temperature and solvents.

2.3.2 Rubidium salts

With close agreement to the protocols which afforded anhydrous K_2CS_3, it was attempted to obtain crystals of Rb_2CS_3. There is only one publication by PHILIPPOT from 1967 on the structure of Rb_2CS_3, which could not be accessed. Linked with that work are however two modifications of the salt,[61] included the PDF-2 database.[viii] The entries reveal that only d_{hkl}-values and no unit cell metrics on the compound were reported. In the progress review of GATTOW from 1992 updates of the anhydrous salt are missing.[19] Thus it was assumed, that the structure has never been described properly so far.
In contrast the crystallographic information on the monohydrate $Rb_2CS_3 \cdot H_2O$ is available and reported isostructural with the potassium homologue.[62] However, in the ICSD the structure is missing.

Solvothermal treatment of Rb_2S_x with CS_2

The growth of pink plank-shaped crystals, shown in figure 2.44, was occurring in the reaction of CS_2 with 'Rb_2S' **48** under solvothermal conditions. The rubidium sulfide precursor was prepared beforehand. Figure 4.13 in the appendix contains the PXRD data of the starting material, stressing that it could not be identified due to the poor crystallinity. However, the 'Rb_2S' educt (batch #2, **48**) was coloured pale yellow as expected for Rb_2S,[63] where in a first attempt (batch #1) an inhomogeneous yellow material was obtained that did not afford crystals under reaction with CS_2. Albeit the low crystallinity, from the PXRD curves, at least a phase change is observed by a different (weakly resolved) reflection pattern between the educt phases #1 and #2. It may be assumed that the desired rubidium sulfide phase was obtained in the later batch.

[viii] Entries of two modifications on Rb_2CS_3 in the PDF-2 database: I [00-021-1046] orange-red, II [00-021-1047] violet-red.

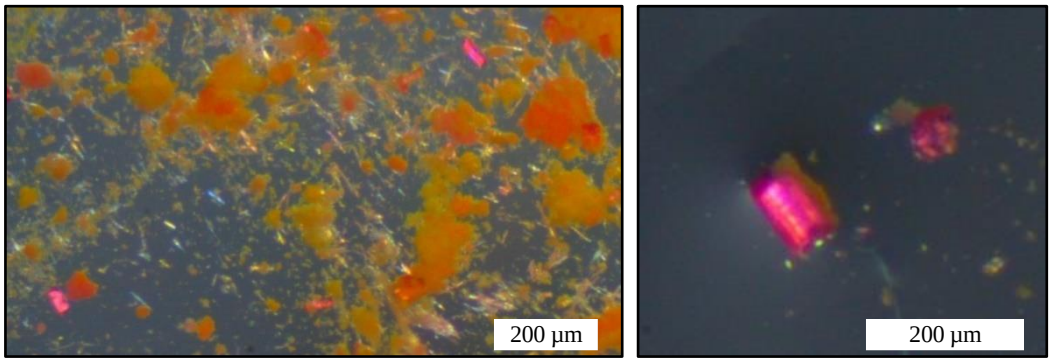

Figure 2.44: Photos of the obtained material from reaction of prepared 'Rb_2S' **48** and CS_2 under solvothermal conditions. The pink coloured crystals were in suspicion to be Rb_2CS_3 **17** and were investigated with SC-XRD. Regrettably, the poor diffraction did not provide data needed for a structure model.

The data obtained from the measurement could not be properly solved in the downstream evaluation. The frames recorded during the measurement offered qualification of the crystal at first glance. However, the scattering was weak, even at a relatively high exposition time of > 42 seconds per frame. The intensities were collected with a signal to noise limit (I/σ) of 10 and indexed with a primitive monoclinic lattice reaching a figure-of-merit of 0,6 within the evaluation software *APEX 3*: a = 676.68(9), b = 1135.2(2), c = 2905.8(4) pm, β = 93.622(6)°, Z = 14. The parameter c of that reduced cell differed from those reported for $Rb_2CS_3 \cdot H_2O$,[62] and the relatively c-axis length could indicate a growing error, e.g., twinning. After integration, the scaling and evaluation of the data yield R_{int} of 14 - 15 % and a signal vs. resolution of 8.1, both describing a poor data quality in the first place. Switching between the space group $P2_1$ or $P2_1/m$ did not help to describe a structure model and to yield decent residuals. Considering a twinned crystal, a simple automatised search for the transformation matrix by the command TWIN did not improve the situation and eventually, the crystal data was discarded. Some trithiocarbonate units and rubidium positions were found in the attempt to model the structure with the diffraction data, but residual fragmental moieties and electron density eventually could not be assigned with chemical reason.

The crystalline species did not decompose too fast keeping the ampoule stoppered. Thus, they could be subjected to µRAMAN spectroscopy which is shifted at this point and is discussed in sub-section 2.4.2.

Rubidium trithiocarbonate Rb_2CS_3

Another attempt to crystalise Rb_2CS_3 was to prepare the salt as a precipitate and attempt recrystallisation in a subsequent step. With the description of YEOMAN used as guideline, a rubidium ethoxide solution, was exposed to H_2S gas and the desired compound was precipitated adding CS_2. The pinkish orange precipitate **16**, which immediately formed, was captured in the photo in figure 2.45. The colouration of the powder persuaded to call it 'Rb_2CS_3' **16** for simplicity. A PXRD of the as obtained powder could not be used to identify the product as the diffraction was too weak.

Figure 2.45: Photograph of the formed rubidium compound 'Rb_2CS_3' **16**.

Thermal analysis

A DTA-TG measurement, shown in figure 2.46, was carried out up to 500 °C. It revealed the compound to release a small mass of volatiles upon heating to 200 °C, which is too small to represent a stoichiometric molecular moiety emitted from the powder. (It may be a sub-stoichiometric amount of adsorbed water.) Then, between 200 – 325 °C, the weigh curve describes a plateau, while the heat flow passes an endothermic signal (peak at 240 °C). Between 325 and 350 °C, an excursive endothermic signal with accompaniment of a steep weight loss and the following incongruent cooling curve, allows to assume irreversible decomposition.

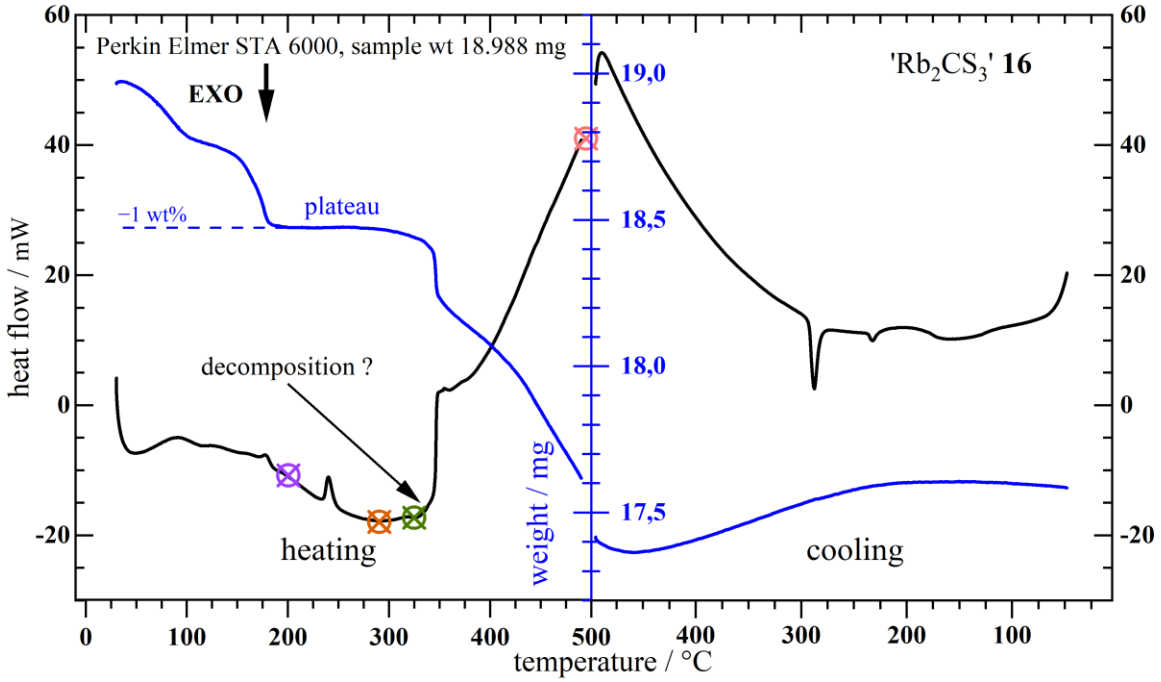

Figure 2.46: Combined DTA heat flow and thermogravimetric plot of precipitated 'Rb_2CS_3' **16**. In the black curve, broad endothermic signals below 180 °C indicate the release of volatiles, supported by a small weight loss of 1 %. At 350 °C the compound decomposes, described by a steep weight loss and the erratic increase in the heat flow signal. Subsequently, the material was treated at different temperatures, where the coloured points on the black curve, mark the max. temperature.

With knowledge of these heat signals, the precipitated powder 'Rb_2CS_3' **16** was conducted to thermal analysis repeatedly up to 200, 290 and 325 °C (indicated by the markings in figure 2.46). The measurements are combined in figure 5.7 in the appendix. All residuals of these DTA-TG measurements were used to collect PXRD data and were also subjected to IR spectroscopy. As seen in figure 2.47, data of the unconditioned product and with previous heating under dynamic vacuum at 125 °C of all methods are compiled. (It shall be noted, that because of a holding step in the measurement up to 325 °C, the material ran into decomposition.)

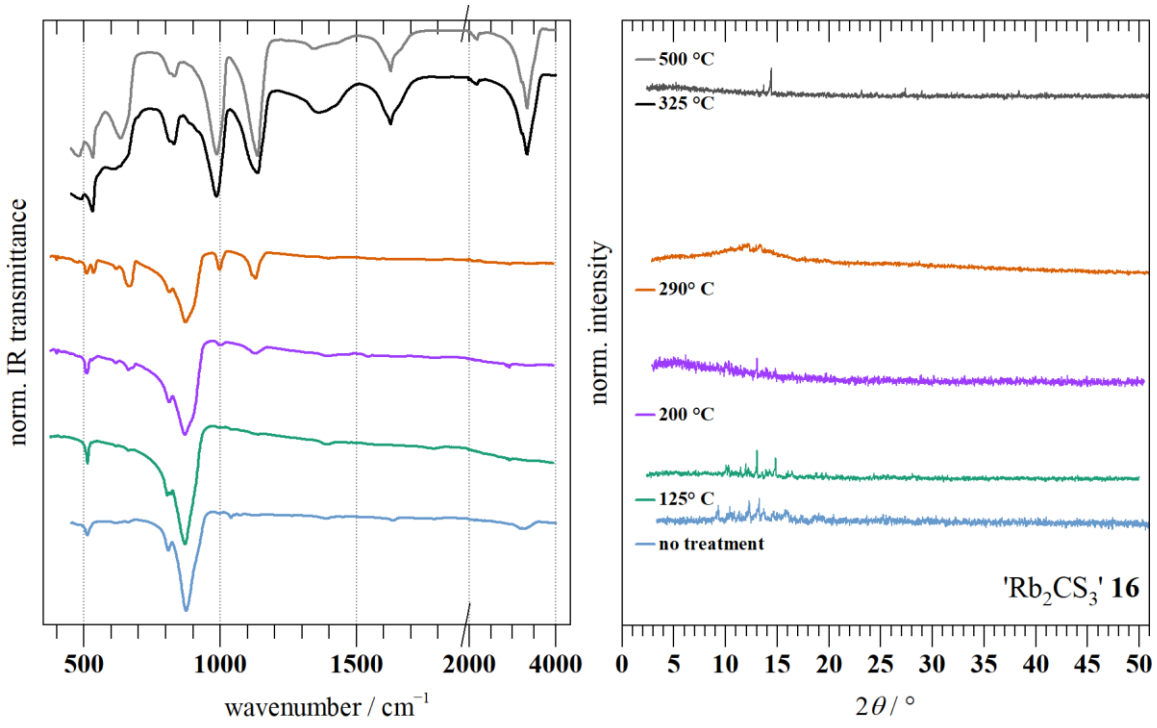

Figure 2.47: IR spectra and PXRD data (left and right, respectively) of 'Rb_2CS_3' **16** and of DTA-TG residuals. The IR spectrum (bottom) changes gradually until the powder was heated higher than 290 °C, followed by decomposition above 325 °C. The PXRD data cannot be used for identification at any time due to the low signal to noise ratio.

The IR spectra reveal the decomposition of the material at about 325 °C, as the absorption pattern between 400 – 4000 cm^{-1} fundamentally change. Before that, the characteristic spectrum of the trithiocarbonate anion can be recognised, which is discussed with more detail and with respect to the other salts in sub-section 2.4.2. Compared to the spectrum of the unconditioned powder (blue line at the bottom), the orange-coloured spectrum (290 °C) contains additional bands or band splitting, suggesting a transformation without cleavage of moieties, because of the constancy of the weight curve (cf. DTA-TG). A weak and broad absorption above 3000 cm^{-1} in the bottom spectrum indicates characteristic water impurity (O−H stretching), which is absent in the turquoise curve above. This probably means, that an adsorbed sub-stoichiometric amount of water could be degassed by treatment at 125 °C under vacuum. Unfortunately, the powder did not crystallise properly at any point under the given conditions, as seen by the low intensity to noise ratio in the PXRD curves.

Solvothermal recrystallisation

The 'Rb_2CS_3' powder **16** was conducted to recrystallisation in ethanol at elevated temperatures in a sealed glass ampoule and on cooling, crystals grew on the ampoule walls, which are shown in figure 2.48.

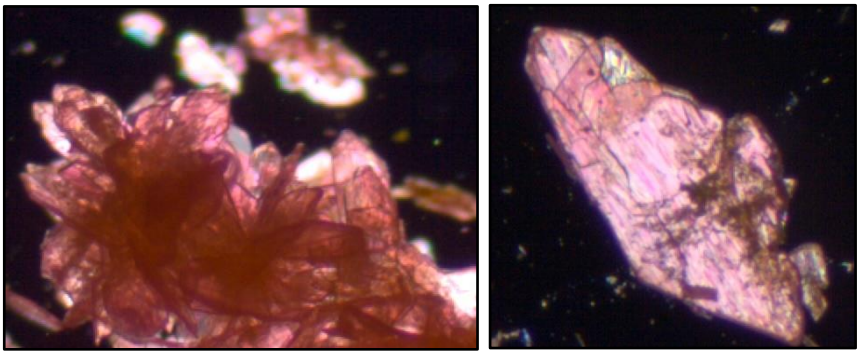

Figure 2.48: Photographs of the crystalline material obtained from recrystallisation of 'Rb_2CS_3' powder **16**. On the left, chunks of intergrown individuals are depicted. They were separated under the microscope, but, as seen on the right, they consisted of flat intergrown domains.

Although the recorded frames demonstrated single crystalline reflections, where no smearing of intensity spots or formation of ring-shaped intensity was observed, SC-XRD data of a recrystallised specimen could not be used for a structure model. Next to the initial triclinic cell, two *c*-centred monoclinic lattices were indexed with unit cell volumes 2.255 nm^3 and 4.494 nm^3, where only the *b* parameter was identical. Again, the R_{int} and signal vs. resolution indicated poor description of the data with the indexed lattice. Integration applying the smaller unit cell volume in the space group *C*2/*m*, was carried out and among unsolved atomic fragments CS_3^{2-} and some Rb^+ positions could be identified. However, in the total picture, residual electron densities that could not be assigned with atoms of suitable weight, denied completing a structure model.

A structure model for Rb_2CS_3 or related derivatives could finally not be obtained by means of SC-XRD.

Although facing troubles in the attempts to work out a structure model, the routes of preparation of the defective crystalline specimens in principle proved useful. It may be advisable to refine the recrystallisation conditions to achieve faultless crystallisation of Rb_2CS_3. A more systematic alteration of the temperature regimes, crystallisation time and/or solvents may be an option.

2.3.3 Caesium salts

Caesium trithiocarbonate Cs_2CS_3

On Cs_2CS_3, X-ray structure reference is scarce, too. However, the structure of the monohydrate $Cs_2CS_3 \cdot H_2O$ was found in the ICSD, originating in a publication of PHILIPPOT and LINDQVIST from 1971.[64] The review of GATTOW and BEHRENDT lists the anhydrous salt Cs_2CS_3 to be featured in the same unacquainted report as anhydrous Rb_2CS_3, claiming two modifications – *Form I* and *Form II* -without further details.[1,61] Linking to the original report, entries on these modifications are included in the PDF-2 database adding only information of different colours (dark and light red) to some d_{hkl}-values.[ix] Any crystal metrics are missing. This motivated to attempt crystallisation of the anhydrous compound in order to acquaint a structure model.

Among other experiments (cf. below), following the script of YEOMAN once more, caesium was dissolved in ethanol and turned into the hydrosulfide on H_2S introduction. An immediately formed precipitate was obtained upon addition of CS_2 to the basic ethanolic solution. The dried product was called 'Cs_2CS_3' **19** and PXRD was carried out.

X-ray powder diffraction

Lacking a single crystal phase to use in a RIETVELD refinement, the PXRD data qualified for treatment with an indexing routine implemented in the *Topas* program-suite. Only BRAVAIS lattices belonging to the orthorhombic and monoclinic lattice systems were used as possible solutions. The cubic, hexagonal and tetragonal systems were left out as they were not expected, taking into account, that the so far known alkali trithiocarbonates did not form crystals of such high lattice symmetry. The program gave out a number of 2999 different unit cells and space groups. To evaluate this large number of possible unit cell metrics, the volumes were considered first. Simply speaking, a large volume allows a large number of atomic sites in the unit cell, making it arbitrarily possible to fit experimental data. Thus, options where the volume was >> 3 nm^3 were discarded. On the other hand, cell volumes < 2 nm^3 in the result list majorly called for a triclinic lattice (space group $P\bar{1}$) allowing the alteration of all six lattice parameters a, b, c, α, β and γ in the subsequent PAWLEY refinement, which again arbitrarily provided a good fitting.

[ix] PDF-2-database entries on Cs_2CS_3: I [00-021-0226] dark red, II [00-021-0227] light red

Eventually, the low volumes < 3 nm^3 with non-triclinic lattices were filtered out and furtherly sorted by their order anisotropy of the lattice parameters. Thereby, more options could be left out, as the parameters sometimes diverged so that the form of the cell was converging a plane instead of a parallelepiped. Still the number of options remained large, thus eight cells obtained in this way were picked out. A PAWLEY refinement for the PXRD data of 'Cs_2CS_3' **19** for 2θ = 2.5 to 35° was carried out with these eight cells. The results are given in table 2.6, where refined cell parameters are written **bold**. All PAWLEY refinements are given for graphical inspection in figure 5.2 in the appendix section 5.2.

Table 2.6: Results on the PAWLEY evaluation of possible unit cells obtained from an indexing routine within the *Topas* programme.

#no.	Crystal system, space group	Indexed unit cell parameters		**Refined** unit cell parameters		R_p, R_{wp}, R_{exp}	Goodness-of-fit R_{wp}/R_{exp}
		a, *b*, *c* / pm	β/ °	*a*, *b*, *c* / pm	β/ °		
# 1	orthorhombic, *P*222	1241.41, 701.79, 2653.18	90	**1242.90, 702.36, 2653.14**		5.67, 8.67, 0.73	11.9
# 2	orthorhombic, $P2_12_12_1$	795.11, 2419.86, 1438.44	90	**795.41, 2414.08, 1438.95**		7.53, 12.59, 0.68	18.5
# 3	orthorhombic, $P2_12_12$	1242.92, 702.09, 2652.47	90	**1242.98, 702.42, 2653.03**		5.94, 9.12, 0.73	12.5
# 4	orthorhombic, $Pca2_1$	1335.57, 3663.27, 623,00	90	**1346.51, 3637.16, 630,60**		5.87, 9.38, 0.66	14.3
#5	monoclinic, *P*2	1732.74, 672.60, 1389.45	108.348	**1736.29, 674.30, 1392.61**	**108.652**	6.10, 9.94, 0.66	15.0
# 6	monoclinic, $P2_1/c$	1900.60, 1711.16, 723.37	108.630	**1895.51, 1710.45, 723.34**	**108.42**	4.55, 7.78, 0.54	14.3
#7	monoclinic, *P*2	1375.26, 415.68, 2800.74	115.571	**1382.00, 416.41, 2794.91**	**115.57**	5.38, 9.06, 0.66	13.8
# 8	monoclinic, $P2_1$	1029.12, 1332.44, 1301.12	107.54	**1025.50, 1327.76, 1298.55**	**107.60**	6.14, 9.99, 0.65	14.5

It shall be remembered, that from a PAWLEY refinement no atomic positions or information of the atomic structure can be learned. The method simply provides to handle a recorded PXRD curve in a mathematical algorithm. In short, all sites in the volume of the unit cell are iteratively filled to run through all possible d_{hkl} lattice spacings. With respect to the

space group symmetry the extinction conditions are changed. The calculated intensity is unlimited as atomic form factors are not considered.

It can be obtained, that none of the cells apply favourably, considering the R_{wp} and goodness-of-fit to be relatively large (the latter should converge unity). Furthermore, as still the graphical output was relatively decent for all refinements, it may be concluded, that in the orthorhombic and monoclinic lattice systems, the degree of freedom for the refinement is too high, to yield meaningful results.

Caesium trithiocarbonate hydrate $Cs_2CS_3 \cdot H_2O$

Abundantly, a pink microcrystalline precipitate **20** was obtained substituting caesium metal with $CsOH \cdot H_2O$ as a starting material. The hydroxide was converted to hydrosulfide, which reacted with CS_2 (cf. equation 2.3).

$$2\ CsOH \cdot H_2O + H_2S \xrightarrow[+\ CS_2]{\text{ethanol, 60 °C}} Cs_2CS_3 \cdot H_2O + 2\ H_2O \qquad 2.3$$

The products, shown on the photos in figure 2.49, still contained water of crystallisation after a mild drying step (left) or solvothermal recrystallisation in ethanol (middle and right), respectively.

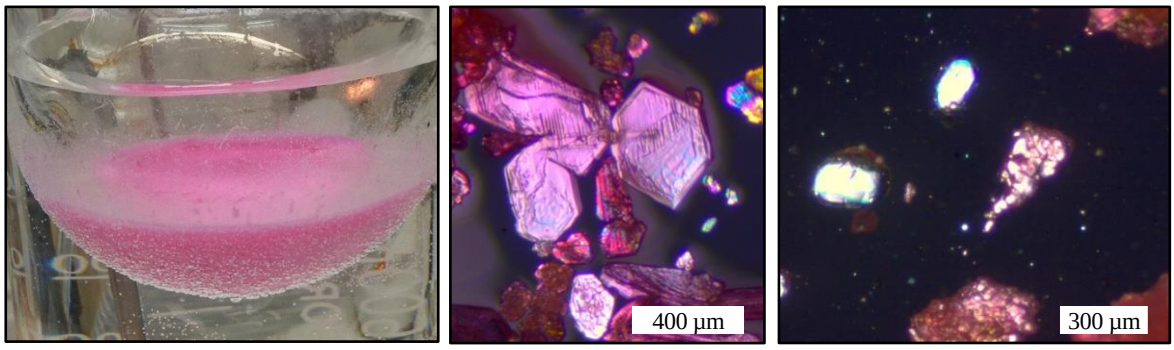

Figure 2.49: Product obtained after addition of CS_2 to a saturated solution of CsOH after treatment with H_2S (left). The powder could be recrystallised, yielding crystals (middle). A crystallite was identified with $Cs_2CS_3 \cdot H_2O$ **20c** by indexing. On the right crystalline residuals are shown. The colourless crystals contained thiosulfate (decomposition product) and were discarded, but the pink crystals were eventually used to collect SC-XRD data.

The prepared $Cs_2CS_3 \cdot H_2O$ powder **20** was investigated with PXRD but showed low crystallinity, and the data quality was unsuitable for a RIETVELD refinement on the basis of the crystal phase information of $Cs_2CS_3 \cdot H_2O$.

The obtained crystals could be indexed with the metrics of the published and available crystal structure by PHILIPPOT.[64] For the sake of confirmation of the earlier structure, it was eventually decided to collect a new set of single crystal data for $Cs_2CS_3 \cdot H_2O$ **20c**.
The powder precipitate (cf. figure 2.49 (left)) was recrystallised twice on other routes, namely apart from solvothermal condition. Interestingly, both colouration and habitus of the single crystals were different, which is seen in figure 2.50, where both the recrystallised solids are depicted. All methods yielded the same unit cell, identical with that of the published structure of $Cs_2CS_3 \cdot H_2O$. Thus, the measurement of only the specimen from the solvothermal method, i.e., **20c** was executed.

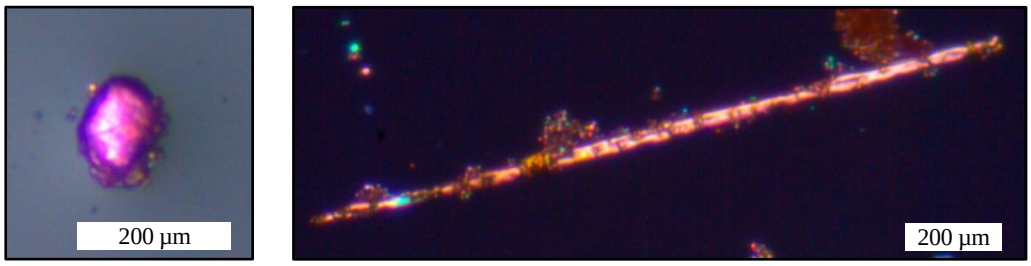

Figure 2.50: Photos of crystalline material obtained from recrystallisation of $Cs_2CS_3 \cdot H_2O$ powder **20**. On the left, isotropic irregular shaped crystallites **21** from experiments at RT and on the right needle-shaped crystals **22** grown during cooling of solution.

Crystal structure model

$Cs_2CS_3 \cdot H_2O$ **20c** crystallised in an orthorhombic lattice using the space group $P2_12_12_1$ (no. 19). Upon data evaluation, a twinning of the specimen used for data collection was noticed. This was not unexpected, as in the space group $P2_12_12_1$ enantiomorphic growth is commonly occurring. The problem was mediated within in the *ShelX* solution software, treating the *hkl* reflections with the corresponding inversion matrix, which excluded the reflections of the twin domain automatically. The domains were almost equally scaled with *flack* parameters of 0.55(3) and 0.45(3). Unaccountably, the statistics in the measurement output achieved 100 % data completeness for the integration but in with the final structure solution, only 90 % completeness was obtained.
Four formula units are included in the unit cell, comprising two non-equivalent caesium cations one trithiocarbonate anion and one molecule of water of crystallisation. All atoms occupy regular sites, thus the symmetry of the trithiocarbonate anion is free of lattice symmetry operations. The unit cell is depicted in figure 2.51 viewing along the crystallographic *a*-axis. The eponymous two-fold screw axes are the only symmetry element in the lattice of the polar space group. In figure 2.51 parallel to the viewing direction two-fold screw axes are at ¼ and ¾ *b* on the cell edges and the vertical cell centre (½ *c*). There

are three non-equivalent C1−S bonds with lengths of 172.3(5) (S1), 172.4(5) (S2) and 170.7(5) pm. The angles at the anion are 118.9(3)° (S1−C1−S2), 120.5(3)° (S1−C1−S3) and 120.6(3)° (S2−C1−S3), which almost shows no distortion from the ideal trigonal shape and for simplicity can be called planar within the margin of uncertainty.

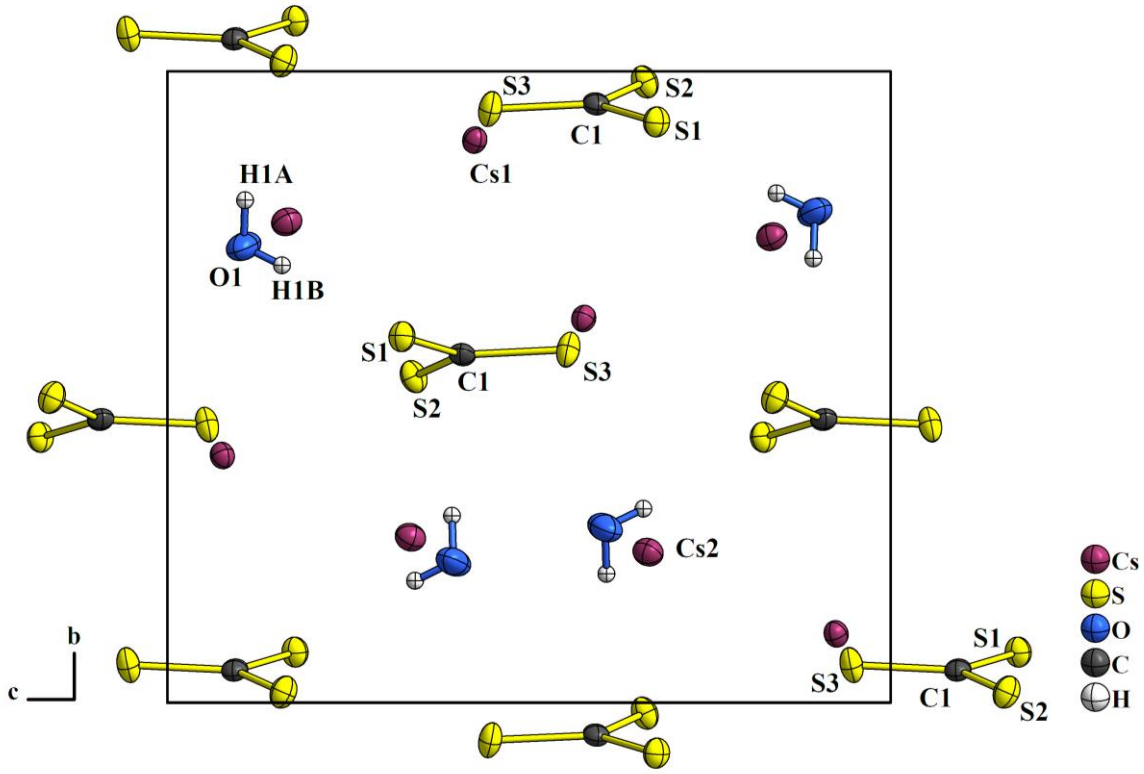

Figure 2.51: Unit cell of $Cs_2CS_3 \cdot H_2O$ **20c** in view along the *a*-axis. All non-hydrogen atomic displacement ellipsoids are drawn at 70 % probability.

The coordination of the Cs^+ ions are found to differ from each other. On Cs1, below 400 pm four trithiocarbonate anions only perform bidentate coordination. Additionally, one molecule of water is in range of possible dipole−cation interaction. In figure 2.52 the coordination is shown in the upper part of the unit cell. The shortest atomic distance is Cs1···O1 with 337.7(4) pm. The ionic interaction with sulfur ranges between 349.1(1) and 380.5(1) pm, where the mean value is 361.6 pm. One long C1−S2 distance of 420.9(1) pm may be neglected.

Cs2 in turn has six sulfur atoms of five different anions in close range for ionic interaction. Thus, Cs2 is coordinated in monodentate fashion only. Two near H_2O molecules are likely to orient by dipole−cation interactions towards the Cs2 cation. The coordination is depicted in figure 2.52 in the lower part of the unit cell. Again, the dipole interaction with water molecules of crystallisation is of the closes distance with 315.6(5) and 320.2(5) pm. The mean value of the monodentate anion coordination is 362.3 pm, which is of the same value

order as obtained for the bidentate coordination of Cs1. Compared with hydrated salts of caesium ions, the $H_2O\cdots Cs$ interaction are within range of expected values. This also holds for the ionic Cs−S interaction. In $Cs_2CO_3 \cdot 3\ H_2O$ the respective distances were reported to be 318.8 – 349.7 pm and in $Cs_2(S_5) \cdot H_2O$ both the dipole−cation and the ionic interactions are of comparable values with 323 pm ($H_2O\cdots Cs$) and 356.3 – 374.2 pm (Cs−S), respectively.[65] Hydrogen bonds of the type O−H···S can be only determined from the orientation and positions of the oxygen and sulfur, as the hydrogen atoms have been fixed to the oxygen atoms by calculation. There are four O···S distances of which only two can be ranked as close enough for moderate hydrogen bonding with 324.2(5) and 333.0(4) pm, respectively. Two more long distances of 373.9(5) and 387.9(4) pm may comprise dispersion interaction with hydrogen atoms attached to O1.[38]

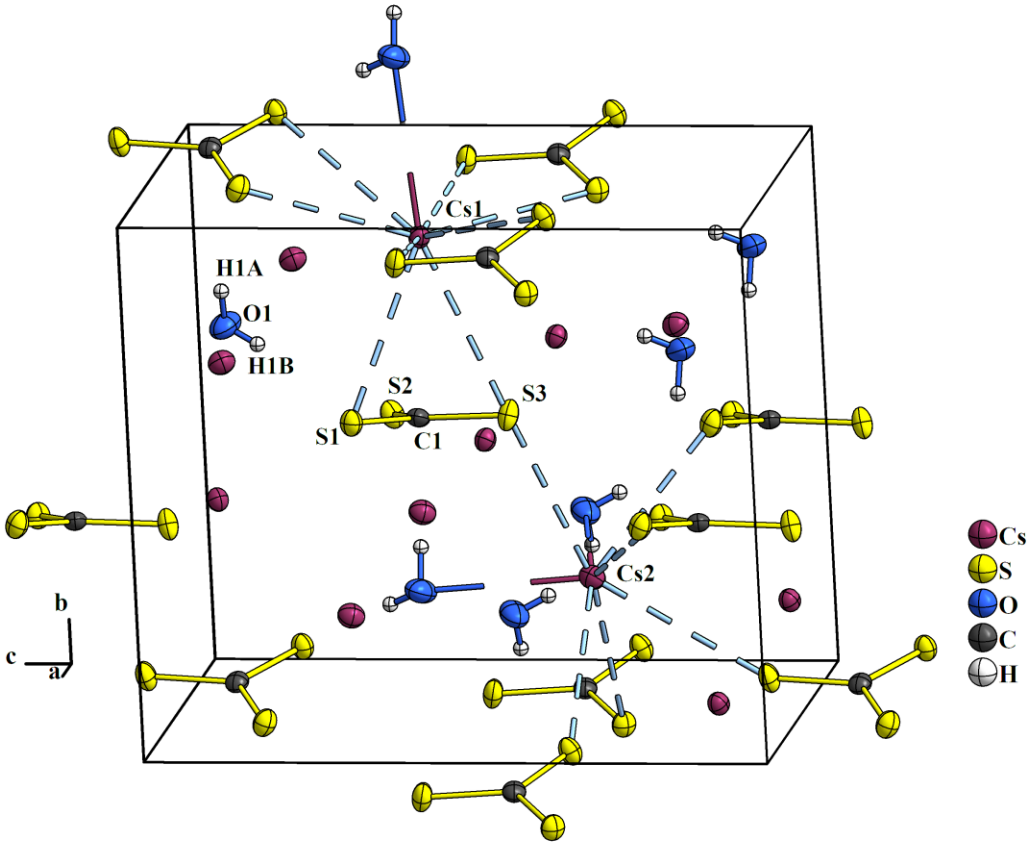

Figure 2.52: Coordination of the two non-equivalent caesium sites in $Cs_2CS_3 \cdot H_2O$ **20c**. All non- hydrogen atomic displacement ellipsoids are drawn at 70 % probability.

Thermal analysis

It was tried to withdraw the water of crystallisation from the $Cs_2CS_3 \cdot H_2O$ **20** powder, to apply recrystallisation methods afterwards, hoping to obtain crystals of the anhydrous compound for structure investigation.

To gain knowledge of suitable drying temperatures for this undertaking, $Cs_2CS_3 \cdot H_2O$ **20** was conducted repeatedly to thermal analyses between iterative drying treatments. Figure 5.8 in the appendix section 5.3 shows the DTA data of the differently conditioned powders up to 1050 °C. As seen from these thermal analyses of $Cs_2CS_3 \cdot H_2O$ **20**, an endothermic peak at about 100 °C suggested the evaporation of water of crystallisation from the solid compound. In consistence, the powder was finally treated at 200 °C under dynamic vacuum. Thereafter, a DTA-TG measurement, which is plotted in figure 2.53, confirmed the conditioned product ('Cs_2CS_3' **20t**) to be free of volatiles in the range up to about 400 °C as the weight curve stays constant after the levelling of the tuning bend at the start of the measurement. Comparable with the heat flow signals of 'Rb_2CS_3' **16**, endothermic signals occur indicating phase transformations just above 200 and at about 300 °C.

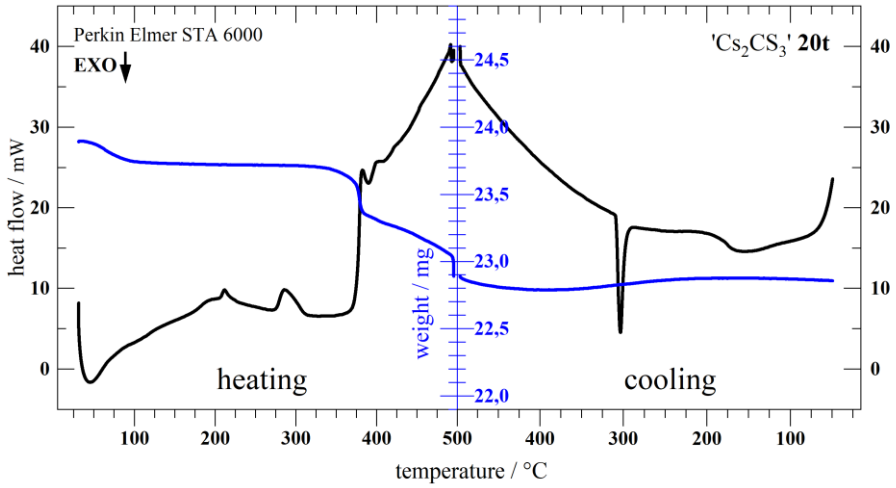

Figure 2.53: DTA- (black) and thermogravimetry (blue) of the starting material after treatment at 200 °C (**20t**). Upon heating, in the region between 100 to 400 °C no change in sample weight is observed. Thus, the signals in the heat flow curve, cannot represent evaporation events. The tuning bend at the start and end are neglected from discussion.

The PXRD pattern of the conditioned $Cs_2CS_3 \cdot H_2O$ **20t** was not found substantially altered from the unconditioned after the drying process at 200 °C, which is in contrast to the diffraction pattern of the residuals from the DTA-TG treatment up to 500 °C. The PXRD data is shown for comparison in figure 2.54. Due to the low signal to noise ratio, the powder data was not suitable for a refinement like seen above. Nonetheless, comparison with the d_{hkl} values of *Form I* published by PHILIPPOT,[61] only available *via* the PDF-2 database, was found in rough agreement, as shown by the blue arrows in figure 2.54.

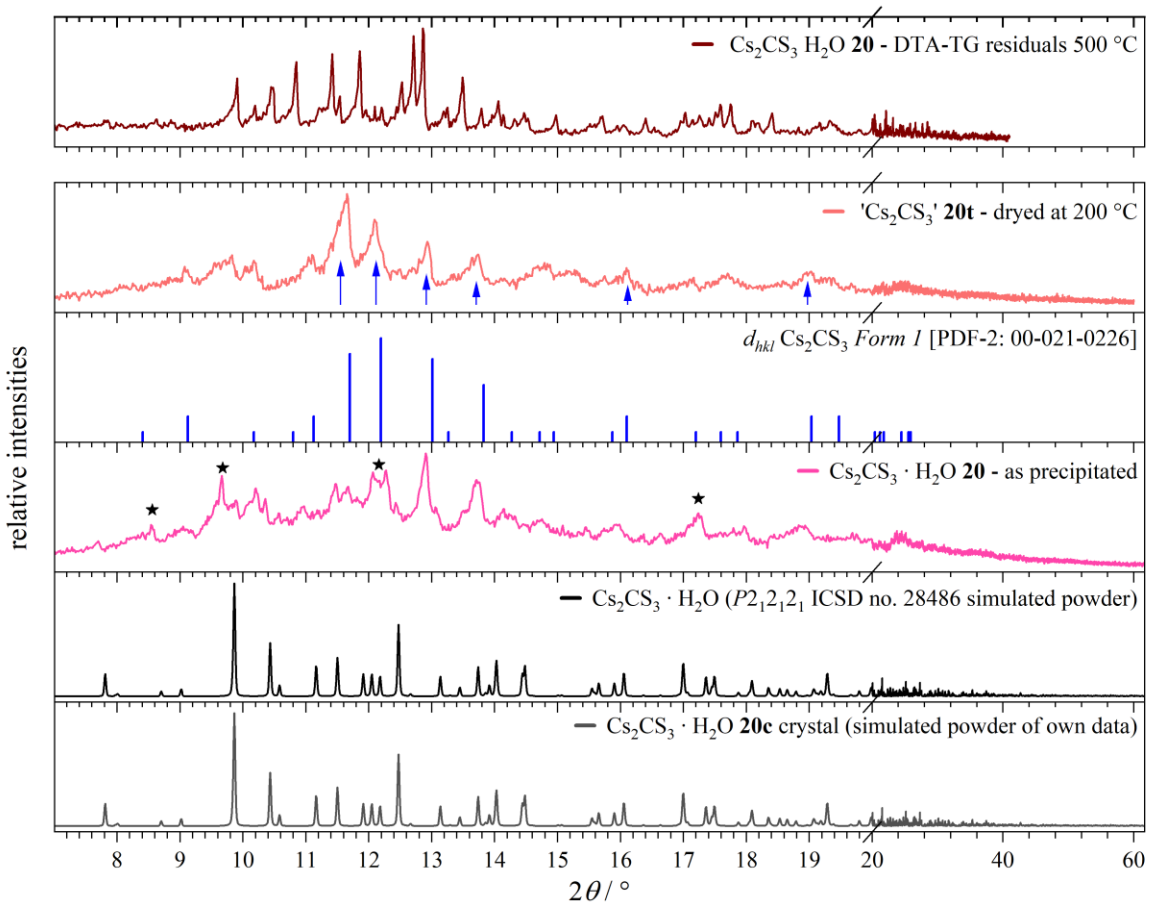

Figure 2.54: PXRD graphs of $Cs_2CS_3 \cdot H_2O$ **20** after different heating treatments. Going from bottom to top, two simulated patterns based on published as well as structure data of **20c** show accordance among each other. The precipitated powder **20** (pink) is poor in crystallinity and does not match the intense signals of the single crystal simulations. Asterisks mark intensities, that are not accord with the red curve of **20t**. This in turn roughly match with the d_{hkl} intensities of Cs_2CS_3 (*Form I*), given as blue lines (and arrows). On top, the separated diagram with diffraction data of the DTA-TG residuals shows crystallinity but no coincidence with the other phases below.

Only the measurement of the residuals from the DTA-TG measurement shows reflections of a notably crystalline material. In agreement with the erratic loss in weight and steep rise of the heat flow in figure 2.53, decomposition of the material should without doubt be at about 375 °C. Based on the dark brown colour of the residual and the clear signs of decomposition in the DTA-TG measurement, it could be assumed to identify a caesium polysulfide, as most likely CS_2 is cleaved and emitted from the powder, but the PXRD data of the residuals could not be assigned with only one distinct sulfide phase.

Caesium trithiocarbonate methanol $Cs_2CS_3 \cdot \frac{1}{6}$ MeOH and caesium trithiocarbonate perthiocarbonate $Cs_5(CS_3)[CS_2(S_2)]_{1.5}$

The conditioned powder of 'Cs_2CS_3' **20t** was recrystallised under solvothermal conditions. With majority, orange red crystals alongside a few yellow crystals were obtained and both were successfully subjected to SC-XRD. The crystalline species are shown on the photographs in figure 2.55. None of them were identified with the desired anhydrous Cs_2CS_3, but yet unknown caesium thiocarbonates.

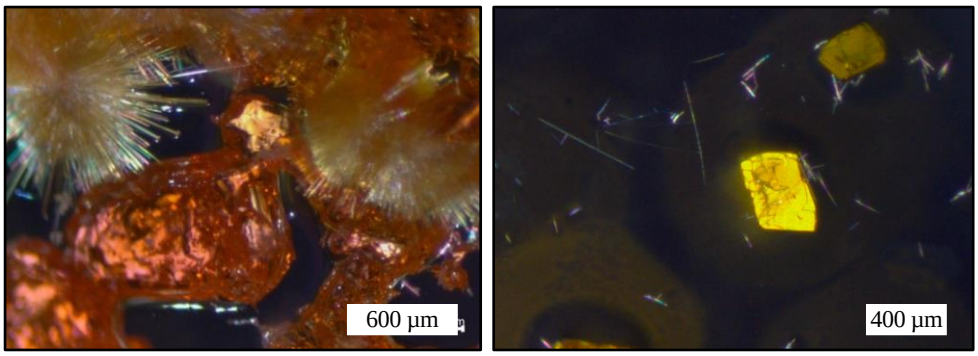

Figure 2.55: Photos of crystals obtained from solvothermal recrystallisation of 'Cs_2CS_3' **20t**. The majority of the obtained product were orange red crystals, which were identified as $Cs_2CS_3 \cdot \frac{1}{6}$ MeOH **24** (left). A minor phase, coloured in a bright intense yellow was identified as $Cs_5(CS_3)[CS_2(S_2)]_{1.5}$ **25** (right).

Crystal structure model

$Cs_2CS_3 \cdot \frac{1}{6}$ MeOH **24**, the orange red compound, crystallised with four formula units per unit cell in a monoclinic lattice. The structure model of **24** is unappealing, since the formula unit consists of twelve non-equivalent caesium ions that are charge balanced by six different trithiocarbonate units and one neutral molecule of methanol. As the number of regular lattice positions is increasing proportional to the cell volume (> 4.7 nm^3), it is not surprising that such many different sites are inhabiting the unit cell.

Attempts to find a structure model with a lower cell volume by an increase of symmetry elements, have been undertaken. At last, the residuals of the refinement, i.e., the most likely way to describe the data, was best in the displayed fashion.

Figure 2.56 depicts the crystal structure model of the orange red compound. All atoms occupy regular 4a sites obeying the $2_1/n$ symmetry elements in a primitive monoclinic lattice. The structure is not isotypic with the monohydrate, which crystallised in the orthorhombic space group $P2_12_12_1$.

As there are six trithiocarbonate units and even double the number of caesium ions per unit cell, it is difficult to see the symmetries in the structure. In figure 2.56 the view along the *b*-axis offers the best way to understand the set up. In the parallel projection, the trithiocarbonate anions seem to be *aligned* roughly with each other, but individually tilted and rotated. As a guide to the eye connections between the central carbon atoms of the CS_3^{2-} ions are drawn. Still, it is not that simple, as these marking connections have components in *b*, i.e., perpendicular to the screen plane. The distribution of caesium ions approximates locations between these grey lines. Each quarter of the cell in view along *b* has the two-fold screw axis, which is parallel to the viewing direction, located in the centre. With the blue coloured atomic ellipsoids for oxygen sites, the screw axis location can be simply obtained in the virtual middle between these sites. In the corners without the methanol molecule, the screw axis is found between the C6 sites.

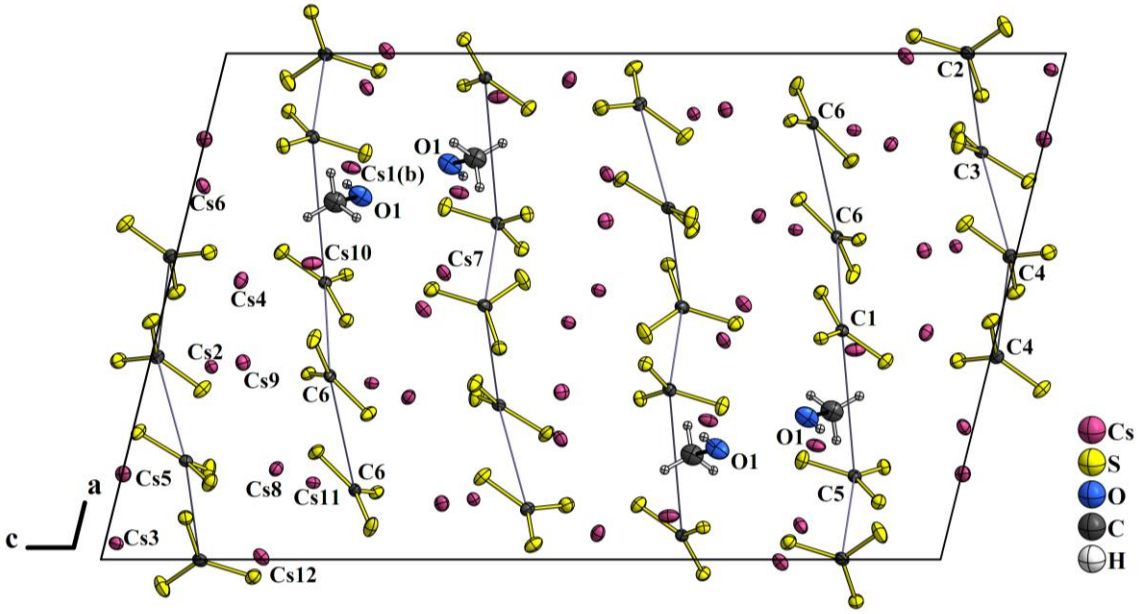

Figure 2.56: Unit cell of $Cs_2CS_3 \cdot \frac{1}{6}$ MeOH **24**. The view along the crystallographic *b*-axis gives overview on the manifold structure. All non-hydrogen atom displacement ellipsoids are drawn at 70 % probability. The connection of the CS_3^{2-} molecules between their central carbon atoms has no physical meaning it is drawn as guide to the eye.

It is not unusual to trap small solvent molecules in a solid structure, nevertheless it can be noted with interest, that only one methanol molecule per formula unit is included. The fraction of solvent molecules is quite low compared to the content of the unit cell, and one comes across the thought of the methanol molecule being one reason for the low symmetry setup of the structure. The protons at the methyl and hydroxy group of the methanol molecule are fixed in place using the *ShelX* command HFIX. Furthermore, the hydroxy

proton was fixed in distance to the oxygen atom with DFIX of 80 pm, and the proton H7BA to the methyl carbon atom C7 of 100 pm. The ISOR command was used on the non-hydrogen solvent atoms to overcome errors due to too high anisotropy of the displacement parameters. This was also performed for the invisible caesium atom Cs1(a). It occupies a position close to Cs1(b), which is shown in figure 2.57. Both ions are contributing to the sum of electron density of one unique caesium ion. However, the best option for the structure solution was to split this position into two distinct sites (a) and (b), since otherwise too much electron density resides shifted from the location of Cs1(b). The occupancy is shared to about 15 % on Cs1(a) and 85 % on Cs1(b). shows the close-up range of that distorted site and explains the surrounding coordination.

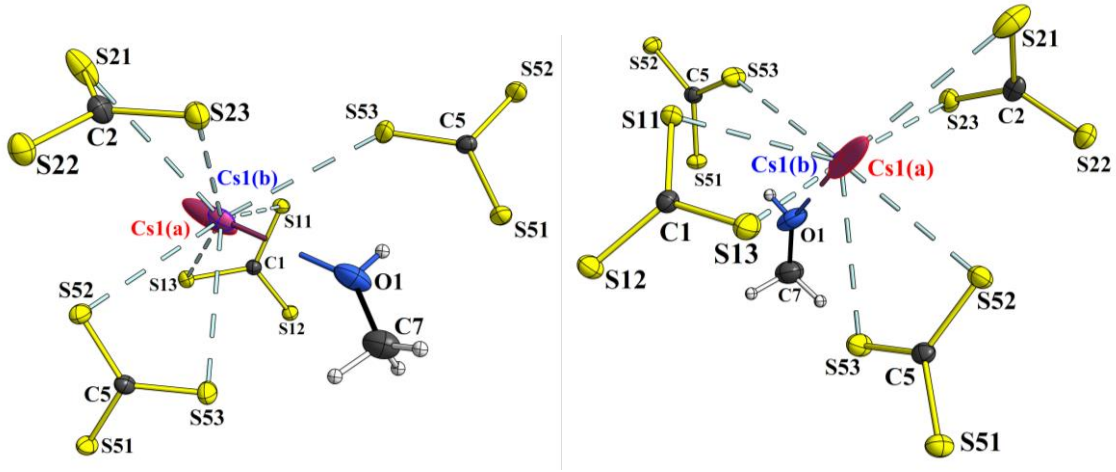

Figure 2.57: Demonstration of the coordination of the distorted Cs1 site in $Cs_2CS_3 \cdot \frac{1}{6}$ MeOH **24** with the view from two angles.

It is shown, that on the distorted Cs1 site, the incorporated methanol molecule is involved in close range. The O1 molecule is indeed the closest coordinator of the Cs1(b) ion, with 318.3(3) pm. Additionally, seven ionic Cs−S interactions are in low distance, ranging from 339.7(1) (S11) to 387.0(1) pm (S21), where the former is significantly shorter than the average Cs1(b)−S distance of 357 pm. The number and style of coordination of the Cs1(a) ion is conserved, but due to the slight position shift, the closest coordination partner is now S52 with 332.9(9) pm. Still the O1 atom lies close by at 346(2) pm, but as seen in figure 2.57, the coordination runs through the position of Cs1(b), which explains the increased distance. Compared with most of the other unique caesium ions inheriting the structure and coordinated by eight or even nine sulfur atoms, the Cs1 site is in lack of one anionic coordination, as the methanol molecule is naturally neutral in charge. Regarding the preparation and the use of methanol as solvent, it is very unlikely, that the methanol molecule was deprotonated during the recrystallisation and there is doubt in the existence

of a methylate instead of the methanol molecule. Thus, the Cs1 site is only coordinated by seven anionic sulfur atoms, of which three pairs belong to the same trithiocarbonate anion. This can be used to draw the conclusion of a weaker stabilisation of the cation, which could open the discussion of an increased movability. However, as there is another caesium ion (Cs7) that is also hetero coordinated with contribution of the oxide atom of methanol. The direct comparison of these caesium ions affords indeed the Cs7−O1 bond to be in reasonable distance of 336.7(3) pm for a dipolar interaction, like the distorted Cs1 site. Furthermore, three pairwise and one single sulfur bond is found in the connectivity list. At last, from a structural point of view, the reason for the disorder of only one caesium site in the structure, namely Cs1(a) and (b), remains unknown. It shall furthermore be emphasised, that the structure was solved by the method of a split position in case of Cs1, but moreover, at all caesium sites remains a cloud of electron density, which is naturally explained with the size of the ions and their promoted soft electron cloud. Overall, each caesium cation is coordinated by at least eight individuals, which is the expected number for alkali ions.[16]

Crystal structure model

The space group $P2_1/n$ was determined on the mixed trithio-perthiocarbonate $Cs_5(CS_3)[CS_2(S_2)]_{1.5}$ **25**, which was discovered to be the identity of the yellow side product. In contrast to the large number of unique molecules and ions in the unit cell of **24**, the yellow side product **25** contains only one unique trithiocarbonate anion, two crystallographically distinct perthiocarbonate anions, of which one is refined with a disorder, and five different caesium ion sites. The unit cell is shown in figure 2.58.

At first glance, the structure, and the symmetry properties of the mixed trithio-perthiocarbonate salt is quite simple. However, as the inversion centre present at each corner and each face centre of the cell frame, the perthiocarbonate molecule of the C3 atom is issued with disorder. It is residing in the inversion centre of the *c*-plane and was described with a four-fold orientation disorder. In figure 2.58 this disorder of the perthiocarbonate anion is omitted for clarity and is therefore graphically demonstrated in figure 2.59.

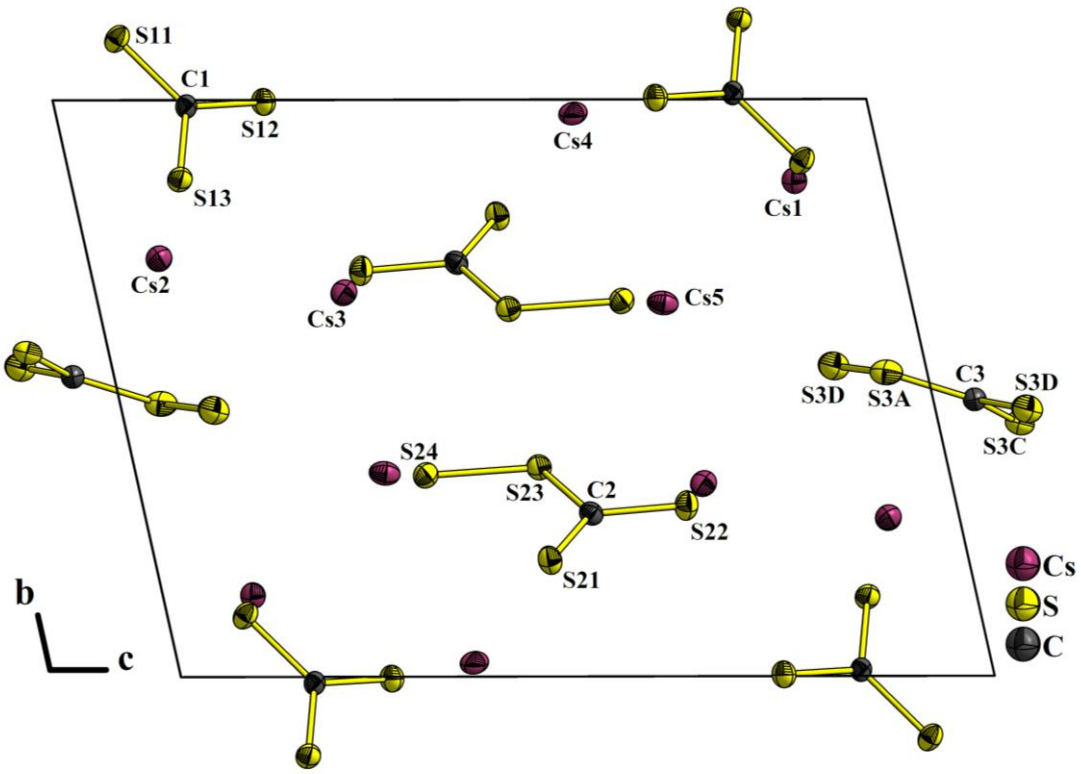

Figure 2.58: Unit cell display of $Cs_5(CS_3)[CS_2(S_2)]_{1.5}$ **25** in view along the *a*-axis. Inversion centres on each corner, cell edge centre and cell centre are the only points of symmetry in this triclinic lattice. Atomic displacement ellipsoids are drawn with 70 % probability.

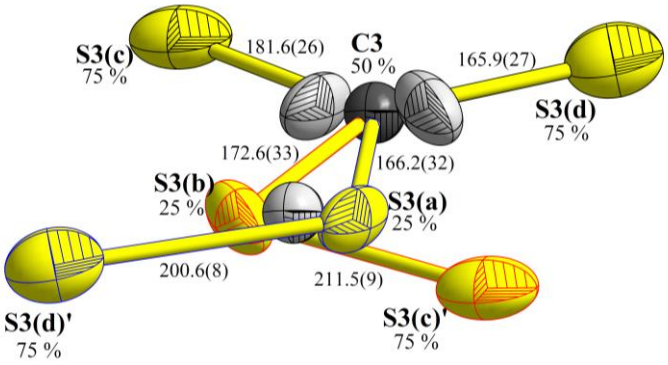

Figure 2.59: Construction of the four-fold disorder of the perthiocarbonate anion in the structure of $Cs_5(CS_3)[CS_2(S_2)]_{1.5}$ **25**. The inversion centre is located in virtual the middle. The near C3 and the far sulfur S3A and B atoms are drawn grey as they are identical but inverted to the construction showed in saturated colouration. The fraction of occupation is given in percent next to each atom. Sulfur displacement ellipsoids are drawn at 70 % probability.

Adding up to four differently oriented perthiocarbonate anions, all atomic sites a fractioned in occupation. The carbon is occupied by 50 % with respect to the inversion. Then, there is one quarter probability for each half-occupied carbon to connect to the S3(a) (blue) or (b) (red) site, with the S−S bonding to S3(d) or (c), respectively. Since each half-occupied carbon connects to either S3(a) (blue) or (b), these sites are occupied with only 25 %. S3(c) and (d) naturally obey the inversion symmetry operation as well and comprise the thiocarbonylthio group (black bold). Consistently the occupation sums up to 75 % at the S3(c) and (d) atom. It shall be emphasised, that all atoms were refined with free occupation, before fixing the values mentioned above. Furthermore, the C3 atom needed isotropic displacement to prevent it becoming *non-positive-definite*, i.e., the volume of the ellipsoid becomes negative.

Different *ShelX* compatible commands were used to analyse the best way to describe the disordered moiety. Including to see if the site could probably be a disordered CS_3^{2-} ion, the above shown solution was concluded, negating CS_3^{2-} at that position.

Generally, the perthiocarbonate can be compared with those being described in the structures of $Na_2[CS_2(S_2)]$ and $K_2[CS_2(S_2)]$ (cf. above.). However, within the C2−S bonds in the CS_3 moiety, both the non-bridging sulfur atoms S21 and S22 are decreased in length of 168.9(4) and 170.7(4) pm, respectively, compared to the bridging S23, ranging 174.8(4) pm from C2. With a little more weight, considering the small difference, the C=S double bond can be assigned to the C2−S21 bond. S21 is the *cis* sided sulfur atom with respect to the S−S orientation. The persulfide group forms a S−S bond of 203.5(1) pm length, with is in accordance with the earlier described structures. Considering the torsion angle S22−C2−S23−S24 with 179.2(2) ° the anion molecule can for simplicity be called *planar*, not being influenced by crystal lattice symmetry operations.

There are five non-equivalent cationic caesium sites found in the unit cell. Charge balance is performed by the dianionic character of the thiocarbonate molecules in which the negative charges are oscillating between the sulfur atoms. For the trithiocarbonate dianion the distribution of negative charge is shared among the three sulfur atoms. In the perthiocarbonate anion the situation should be different, as the bridging sulfur, (i.e., S23, S3(a) and S3(b)) is not able to stabilise an electron without exceeding its filled valence shell. Because the spatial probability of negative charge is here lower than at the three other sulfur atoms in the perthiocarbonate anion, contribution of S23, S3(a) or S3(b) are considered of minor importance regarding the caesium coordination. It was shown with HMO-approximations, that upon transition from CS_3^{2-} to $CS_2(S_2)^{2-}$, the π-bonding order of

the CS_3 moieties does not significantly change. Thus, the π-bonding character of the S−S bond is only fractional (< 0.1). However, this rough approximation supports the stabilised negative charges to reside at either one of the three terminal non-bridging sulfur atoms.[66]
T-he number of Cs−S coordination of each different caesium atom is nine, except only eight for Cs4. Considering the distances of strong ionic interaction below 400 pm, coordination by the sulfur atoms being attached to the distorted perthiocarbonate anion was counted with respect to the display in figure 2.58, where only one of the four possible orientations is drawn. The shortest Cs−S bonding interaction is 344.5(1) (Cs1−S11) and the longest is 388.9(1) pm (Cs3−S12). The mean Cs−S distances are 363 pm (Cs1), 366 pm (Cs2), 365 pm (Cs3), 360 pm (Cs4) and 359 pm (Cs5).
For Cs^+ ions an ionic radius of 188 to 192 pm is reported for coordination numbers eight and nine, respectively. For S^{2-} ions a radius of 170 pm can be assumed.[16,67] This sums up to ionic distances in the regime of roughly 358 to 362 pm for the Cs−S bonds. Albeit, these tabulated ionic radii are only considering oxides and fluorides, the values fit with the structure model.

2.3.4 On the perthiodicarbonate anion

The perthiodicarbonate anion has scarcely been covered in the literature. Reciting the review of GATTOW and BEHRENDT (again the original publication was not available), in 1975 SILBER et al. mentioned the $C_2S_6^{2-}$ anion as a product from tetramethyl ammonium trithiocarbonate in solution with CS_2 and methanol for the first time. The anion could be elucidated, and their crystal structure is accessible in the CSD database. They were able to determine the structure of the molecule anion to consist of two planar trithiocarbonate units, connected *via* a persulfide bridge. It crystallised with one half CS_2 solvate molecule per formula unit.[1,68] Five years later, formation of $(Et_4N)_2(C_2S_6)$ was believed upon reduction of CS_2 on a sulfur cathode using a conducting salt bearing the cation in acetonitrile solution. At that time, due to the sensitivity towards moisture, the structure of the perthiodicarbonate anion could not be obtained. However, the authors used other methods to exclude the adduct $CS_2(S_2)^{2-} \cdot CS_2$ or other thiocarbonate species and attempts to solve crystal data resulted in a triclinic lattice.[69] In the progress review by GATTOW from 1992, the perthiodicarbonate anion is not further mentioned and to the best of the authors knowledge of this thesis, it was not before 1995, when a crystal structure with the $C_2S_6^{2-}$ anion was described again. Alongside some new trithiocarbonato complexes, MÜLLER et al. elucidated the structure of $(Ph_4P)_2(C_2S_6)$.[70] Very recently a new publication containing the crystal structure of $(Et_4N)_2(C_2S_6)$ was published.[71] The report features two sets of crystal data at 90 and 150 K, respectively, and describes the preparation according to a patent by GREEN and YOUNG, who claimed the compound for the use as pesticide. From an aqueous solution of $(Et_4N)_2S_2$ upon addition of CS_2, the perthiodicarbonate precipitates as an orange solid. It is stable towards the ambient air after it was washed dry from water with *i*-propanol and diethyl ether. The product is said to be sparingly soluble in water.[71,72] The behaviour towards moisture stands in conflict with the earlier work mentioned above, telling the material is hygroscopic, back then making it impossible to identify the product crystallographically. Interestingly, the new publication by BERNHARDT does not discuss these different findings.[71]

Caesium perthiodicarbonate carbon disulfide $Cs_2(C_2S_6) \cdot CS_2$

As demonstrated above, the reaction under solvothermal conditions of alkali sulfides with CS_2 was successful for the crystallisation of some alkali trithiocarbonates. To try this route aiming to crystallise Cs_2CS_3, starting material, namely caesium sulfide, had to be prepared beforehand. The PXRD data of the obtained precursor, did not confirm the desired phase

and could be analysed to consist of the sulfur richer Cs_2S_3 **49**, which is shown in a refinement of the PXRD curve in figure 4.14, in the experimental chapter. The formation of the trisulfide could at last be explained with errors in the correct scaling of the mass of sulfur needed, proportional to the mass of caesium. It was seen for the reaction of K_2S with CS_2 (cf. above), that small impurities of K_2S_2 in the precursing material are excusable and K_2CS_3 was obtained successfully. For this reason, a slight excess of sulfur was scaled into the reaction with caesium, to avoid residual of the highly reactive metal to be left unconverted. However, trying to meet the correct stoichiometry, a second batch of caesium sulfide was prepared. This time, the PXRD displayed lower crystallinity and was refined as a caesium polysulfide multiphase (cf. figure 4.15).

Still, reactions of both the first and second batch of the sulfide starting material with CS_2 under solvothermal conditions were carried out. The powder of the second batch did not afford crystals after treatment with CS_2, and the colour of the solution remained clear indicating inert behaviour of the prepared polysulfide powder. In turn, with the first batch (Cs_2S_3 **49**), brownish yellow crystals were obtained, shown on the photograph in figure 2.60 that could be used to collect single crystal data. They were identified as the first perthiodicarbonate $C_2S_6^{2-}$ crystallised with the caesium ions and a solvate molecule of CS_2. Thus far, no other compound and particularly, none with inorganic cations, is known featuring the perthiodicarbonate anion.

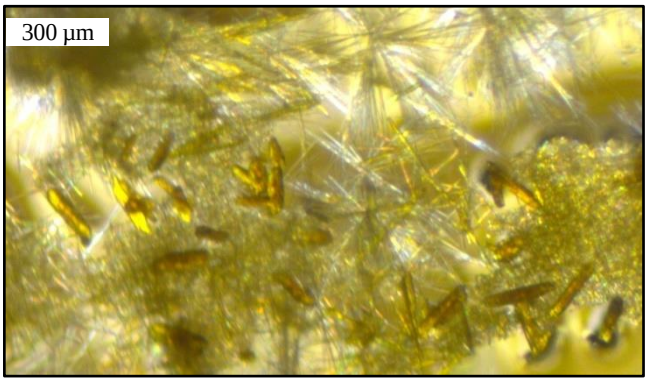

Figure 2.60: Covered in unidentified colourless side products, a few brownish yellow plank-shaped crystals of $Cs_2(C_2S_6) \cdot CS_2$ **33** were discovered.

Crystal structure model

In the crystal structure model of $Cs_2(C_2S_6) \cdot CS_2$ **33**, four formula units obey the space group symmetry $P2_1/c$ (no. 14) in a primitive monoclinic lattice. All atoms occupy the regular lattice site 4e. An extended structure fragment exceeding the unit cell is shown in figure 2.61.

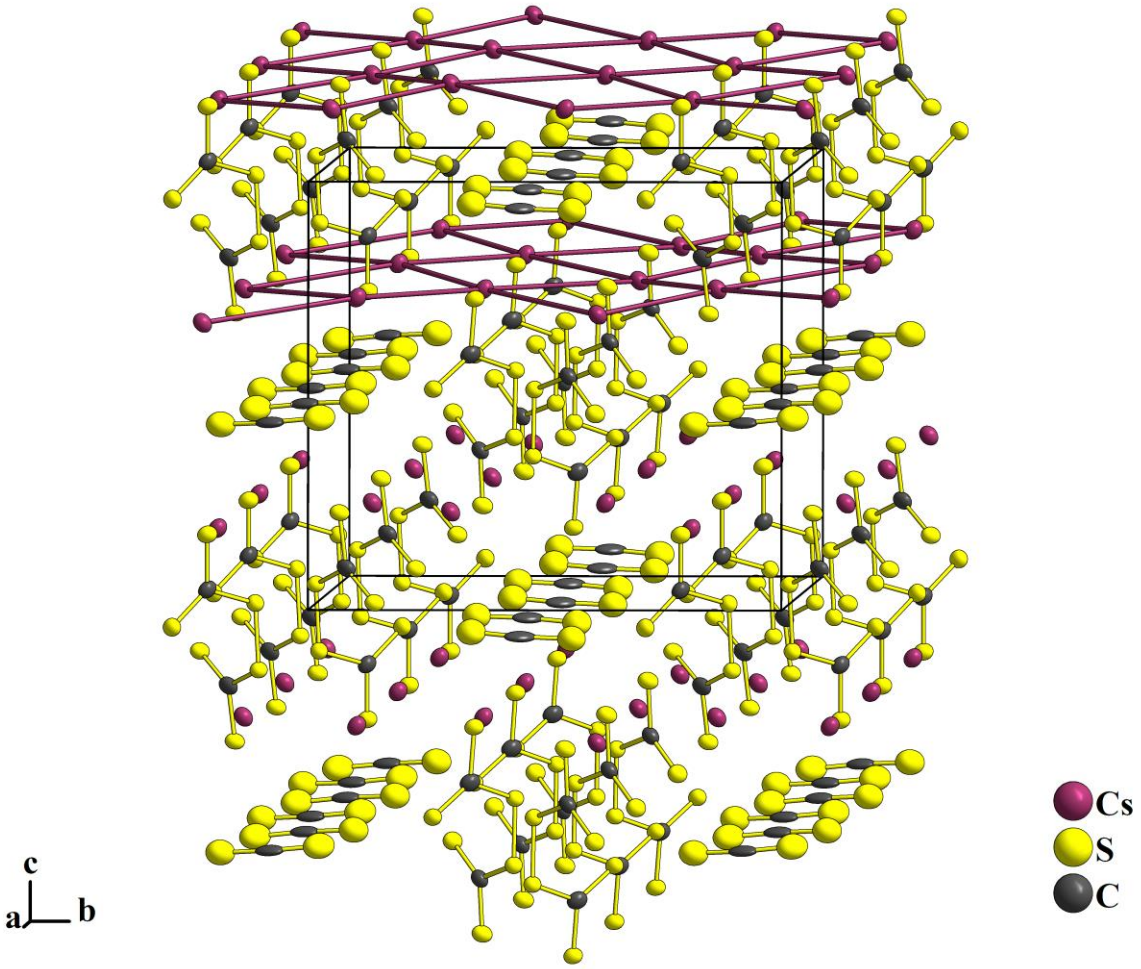

Figure 2.61: Grown structure of $Cs_2(C_2S_6) \cdot CS_2$ **33**. The caesium ions are drawn connected in the top section for better visibility of their layered fashion. All atomic displacement ellipsoids are drawn at 50 % probability. The large ellipsoids of the CS_2 molecules are discussed below.

In the upper part of the depiction of the extended structure, indicated by connections between the caesium ions, their checked pattern layer like distribution in the room becomes visible. The layers are roughly parallel to the *c*-plane and a packing motif along the *c*-axis in the style of ABAB. The A- and B layers are shifted parallel against each other. In each layer both non-equivalent caesium ions are involved in the way that the connections are drawn as a guide-to-the-eye. However, in this Cs1 only has *connection* to Cs2 cations. The terminal sulfur atoms S13 and S23 are located in the centres of the distorted squares of the checked pattern of the cationic layers (cf. figure 2.61). Thus, the anions connect the separated layers of cations. However, the room virtually filled by rows of perthiocarbonate anions along the *a*-axis is alternatively interrupted by the CS_2 molecules. Their linear

molecule axes are ordered parallel to each other and like the anions they translate along the *a*-direction.

The ionic interaction of $C_2S_6^{2-}$ with the Cs^+ is depicted in figure 2.62 for the Cs1 and Cs2 site on the left and right, respectively.

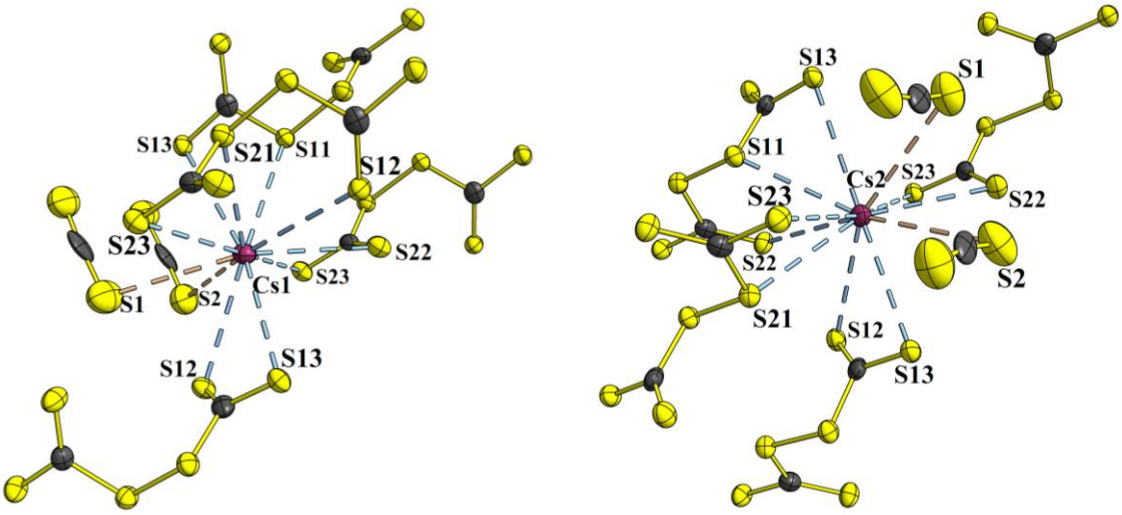

Figure 2.62: Coordination of the cations Cs1 and Cs2 in $Cs_2(C_2S_6) \cdot CS_2$ **34** on the left and right, respectively. All atomic displacement ellipsoids are drawn at 50 % probability. Note, the dashed ionic interactions are coloured in blue and orange for those with the CS_2 molecules.

Particularly, the atomic displacement ellipsoids of the sulfur atoms of the CS_2 molecules are much bigger compared to those of the anions, indicating errors in the solution. As seen above, in other crystal structures, disorder of the thiocarbonate groups is a frequent issue. It was thus tried to fit the moiety with disordered trithio-, perthio- or perthiodicarbonate anions, however, here, it was not possible to fill the room differently than as shown. The C=S distances 152(1) and 157(1) pm are reasonable for a CS_2 molecule compared with the value of 152.8 pm in $(Me_4N)_2(C_2S_6) \cdot ½\ CS_2$.[68]

The spheres around the caesium ions are occupied by four $C_2S_6^{2-}$ anions and two CS_2 molecules, which all offer Cs−S distances lower than 400 pm, considering these to indicate interaction. Of course, the strongest type of interaction in this compound should be due to the coulomb fields of the ions. The perthiodicarbonate carries two negative charges, which are expected at one of the terminal sulfur atoms but delocalised in their π-electron system. Probability of the free charges to be located at or in the S−S bridging, i.e., the perthio groups, is assumed low, as this would destabilise the molecule by occupying anti-bonding orbitals. A similar reason was addressed about the bridging sulfur atom in the perthiocarbonate $CS_2(S_2)^{2-}$ anion. However, for both cations nine close ranged sulfur atoms

between 353.4(3) (C1−S11) and 386.3(3) pm (C2−S22) are present. The mean value is 365.1 and 367.0 pm for Cs1 and Cs2, respectively. The shortest and longest Cs−S distances between the cations and the CS_2 molecules are considerably long with 376.1(5) and 404.4(6) pm, respectively. This rises evidence for the neutral molecule to be less strongly bound to the cations.

As introduced, carbon disulfide was also included in the first ever mentioned structure of $(Me_4N)_2(C_2S_6) \cdot ½\ CS_2$,[68] which was also called a clathrate for this reason.[69] The crystal data was recorded at RT, making it doubtful to resolve the CS_2 molecule in an ordered fashion. The methyl groups on the $(Me_4N)^+$ cations are sterically masking the positive charge at the nitrogen atom and one can retrieve the distances between sulfur and the closest methyl group carbon atoms of six $(Me_4N)^+$ ions from the published data, obtaining values above 362 pm.

The above stated assumption of low or maybe even no interaction with the cations further agrees with the neutrality and *non-polarity* of CS_2, leaving no reason for dipole-cation interaction. Residual electron density peaks at the CS_2 in the structure data may indicate the neutral molecules to more or less freely move along the one-dimensional cavities depicted in figure 2.61. In conclusion, the trapping of CS_2 molecules is reasonable to explain with weaker dispersion interaction, e.g., VAN-DER-WAALS interaction, considering the relatively soft polarisable electron shells of the involved atoms. In this picture, the presence of weak attraction between the soft Cs^+ and sulfur atoms of CS_2, can be assumed.

Furthermore, following the technique described by MÜLLER et al., coincidently the orange $(Ph_4P)_2(C_2S_6)$ **34** was crystallised. It formed upon reaction of a solution of K_2CS_3 in DMSO treated with aqueous $(Ph_4P)Cl$.[70] A specimen is captured on the photo in figure 2.63. As the structure was published earlier, it is left out at this point. However, the structure of the $C_2S_6^{2-}$was obtained once more and could be compared to those determined in the caesium compound **33**.

In principle, the bulky phosphonium cations arrange in layers and enfold the $C_2S_6^{2-}$ ions, which thereby are separated individually. All atoms in the primitive monoclinic lattice with the space group $P2_1/c$ (no. 14) occupy regular sites.

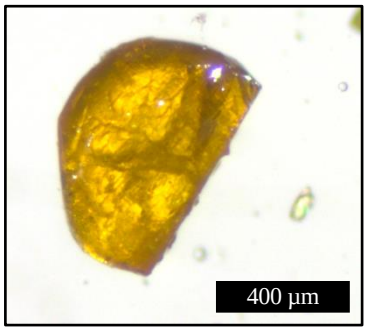

Figure 2.63: Crystallite of tetraphenyl phosphonium perthiodicarbonate $(Ph_4P)_2(C_2S_6)$ **34**.

X-ray structure of $C_2S_6^{2-}$

In figure 2.64 the perthiodicarbonate anion as determined in the structures of $Cs(C_2S_6) \cdot CS_2$ **33** and $(Ph_4P)_2(C_2S_6)$ **34** are compared. Within the accuracy of the measurement, the carbon atoms share planarity with the adjacent sulfur atoms. In $Cs(C_2S_6) \cdot CS_2$ **33** the planarity deviates by about 4° considering the persulfide of the other trithiocarbonate moiety, e.g., S11 is not in plane with the CS_3 moiety of C2 and vice versa. This distortion is much larger in $(Ph_4P)_2(C_2S_6)$ **34**, where the dihedral angle S21−S11−C1−S13 is 11.3°, while that of S11−S21−C2−S23 is 2.8°. The dihedral angles between the CS_3 moieties *via* the perthio bridge, is 89.1(6) and 93.6(2)° in $Cs(C_2S_6) \cdot CS_2$ **33** and $(Ph_4P)_2(C_2S_6)$ **34**, respectively, which is comparable with the tetramethyl (87.12°) and tetraethyl (86,92°) ammonium slats.[71]

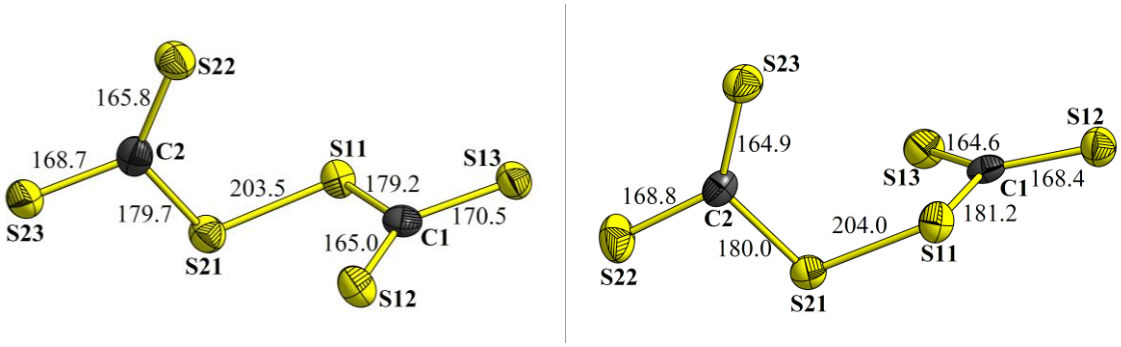

Figure 2.64: Close up depiction of the perthiodicarbonate anion $C_2S_6^{2-}$ determined to be included in the crystal structures of $Cs_2(C_2S_6) \cdot CS_2$ **33** on the left and $(Ph_4P)_2(C_2S_6)$ **34** on the right. The numbers are the bond lengths in pm. In both structures, none of the molecule atoms occupy special lattice positions. All displacement ellipsoids are drawn at 50 % probability.

Indicated by the significantly shorter C−S bond lengths, given in figure 2.64, the C=S double bond is delocalised between S12 and S13 as well as S22 and S23, and a negative charge is oscillating between the sulfur atoms. In **33** (in **34**), the respective S−C−S angle is

128.9(8)° (130.2(3)°) at S12−C1−S13 and 129.6(7)° (129.8(3)°) at S22−C2−S23, which is significantly increased from the ideal 120° in the trithiocarbonate geometry. The S−S bond length is comparable to that in perthiocarbonate anions and lies in the range of distances reported for S−S single bonds in S_8 and S_x^{2-} chains.[13] Accordingly, the C−S bond towards the perthio moiety is expected a single bond, approved through determination to about 180 pm. The C−S−S−C dihedral angle in this molecule section can be understood as a result of the sp^2-hybridisation, i.e., the repulsion of the two lone pairs of each of the sulfur atoms occupying the p_z-orbital orthogaonal to the CS_3 plane and one sp^2-orbital in plane directed into free space. For approval, the anion structure of the oxygen homologue, $C_2O_6^{2-}$ in $K_2C_2O_6$, where the C−O−O−C dihedral angle is also 93°, can be taken into account.[73] The related $Rb_2C_2O_6$ was found to crystallise isotypically, however, the dihedral angle of the peroxodicarbonate anion is 175°, i.e., almost planar, suggesting a sp^3-hybridisation in consideration of the lone pair orbital repulsion.[74] At last the ion packing and intermolecular interactions in the crystal seem to influence the absolute structure quite variably.

It is known, that sulfur is able to form stable homonuclear chain ions S_x^{2-} ($x >> 4$), and that compared to its smaller homologue, oxygen, is suffering from this lone pair repulsion, making it not possible to exceed O_x^{2-} moieties above $x = 4$. In the analogous peroxodicarbonate $C_2O_6^{2-}$ occupation of anti-bonding π^*-orbitals weakens the peroxo group bond, leading to an increase of the bond length in such a molecule anion. For sulfur, with its larger and softer electron cloud, the occupation of orbitals as said above does not severely affect the bond length in the perhtio group.

2.4 Spectroscopy of trithiocarbonic acid and alkali thiocarbonate compounds

2.4.1 IR spectroscopy on trithiocarbonic acid

Generally, it is convenient to derive salts, esters, etc. from their parent acid. However, in a preparative view, many of the 1,1-dithiolate acids are actually prepared from their associated salts, esters, etc. formed from reaction of the respective moieties with CS_2 in the first place.[1]

As mentioned in the introduction, $SC(SH)_2$ is a red liquid at RT, tempting to be called an *oil* as it behaves hydrophobic, which can be seen in figure 2.65. The *hydrophobic* nature was quantified by solution experiments with different solvents, where the solubility of $SC(SH)_2$ in water is only 0.1 mol/L.[75] Thus, speaking of the trithiocarbonic acid, herein the *pure* liquid $SC(SH)_2$ is meant, where for instance hydrochloric acid is always an aqueous solution of HCl.

Figure 2.65: From the aqueous solution of K_2CS_3 **9** and 10 % hydrochloric acid (yellow) using a standard glass funnel, the red $SC(SH)_2$ **1** separates in an insoluble phase at the bottom. Bubble evolution (H_2S ↑) was observed during the process.

Extensive work on literally all properties of $SC(SH)_2$, including the determination of the crystal structure, have been published during the second half of the last century. Major effort in this regard was spent by GATTOW, KREBS and co-workers, who characterised the acid unequivocally.[22,75,76,77] $SC(SH)_2$ is very volatile and irreversibly decomposes soon according to the reported equation 2.4.[77] It cannot be distilled and attempts to store larger volumes of the order of 10 mL at low temperature in a PTFE tape sealed crew lid vial did not stop an obnoxious odour to be released supporting its poor stability. Fresh preparation was of low yield compared to the consumed amounts of K_2CS_3 **9** used for preparation.

Attempts to use the acid as a reagent in preliminary experiments aiming for new routes to prepare trithiocarbonates were of modest results and could not develop as a key topic in this work.

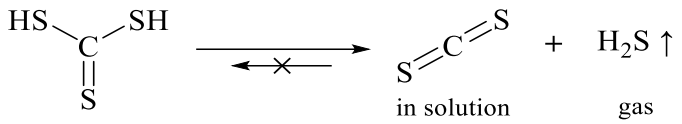

2.4

Infrared spectroscopy

A simple method to prove the successful preparation of $SC(HS)_2$ was to record an IR spectrum, which is shown in figure 2.66. Naturally, the IR properties of $SC(SH)_2$ were already known, which was used for confirmation of the assigned modes.

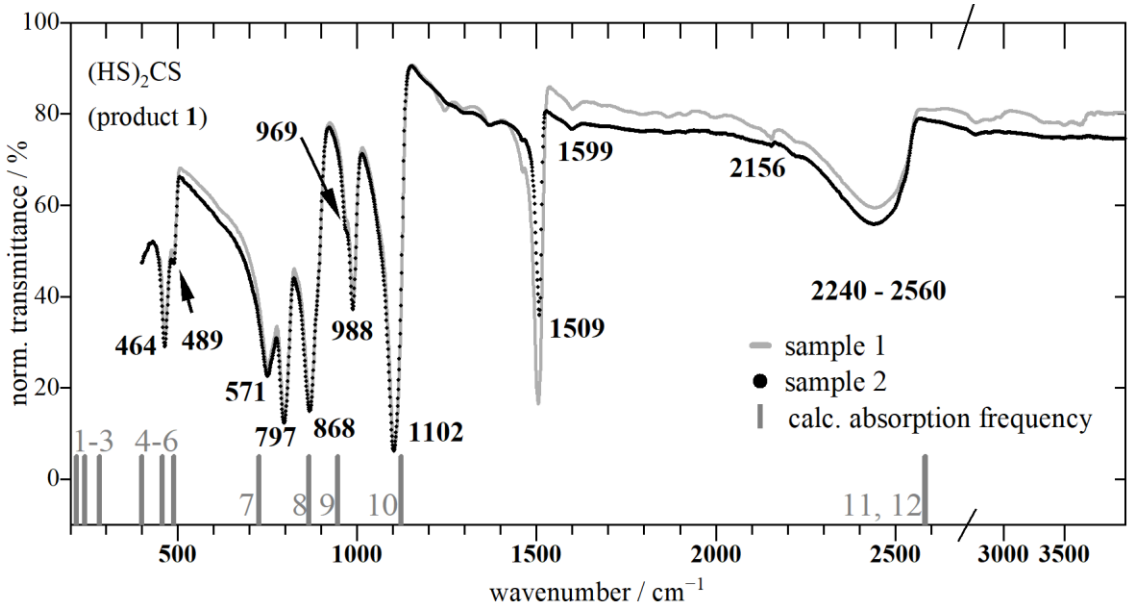

Figure 2.66: IR spectrum of $SC(SH)_2$ **1** of two individual samples (black solid and blue dotted) from different batches. At the bottom, the grey vertical lines mark the position of calculated modes individually numbered (details are given in the paragraph).

The IR modes assigned in the spectrum of two individual batches of $SC(SH)_2$ **1** almost perfectly match the data from the original reference. In the exact values and those published by GATTOW, KREBS and MÜLLER in 1967, who assigned the planar $SC(SH)_2$ molecule with C_{2v} point symmetry,[78] are presented.

As the acid successively decomposes, a sharp C=S stretching mode $\nu(CS_2)$ at about 1500 cm^{-1} originating from CS_2, which is dissolved in the main phase of $SC(SH)_2$ was obtained in addition to the inherent modes of the $SC(SH)_2$.

The spectrum was complemented with the calculated values of vibrations which based on the molecule structure described in the crystal structure model published by KREBS et al. in 1980. The geometry optimisation is summarised in table 5.11 on page 260 in the appendix section. The best agreement with the X-ray structure model was obtained with a PBE0 hybrid functional with implementation of cc−pVTZ base set for the carbon and sulfur atoms.[79,80,81]A slight decrease or increase in the optimised bond lengths are due to the calculation of the molecule in isolation, while experimentally, the bridging S−H···S hydrogen bonds between the molecules should result in elongation bonds. For the comparison, care must moreover be taken, as the calculation is based on a solid state structure at low temperature (140 K), while the measurement data and the reference values stemmed from $SC(SH)_2$ in the liquid aggregate state at RT. Table 2.7 summarises the absorption centres of experimental data and the calculated frequencies (cf. numbers in diagram) of this work with those published earlier. The molecule symmetry C_{2v} was confirmed in the optimisation calculation, although in the solid state it is reduced to C_s because the two C−S−H connections, interacting with surrounding molecules *via* hydrogen bonds, are asymmetric about the C=S bond.[33]

Table 2.7: IR data comparison for $SC(SH)_2$ with assignment of absorption characteristics. All values are given in cm^{-1}, irreducible characters are given elsewhere.[78]

	this work		references	
vibration character[78]	calculation (no.)	experiment*	GATTOW et al.[75]	MÜLLER et al. [78]
T		RT	RT[?]	263 K
$\delta_{ip}(CS_3)$	218 - 281 (1 - 3)	not included	not included	~ 200 - 300
$\gamma(CS_3)$, ν_s(C−S)	399, 456, 488 (4 - 6)	464 m 489 sh	462 m	465 487
γ_{op}(CSH)	727 (7)	751 s	752 m	755[?]
δ(CSH)	866 (8)	797 s 868 s	802 s 875 s 895 m	805 876
ν_{as}(C−S)	946 (9)	969 sh 988 m	972 m 990 s	990
ν(C=S)	1122 (10)	1102 vs	1115 s	1115
CS_2[a]	–	[a]1509 s	1522 w	
		[b]1599 vw	1605 w 2150 vw	
		[b]2156 vw		
ν_s(SH), ν_{as}(SH)	2583, 25843 (11, 12)	2240 – 2560 bm	2500 s	~ 2500

* Sample 2; S^{I}double/S^{II}single bound sulfur; v very, w weak, m medium, s strong, b broad, sh shoulder; [?]uncertain, [a] C=S stretch, [b] non-fundamental combination absorption of e.g., ν(C=S) + ν_s(C−S).

The calculated modes no. 11 and 12 (at almost the same frequency) are asymmetric and symmetric S−H valence stretching vibrations (ν_s(SH), ν_{as}(SH)) of the protonated sulfide atoms, respectively. In the recorded spectrum these modes are included with a shift towards lower energy, consistent with the comparison of a solid (calculation, stronger bonds) and a liquid (IR experiment). The detected IR signal centred at 2441 cm^{-1} is relatively broad, which supports the intermolecular S−H···S hydrogen bonds to be modulated in the liquid state. (Diluting of $SC(SH)_2$ in CCl_4 results in sharpening of that absorption due to depletion of intermolecular S−H···S association.[75]) With agreement the calculated modes 7 - 10 match the centre of intensities in the data, which are furthermore consistent with the reports (cf. table 2.7). The frequency window between 700 and 1000 cm^{-1} features resonances with several out-of- and in-plane deformation absorptions (γ_{op} and δ_{ip}, respectively) as well as symmetric C−S stretching modes ν_s(C−S).

Finally, the peak at 464 cm^{-1} (with shoulder at 498 cm^{-1}) can be either assigned with the calculated out-of-plane γ vibration (no. 5) of the carbon atom from the CS_3 plane, or the symmetrical C−S valence stretching (no. 6). In anticipation of the IR spectra discussed for alkali and barium trithiocarbonates below, both vibrations should be observed in IR and are likely to overlap. The output modes 1 – 4 below 400 cm^{-1} agree with the characterisation in the reference, but the data collection was limited to as low as 400 cm^{-1}.

2.4.2 IR, RAMAN and UV-Vis spectroscopy on thiocarbonate salts

The trithiocarbonate molecule anion has $N = 4$ atoms, thus $3N-6 = 6$ degrees of freedom for vibration (non-linear molecule) should be expected.[82] Due to its trigonal planar shape, it can be characterised ideally with D_{3h} symmetry within the group theory. Proper assignment and classification of vibrational modes call for the group theoretical fundamentals, namely, application of the character tables of the respective point groups. However, at this point, the full derivation is neglected, as previous work in this concern is referred in the following.
In line with earlier investigations, it was found that the ideal D_{3h} point symmetry of the CS_3^{2-} ion is however lowered due to the influence of the COULOMB field in the ionic crystal.[82] This *site symmetry effect* is typical for molecules in the crystal lattice (i.e., interaction with surrounding moieties). Therefore, the trithiocarbonate anion in solid state is unlikely to a strictly apply to D_{3h} symmetry, but depending on crystal lattice site symmetry, the point groups C_{2v}, C_2 or C_s are frequent. As displayed in table 2.8, this results in splitting of degenerated normal modes of D_{3h} as well as activating all six resulting normal modes to both IR and RAMAN.[83,84] Furthermore, the interaction between molecules may be represented by combination, thus more than the number of fundamental modes may be observed.

Table 2.8: Correlation between the point symmetry and their IR and RAMAN activity for ideal D_{3h} and sub-groups.[83]

molecule symmetry		molecule symmetry	
vibration	D_{3h}	vibration	C_{2v}, C_2, C_s
$\delta_{ip}(CS_3)$	d IR (+ R)	$\delta_{ip}(CS_3)$	IR + R
			IR + R
$\nu_s(C-S)$	R	$\nu_s(C-S)$	IR + R
$\gamma_{op}(CS_3)$	IR	$\gamma_{op}(CS_3)$	IR + R
$\nu_{as}(C-S)$	d IR (+ R)	$\nu_{as}(C-S)$	IR + R
			IR + R

R = RAMAN, d = degenerate

For example, the total symmetric C−S stretching vibration ν_s(C−S) of all three sulfur atoms bound to the carbon, should be RAMAN active only, as the dipole moment of the CS_3^{2-} molecule is not changed and therefore the vibration is invisible in the infrared. Due to the symmetry reduction resulting from the crystal interaction in the solid state this mode becomes visible in IR too, which was concluded in 1965 from investigation of some heavy metal trithiocarbonates.[82,83]. This means that deviations of planarity, non-equivalent C−S bond lengths or intramolecular deviation in the S−C−S angles which were determined

within the limits of experimental uncertainty theoretically influence the vibrational spectra. However, in truth these crystallographic details are masked in the spectra and cannot be expected to be determined in a one-to-one fashion. One reason for that is the temperature difference in the analytic methods (X-ray crystal data at 100 or 150 K vs. IR and RAMAN at RT). With rising temperature, increased deviation from the determined structure is reasonable due to the stronger molecule vibration.

To bring the single crystal structure with the vibrational data together, supporting calculation of the molecule were considered. DFT (and occasionally MP2) based geometry optimisations were carried out to subsequently simulate IR and RAMAN frequencies. Using a tolerance factor for the implemented molecule structure obtained by SC-XRD, allowed to adjust the limits of geometry change. Thus, with *no tolerance* the CS_3^{2-} anion was left in the lowest C_1 symmetry and increasing the factor allowed to compute higher possible molecule symmetries. However, it was found, for the trithiocarbonate that using the same hybrid functionals and atomic base sets but changing the symmetry tolerance, afforded no change in the optimised structure. In table 5.12 in the appendix, the calculated values for the isotropic C−S bond length applying the hybrid functional PBE0 with different base sets for the atoms are listed.

IR and RAMAN spectroscopy on alkali and barium salts

The spectra of K_2CS_3 **9** (powder), $K_2CS_3 \cdot H_2O$ **10** (powder) and $K_2[CS_2(S_2)]$ **29** (crystals) are summarised in figure 2.67 for the purpose of direct comparison of the trithio- and perthiocarbonate anions in the solid structures discussed above. Note, that for each compound the IR and RAMAN spectra are drawn at the top and bottom of the respective diagram, respectively. It was expected to see additional pronounced S−S vibration of the perthiocarbonate in the RAMAN spectrum. The ATR-IR and RAMAN spectra of powder samples of '$LiCS_3$' **2**, 'Rb_2CS_3 **16**', 'Cs_2CS_3' **20t**, and $BaCS_3$ **26** are plotted in figure 2.68. In first iteration, all the spectra of samples expected to include trithiocarbonate show widely similar IR absorptions and RAMAN intensities.

Fortunately, the powders (PXRD) of K_2CS_3 **9** and $BaCS_3$ **26** could be identified sustainably with the structure model previously discussed (cf. graphical RIETVELD refinements). It was seen that there are three non-equivalent CS_3^{2-} anions, i.e., three anion site symmetries, in the crystal structure of K_2CS_3 **12**. For in the crystal structure of $BaCS_3$ **27**, in turn, there is just one unambiguous anion. However, in the powders, the strict crystallographic site

symmetry of the single crystal must be considered softened by cancellation of the long-range order and cumulation of additional intrinsic impurities (e.g., lattice defects).

As the crystallographically indistinct compounds ‘$LiCS_3$’ **2**, ‘Rb_2CS_3’ **16**, ‘Cs_2CS_3’ **20t**, as well show the expected spectroscopic properties of CS_3^{2-}, it is inferred, that they all include a 1,1-dithiolate and most probably a trithiocarbonate ion. In particular, the powder samples of ‘Li_2CS_3’ **2** and ‘Rb_2CS_3’ **16** could not be compared/identified using PXRD data. Hence, for those products, although the structure remains is unknown, the presence of a thiocarbonate can be eventually confirmed from the spectra.

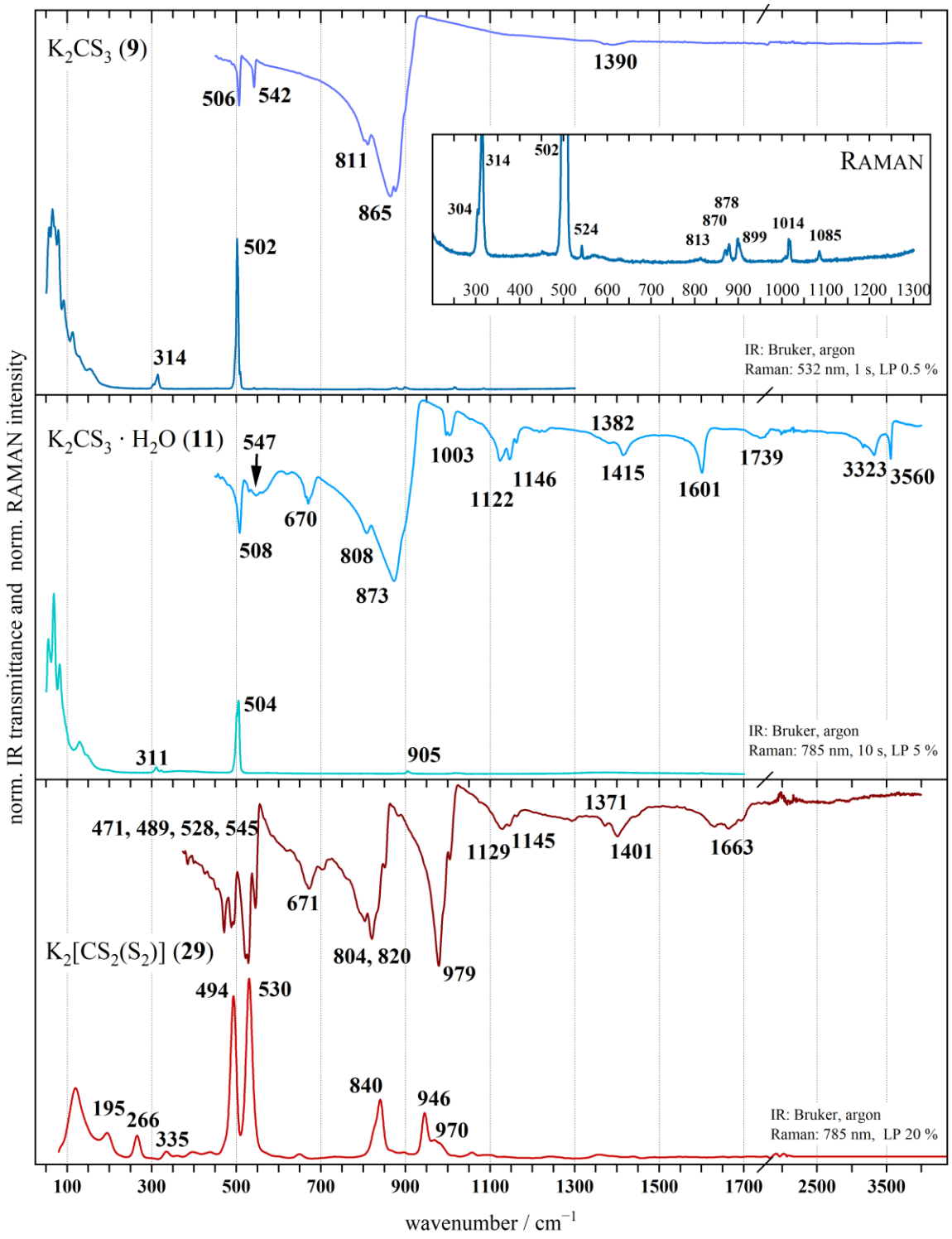

Figure 2.67: IR (top) and RAMAN (bottom) spectra of the potassium salts K_2CS_3 **9** (top field), $K_2CS_3 \cdot H_2O$ **11** (mid field) and $K_2[CS_2(S_2)]$ **29** (bottom field). Insets show enlarged Raman data. Numbers give peak centre location in cm^{-1}. Measurement specifications at the bottom right of each field.

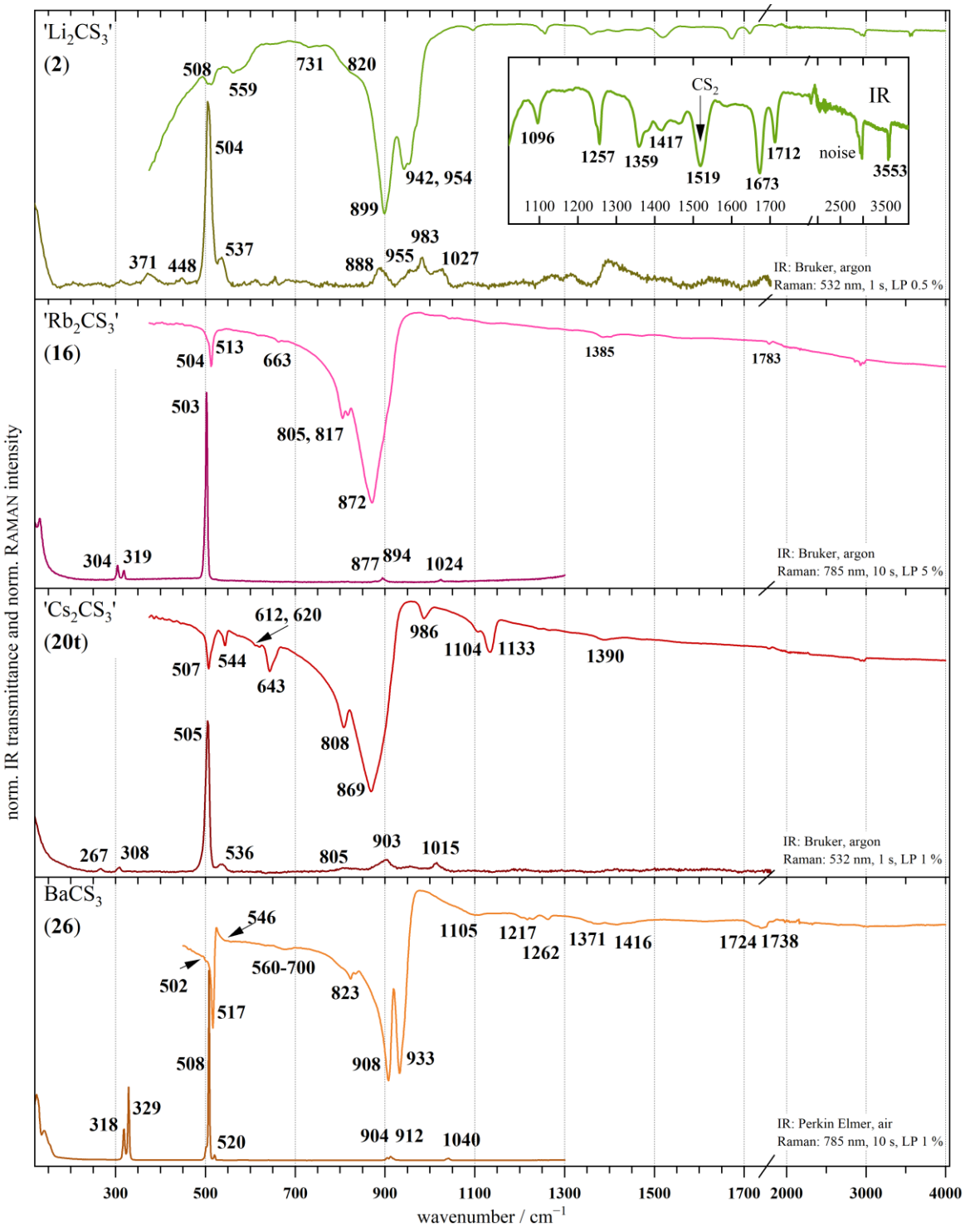

Figure 2.68: IR (top) and RAMAN (bottom) spectra of obtained powder of 'Li_2CS_3' **2** (top field), 'Rb_2CS_3' **16** (top mid field), 'Cs_2CS_3' **20t** (bottom mid field) and $BaCS_3$ **26** (bottom field). Numbers give peak centre location in cm^{-1}. For measurement specifications see corners.

At low wavenumbers, broad RAMAN peaks below 250 cm^{-1} originating in lattice vibrations have been recorded but are not discussed. Since solids were used, they are likely to occur from lattice vibrations and do not necessarily belong to certain molecular vibration.[84]
Between 300 and 350 cm^{-1} it was observed that the degeneracy of the CS_3-in-plane deformation vibration δ_{ip}(C−S) is cancelled and split in two RAMAN modes, due to site symmetry reduction (cf. table 2.8).[83] Comparing the RAMAN spectra in figure 2.67 and 2.68 there are apparently different grades of this phenomenon. For instance, in the spectrum of K_2CS_3 **9**, the peak at 304 cm^{-1} is resolved as a shoulder of the more prominent mode at 313 cm^{-1}, i.e., energetically close. In turn, in the spectra of 'Rb_2CS_3' **16**, 'Cs_2CS_3' **20t** and $BaCS_3$ **26**, two individual bands are relatively well resolved, indicating an larger energy difference of the deformation mode. The signals in the RAMAN spectrum of 'Li_2CS_3' **2** are of too low resolution, but still broad signals could be detected in this region, approving for $\delta_{ip}(CS_3)$.
At around 500 cm^{-1} the total symmetric C−S stretching mode ν_s(C−S) (IR inactive only for D_{3h}) is located. As expected, there was a strong and acute peak in all RAMAN spectra detected. Significantly difference is seen in the spectrum recorded on $K_2[CS_2(S_2)]$ **29** crystals, where two strong bands are detected, which are discussed below. In the IR, at the almost same wavenumbers, a relatively strong group of absorptions is observed. The out-of-plane deformation vibration $\gamma_{op}(CS_3)$ (with D_{3h} only active in IR) is located close to ν_s(C−S), at a similar wavenumber.[83] Additionally, moving towards higher wave numbers, a second IR absorption (ca. 540 – 560 cm^{-1}) could be measured for K_2CS_3 **9**, 'Li_2CS_3' **2**, 'Cs_2CS_3' **20t** but not for 'Rb_2CS_3' **16** and for $BaCS_3$ **26** the peak is smeared to a broad bump. In the RAMAN spectra at this position, a weak mode is found (520 – 530 cm^{-1}; very weak for 'Rb_2CS_3' **16**). This spectral range is thus summarised to show both the strong RAMAN peak of ν_s(C−S) and the IR absorptions of $\gamma_{op}(CS_3)$, which might be split in analogy to δ_{ip}(C−S) or due to the site effect. In IR it is thinkable that the total symmetric valence stretching vibration ν_s(C−S) is observed because of molecule symmetry lowering. In this sense, ν_s(C−S) may become active (cf. table 2.8), but should still be weak and likely to be overlapped by the IR active deformation mode(s) $\gamma_{op}(CS_3)$. Vice versa, this deformation vibration may also occur weakly in the RAMAN spectra on the right of the intense band valence stretching band.[46]
Moving towards higher energy, modes unsuitable for the trithiocarbonate anion are observed. For instance, 'Cs_2CS_3' **20t** absorbed IR radiation at 612, 620 and 643 cm^{-1}. 'Li_2CS_3' **2** (731 cm^{-1}), $K_2CS_3 \cdot H_2O$ **11** (670 cm^{-1}) $K_2[CS_2(S_2)]$ **29** (671 cm^{-1}) and $BaCS_3$

26 exhibits a broad absorption in a similar region, which also holds for 'Rb_2CS_3' **16** (very weak). In earlier publications, an absorption at 668 cm^{-1} was reported and proposed to originate from an overtone of doubled frequency of $\delta_{ip}(CS_3)$.[83] Otherwise, these signals could be assigned to impurities (e.g., oxidation products) of foreign origin. At this point the PXRD analysis is referred, where some indications for contamination by other phases were seen. Although these could not be elucidated by structure information, for example, contamination with carbonate (CO_3^{2-}), thiosulfate $(S_2O_3)^{2-}$ or polysulfides (S_x^{2-}) is imaginable. Moreover, liberational modes of water of crystallisation usually show up between 200 and 600 cm^{-1}. H_2O however should always add O−H modes above 1600 and 3500 cm^{-1} to a spectrum (bending and valence stretching, respectively), and except for $K_2CS_3 \cdot H_2O$ **11** such cannot be observed properly.[84] In conclusion, a reason for additional (non-fundamental) modes should be the combination of fundamentals in the case for 'Cs_2CS_3' **20t**, $K_2CS_3 \cdot H_2O$ **11** and $K_2[CS_2(S_2)]$ **29**, where these foreign absorptions are relatively well pronounced. However, they could at last not be explained unambigously in consideration of the fundamental vibrations of trithiocarbonate. In the other spectra the influence of impurities cannot be excluded.

The neighbouring and most intense IR absorptions are found roughly between 800 and 950 cm^{-1} for the alkali and barium thiocarbonates. In the ideal symmetry (D_{3h}) the degenerate asymmetric ν_{as}(C−S) stretching vibration is found here. Lowering the symmetry to C_{2v} (or C_2, C_s, …) gives two groups of absorptions, likewise already seen in the RAMAN bands near 300 cm^{-1}.[46] An extreme divergence from D_{3h} is described with the structure of the perthiocarbonate $CS_2(S_2)^{2-}$, which possesses C_s symmetry (cf. below).

The earlier published investigation of $PbCS_3$ and Tl_2CS_3 have been meaningful in this regard, concluding, the stronger the distortion of the molecule anion (i.e., stronger the divergence from D_{3h}), the larger the splitting of the doubly degenerate asymmetric valence stretching ν_{as}(C−S).[83]

The IR spectra in figure 2.67 and 2.68 show different courses of the curves in this region. Generally, the strong absorption is split or contains a shoulder or both. In the spectra of K_2CS_3 **9**, $K_2CS_3 \cdot H_2O$ **11**, 'Rb_2CS_3' **16** and 'Cs_2CS_3' **20t**, a medium strong shoulder at lower wavenumbers accompanies the local strong absorption, indicating a less extreme deviation from D_{3h} symmetry of the CS_3^{2-} ions. Interestingly, in the IR spectrum of K_2CS_3 **9** both absorptions are split to individual peaks, separated about only a couple of wavenumbers, which could be due to the individual molecules in the solid structure. The product 'Li_2CS_3' **2** absorbed only weakly at 820 cm^{-1} and the intense absorption above is indeed bisect (899

and 942 cm^{-1}). This may be compared with the IR curve of $BaCS_3$, which yields no absolute exclusion of the trithiocarbonate anion or a similar structured 1,1-dithiolate to be part of the compound 'Li_2CS_3' **2**. The IR spectrum of $BaCS_3$ **26** is designed with two strong absorptions in this region, too, which is in agreement with earlier publications. $BaCS_3$ was investigated by different authors and at last, by partial isotope substitution with ^{13}C, it was concluded that the origin for the shoulder (here 823 cm^{-1}) should be a ν_s(C−S) + δ_{ip}(CS_3) combination.[55,82,85] The contribution of the isotope substitution was found only to change the δ_{op}(CS_3) signal (near 500 cm^{-1}) with respect to its intensity and its frequency and thus was denied to take part in the combination vibration.[82]

With this, the shoulder in the spectrum of $BaCS_3$ **26** at 823 cm^{-1} should be the claimed combination vibration in figure 2.68. The strong absorptions at 908 and 933 cm^{-1} are in turn again due to the symmetry lowering and removal of the degeneracy of ν_{as}(C−S). It is shifted to higher energy due to a reasonably stronger crystal field effect stemming from the divalent Ba^{2+} ions.

The IR region above 1000 cm^{-1} in the spectrum of 'Li_2CS_3' **2** is however demonstrating a large number of absorptions not suitable to assign with molecule vibrations of CS_3^{2-} only. According to textbooks, roughly between 1000 and 2500 cm^{-1}, typically interatomic valence vibrations between nitrogen, carbon, oxygen and sulfur can be found.[86] It is henceforth not possible to interpret the spectra of 'Li_2CS_3' **2** unambiguously.

Generally, for all RAMAN signals and IR absorptions above 1000 cm^{-1} similar impurity considerations as already mentioned apply. But also overtones or combination vibrations might be due to signals at higher wavenumbers.[35] The pronunciation of absorption near 1100 – 1150 cm^{-1} in the IR spectra of 'Cs_2CS_3' **20t** was found to increase with the conditioning of the prepared $Cs_2CS_3 \cdot H_2O$ **20** (obtained in the first place), which is shown in figure 2.69. The IR band is in suspicion of comprising a C=S double bond valence stretching, i.e., a certain degree of confinement of the π-electron system due to the crystal site of the CS_3^{2-} anion. This can be observed not only in the spectrum of 'Cs_2CS_3' **20t**, but $K_2CS_3 \cdot H_2O$ **11**, $K_2[CS_2(S_2)]$ **29**, 'Li_2CS_3' **2** and $BaCS_3$ **26**.

Not only these higher frequent modes emerged as a result of the thermal treatment of $Cs_2CS_3 \cdot H_2O$ **20**. The above discussed non-fundamental absorption near 650 cm^{-1} resolves better after the powder was dried at 200 °C compared to the spectrum of the unconditioned product **20**. The δ_{ip}(CS_3) mode at 519 cm^{-1} is split after the drying steps and sharpens in the spectrum of **20t**. The main group of absorptions from ν_{as}(C−S) between 800 and 900 cm^{-1} remain relatively unchanged. This may be read as an indication for thermal curing and

ordering of the molecules after the removal of crystal water. The removal of water of crystallisation by the thermal treatments indicated in the DTA-TG measurement is confirmed, considering the vanishing of these absorptions. The O–H stretching modes above 3000 cm^{-1} and a peak indicating crystal water at 1627 cm^{-1} in the bottom spectrum confirm the powder to consist of $Cs_2CS_3 \cdot H_2O$ **20**, which was also derived from the recrystallisation and subsequent results by means of SC-XRD.

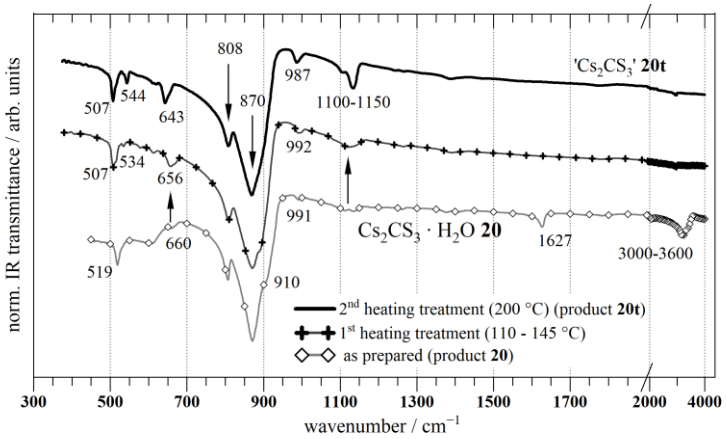

Figure 2.69: IR spectra of different conditioning steps of 'Cs_2CS_3' **20** based on the results of thermal analysis. Several absorption band changes are discussed in the paragraph.

From their main absorption of IR light and their RAMAN scattering, it can be stated that a (tri)thiocarbonate anion or CS_3 moiety is likely to be present in all compounds.

In table 2.9 a compilating list of the IR absorption and RAMAN band centres are assigned for the thiocarbonate salts as explained above. To support the experimental data, values obtained from calculation on DFT level are given.

Table 2.9: Assignment of the characteristic virbations of CS_3^{2-} with the experimental signals of each compound (all numbers are given in cm^{-1}). In the bottom part calculated wavenumbers are listed with IR and RAMAN activity in parenthesis. Note, by calculation in D_{3h} the selection rule applies for some characters.

		vibration characters of CS_3^{2-} ($D_{3h} \rightarrow C_{2v}$)			
compound		$\delta_{ip}(CS_3)$	$\nu_s(C{-}S)$	$\gamma_{op}(CS_3)$	$\nu_{as}(C{-}S)$
K_2CS_3 **9**	IR		506 m	542 m	811 s 865 vs
	R	304 sh 314 m	502 vs		
$K_2CS_3 \cdot H_2O$ **11**	IR		508 m	574 bw	808 m 873 s
	R	311 w 322 vw	504 s		905 vw
'Li_2CS_3' **2**	IR		508 w	559 bw	820 sh 899 vs 942 s
	R	312 bw 371 w?	504 vs	537 m	888 m? 955 m? 983 m?
'Rb_2CS_3' **16**	IR		504 m	513 sh	805 s 817 s 872 vs
	R	304 w 319 w	503 vs		877 vw 894 vw
'Cs_2CS_3' **20t**	IR		507 m	544 w	808 s 869 vs
	R	267 vw 308 w	505 vs	536 m	805 bw 903 m
$BaCS_3$ **26**	IR		502 sh 517 s	546 bw	823 w 908 vs 933 vs
	R	318 m 329 s	508 vs	520 w	904 w 912 w
functional (base set)		calculated IR and RAMAN frequencies# (D_{3h})			
PBE0 (cc-pVTZ)		295 (IR w + R s) 499 (R s)		525 (IR s) 898 (IR s + R w)	

v very, w weak, m medium, s strong, b broad, sh shoulder; ? uncertain; #the calculation was carried out with the optimised structure model of CS_3^{2-} determined in the structure model of $Cs_2CS_3 \cdot$ ⅙ MeOH **24**, namely using the anion centred with atom C2.

The isolated $CS_2(S_2)^{2-}$ anion is naturally lower in symmetry than the isolated CS_3^{2-} anion, as carbon carries one disulfide for a sulfide at one of the three covalent bonds. Therefore, as expected by addition of an atom in the molecule more modes in RAMAN and absorptions in IR have been described. In 1966 the tetrahedral shape, was denied by by IR spectroscopy, assigning the $CS_2(S_2)^{2-}$ molecule anion with the point symmetry C_{2v}.[66] Based on the structure of $CS_2(S_2)^{2-}$ in the model for $K_2[CS_2(S_2)]$ **29**, the C−S−S moiety comprises an angle < 180°, decreasing the symmetry to $C_{s.\,A}$ geometry optimisation was carried out as well, approximitaly giving the ground state vibtations, which can be expected in the eperimental data.

The spectra of the perthiocarbonate anion are given comparative in figure 2.67 alongside other potassium thiocarbonates. They could be assigned in agreement with early vibration spectroscopy, investigating $(H_4N)_2[CS_2(S_2)]$ and $K_2[CS_2(S_2)] \cdot MeOH$,[66,87] which is tabulated below in table 2.10.

Above 1000 cm^{-1} no fundamental molecule vibrations are expected. However, like in the spectra of the trithiocarbonate compounds, IR and some very weak Raman signals are detected. In the IR spectrum of the perthiocarbonate anion, the absorption at 1100 to 1200 cm^{-1} could be due to C=S vibration, which should not be seen from fundamental considerations. Above that, groups of weak absorptions between 1300 and 1800 cm^{-1} indicate either impurities or non-fundamental combinations or overtones. As for the collection of IR data the material was taken straight out of the ampoule maybe educts and unknown side products were accidently included. The absorptions above 1300 cm^{-1} remain unassigned.

With $CS_2(S_2)^{2-}$ as an exaggerated example for breaking the D_{3h} symmetry, naturally two groups of stretching vibrations ν_{as}(C−S) have been determined.[32,87] In this work, similar groups of IR absorptions have been detected at 820 and 979 cm^{-1} as seen in figure 2.67 (bottom field). In the crystal structure model there are three non-equivalent molecule anions determined (of which one is disordered, cf. crystal structure of $K_2[CS_2(S_2)]$ **29**, page 38). Differences in the IR absorptions of ~ 20 – 30 cm^{-1} are likely indicating the different molecule sites in the crystal, which had been claimed for the methanol solvate before.[87] The µRAMAN method applied here on single crystals of $K_2[CS_2(S_2)]$ **29** allowed to resolve corresponding modes at around 840 and 946, 970 cm^{-1}. Careful inspection of earlier published reference spectra showed very weak signals at these positions in RAMAN data, too, that however had not been discussed.[46,87]

Like in the spectra of trithiocarbonates, the degeneration of the in-plane deformation of the CS_3 moiety $\delta_{ip}(CS_3)$ is also cancelled. At a wavelength around 300 cm^{-1} in the RAMAN spectrum two corresponding signals are resolved.

Significant for $CS_2(S_2)^{2-}$ are the experimental RAMAN bands in the area around 500 cm^{-1}, as unlikely CS_3^{2-} two strong intensities are detected. Here, at 530 cm^{-1}, it was tempting to assign the band with the synchronic stretching mode of all sulfur atoms ν_s(C−S), which in molecule symmetry C_s become IR active, too. In the references the vibration at higher wavenumber was designated this way as well. However, the calculated vibration at 537 cm^{-1} gives rise to assign ν(S−S) at this frequency, by inspection of the mode animation. The respective group of IR absorptions at 545 and 528 cm^{-1} cannot be assigned with symmetric stretching ν_s(C−S) or ν(S−S) without fail. The strong mode at 494 cm^{-1} in the RAMAN spectrum should in consideration of the calculation mark ν_s(C−S), while in IR the more active out of plane deformation $\gamma_{op}(CS_3)$ was assigned at 489 and/or 471 cm^{-1}. Lacking RAMAN spectra, similar problems occurred during earlier investigation of ammonium

perthiocarbonate, reporting IR signals at 519 and 485 cm^{-1}.[66] The spectral IR region between 470 and 550 cm^{-1} cannot be distinctively assigned in figure 2.67. Furthermore, manipulations are imaginable, as the S−S stretching should able to couple with the ν_s(C−S) and $\gamma_{op}(CS_3)$.

Not least, the RAMAN spectrum showed a peak at 195 cm^{-1} that was also described by BUENO et al. on $K_2[CS_2(S_2)] \cdot MeOH$ stemming from a deformation mode δ(C−S−S).

Table 2.10: Assignment of the characteristic virbations of $CS_2(S_2)^{2-}$ with the experimental signals of $K_2[CS_2(S_2)]$ **29** (all numbers are given in cm^{-1}). Reference values are added for comparison. In the right collumn, calculated wavenumbers are listed.

	this work, $K_2[CS_2(S_2)]$ **29**		$(H_4N)_2[CS_2(S_2)]$[66]	$K_2[CS_2(S_2)] \cdot MeOH$[87]		DFT calculation
vibration character	IR	RAMAN	IR	IR	RAMAN	PBE0 (cc-pVTZ) [scaled˜]
ν_{as}(C−S)(*)	979 vs 823 s 804 s	970 sh? 946 m? 840 m?	955 m 825 m	974 vs 838 vs		1017 822 [970 784]
impurity	671?			600 – 700?		
ν(S−S)		530 vs	expected 400 – 500, too weak	494 s	495 vs	537 [510]
ν_s(C−S)(**)	545 m 528 vs	494 s	519 m,	539 vs (535 sh)[a]	537 s	492 [469]
$\gamma_{op}(CS_3)$(**)	489 m 471m		485 m	478 m	481 w	487 [465]
$\delta_{ip}(CS_3)$		335 w 266 w	out of range	334 m 273 w	338 m, 273 w	325 254 137 [310 242 130]
δ(S−C−S−S)		195 w			194 m	109 [103]

v very, w weak, m medium, s strong, b broad, sh shoulder; ? uncertain; (*) both peaks are expected to include contribution of the single and the bridging sulfur atoms; (**) not assigned unambiguously; [a] shoulder vibration from two non-equivalent anions in the solid structure; ˜scaling factor 0.954[81]

*µRAMAN spectroscopy on 'Rb$_2$CS$_3$' **17** and K$_5$[CS$_2$(Se$_2$)]$_{1.5}$(CS$_3$) · H$_2$O **15***

Enhanced by focussing the LASER through a microscope, µRAMAN spectroscopy allowed to probe very small specimen. Therefore, RAMAN spectra of the little pink crystals of 'Rb$_2$CS$_3$' **17** that could not be identified with SC-XRD (cf. figure 2.44) and the red crystals of $K_5[CS_2(Se_2)]_{1.5}(CS_3) \cdot H_2O$ **15** could be obtained. (Note, above the precipitated powder material 'Rb$_2$CS$_3$' **16** was characterised.)

The spectrum of 'Rb$_2$CS$_3$' **17** could clearly be assigned with the expected fundamental vibrations of the CS_3^{2-} ion, allowing to claim the crystallised product with the formula Rb_2CS_3. Figure 2.70 shows the spectrum, where the bands are assigned in accordance with table 2.9.

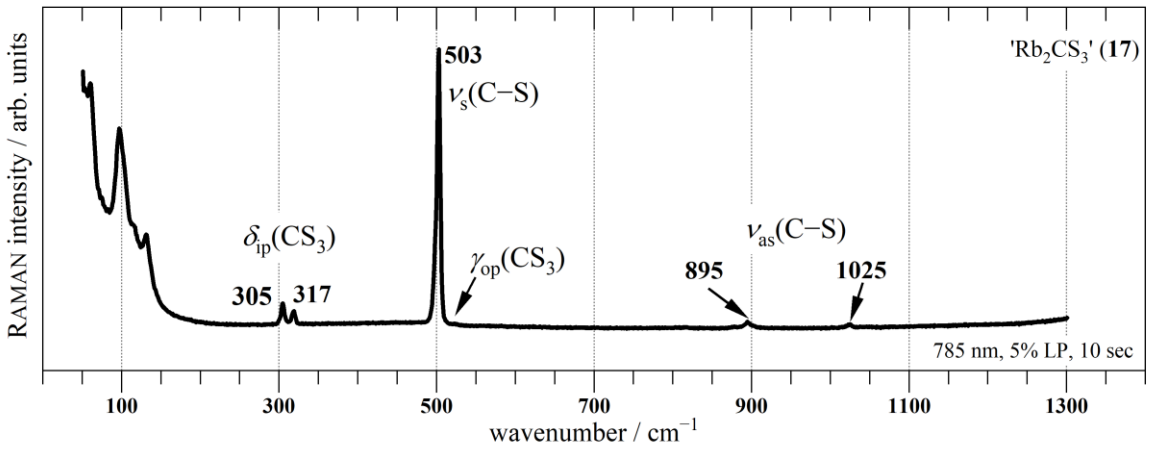

Figure 2.70: RAMAN spectrum of 'Rb_2CS_3' **17** with assignment of the bands according to the discussion above and their peak centres in cm^{-1}. $\gamma_{op}(CS_3)$ is very weak as it is even invisible in D_{3h}).

The mixed anions in the structure of $K_5[CS_2(Se_2)]_{1.5}(CS_3) \cdot H_2O$ **15** make it difficult to evaluate the spectrum without fail. The structure of the new anion $CS_2(Se_2)^{2-}$ was treated in a geometry optimisation using the familiar hybrid functional PBE0 with the base set cc-pVTZ for all atoms, as this worked well for trithio- and perthiocarbonates. The calculated RAMAN spectrum was used for support of the experimental data. Additionally, the RAMAN properties of CS_3^{2-} are considered to evaluate the data, since both anions were included in the crystals. However, as justified in the description of the crystal structure model, the moiety might also be identified with CS_2Se^{2-} (cf. above). Indeed, the spectrum could help to confirm the latter anion, because several vibration characters should change, substituting a sulfur atom for the heavier homologue. To assess this, reference data for CS_2Se^{2-} could fortunately be consulted. The RAMAN spectrum of $BaCS_2Se$ was included in a paper of MÜLLER et al.,[46] who earlier investigated the change in vibration spectroscopy upon substitution of selenium for sulfur on the trithiocarbonate anion CS_3^{2-}. They concluded a decreasing in the wavenumbers upon addition of selenium in the molecule, which they justified from comparison and similarity with the interhalogenboranes BCl_yBr_x, with x + y = 3.

Figure 2.71 shows the recorded spectrum and table 2.11 assigns the bands according to the considerations below.

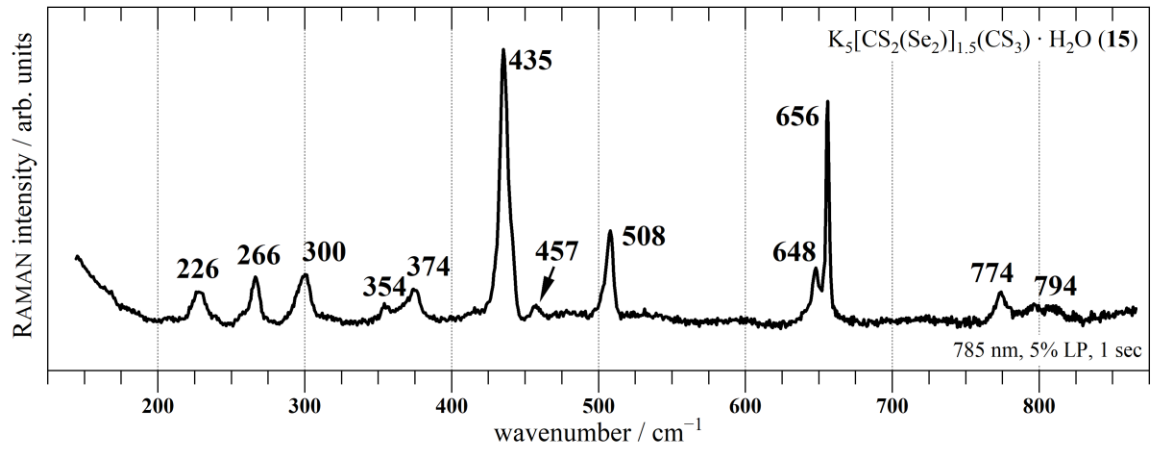

Figure 2.71: RAMAN spectrum of $K_5[CS_2(Se_2)]_{1.5}(CS_3) \cdot H_2O$ **15** with the peak centres in cm^{-1}.

Basically, the geometry of $CS_2(Se_2)^{2-}$ is very similar to $CS_2(S_2)^{2-}$, allowing to assume a similar spectrum. The peak centres should however shift to lower wavenumbers due to the substitution with heavier elements. But considering lattice site effects this must not generally be the observed trend. Calculation of the vibration spectrum gave a dihedral bending mode δ(S−C−Se−Se) at 67 cm^{-1} and the in-plane deformation $\delta_{ip}(CS_2Se_2)$ at 84 cm^{-1}, involving the terminal selenium and the *cis*-sulfur atoms. Both are not included in the spectral range in figure 2.71.

Two more deformation vibrations should be considered for the bands at 226 and 266 cm^{-1}, which is in line with the calculation and comparable with the experimental values for $CS_2(Se_2)^{2-}$.[46] Using the visualisation tool, giving a graphical demonstration, allowed to assign the bands more sustainable. The Se−Se valence stretching is reduced by about 200 cm^{-1} compared to the related $CS_2(S_2)^{2-}$ including an S−S vibration (cf. above). At 300 cm^{-1} the spectrum shows a medium strong band, which could be assigned with the perselenide stretching ν(Se−Se). Interestingly, in the published spectrum of CS_2Se^{2-} an impurity signal at 299 cm^{-1}, which was not further discussed was observed.[46] Probably in the earlier investigations some $CS_2(Se_2)^{2-}$ was included in the samples and remained unnoticed.

The signals at 354 and 374 cm^{-1} are not featured in the calculation and lie somewhat higher than the expected $\delta_{ip}(CS_3)$, which was shown in other spectra above. Still, this is a reasonable way to explain these signals, as a variety of intermolecular interactions might influence these fundamental modes. Nicely, the symmetric valence stretching is resolved at 435 cm^{-1}, which was also assigned for CS_2Se^{2-} at a similar wavelength (442 cm^{-1}),[46] and could be expected with strong intensity. Also, the weak peak on the right was found by the referred authors, although shifted to higher wavenumbers. This should resemble the out of

plane vibration which becomes RAMAN active for molecules with C_s symmetry, which holds for $CS_2(Se_2)^{2-}$ (cf. above).

Neither the calculation of $CS_2(Se_2)^{2-}$, nor the references on the seleno derivatives noted the strong bands observed at 508, 648 and 656 cm^{-1}. Of those, the first one is easily assigned with the strong symmetric stretching of the CS_3^{2-} molecule, which was expected here after knowledge of the crystal structure. The latter two bands could be either impurities or non-fundamentals, but it was found, that also liquid CS_2 might be most plausible explanation, as the crystal of **15** was measured through the ampoule wall and surrounded by educt residuals, amongst others CS_2. A strong symmetric S=C=S stretching can be expected in RAMAN spectra at ~655 cm^{-1}, perfectly agreeing with the spectrum above.[88] The shoulder at 648 cm^{-1} could be a modulation due to other dissolved specimen in the product mix.

A weak RAMAN signal was calculated at 765 and could fit with the experimental data showing a band at 774 cm^{-1}. It should include asymmetric valence stretching, which is not intense. At last, the molecule symmetry demands a second weak mode for asymmetric vibration, which was consistently calculated at 1037 cm^{-1}. Unfortunately, no signals were obtained in that region, even in spectra reaching wavenumbers beyond 3000 cm^{-1}, not covered in figure 2.71. Although energetically lowered, the bulky broad signal at 794 cm^{-1} could again stem from CS_3^{2-} (cf. Table 2.9), but also CS_2 exhibits a weak mode at ~800 cm^{-1}, eventually leaving the signal assigned ambiguous.

Table 2.11: Assignment of the experimental RAMAN bands of $CS_2(Se_2)^{2-}$ as determined in $K_5[CS_2(Se_2)]_{1.5}(CS_3) \cdot H_2O$ **15** (all numbers are given in cm^{-1}). Reference values are added for comparison. In the right collumn, calculated wavenumbers are listed.

	this work, $K_5[CS_2(Se_2)]_{1.5}(CS_3) \cdot H_2O$ **15**	MÜLLER et al., CS_2Se^{2-}[46]		DFT calculation
vibration character	RAMAN	RAMAN	IR	PBE0 (cc-pVTZ)
$\delta(CS_2)$	794 bw(*)			
$\boldsymbol{\nu_{as}(Se_2-C-S_2)}$	774 w nA	925 w 833 w	925 vs 840 vs	1037 765
$\nu_s(CS_2)$	656 s(*) 648 sh(*)			
$\nu_s(C-S)$(**)	508 m			
$\boldsymbol{\gamma_{op}(CS_2Se_2)}$	457 w	485 w	480 m	460
$\boldsymbol{\nu_s(Se_2-C-S_2)}$	435 vs	442 vs	442 w	433
$\delta_{ip}(CS_3)$ (**)	374 w 354 w			
$\boldsymbol{\nu(Se-Se)}$	300 m			294
$\boldsymbol{\delta_{ip}(CS_2Se_2)}$	266 m 226 m?	284 m, 265w	impurity?	250 203 84
$\boldsymbol{\delta(S-C-Se-Se)}$	nA			66

v very, w weak, m medium, s strong, b broad, sh shoulder; ? uncertain; (*) CS_2 impurity[88]; (**) from additional CS_3^{2-};

UV-vis spectroscopy

The products K_2CS_3 **9** and $BaCS_3$ **26** were conducted to UV-vis spectroscopy. The alkali and alkaline earth trithiocarbonates have been investigated in this regard before: Two types of light absorption bands have been detected in the range of 530 to 430 nm and 410 to 350 nm. They were suggested a $n \rightarrow \pi^*$ and a $\pi \rightarrow \pi^*$ transition, respectively.[89] Trithiocarbonic acid has also been assigned with these transitions at 465 and 290 nm, respectively. Only the $n \rightarrow \pi^*$ transitions lie in the visible spectrum, thus contribute to the colour of the compounds, while the $\pi \rightarrow \pi^*$ is already in the near ultraviolet. Figure 2.72 shows the UV-vis spectra of the products, which for this purpose were diluted in KBr and pressed to a pellet.

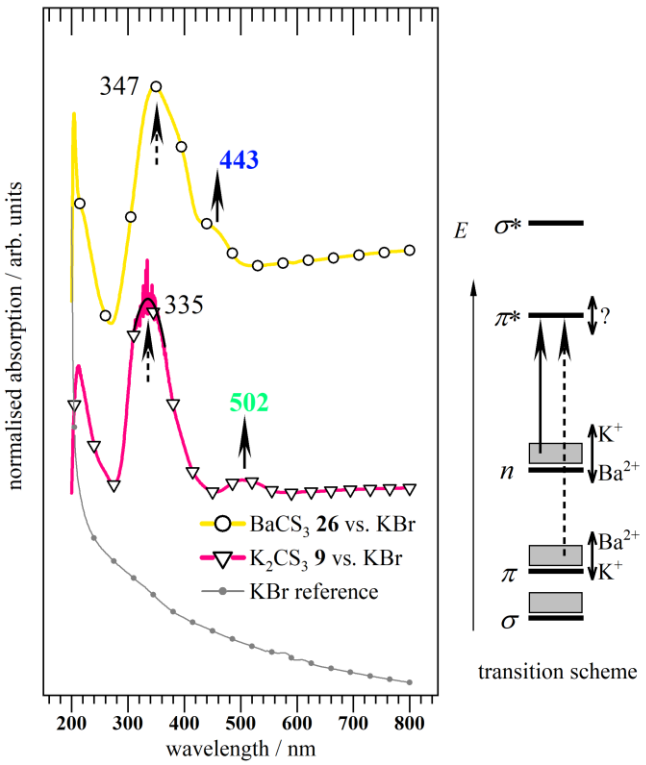

Figure 2.72: UV-Vis spectra of K_2CS_3 **9** and $BaCS_3$ **26**. The two expected absorption peaks are given in nm and are assigned by the arrow type (dashed and solid). On the right a simplified scheme explains the transitions. From filled states (grey boxes) by light absorption electrons can get excited (arrows) to higher empty states .

The bright colours of trithiocarbonic acid (intense red, cf. figure 2.65) and its potassium and barium salts (pink and yellow, respectively) demonstrate absorption of visible light. Apparently, a dramatic energy difference of the involved electron states occurs changing the chemical surrounding of the trithiocarbonate anion. In figure 2.72, the colours of numbers giving the absorption at 443 and 502 nm for the barium and potassium compound are represented, respectively. For the human eyes, this results in the complementary colouration of the actual compounds mimicked in the line colours. Given the stylised molecular orbital model on the right explains the electron transitions in a simplified way. It is seen that the free electrons located in the band gap of the combined orbitals (n) can get excited to the free anti-bonding π^* level. A larger energy difference is present between the bonding π-level and the anti-bonding π^* states, although direct comparison shows this high energy transition to be relatively constant upon cation substitution. From the picture, it can be assumed that the electric field of the cations K^+ or Ba^{2+} manipulate the energy levels of the orbitals inhabited by the relevant electrons on the CS_3^{2-} ions. Assuming the π^*-level not to change dramatically upon substitution of the cations, the energy distance between the π

and *n* states are tuned markedly. Compared to $BaCS_3$ **26**, more energy is needed to excite $\pi \rightarrow \pi^*$ in K_2CS_3 **9**, whereas the free states are at a level allowing the transfer $n \rightarrow \pi^*$ to consume less energy.

SEIDEL published the absorption bands of other alkali and alkaline earth carbonates in 1969, stressing that he also investigated the substitution on the trichalcogencarbonate anion with the heavier sulfur and selenium homologues. Qualitatively. the limited reinvestigation shown here is in line with the former data, listing the absorptions for K_2CS_3 **9** at 526 and 381 nm and for $BaCS_3$ **26** at 455 and 391 nm. It was claimed the stability of the molecule anions can be reflected in consideration of their absorptions. $BaCO_3$ only absorbs high energetic light at 213 nm, whereas both absorption bands are shifted into the visible spectrum in $BaCSe_3$ (599 and 532 nm) explaining its dark violet colour.[89] In line is the here presented finding, that $BaCS_3$ is positioned in the middle, having one absorption in the near UV and another in the visible.

2.5 1,1-Dithiolates in the system of NH_3 and CS_2

As in the section above, for the formation of thiocarbonates, carbon disulfide is treated under basic conditions. In addition to alkoxide or hydroxide solutions of alkali and alkaline earth metals, reactions of ammonia and carbon disulfide afford thiocarbonates. As both compounds are of fundamental and historical importance in chemistry, naturally, the interplay of the species has been investigated enthusiastically before.

Of course, ammonia can act as a nucleophile and is able to attack the C=S double bonds in CS_2 with the lone electron pair at the nitrogen atom. This direct nucleophile addition results in formation of the dithiocarbamate anion $S_2C(NH_2)^-$. It can be assumed that ZEISE already had the compound at hand, which he called *das schwefelbrintige anthrazothionsaure Salz*.[8]

At elevated pressure and temperature, NH_3 and CS_2 yield $(H_4N)SCN$, which stands in thermodynamic balance with thiourea. Furthermore, the products of the reaction between ammonia and carbon disulfide can be transformed into one another by adjustment of the thermodynamic conditions, which is depicted in the reaction scheme below.[1]

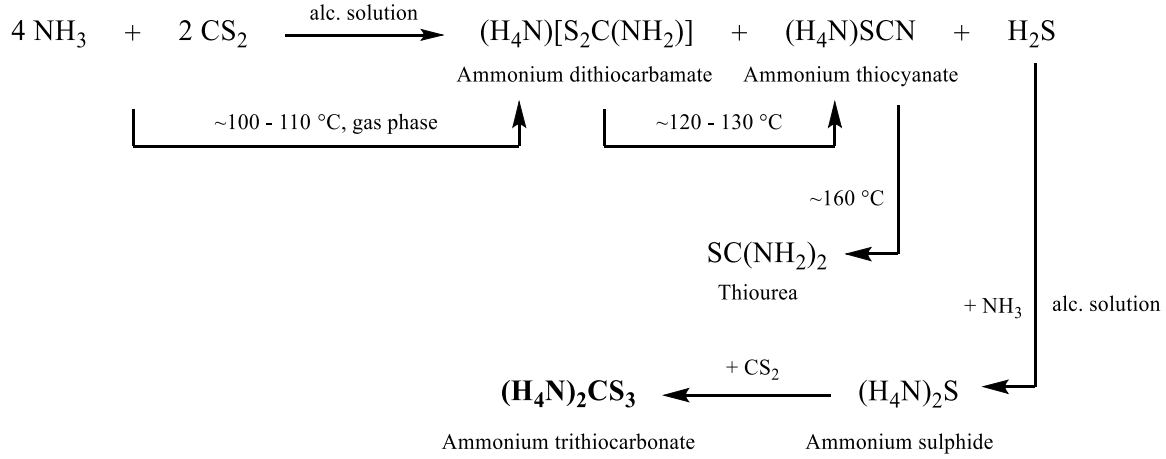

Scheme 2: Reaction variability in the system of NH_3 and CS_2.[1]

Control over the system of NH_3 and CS_2 is challenging as a variety of side products can form and might be obtained in parallel. Motivated by the absence of entries in the CSD, it was attempted to obtain ammonium trithiocarbonate for single crystal investigations.

2.5.1 Ammonium salts of trithiocarbonate and dithiocarbamate

The fundamental preparative method used here, was followed from the early description of YEOMAN but other methods are existent. Likewise the formation of alkali and alkali earth trithiocarbonates, it was written, that solutions of $(H_4N)_2S$ can be treated with CS_2 (right

corner in the reaction scheme above) to afford the trithiocarbonate salt.[3–5] As described in section 4.2.9 and 0.0.1081814352, ammonia was therefore dissolved in ethanol, affording the starting solution, which was treated with hydrogen sulfide. The formation of $(H_4N)_2S$ was assumed as under introduction of the gas a colourless solid formed, which was captured in figure 2.73 (middle). An orange solid, was subsequently obtained from the reaction of colourless precipitated $(H_4N)_2S$ with CS_2 in ethanol.

Figure 2.73: Photo of a SCHLENK tube containing absolute ethanol covered with liquid NH_3 separated in two phases at first (left). Colourless crystalline solid, precipitated after the ethanolic solution of NH_3 (left) was treated with H_2S gas (middle). Orange solid was obtained from the solution of $(H_4N)_2S$ (middle) with CS_2 (right). Discolouration is indicated in the upper areas of the round bottom flask and may be a sign for decomposition.

The orange material was quite unstable when exposed to ambient atmosphere and successively became colourless. The dried orange powder was examined under argon with a microscope, and it was found that it consisted of at least two phases: Orange carrot-like crystallites and a microcrystalline powder of yellowish white colour (cf. figure 2.74). The orange crystals qualified for SC-XRD and their identity could be determined as a mixed trithiocarbonate dithiocarbamate $(H_4N)_5(CS_3)_2[S_2C(NH_2)]$ **31**. Apparently, NH_3 was not completely converted to $(H_4N)_2S$ and the residues reacted in parallel with CS_2 to yield $S_2C(NH_2)^-$, while $(H_4N)_2S$ was converted to CS_3^{2-}, because both these anions crystallised simultaneously. Furthermore, upon the addition of CS_2 to the alcoholic dispersion carrying $(H_4N)_2S$ (cf. figure 2.73 (middle)), the ignition of the back reaction of NH_3 and H_2S may occur (cf. on the right in scheme 2).

$(H_4N)[S_2C(NH_2)]$ **32** seems to be the more stable product under these conditions, as if the concentrated ammonia solution is not exchanged for fresh ethanol after the precipitation of $(H_4N)_2S$, the desired orange compound decomposed quickly to yield bright yellow crystals of **32**. Indeed, the microcrystalline yellowish white side product in figure 2.74 could be

confirmed to be $(H_4N)[S_2C(NH_2)]$ **32**, confirming it to be thermodynamically favoured over $(H_4N)_2CS_3$.

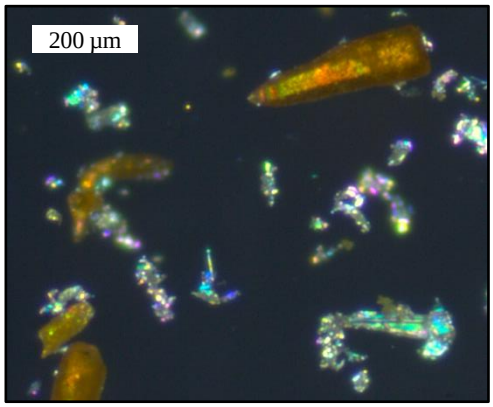

Figure 2.74: Microscope photograph of the product mixture that included orange carrot-shaped crystals of $(H_4N)_5(CS_3)_2[S_2C(NH_2)]$ **31**. The almost colourless side product was confirmed to be microcrystalline $(H_4N)[S_2C(NH_2)]$ **32**.

In short, the reaction comprises the concurrence between S^{2-} and NH_3 to react with CS_2. The dithiocarbamate carries only one negative charge, stereo chemically stabilised between the two sulfur atoms. The nitrogen atom of the amino group moreover has a higher electronegativity than carbon and is able to mediate the negative charge cloud of the thiocarbonylthio group. In turn, the trithiocarbonate has two negative charges that are distributed over the relatively non-polar molecule bonds (PAULING: $E_N(C) = 2.55$, $E_N(S) = 2.58$).[52] It is therefore remarkable that co-crystallisation of the trithiocarbonate and the dithiocarbamate did occur.

As another measure for the stability of both the anions, the corresponding acids may be taken for comparison. Dithiocarbamic acid $(HS)SC(NH_2)$ is solid at RT, crystalising as dimers of neutral molecules with strong S−H···N hydrogen bonds further linked by additional S−H···S hydrogen interactions.[90] In contrast, trithiocarbonic acid $(HS)_2CS$ (cf. sub-section 2.4.1) is liquid and irreversibly decomposes at RT.[6]

Considering the literature landscape, compounds with mixed trithiocarbonate and dithiocarbamate anion have not been reported yet.

Ammonium trithiocarbonate dithiocarbamate $(H_4N)_5(CS_3)_2[S_2C(NH_2)]$

Crystal structure model

The orange carrot-like crystals (in figure 2.74), determined as $(H_4N)_5(CS_3)_2[S_2C(NH_2)]$ **31** crystallised in a primitive trigonal lattice with three formula units per unit cell. All atoms occupy regular lattice positions (3a) and only obey a three-fold screw axis along the

crystallographic *c*-axis, i.e., the space group was defined as $P3_1$ (No. 144). As seen by the view along different crystal directions in figure 2.75, the anions are located close by the three-fold screw axis, without a certain orientation. Trithiocarbonate anions are found near the corner and one of the screw-axis centres inside the unit cell, as the dithiocarbamate anion is sitting by the other. Within the scope of the standard uncertainty of the locations of the atoms, both the anions are planar. The planarity of $S_2C(NH_2)^-$ was confirmed below in the structure of the ammonium salt **32** and was earlier reported.[91]

The ammonium cations are distributed around the anions with no special fashion, connecting to the nearest anions to form a hydrogen-bound network in addition to ionic interaction. All hydrogen atoms of the ammonium ions could be located with help of the residual electron density during solution of the data. They were tetrahedrally arranged around the nitrogen atoms in reasonable N−H distance of 78(4) to 95(4) pm. The N−H bonds in the amino group at the dithiocarbamate anion was fit with the value of 88 pm, which is equal to the reported dithiocarbamate structure.[91] The coordination distances and angles of the ammonium ions that interact *via* hydrogen bonds are visualised in figure 2.76, 2.77 and 2.78 for the different anions in the structure, respectively.

The N−H···S hydrogen bonds can be considered of moderate to weak according to the categorisation given by STEINER. In this, the qualitative terms *strong* or *strongly covalent* (~220 – 250pm), *moderate* or *mostly electrostatic* (~250 – 320 pm) and *weak* or *dispersive* (320 – 400 pm) are used with regard to the acceptor ··· donator distance to characterise possible hydrogen bonding.[38] The proton acceptor atoms are exclusively the sulfur atoms of the anions. The more linear (close to 180°) and shorter the H···S distance, the stronger the hydrogen bond. In the structure of **31** the geometries of hydrogen bonds vary between H···S distances of 234.9 and 299.8 pm and N−H···S angles 105(3) and 176(3)°, although angles from 110 to 90° and below are doubtful for the character of a hydrogen bond.[38] Only two N−H···S angles amount to < 110°, therefore they are qualified very weak. There are three to five hydrogen-bound ammonium anions around each sulfur atom except for S21 and S23, for which one coordination each is performed by the amino group a dithiocarbamate anion (cf. figure 2.77 and 2.78). The amino group hydrogen bonds demonstrate S···H distances (N−H···S angles) of 267.8 pm (168(1)°) and 264.4 pm (169(1)°), for S21 and S23, respectively, which are close to the distance mean value of all hydrogen bonds in this structure. This is stressing the deviating character of the two present anions. In the dithiocarbamate anion the covalent character is relatively increased, due to only one negative charge. As mentioned above, this charge is balanced between the sulfur

atoms, while the C−NH_2 group should majorly be left non-charged acting only electrostatically due to its polarisation.

Some of the hydrogen bonds are bifurcated, with the hydrogen atom shared by two sulfur acceptors, which goes along with either smaller angles of the N−H···S bonds in the range of 134 to 158° of similar H···S distance, or one clearly favoured shorter and straighter interaction in contrast to the other. Finally, as the hydrogen atoms cannot be localised from X-ray diffraction data ideally, i.e., without large standard uncertainty, the N···S distances of the hydrogen bonds should be noticed. They range between 324.6(3) (N6···S11) and 354.3(2) pm (N1···S21). Compared with the solid state structures of α- and β-(H_4N)[$S_2C(NH_2)$], the donor acceptor distances agree.[91]

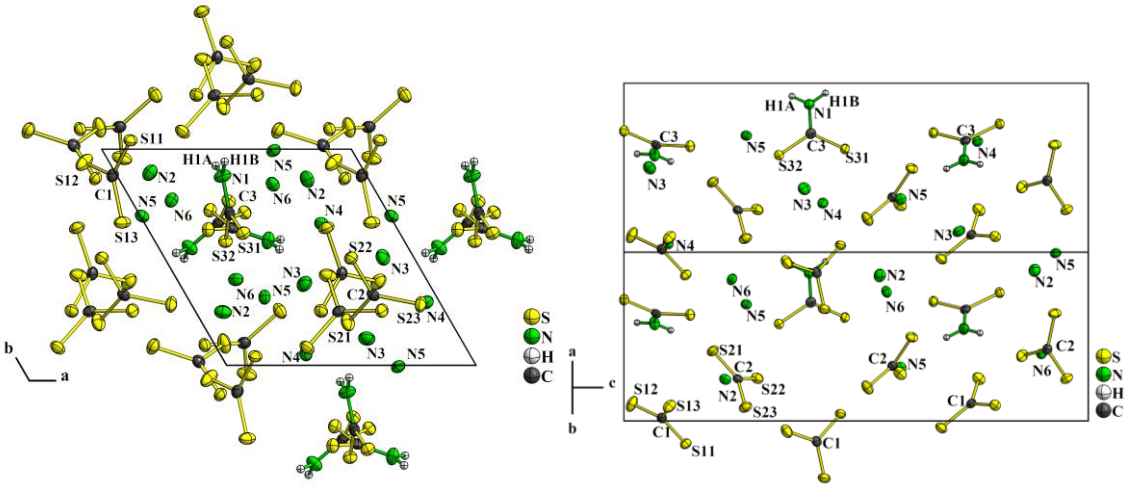

Figure 2.75: Extended unit cell of (H_4N)$_5$(CS_3)$_2$[$S_2C(NH_2)$] **31** with view along the *c*-axis and along [110] (left and right, respectively). Displacement ellipsoids are drawn at 70 % probability. Hydrogen atoms of ammonium ions are omitted for clarity.

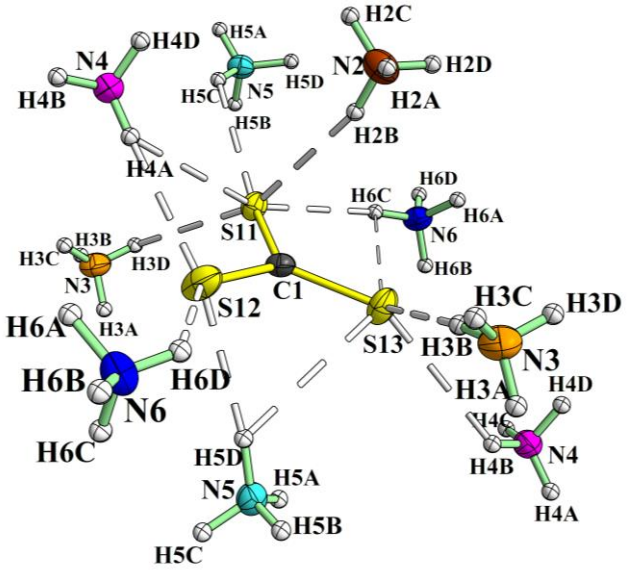

Figure 2.76: Coordination of the trithiocarbonate anion of C1, located at the corner of the unit cell. All non-hydrogen atoms are drawn with displacement ellipsoids of 70 % probability. The dashed lines represent the hydrogen bonds. For the reason of a small angle < 110°, i.e., very weak hydrogen bonding, the connection H6C···S13 is drawn thin.

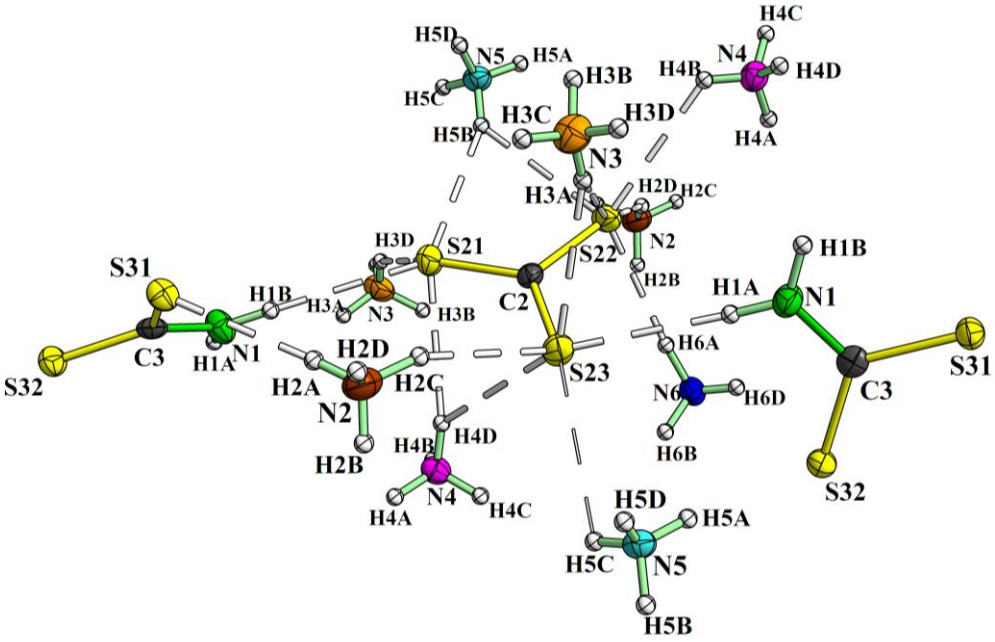

Figure 2.77: Coordination of the trithiocarbonate anion of C2, located near one of the two centres of the three-fold screw axis inside the unit cell. All non-hydrogen atoms are drawn with displacement ellipsoids of 70 % probability. The dashed lines represent the hydrogen bonds. For the reason of a small angle < 110°, i.e., very weak hydrogen bonding, the connection H5D···S23 is drawn thin.

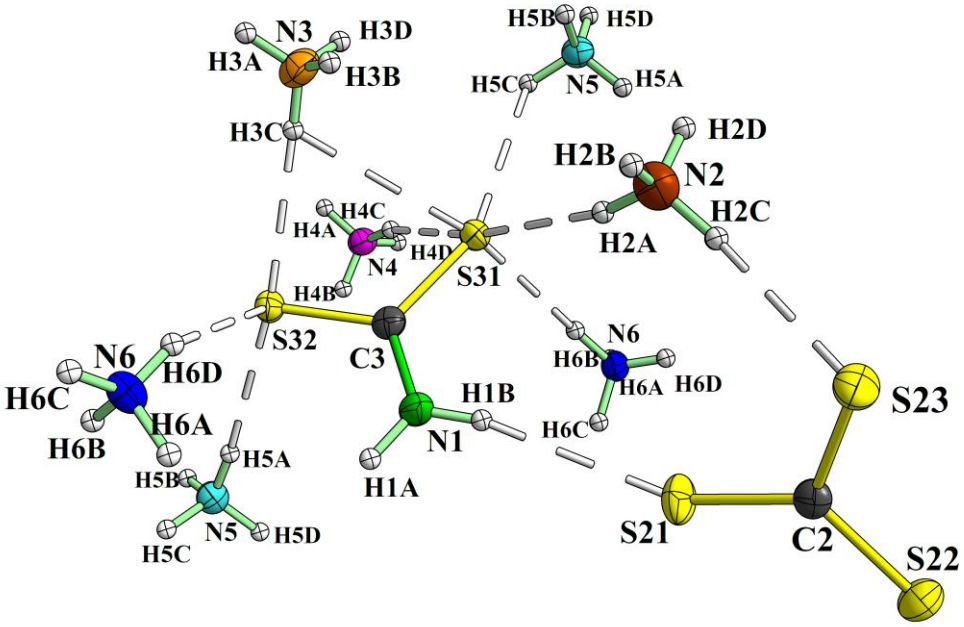

Figure 2.78: Coordination of the dithiocarbamate anion of C3, located near one of the two centres of the three-fold screw axis inside the unit cell. All non-hydrogen atoms are drawn with displacement ellipsoids of 70 % probability. The dashed lines represent the hydrogen bonds.

X-ray powder diffraction

As mentioned above, the product from which **31** was isolated as the main phase was obviously mixed with at least one second phase. This was identified by analysis of the PXRD data in a RIETVELD routine. The graphical result is given in figure 2.79. It was found, that **31** was obtained together with $(H_4N)[S_2C(NH_2)]$, which was expected as explained above.

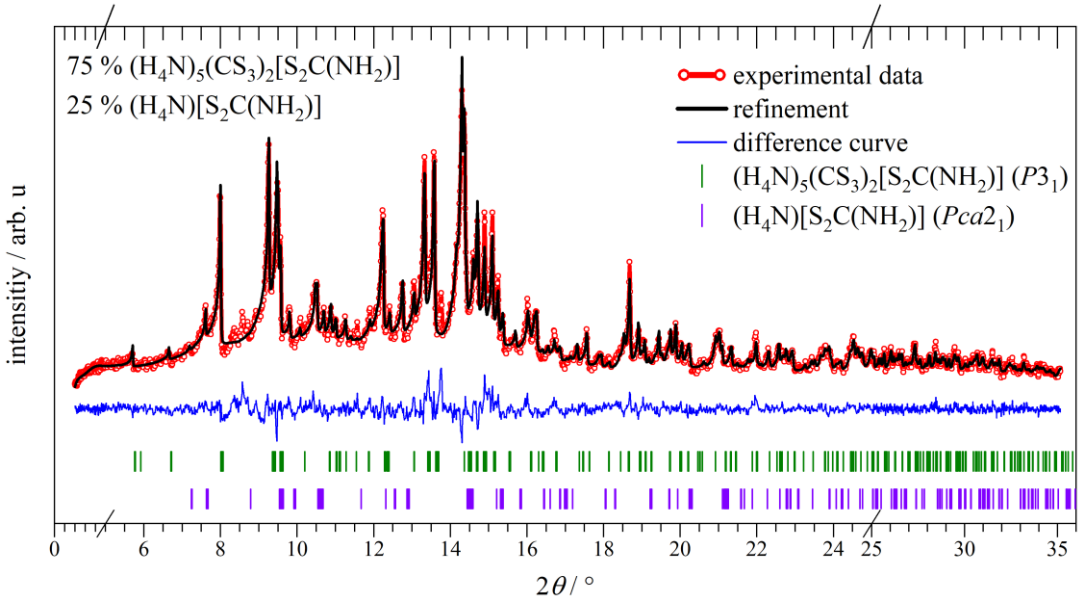

Figure 2.79: RIETVELD refinement of the obtained phase mix including crystals of $(H_4N)_5(CS_3)[S_2C(NH_2)]$ **31** and the expected impurity by $(H_4N)[S_2C(NH_2)]$.

Ammonium dithiocarbamate $(H_4N)[S_2C(NH_2)]$

The crystal structures of ammonium dithiocarbamate can be found in the ICSD, where a low temperature α- and a metastable high temperature β-modification were deposited. The entries originate from the reinvestigations of TESKE and BENSCH in 2010 but the crystal structure was investigated as early as 1967.[91] Noteworthy, they prepared $(H_4N)[S_2C(NH_2)]$ by adding concentrated ammonia solution – assumingly aqueous – to a solution of CS_2 in ethanol and obtained the salts subsequently increasing the volume with ethanol. The use of aqueous ammonia solution points up the stability of the dithiocarbamate anion towards hydrolysis. Stirring the mixture and storing it cooled at −10 °C, they obtained a colourless to yellow crystalline product. They refer to the yellow colour as to an effect of impurities that had been claimed earlier,[92] and indicate the intermixing of ammonium dithiohydrogencarbonate, $(H_4N)HCS_2O$, which is yellow and isostructural with $(H_4N)[S_2C(NH_2)]$.

Earlier reported preparations where undertaken in THF as a solvent for CS_2, which was converted to the ammonium dithiocarbamate salt by introduction of NH_3 gas.[93]

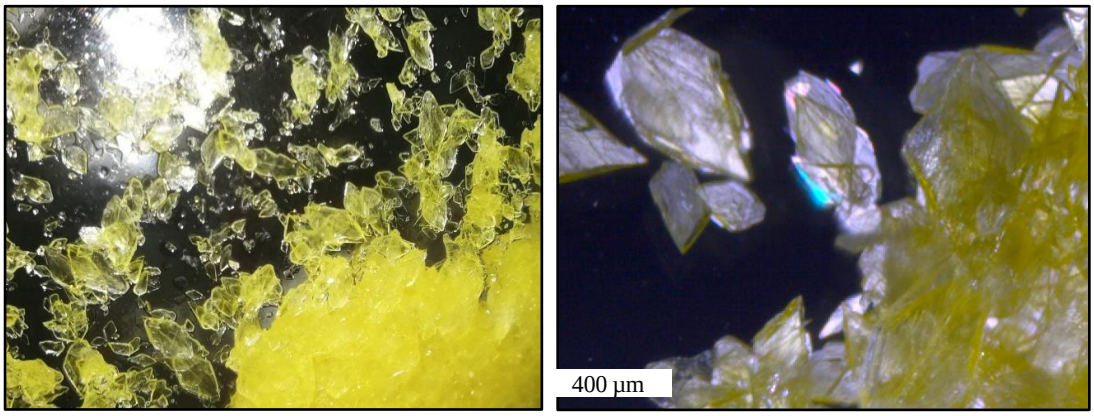

Figure 2.80: Crystals of $(H_4N)[S_2C(NH_2)]$ **32** as obtained in the round bottom flask. Under polarised light the crystals appear to be almost colourless.

Crystal structure model

In this work, the thermodynamically stable low temperature α-modification was (re-)discovered by X-ray diffraction on the crystals shown in figure 2.80. The salt crystallised in the orthorhombic system with a primitive lattice following the symmetries of the space group $Pca2_1$ (No. 29). Clearly, the crystals had yellow colour filling a sample vial but appeared colourless examined individually and with polarisation filter (cf. figure 2.80). From former investigations a phase transition above 60°C was known, but it was shown that the phase transition into the meta stable β-modification happens between 30 – 35 °C and can be cycled between the α- and β-form reversibly.[91]

As both the modifications are already described in detail, including the peculiarities of the hydrogen bonds present in the structures, a graphical illustration of the measured crystal and a description of the coordination is left out at this point. Nevertheless, the compound was taken for reference in the vibrational spectroscopic investigations in section 2.5.3.

2.5.2 Treatment of CS_2 with aqueous NH_3

In addition to the traditional route of precipitation the desired salt from saturated ethanolic solution, the direct reaction of CS_2 with aqueous NH_3 was considered an option in order to pursue the preparation if $(H_4N)_2CS_3$. Remarkably, it has only been shown as recently as 2010 that indeed growth of yellow crystal cuboids can be observed at the wetting interphase of CS_2 under a layer of concentrated aqueous ammonia,[94] which is shown in figure 2.81 (left). Following this the preparation was repeated and the investigation extended by IR measurements. The crystals are unstable at RT and for the SC-XRD measurement, to pick crystallites, an improved cooling set up was necessary, which is shown and described in figure 2.82. They were identified as $(H_7N_2)_2CS_3$ **30** featuring the elusive diamine hydrogen cation $(H_7N_2)^+$, i.e. $[H_3N\cdots H{-}NH_3]^+$.

The thermal instability could be annulled to some extent, as in the deep freezer successive intergrowth yield a multidomain crystal agglomerate of ~1 cm shown in figure 2.81 (right). Increased in size, the material was mechanically stable enough to resist transfer into a cell for inert µRAMAN spectroscopy. Under argon the investigation by IR spectroscopy was carried out for the first time after successful transfer into a glovebox.

Figure 2.81: Photo of the reaction mixture of aqueous ammonia (red phase) with carbon disulfide (colourless) after a couple of hours (left) and after several weeks stored at −20 °C (right). The yellow crystals of $(H_7N_2)_2CS_3$ **30** have formed. The orange red colouration of the aqueous solution is due to the formation of CS_3^{2-} anions. The polycrystals agglomerated to a size, which realised analysis with RAMAN and IR spectroscopy.

Figure 2.82: Set up for inert and cooling crystal sorting for SC-XRD measurements. The DEWAR vessel was filled with liquid nitrogen and nitrogen gas was introduced. The pressure release went through the isolated glass tube that transported the cold stream of nitrogen towards the glass substrate that was placed in the optical axis of the *Stemi 508* microscope, used for crystal sorting. The insert photo was taken through the ocular lens, showing the yellow crystals of $(H_7N_2)_2CS_3$ **30**.

The collected diffraction data was solved in agreement of the results of BENZ, who was able to describe the structure of $(H_4N)_2CS_3 \cdot 2\ NH_3$ in 2010 and inferred the diamine hydrogen cation.[94] Remarkably, it was not published in a journal apart from his dissertation and the structure was not published in the ICSD, although solid state structures of the diamine hydrogen ion are low in number.

Diamine hydrogen trithiocarbonate $(H_7N_2)_2CS_3$

On compounds including the $(H_7N_2)^+$ ion

Although, NAHRINGBAUER et al. could determine a close N···N distance of 287.4(4) pm at 233 K and 286.8(5) pm at 83 K, in a crystal of $(H_4N)(OOC_2H_3) \cdot NH_3$ as early as 1968, they did not refer to the ammonium-ammonia complex with the term *diamine hydrogen* cation. Nevertheless, they did conclude, that the N···N distance must involve a hydrogen bond, i.e., a hydrogen atom of H_4N^+ donated towards the lone pair of a NH_3 molecule. This is

supported as in pure ammonia hydrogen bonds are reported longer with a N···N distance of 338 pm. Moreover, from comparison of the different distances of the acetate ions, decision of the nitrogen atom belonging to the ammonium and the ammonia unit was made.[95] This picture is in accordance with the structure of **30**, showing a much shorter coordination distance of the ammonium fragment compared with the ammonia molecule with the sulfur atoms of the trithiocarbonate molecule. Like in **30**, the ammonium unit is coordinated tetrahedrally, where three different acetate anions and the adjacent ammonia molecule are involved. Only one of three O···N connections, which are meant to resemble hydrogen bonds, is bifurcated with a shorter (288 pm) and a longer (317 pm) distance (T = 83 K).[95] This motif is remarkably close to the arrangement of the three trithiocarbonate groups in nearest distance to the ammonium fragment in **30**, which is shown in figure 2.84.

Another early publication of a crystal structure with a diamine hydrogen cation is given by BERTHOLD et al. on $(H_4N)I \cdot NH_3$., in which due to the disorder of one diamine hydrogen cation along all three axes, could not be described accurately in the cubic lattice system. Only the N···N distance is reported with 269(5) pm, which is about 17 pm (!) shorter than in **30**. It was the first structure, that supported the results of *ab initio* calculations of the hydrogen bond in the diamine hydrogen cation.[96] Depending on the assumptions in the calculations, the N···N distance in the gas phase was calculated to a value in the range of 250 to 296 pm, where the best consensus was with 273.1 pm, reported by SCHEINER et al. The latter authors investigated the proton transport by means of calculation of the molecule in C_{3v} symmetry with different sized basis sets and inclusion of different correlation effects. These predicted the same qualitative potential affecting the proton, which is a double-well potential, and the barrier height for transportation increasing with the N···N distance.[97]

Other than these mentioned values are compiled in table 2.12, describing the geometry of the diamine hydrogen cation and its derivatives with higher resolution.

It was not until 2002 that a well resolved $(N_2H_7)^+$ ion was found in a crystal structure, stabilised inside the cavity of a calix[4]arene[x].[98] An N···N distance of 276.5 pm is reported and the N···H–N angle deviates only about 3.83° from linearity. In this structure, the coordination of the cation is majorly ruled by VAN DER WAALS interactions with the supermolecule. In fact, next to the intramolecular hydrogen bond of the diamine hydrogen cation, the ammonium ion, centred in the calix[4]arene cavity, is bound only to the deprotonated phenol group of the latter. It is worth of note that the authors could therefore resolve the hydrogen sites with difference electron density maps, since no additional dative

[x] Calix[4]arene-25,26,27,28-tetrol, $-[C_6H_3(OH)-Me]-_4$

bonding was observed in the structure. This stands in contrast to the diamine hydrogen cation observed in **30**, where both the ammonium and ammonia fragment are coordinated by the anions *via* hydrogen bonding.

In the same year, X-ray structure investigations on $(H_4N)[Li(NH_3)_4][P(NH_2)S_3] \cdot NH_3$ were published, featuring the diamine hydrogen cation.[99] The compound was obtained from reduction of phosphorous pentasulfide in a solution of lithium in liquid ammonia at 233 K, which diverges from the relatively mild conditions used to obtain **30**. As a reminder, **30** was obtained from CS_2 and concentrated aqueous ammonia kept chilled in the freezer at 253 K. The amidotrithiophosphate is not only an example for a crystal structure including the diamine hydrogen cation, nut also comprises interaction with sulfur, coordinating on $(N_2H_7)^+$. The S···H distances in the hydrogen bonds are reported to value in the range of 245.7 - 298.8 pm,[99] which is in agreement with **30** and furthermore supports to consider the longer distant coordination, drawn thin in figure 2.84, as less strong. Similarly, the sulfur acceptors for hydrogen bonding are designed in the crystal structures of $[H_4N(NH_3)_4][Ca(NH_3)_7]As_3S_6 \cdot 2\ NH_3$ and $[H_4N(NH_3)_4][Ba(NH_3)_8]As_3S_6 \cdot NH_3$. Although, there the simpler diamine hydrogen cation is extended to the tetraamine ammonium complex, the same range of S···H distances are found (255(8) to 299(7) pm).[100]

Details given in table 2.12, the $(N_2H_7)^+$ ion was also found in the structures of $(N_2H_7)F$,[101] $(NH_3)_4[UF_7(NH_3)] \cdot NH_3$,[102] $(N_2H_7)[Al(OC(CF_3)_3)_4]$,[103] and the *closo*-borates $(H_4N)_2B_xH_x \cdot y\ NH_3$ (x = 10, y = ½, 1 / x = 12, y = 1, 2).[104] The latter were investigated with regard to proton conductivity mechanisms. The structures, obtained from synchrotron powder data, display a series of compounds, where the $(N_2H_7)^+$ ion could be stabilised in an extended hydrogen-bound network. Nevertheless, the interconnection between the cationic groups is fashioned by distances with values of 346 to 526 pm,[104] which results in three dimensional networks of much larger loops compared to structures set up with ammonia bridged interconnection of $[H_4N(NH_3)_4]^+$ cations. There, N···H–N bonds do not exceed 338 pm, which is typical for hydrogen bonds of two ammonia molecules of crystallisation.[100,105]

Within the frame of the series of ammonium borate amine structures, the proton conductivity could however not be correlated with the fashion of the $(N_2H_7)^+$ ions, i.e., their geometric and coordinative setup within the structure. The authors conclude that improvement of proton conductivity demand a closer interconnection between the proton carrying moieties them.[104] Overall, the diamine hydrogen cation, $(H_3N{\cdots}H{-}NH_3)^+$, has yet not frequently been elucidated properly in crystal structures. This is due to the low thermal

stability of ammoniates and stays in contrast with the isoelectric ZUNDEL ion, i.e., $(H_2O{-}H{\cdots}OH_2)^+$ and extended hydrated hydronium complexes, which are structurally well-known.[100,105,106]

Table 2.12: The geometry of the hydrogen bond in diamine hydrogen cation $(H_3\mathbf{N{\cdots}H{-}N}H_3)^+$ in a selection of different compounds.

Compound (year published)	N···H / pm	H−N / pm	N···N / pm	N···H−N / °	*T* / K
$(H_7N_2)_2CS_3$ (**30**) (this work)	197(2)	89(2)	286(2)[a]	175	100(2)
$(H_4N)_2CS_3 \cdot 2\ NH_3$[94] (2010)	not given	92(2)	286.5(2)	169(2)	123(2)
$(H_4N)[Li(NH_3)_4][P(NH_2)S_3] \cdot NH_3$[99] (2002)	193.1*	93.8*	286.4	172.5	123
(H_7N_2)calix[4]arene[98] (2002)	168(2)*	110(2)*	276.5	176.2	173(2)
$(N_2H_7)F$[101] (2009)	197(2)	92(2)	289.0(3)	172(2)	123(2)
$(H_4N)_3[UF_7(NH_3)] \cdot NH_3$[102] (2009)	199.3*	89.8*	288.2(6)	177.0*	123(2)
$(H_7N_2)[Al(OC(CF_3)_3)_4]$[103] (2020)	158(1)-163(1)*	109(1)-110(1)*	267.4(5)-270.0(5)	162(1)-179(7)*	100(2)
$(H_4N)_2B_xH_x \cdot y\ NH_3$[104] (2020) ([a]$x$=10,$y$=½; [b]$x$=12, y=1)	156.6[a]-183.7[b]	106.9[b]-112.4[a]	268.9[a]-290.6[b]	180[b]*	388[b], 150[a]

* values withdrawn from published crystal information file.

Crystal structure model

The atomic set up follows the symmetry elements of the space group *C*12/*c*1 in a monoclinic lattice with four formula units per unit cell. The unique CS_3^{2-} anion is symmetrically bisect, as the atoms C1 and S1 occupy the site symmetry 4e, which lies in the two-fold axis along *b*-direction (cf. figure 2.83). All other atoms occupy regular sites (8f) and there is only one unique diamine hydrogen cation present. The bond length C1−S1 is decreased to 169.2 pm and therefore can be assigned with an increased double bond character. The C1−S2 bond in turn is 172.7 pm which makes it rather a single bond and thus more interactive towards the cations. Thus, the ideal D_{3h} symmetry of the trithiocarbonate anion is reduced to C_{2v}, with the difference in the S1−C1−S2 and S2−C1−S2 angles (121.17(4)° and 117.66(8)°, respectively). The triangular anion planes are arranged parallel to each other, but without coincidence or special orientation with the unit cell planes. In the unit cell, the propagation of the ions is realised in an alternating stacking of one trithiocarbonate anion and two cross-oriented $(H_7N_2)^+$ complexes, resulting in ten nearest cations surrounding the anion, taking the carbon atom as a centre. Interestingly, despite their positive charge, two (a and b)of the diamine hydrogen ions are in close range to one another ($H_4N^a{\cdots}NH_3^b$ 343.7(2), $H_3N^a{\cdots}NH_3^b$

391.8(2), $H1A^{a}\cdots H1A^{b}$ 297(2)), assuming an intermolecular interaction *via* hydrogen bonds.[99] Probably, this helps to stabilise two positive charges surrounded by the anions, that form a distorted octahedron.

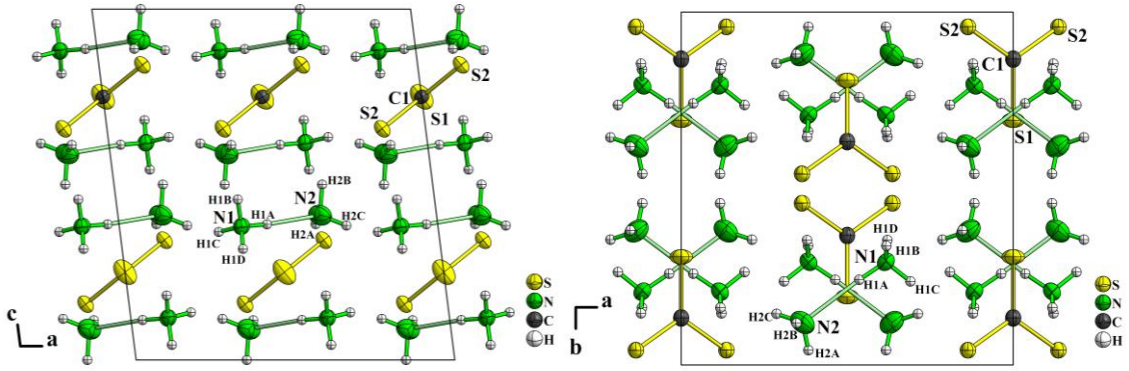

Figure 2.83: Unit cell set up of $(H_7N_2)_2CS_3$ **30** with view along the *b*- and *c*-axis on the left and right, respectively. All non-hydrogen atomic displacement ellipsoids are drawn with 70 % probability. The bond between the special sited atoms C1 and S1 (4e), is pointing towards the viewer in the left picture.

Figure 2.84 shows the coordination arrangement between the CS_3^{2-} and $(N_2H_7)^+$ ions. The hydrogen atoms could be refined free, i.e., their lattice coordinates and isotropic displacement parameters were obtained without empirical restraints. Table 2.12 on page 130 gives the essential values of the hydrogen bond of the diamine hydrogen cation obtained by measurement and compares them with those reported for other compounds. Drawn as red connections in figure 2.84, there are three bifurcated bonds, a shorter (bold) and a longer (fine) for each of the terminal hydrogen atoms of the H_4N^+ fragment of the diamine hydrogen cation. From the consideration of the order of the covalent bonds in the CS_3^{2-} anion (cf. above), the S2 atom is favourable over S1 to perform ionic interactions with cations. Therefore, the terminal H1···S2 distances are short (see values given in figure 2.84), with N1−H···S2 angles close to a straight virtual connection: S2···H1B−N1 = 177°, S2···H1C−N1 = 168° and S2···H1D−N1 = 174°. H1D relates to the second S2 atom of the CS_3^{2-} anion with an increased distance of 300.1 pm. Suggesting a weaker interaction,[38] this and two other even longer distances (S1−H1C/B) are drawn thin in figure 2.84 coordinating the H_4N fragment.

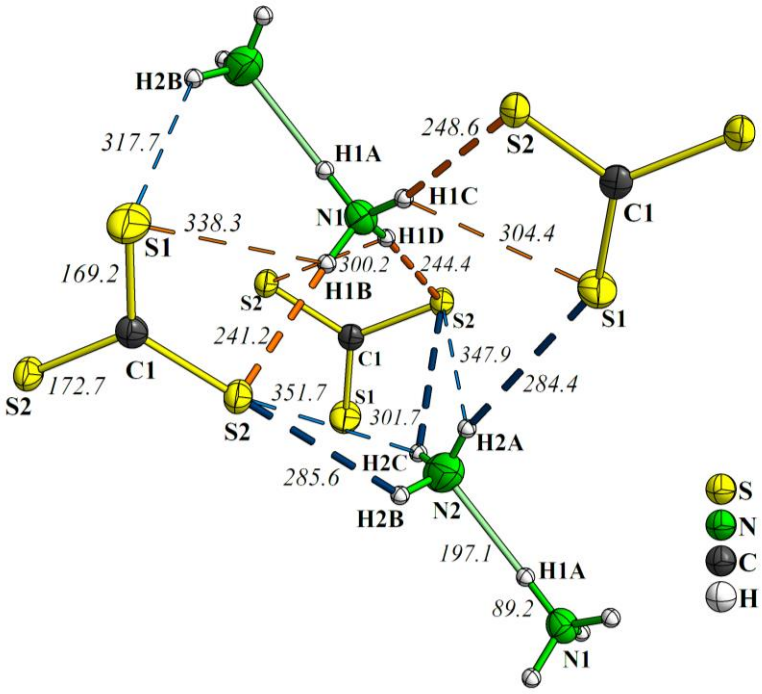

Figure 2.84: Coordination and bonding arrangement in $(H_7N_2)_2CS_3$ **30**. For all non-hydrogen atoms, the atomic displacement ellipsoids are drawn at 70 % probability. The numbers are bond lengths given in pm.

According the number of hydrogen atoms, the NH_3 fragment of the diamine hydrogen ion is bound to the nearest trithiocarbonate anions, with the hydrogen bonds less well oriented for a tetrahedrally shaped fragment (N2−H2B···S2 = 128(1)°, N2−H2B···S2 = 132(2)°). Nevertheless, as drawn in bold dark blue connections in figure 2.84, these shortest bonds stabilise the NH_3 fragment. Assuming dispersive long distant interactions (317.7 – 351.9 pm), each hydrogen atom of the NH_3 unit, is in range of multiple coordination by other sulfur atoms. Note, for the sake of clarity, not all of them are drawn in figure 2.84. However, in consideration of other sulfur compounds (cf. below) an upper limit of ~300 pm was found for S···H distances in S···H−N hydrogen bonds with $(H_7N_2)_2^+$ cations. Although, the ionic character differs from some of the other reported compounds, over all the geometric properties in **30** is found in accordance and suggests neglecting the longer S···H distances mentioned above.

Finally, with the distorted tetrahedral coordination of the NH_3 fragment, the structure solution with a diamine hydrogen cation is evident in the strongest interaction of the NH_3 unit, which is that of the lone pair with the hydrogen atom H1A of the H_4N fragment.

2.5.3 Vibrational molecular spectroscopy

Both IR and RAMAN spectroscopy were conducted on ammonium salts of the mixed trithiocarbonate dithiocarbamate **31**, the pristine dithiocarbamate **32** and of diamine hydrogen trithiocarbonate **30**. As mentioned **30** was temperature sensitive and needed cooling for vibrational spectroscopy investigations. For both methods, the increased size of the intergrown polycrystals of **30** were advantageous. Thanks to that, the sample was mechanically stable enough to be transferred into a glove box, which was equipped with a freezer, running at −40 °C for intermediate and subsequent storage. Thus, it could be realised to analyse diamine hydrogen trithiocarbonate **30** with an ATR-IR device for the first time. µRAMAN spectroscopy on **30** was carried out with use of an inert gas temperature-controlled measuring cell (*THMS 600*, *Linkam Scientific Instruments Ltd.*, Tadworth, UK). It is shown in figure 2.85 and offered to cool the sample chamber down to arbitrary temperature. µRAMAN spectra of **31** and **32** could be measured through the glass wall of the sample vials and IR spectra were recorded likewise with an ATR-IR device in the glovebox. All spectra are given in figure 2.86.

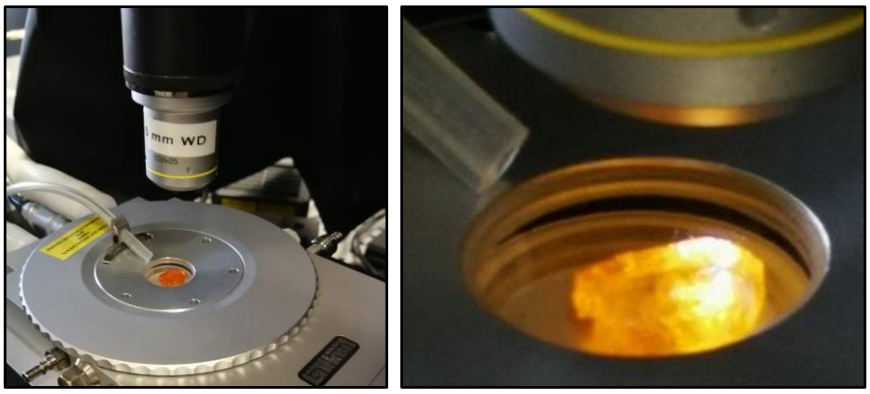

Figure 2.85: Inert gas temperature control chamber holding a large polycrystal of $(H_7N_2)_2CS_3$ **30** was encapsuled in nitrogen (left). Close up photo of the specimen at 100 K.

Diamine hydrogen trithiocarbonate has earlier been investigated with RAMAN spectroscopy by BENZ, who assigned the modes of $N_2H_7^+$ with those of neutral NH_3 (liquid) and H_4N^+. He concluded a shift towards lower energy due to the strong hydrogen bond connecting the individual molecules.[94]

IR and Raman spectroscopy on $(H_7N_2)_2CS_3$

In this work, RAMAN spectra of $(N_2H_7)_2CS_3$ **30** recorded at RT and −170 °C (100 K) allowed to resolve more modes in the high energy regime as expected for the individual NH_3 an H_4N^+, respectively, which is in line with the results of BENZ.[94] No additional downshifted

'N···H−N' modes that could be distinctive for $N_2H_7^+$, could be resolved, not even at low temperature. Beforehand, it was assumed, that the strong hydrogen bond, comprising the principal axis of the molecule, may indicate a stretching vibration at lower wavenumbers than the expected spectral region for N−H valence stretching modes.

In the top area in figure 2.86, for clarity only the band centres of the low temperature RAMAN measurement are written. Signals above 2500 cm^{-1} at RT, which involve only the N−H groups, are altered slightly in position, which is written down in

table 2.13. It must be stressed here, that from the red aqueous mother liquor that was wetting the crystal and passed into the inert gas chamber (cf. figure 2.85), O−H impurity modes, prominent to the high energy region, cannot be excluded to be intermixed in the signals.

For comparison, representative for the H_4N^+ ion, a RAMAN spectrum of $(H_4N)Cl$ was recorded and is plotted below the diagram in figure 2.86 (black line), allowing to see clear difference with the spectra of **30**. At first glance, the very intense modes at 1710 and 3560 cm^{-1}, which for instance belong to the fundamental vibrations of H_4N^+, are not observed in the sprectrum of $(N_2H_7)_2CS_3$ **30**. The experimental ammonium chloride reference was in perfect agreement with earlier investigation of the vibration spectra of the ammonum ion.[107] This indicated already, that in $(N_2H_7)_2CS_3$ **30** indeed no free ammonium ions were present, which supports the SC-XRD structure model. More generally, in the region of N−H stretching vibration expected above 2700 cm^{-1} some accordance can be seen in the IR and RAMAN spectra of $(N_2H_7)_2CS_3$ **30**. Assuming the hydrogen bonding in $N_2H_7^+$ to result in a redshift of the individual modes of H_4N^+ and NH_3, at least it can be learned from the RAMAN spectra that the two highest wavenumbers at 3349 and 3221 cm^{-1} (3365 and 3277 cm^{-1} at RT) should be considerably ordered to the hydrogen-bound NH_3 moiety in $N_2H_7^+$. This is because liquid NH_3 exhibits vibrations at slighly increased wavenumbers.[108] The unspecific broad IR absorption (probably four individual modes) could not be improved, due to the overall challenging circumstances of the IR-ATR measurement, because of the instability of $(H_7N_2)_2CS_3$ **30**, successively releasing liquid decomposition products, naturally including ammonia and most probably ammonium.

Towards lower wavenumbers, some relatively weak peaks at 1656 1414 and 1130 cm^{-1} with complementarily pronounced IR absorptions were detected. Deformation modes of N−H bonds could be assigned in the region 1650 to 1560 cm^{-1},[86] which also describes the character of the intensity at 1414 cm^{-1} that literally has the same shape and position like the band in the spectrum of (H_4N) Cl. At last, it is likely that CS_2 impurities afforded a symmetric stretching between 1050 to 1200 cm^{-1}. The strong IR absorption at 883 cm^{-1} in

company of two weak RAMAN signals at 1037 and 919 cm^{-1} should be results of asymmetric valence stretching on the CS_3^{2-} anion. Followed by that, the very strong symmetric valence stretching, expected for CS_3^{2-} was noted in the RAMAN spectra, whereas in the IR spectrum only a broad absorption is obtained. A series of weak in plane deformation modes of the anion was recorded below 400 cm^{-1}, which was in good agreement to the spectra discussed for alkali and barium trithiocarbonate (cf. sub-section 2.4.2).

Table 2.13: Compilation of RAMAN mode frequencies of $(H_7N_2)_2CS_3$ **30** and $(H_4N)Cl$ and reference data. All numbers given in cm^{-1}.

vibration character	this work, $(H_7N_2)_2CS_3$ **30**		BENZ 2010[94] $(H_4N)_2CS_3 \cdot 2\ NH_3$	this work, $(H_4N)Cl$	$(H_4N)Cl$[107]
	RT	−170 °C	RT?		
ν(N−H)	3365 w	3349 vw	3351 w		
	3277 m	3221 w	3270 s	3148 s	3146
		3076 bw	3223 msh	3056 vs	3041
	3003 bm	2987 m	3020 vs		
	2878 vwsh	2904 w, 2790 w	~2750 – 2300 bsh	2821 m, 2002 m	2828, 2010
δ(NH)	1393 w	1656 w?		1768 m, 1710 vs	1780, 1765, 1710
		1414 w, 1396 wsh		1425 wsh, 1403 m	1440, 1418, 1400
CS_2	1127 w	1130 w			
ν_{as}(C−S)	1022 w	1037 w	1050 w		
	910 m	919 m	908 m		
δ(NH)		643 vw?			
ν_s(C−S)	505 vs	508 vs	503 vs		
$\delta_{ip}(CS_3)$	315 w	390 w	313 m		
		337 w	161 m		
		255 w			
		191 w			

IR and Raman spectroscopy on $(H_4N)_5(CS_3)_2[S_2C(NH_2)]$ and $(H_4N)[S_2C(NH_2)]$

In the RAMAN spectra for the two other compounds, $(H_4N)_5(CS_3)_2[S_2C(NH_2)]$ **31** and $(H_4N)[S_2C(NH_2)]$ **32**, the absence of the very acute signal at 1710 cm^{-1} of the fundamental deformation mode of ammonium is remarkable, because both the compounds were identified including this cation. To some degree this may be a result of the three dimensional hydrogen bonds, that have been derived from the crystal structure models. In ammonium chloride, an increased salt character might allow the cations to deform specifically, which under influence of covalent bonding interactions may be hindered. This statement is

furthermore not conflicting with the observed structural peculiarities of $(H_7N_2)_2CS_3$ **30**, which also comprises such a network of hydrogen bonds. After all, a certain assignment of the experimental data of **31** and **32** with the fundamentals of H_4N^+ was found unpractical due to the extended hydrogen bound network discussed above.

By investigation of the mixed phase product including crystals of $(H_4N)_5(CS_3)_2[S_2C(NH_2)]$ **31** with vibration spectroscopy could identify the pale yellow microcrystalline side product (cf. figure 2.74). As seen in the µRAMAN spectra in the diagram, the unknown solid can be assumed $(H_4N)[S_2C(NH_2)]$, too, because the respective spectra include the same signal pattern. This is the green line in the middle diagram displaying the spectrum of the pale yellow side product, which perfectly matches the bands in the diagram at the bottom, showing the RAMAN spectrum of $(H_4N)[S_2C(NH_2)]$ **32**. This is in accordance with the PXRD analysis (cf. above).

Two RAMAN bands (brown line) were detected focussing on the orange carrot-shaped crystals of $(H_4N)_5(CS_3)_2[S_2C(NH_2)]$ **31**, which without doubts could be assigned to CS_3^{2-}. They are the strong symmetric valence stretching and the weak out of plane deformation near 500 cm^{-1} and are of consistently missing in the RAMAN spectra of only dithiocarbamate $S_2C(NH_2)^-$. However, as in the crystal of **31** also dithiocarbamate was included, the representative modes are added in the spectrum. Bands of low RAMAN activity like in plane deformation (~200 – 350 cm^{-1}) and asymmetric valence stretching (~800 – 950 cm^{-1}) belonging to CS_3^{2-} are less well resolved. This also holds for the high frequency region in the spectrum of $(H_4N)_5(CS_3)_2[S_2C(NH_2)]$ **31**, where albeit the presence of dithiocarbamate (cf. bottom diagram **32**), only a broad bump was detected. The weak signal is too unspecific for evaluation and since ammonium cations were present, probable differences between cation and anion N−H valence stretching is not possible.

The IR spectra of $(H_4N)_5(CS_3)_2[S_2C(NH_2)]$ **31** and $(H_4N)S_2C(NH_2)$ **32** are almost identical. For clarity, peak centres of matching absorptions are only given in the bottom field. Thus, marking only one very different rather weak peak in the spectrum of **31** at 892 cm^{-1}, which could indicate the expected CS_3^{2-} asymmetric valence stretching (cf. alkali salts, sub-section 2.4.2). At highest wavenumbers (> 3200 cm^{-1}) two medium strong absorptions in both the spectra of **31** and **32** are found, which can be assigned with anti- and symmetric N−H valence stretching of the amide group of the dithiocarbamate. The modes are also seen in the RAMAN spectra.[84] At slightly lower wavenumbers, the typical ammonium cation vibration is mixed into the spectrum. This is sustained, taking the experimental $(H_4N)Cl$ curve for comparison into account.

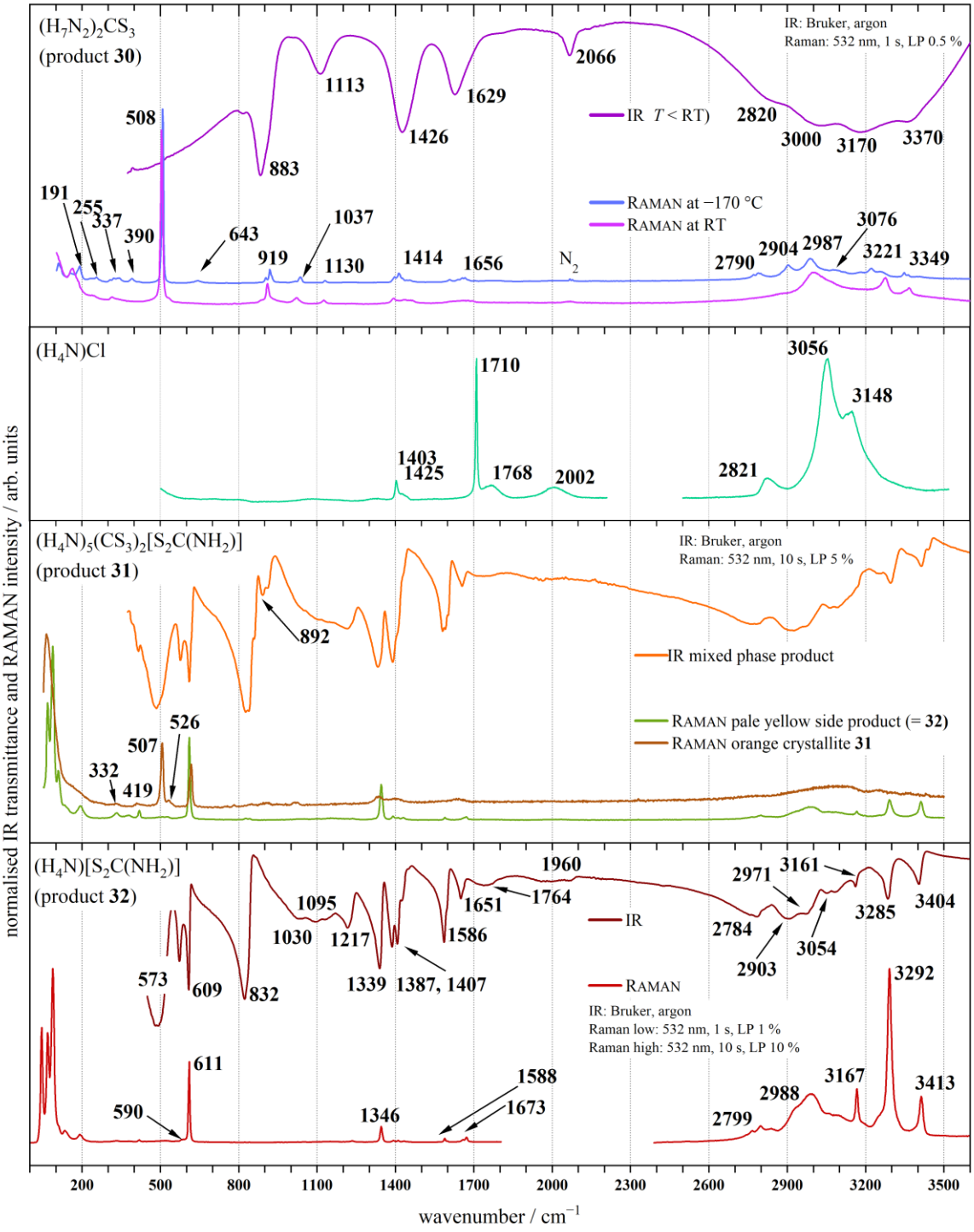

Figure 2.86: Vibrational spectra of the products obtained in the system of NH_3 and CS_2. $(H_7N_2)_2CS_3$ **30** (top), $(H_4N)_5(CS_3)_2[S_2C(NH_2]$ **31** (bottom mid) and $(H_4N)[S_2C(NH_2)]$ **32** (bottom) as well as $(H_4N)Cl$ (top mid) for reference. Mode centres are given in cm^{-1}.

From molecule symmetry considerations, the $S_2C(NH_2)^-$ anion ideally possesses C_{2v} symmetry, assuming the hydrogen atoms co-planar with the S_2CN backbone (like obtained in the crystal structures). As stated above, six atoms in the non-linear molecule give 12 ground state vibrations to be expected that should be both IR and RAMAN active.[109] The assignment of the modes and support of the results with earlier publications as well as the calculated values as approximates is arranged in table 2.14. The X-ray $S_2C(NH_2)^-$ structure was used in a DFT and MPT level calculation to optimise its geometry. The resulting molecule bond lengths and angles are found in table 5.15 and was used to compute its RAMAN and IR vibration frequencies. In consideration of the respective vibration animations, the vibration character could be assigned sustainably. The calculated wavenumbers matched the references and the collected experimental data of this work. An exception has to be made for the high frequent N−H valence stretching modes, which are calculated to have much higher wavenumbers, displaying errors in the used DFT method to handle hydrogen atoms and their covalent bonds.

It has to be noted at last that most probable intermolecular interaction in the crystalline species act out combinations of fundamental vibration and lattice overtones, which demands a certain degree of freedom for the assignment. For instance, absorptions near 1000 or 1600 – 1700 cm^{-1} cannot be assigned unambiguously, which may have their origin in a combination vibration. Impurity vibrations may also occur.

Table 2.14: Assignment of experimental IR absorption and RAMAN shift intensities of $(H_4N)S_2C(NH_2)$ **32** in consideration of calculation and experimental reference data.

vibration character	this work, $(H_4N)S_2C(NH_2)$ **32**			references	
	experimental		calculation	experimental	
	IR	RAMAN	IR / RAMAN	IR[90]	RAMAN[109]
ν(N−H)	3404 m 3285 m	3413 (**31**3412) m 3292 (**31**3290) s	3746 ‡ 3586 ‡	3300 vssh 3250 vs	3290 3200
ν(N−H)(*)	3161 w 3054 w 2971 bw 2903bm 2784 bm	3167 m ~3050 sh 2988 bm 2799 m		3150 s ~3000-2500 sh	
ν(H_4N^+)(**)	~1960 vbw			2060 m	
	1746 bm 1651 m	1673 vw			
$\delta(NH_x)$	1586 s	1588 vw	1555	1590 sh 1570 vs	1588
$\delta(H_4N^+)$(**)	1387 s 1407 s	1392 vw		1395 vs	
ν(N−C)	1339 s	1346 m	1268	1322 m	1344
$\delta_{ip,as}(C-NH_2)$	1217 m		1250	1238 m, 1200 m	1217
ν(C=S)?, δ(C−N)?, lattice	1095 bm 1030 sh				1147
$\delta_{ip,s}(C-NH_2)$, ν_{as}(C−S)	832 vs		881	860 vs 844 vssh	859
ν_s(C−S)	609 s	611 vs	638 605	619 s	612
$\delta_{op}(NCS_2)$	573 s	590 w	578	579 m	
δ_{ip}(C−S), $\gamma_{ip}(C-NH_2)$	492 bs	**31**419 w **31**332 vw	405 319		433 418, 332 197

v very, w weak, m medium, s strong, b broad, sh shoulder; ?uncertain; (*)ammonium vibration, not occurring in alkali dithiocarbamates[110]; ‡ too high frequent, failure of calculation of hydrogen atoms; (**)combination of ammonium fundamentals with lattice modes[84]; **31**pale yellow side product in **31** (green line in middle diagram)

2.6 Thiocarbonate complexes of transition, p-block and 4f-metals

Dithiolato complexes with ligand structures according to $S_2C{-}X$ can be realised in great variation.[1,12,19,93,111,112–114] The known homoleptic trithiocarbonato complexes, belonging to that group of 1,1-dithiolato complexes are listed in table 2.15.

Table 2.15: Known homoleptic trithiocarbonato complexes of transition and p-block metals.

colour	complex	reference
yellow	$[Sn(CS_3)_2]^{2-}$	[115,70]
yellow	$[As(CS_3)_3]^{3-}$	[115,70,116]
yellow – orange	$[Sb(CS_3)_3]^{3-}$	[115,70]
orange	$[Bi(CS_3)_3]^{3-}$	[115,70,116]
light brown	$[Cu(CS_3)_n]^{n-}$	[115,70]
	$[Au_2(CS_3)_2]^{2-}$	[117,118]
	$[Au(CS_3)_2]^{-}$	[117]
	$[Au^{I}_n\{Au^{III}(CS_3)_2\}_{n+1}]^{-}$ ($n \approx 6$)	[117]
light yellow	$[Zn(CS_3)_2]^{2-}$	[115,70,119]
light yellow	$[Cd(CS_3)_2]^{2-}$	[115,70]
light green	$[Cr(CS_3)_3]^{3-}$	[115]
black	$[Fe(CS_3)_3]^{3-}$	[116]
blue-black	$[Co(CS_3)_2]^{2-}$	[120]
olive green	$[Co(CS_3)_3]^{3-}$	[115,70]
red	$[Ni(CS_3)_2]^{2-}$	[121,113,114,122,123,119]
brown – red	$[Pd(CS_3)_2]^{2-}$	[113,122]
yellow – orange	$[Pt(CS_3)_2]^{2-}$	[113,122]

Among the very first investigators of the chemistry of transition metals with CS_2 were WIEDE and HOFMANN, who reported on $Ni(NH_3)_3CS_3$ in 1896,[124] and one year later HOFMANN added a report on $Pt(NH_3)_2S_3C \cdot H_2O$.[125] During the 1960s and 70s based on different analytic methods, the compounds could be verified with the corrected sum formulas $[Ni(NH_3)_6][Ni(CS_3)_2]$ and $[Pt(NH_3)_4][Pt(CS_3)_2] \cdot 2\ H_2O$, respectively. MCKECHNIE et al. elucidated the first three crystal structure discovering trithiocarbonate anions as bidentate ligands, which was that of $[Ph_4As]_2[Ni(CS_3)_2]$ in 1967.[121] The structure was used in combination with results of vibrational spectroscopy and magnetic measurements to prove the compounds of HOFMANN and co-workers to be two-centre complexes.[115,122,123] MÜLLER et al. were among those, who re-investigated the falsely interpreted $Ni(NH_3)_3CS_3$. They prepared $[Ni(NH_3)_6][Ni(CS_3)_2]$ by use of

$K_2[Ni(CS_3)_2] \cdot ½$ dioxane as starting material. This potassium complex again was obtained as amorphous brown-red powder and converted with $[Ni(NH_3)_4]^{2+}$ in dioxane.[115]

In 2010, BENZ finally described the crystal structures of $[Ni(NH_3)_6][Ni(CS_3)_2]$ and $[Pt(NH_3)_6][Pt(CS_3)_2]$ for the first time, stressing, that they consist of a paramagnetic octahedral-shaped cation and a diamagnetic square-planar-shaped anion. Indeed, this was the first and yet only crystal structure describing bis(trithiocarbonato) platinate(II),[94] stressing that the Pd^{2+} analogue is yet absent from crystallographic databases. Practically, BENZ used the conversion of CS_2 in concentrated ammonia solution with the respective d^8 transition metal ion to obtain the two-centre complex compounds.

In this work, this method was attempted only once using $NiCl_2$ as starting material. This afforded large blue crystals of $[Ni(NH_3)_6]Cl_2$, which were not investigated any further, next to an unidentified purple solid, depicted in figure 2.87 . Unfortunately, the purple microcrystalline species was unsuitable for SC-XRD analysis.

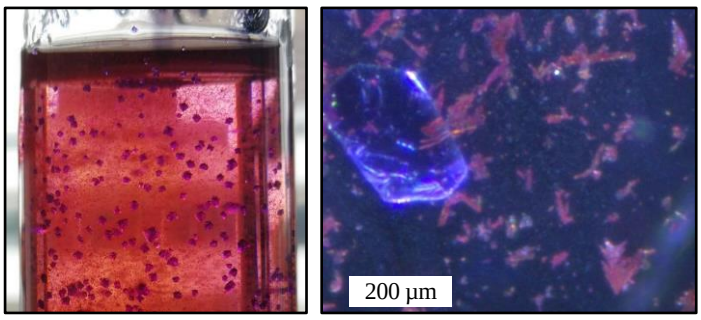

Figure 2.87: Blue crystals of $[Ni(NH_3)]Cl_2$ and a purple crystalline solid obtained from the aqueous ammonia solution with CS_2.

COUCOUVANIS, FACKLER and co-workers prepared the bis(trithiocarbonato) complexes with use of an alkali trithiocarbonate precursor. They stirred aqueous potassium hydroxide into a solution of CS_2 in DMF, which turned red after 5 minutes indicating formation of CS_3^{2-}. This solution was then brought to reaction with $Ni(CH_3COO)_2$, $PdCl_2$ or $K_2[PtCl_4]$ in ethanol to afford red to orange solutions containing the anionic bis(trithiocarbonato) metal(II) complex, respectively. By addition of an aqueous solution of tetraphenyl arsonium cations $(Ph_4As)^+$, the crude solid products including $[Ni(CS_3)_2]^{2-}$, $[Pd(CS_3)_2]^{2-}$ and $[Pt(CS_3)_2]^{2-}$ were obtained, respectively.[113,114] They have been investigated with IR, RAMAN and UV-vis,[113] and could all be determined diamagnetic with *electron spin resonance* ESR.[113] Accordingly, the d^8 transition metal centres are coordinated in a square-planar geometry by four sulfur donators of two trithiocarbonato chelate ligands, stabilising their low spin electron state. Similarly, the preparation with other volume consuming

monocations, exchanging the alkyl or aryl groups are mentioned, however recrystallisation and SC-XRD analysis were not performed.

These monocations, so-called *phase transfer catalysts* (PTC), basically allow transfer of inorganic molecules/complexes, dissolved in inorganic solvent to organic solutions/solvents and subsequent crystallisation.[126] This was also applied by MÜLLER, KRICKEMEYER et al., who discovered the crystal structures of a series of trithiocarbonato complexes: $[Sn(CS_3)_2]^{2-}$, $[M^{III}(CS_3)_3]^{3-}$ (M = As, Sb, Bi),[70] and $[Fe(CS_3)_3]^{3-}$.[116]

SEIDEL and DE BOER covered an aqueous solution of [Ni en_3]Cl_2 (en = ethane-1,2-diamine) with trithiocarbonic acid $(HS)_2CS$ in toluene to obtain [Ni en_3][Ni$(CS_3)_2$].[123] Like the hexaammine nickel(II) salt obtained by HOFMANN et al. (cf. above), the obtained two centre complex salt exhibits both a paramagnetic cation and a diamagnetic anion of Ni^{2+}.

Other than the use as a precursor mentioned above, a paper on the magnetic susceptibility of potassium bis(trithiocarbonato) nickelate(II) was published by JOHRI and KAUSHIK in 1968. It could not be accessed and from the brief listing in *Carbon Sulfides and their Inorganic Complex Chemistry* no details are obtained.[1,127] For potassium bis(trithiocarbonato) palladate(II) and platinate(II) nothing stands written.

The complex anion $[Co(CS_3)_3]^{3-}$ was included in an early work of MÜLLER et al. alongside with other trithiocarbonato metal complex anions. Already in 1973 the use of cationic PTCs afforded solid material for UV/Vis characterisation.[115] In a re-investigation of this compound, MÜLLER and co-workers were unable to prepare suitable crystals for SC-XRD in 1995, but discovered the complex to be centred with diamagnetic d^6 Co^{3+}.[70] Much earlier, SEIDEL and BRUHN reported the Co^{2+} complex anion in $[Co(NH_3)_6][Co(CS_3)_2]$ and other compounds.[120] BENZ work contains the first X-ray structure analysis of another two-centre cobalt complex $[Co(NH_3)_6]_3[Co(CS_3)_3]_2 \cdot 6\,NH_3$, which in analogy to the nickel compound (cf. above) was first mentioned in early works of HOFMANN.[94,124,125] It is therefore questionable if the Co^{2+} complex anion reported by SEIDEL and BRUHN really exists, since it does not occur elsewhere and the determination of the authors was based on element analysis and qualitative comparison of IR spectra only.[120] Crucial magnetic investigation is missing elucidating the oxidation state of the metal centre.

2.6.1 The Ni^{2+}, Pd^{2+}, Pt^{2+} and Co^{3+} trithiocarbonato complexes

In order to investigate a new pathway for the preparation of thiocarbonate compounds including transition metal complexes, acetates of Ni^{2+}, Pd^{2+} and Pt^{2+} as well as $CoCl_2$ were put to reaction with K_2CS_3 **9** under solvothermal conditions. Crystalline compounds suitable for X-ray structure analysis including the trithiocarbonato complexes $[Ni(CS_3)_2]^{2-}$ **35**, $[Pd(CS_3)_2]^{2-}$ **36**, $[Pt(CS_3)_2]^{2-}$ **37**, $[Co(CS_3)_3]^{3-}$ **38** were obtained. On the photographs in the figure 2.88 to 2.92 the crystal specimens are depicted. As expected from the literature on transition metal dithiolato complexes, the trithiocarbonate anion introduced from the potassium salt was found to react as a bidentate ligand for the transition metals. For the first time, the obtained transition metal complexes could be crystallographically elucidated with potassium ions to compensate the negative charges on the complex, denying a mandatory presence of PTC cations, e.g. tetraphenylphosphonium $[Ph_4P]^+$.[1] As supplement, the latter phosphonium cation was used to obtain a second crystal including the Pd^{2+}-centred complex: $[Ph_4P]_2[Pd(CS_3)_2]$ **39**.

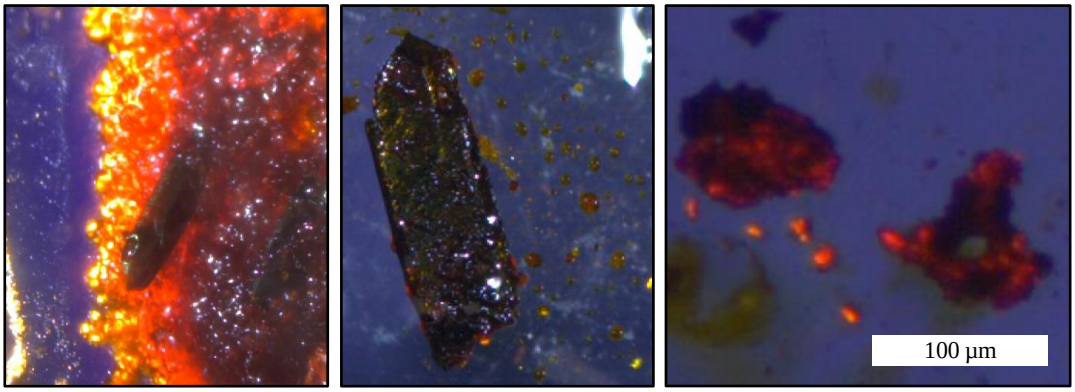

Figure 2.88: Microscope photographs of the products obtained from the reaction of K_2CS_3 **9** with nickel(II) acetate tetrahydrate. A dark monolith of $K_2[Ni(CS_3)_2]$ **35** were obtained, grown from the reaction mass (left). Isolation (middle) and careful breaking of the dark crystal (≈ mm) into smaller pieces disclosed a red colour (bottom right).

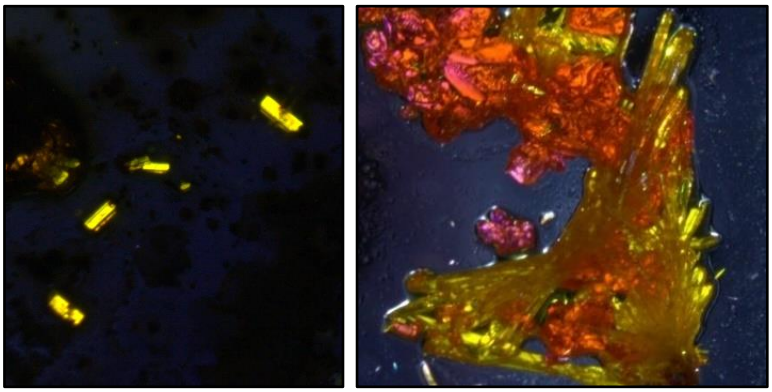

Figure 2.89: Yellow crystals of $K_2[Pd(CS_3)_2] \cdot EtOH$ **36** from two separate reactions with different morphologies. The photo on the left shows the specimens used for SC-XRD structure analysis. The right photograph displays the orange-pink starting material, which recrystallised alongside. Before conduction to RAMAN spectroscopy, the reproduced crystals were indexed with the same cell as **36**.

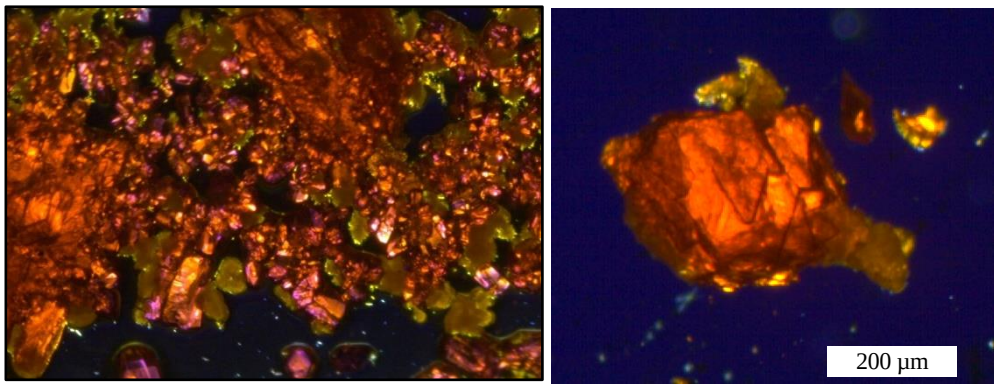

Figure 2.90: Overview of the crystalline products obtained from the solvothermal reaction with platinum(II) acetate (left). Example of orange crystalline $K_2[Pt(CS_3)_2]$ **37** (right). In reproduction, differentiation of recrystallised starting material **9** and $K_2[Pt(CS_3)_2]$ **37** was ensured by crystal lattice indexing.

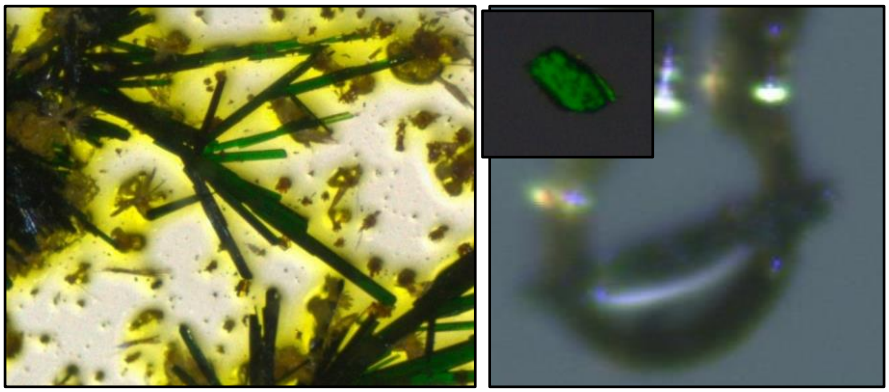

Figure 2.91: Overview of the green $K_5[Co(CS_3)_3]CS_3$ **38**, which was obtained alongside with and $K_7(CS_3)_3Cl \cdot H_2O$ **14** (not shown) as discussed in section 2.1.2 and probably other unidentified products (left). The green needle shaped crystals were fragile and quickly weathered after removal from the ampoule. Small specimen (inset) did not diffract properly under radiation with X-ray. Eventually, one larger needle-shaped crystal was used for data collection **38**. Mounting loop carrying the crystal during the measurement (right).

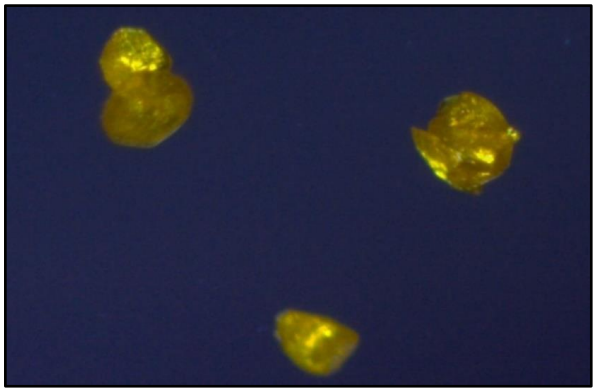

Figure 2.92: Yellow crystals of $[Ph_4P]_2[Pd(CS_3)_2]$ **39**.

The crystals were investigated with µRAMAN spectroscopy, allowing to focus the probe LASER on the crystalline specimens with high accuracy. The obtained spectra are discussed below compiling the RAMAN spectroscopy of all complex compounds. The consecutive investigation of the solids with an ATR-IR device included the problem that the crystals were not obtained in abundant yield and moreover the samples used for the ATR-IR investigation could easily include side products or educts of the reactions. Using inert oil to keep the crystals from weathering, gave no useful IR spectra, as the already less well resolved fingerprint region was additionally mixed with dominant absorption from the oil.

Potassium bis(trithiocarbonato) nickelate(II) and platinate(II)

Crystal structure model

$K_2[Ni(CS_3)2]$ **35** and $K_2[Pt(CS_3)_2]$ **37** were found to crystallise isostructurally in the monoclinic crystal system. The four formula units per unit cell could be differentiated with two non-equivalent transition metal centres (Ni1/Pt1 and Ni2/Pt2) occupying the inversion centres 2a and 2d in the space group $P12_1/c1$ (No. 14). By that inversion sites the two trithiocarbonato ligands are symmetry equivalent on each metal centre. The Ni^{2+} and Pt^{2+} ion centres of the complex anions are coordinated by four sulfur atoms of two trithiocarbonato ligands and span a rectangular plane. Thus, a typical, although distorted, square-planar coordination geometry is realised. The point symmetry of the complex anions deviates slightly from ideal D_{2h}. For the Ni2/Pt2 centred complex anions this deviation from planarity was determined within the range of accuracy. In numbers, the dihedral angles S23−C2−S21−Ni2/Pt2 and C2−S22−Ni2/Pt2−S21 are 174.63(7)/176.1(6)° and 178.01(3)/177.9(3)°, respectively. The bidentate trithiocarbonato ligands are co-planar with the four-fold coordination plane.

All non-transition metal atoms in the structure occupy regular sites (4a). Figure 2.93 shows the extended filling of the unit cell of **35** in a tilted view along the *a*-axis. A close display of the geometry of the complex anions is given in figure 2.94.

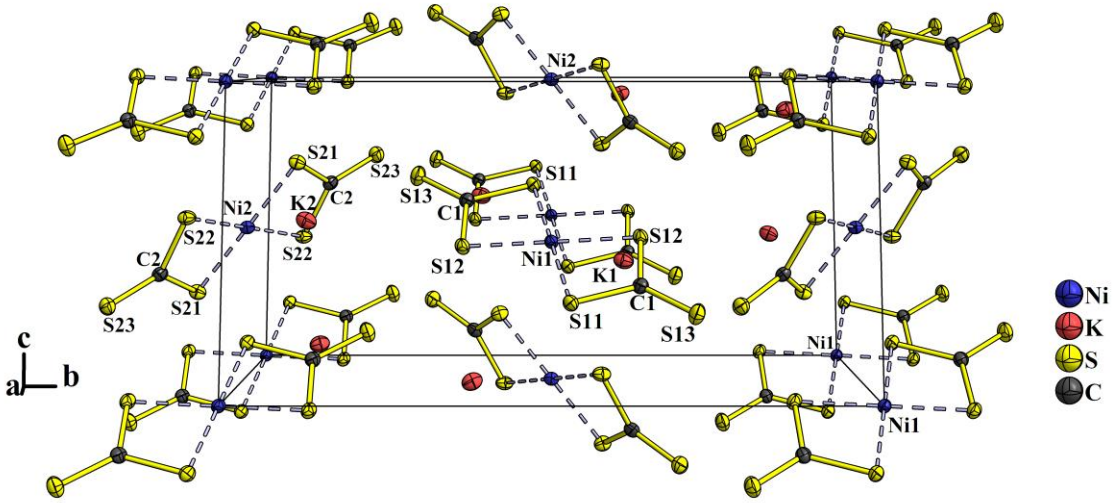

Figure 2.93: Extended display of the unit cell of $K_2[Ni(CS_3)_2]$ **35** with view along the *a*-axis. All displacement ellipsoids are drawn at 70 % probability. All nickel atoms occupy special lattice sites of inversion, located at either the cell corners or in the cell face centres.

The shape of the trithiocarbonato ligands is altered from that seen in structures of the free trithiocarbonate anion, which is in accordance with reported documentation.[94,121] The bidentate coordination of one trithiocarbonato ligand with the metal centre M describes a four-membered circle CS_2M. The endocyclic C−S bond lengths and S−C−S angle are increased and compressed, respectively, compared to the values for the exocyclic geometry. The exocyclic C−S bonds of the non-coordinating sulfur atom in the Ni^{2+} (Pt^{2+}) complex are only 165.6 pm (166.8 pm) and thus characterised rather as a double bond. Therefore, the two negative charges of the trithiocarbonato ligand should reside at the donor sulfur atoms S11, 12, 21 and 22 with major probability, which agrees with their longer, more single bonding character. However, the delocalised π-system should be maintained. The anti-bonding π*-orbital of CS_3^{2-} is empty and allows partial π-back donation of the electrons filled in the d-orbitals of the complex centre ion. The compression of the endocyclic angle, which is also the reason for the divergence of the ideal square-shape of the coordination, is a result of the interplay between the electron orbital repulsion with simultaneous attractive dative interaction as well as π-back donation between the metal centre and the ligands. In the square-planar ligand field, the d_{xy}-orbital of the d^8 metal ions is the energetically highest occupied and lies in coordination plane.[128]

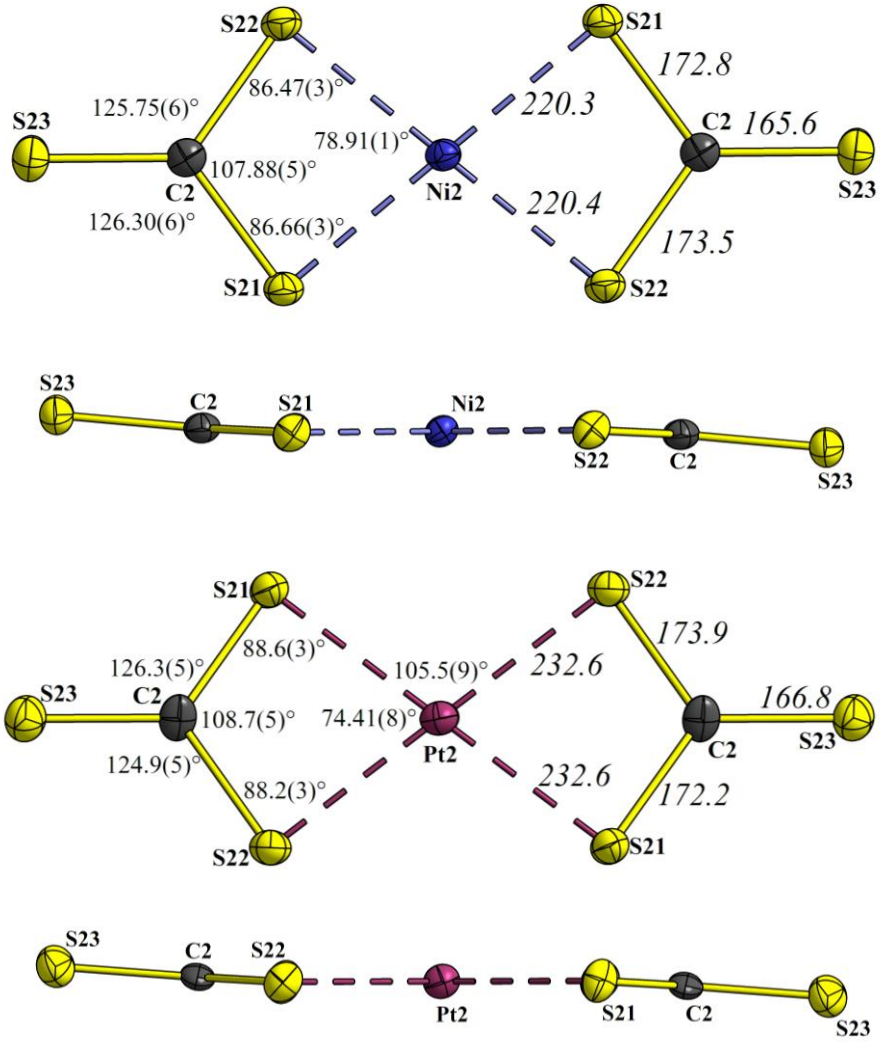

Figure 2.94: Top and side view of the complex anions $[Ni(CS_3)_2]^{2-}$ and $[Pt(CS_3)_2]^{2-}$ in the structure of **35** and **37**. Numbers in the top view are bond lengths in pm (italic) and angles, respectively. The metal centres coincide with lattice centres of inversion, i.e., the ligands are symmetry equivalent. As seen in side view, the complex structure deviate slightly from ideal planarity. Compared with the non-equivalent Ni1 and Pt1 complex (not shown here), planarity is found within the accuracy of measurement. All atomic displacement ellipsoids drawn with 70 % probability.

There are two crystallographically different potassium cations in the structure connecting the complex anions with ionic bonding. A closer look at the cationic surrounding of the Ni^{2+} complex anions is given in figure 2.95. Both the cations receive nine closest partially negative sulfur coordination partners (K−S) in the range of 315.8 to 358.2 (K1) and 320.7 to 369.2 pm (K2) in **35**. Two potassium ions (K1 and K2) are multiplied by inversion around the metal centres, spanning distorted squares. The planes of these squares are perpendicularly oriented towards the sulfur coordination plane of the metal centre and share

edges moving from one complex centre to the adjacent. This is demonstrated in figure 2.95. The potassium cations are virtually directed towards the electron filled d-orbitals of $Ni^{2+}$with *z*-component, suggesting an electrostatic interaction. The Ni···K distance for that is 365.4 to 398.1 pm. The same structure characteristics is naturally observed in the isostructural Pt^{2+} compound **37**, where the ionic K−S interaction ranges between 323.5 and 375.8 pm and K···Ni distances are 358.2 to 393.6 pm.

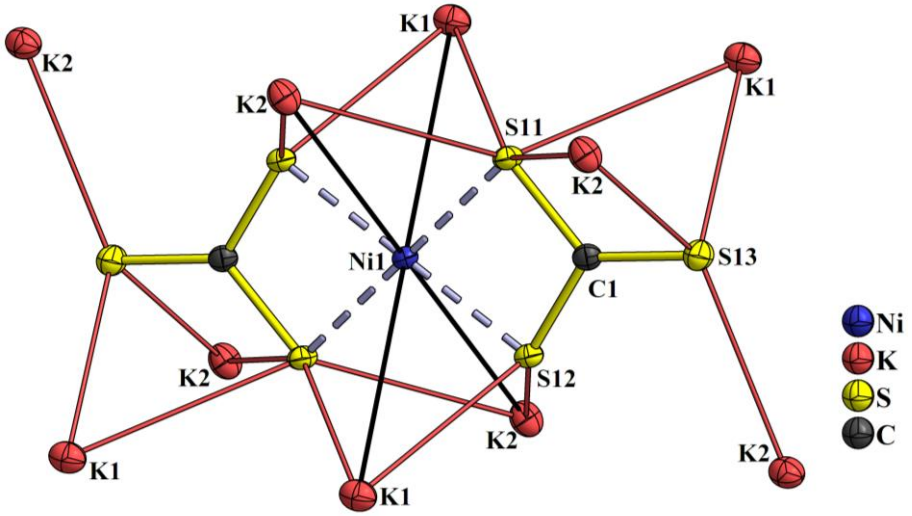

Figure 2.95: Potassium cations surrounding the complex anion $[Ni(CS_3)_2]^{2-}$ **35**. The ionic K−S interaction is drawn solid for better clarity. The K−Ni connections are drawn solid black to support visualisation of the distorted square-planar cation arrangement perpendicular to the nickel coordination by sulfur donators. All displacement ellipsoids are drawn at 70 % probability.

In some square-planar complexes of the d^8 metal ions Ni^{2+}, Pd^{2+} and Pt^{2+} with simpler ligand structures, it was discovered that parallel ordering of the four-fold coordination planes can occur. This builds up a perpendicular metal centre axis with relatively short metal···metal distances. Among the oldest examples is the green MAGNUS salt $[Pt(NH_3)_4][PtCl_4]$ (Pt···Pt distance 330 pm) and VAUQUELIN's salt, the palladium isomer (Pd···Pd 325 pm).[129] The former owes its unusual colour to the electric interaction between the metal centres.[130,131] In the structure of the isomeric pink MAGNUS salt, the Pt···Pt distances are > 500 pm and the square-planes of the individual complex ions are not in parallel order, overall showing no metal···metal interaction.[130,132]

Besides, upon sub-stoichiometric oxidation with chloride, $K_2[Pt(CN)_4]$ (Pt···Pt ≈ 350 pm), becomes one-dimensionally conducting along the axis of the intermolecular metal interaction, as the Pt···Pt distance is decreasing to a point (≈ 280 pm) that perturbation of the metal ion orbitals results in formation of an electron band.[131][133] This is explained as

the overlap of the filled d_z^2-orbitals along the metal axis becomes more and more probable with converging of the metal centres to one another. Under simultaneous oxidation, electrons from this band are withdrawn, leaving vacant electron states, which promote electric conduction in this band. In the previously mentioned $[Ni(NH_3)_6][Ni(CS_3)_2]$, this overlap cannot happen due to the octahedral coordination of Ni^{2+} with six amine ligands. In turn, as $[Pt(NH_3)_4][Pt(CS_3)_2]$ is set up by both square-planar anion and cation complexes, short Pt···Pt distances (≈ 353 pm) are found in the crystal structure by their parallel order.[94] Other properties of these compounds that can involve intermetallic interaction, like the solubility or vapochroism, have been investigated.[131]

Regarding these columnar structure motifs, in figure 2.96 the lattice of **35** is shown in view towards the (101) plane. As seen, the Ni1 and Ni2 centres are alternately rowed up in a virtual metal ion axis. However, the coordination planes are alternatively oriented perpendicular to one another by rotation around the virtual C···Ni···C axis. The exact intermolecular angle between the planes for the nickel compound **35** is 89.79(3)°. In the structure of the Pt^{2+} compound **37** the angle values 89.4(3)°. Moreover, the shortest Ni···Ni (Pt···Pt) distance is about 500 pm (Ni···Ni 504.12(4) pm **35**, Pt···Pt 499.5(1) pm **37**), which is too far for significant orbital overlapping, not to mention the failure to order in parallel, which is mandatory.

In the same figure, one can describe the arrangement of the complex anions as a herringbone pattern, which is the result of the two-fold screw translation along the *b*-axis and the orientation of the two crystallographically non-identical anions towards each other. Finally, from these geometric considerations in no lattice direction metal···metal interactions can be derived.

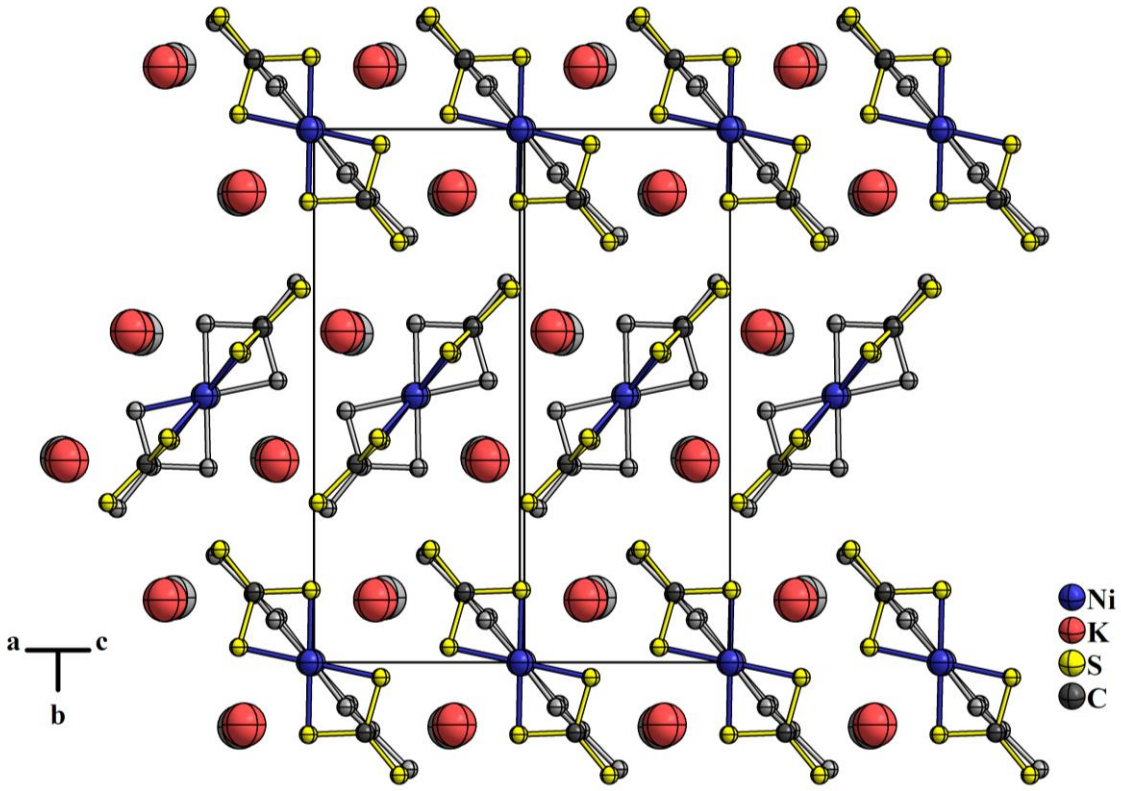

Figure 2.96: View towards the (101) plane in the atomic lattice of **35**. The atoms on top and in the layer below are drawn coloured and grey, respectively. They are virtually piled up along their Ni^{2+} centres (metal···metal distance > 500 pm). Their coordination square-planes are alternatively flipped about ~90°. Along the crystallographical *b*-axis a two-fold screw rotation coincides, resulting in a herringbone pattern arranged by the complex anions.

Most likely, large sterically challenging PTC cations used to crystallise trithiocarbonato complexes earlier, sterically prohibit a formation of the stacking motif in the solid state. However, as much smaller potassium ions are used to compensate the negative charges in the structures of **35** and **37**, the cation size cannot only account for the stacking and formation of metal···metal interaction. It can be assumed, that for a successful pairing of coordinative square-planes, moieties of opposite charge sign have to be present, like in $[Pt(NH_3)][Pt(CS_3)_2]$. In fact, it was moreover proposed that occasionally a requisite for successful columnar packing is an electrostatic interlocking of the ligands. For example, bis(di*alkyl*dioximato) complexes of Ni^{2+}, Pd^{2+} and Pt^{2+} cancel columnar packing of the square-planes, when larger alkyl functions than methyl are substituted on the bidentate ligand. But, for instance in bis(diacetyldioximato), e.g., $[Ni(C_4H_8N_2O_2)_2]$, the ligands along the metal···metal chain are staggered by 90° allowing the methyl groups of the ligand to interlock.[131]

Potassium bis(trithiocarbonato) palladate(II) ethanol

Crystal structure model

In contrast to the structures comprising the homologous complexes of Ni^{2+} and Pt^{2+} presented above, the bis(trithiocarbonato) palladate(II) anion crystallised with potassium cations and an additional ethanol molecule to give $K_2[Pd(CS_3)_2] \cdot C_2H_5OH$ **36**. The unit cell contains two formula units and applies the monoclinic system with the space group $P2_1/m$. (No. 11).

Chemically, the complex palladate anion in **36** is set up likewise in the nickel and platinum compounds. Two bidentate trithiocarbonato ligands coordinate the Pd^{2+} ion with two sulfur donators each. Like in **35** and **37** (cf. above), the square-plane spanned by the sulfur donators is deformed to a rectangle. In the crystal structure of **36**, the virtual C···Pd···C line lies in the mirror plane. In this way, the exocyclic sulfur atoms S21 and S22, the carbon atoms C1 and C2 and the Pd atom occupy the mirror site 2e in the lattice. This symmetry element demands two non-equivalent trithiocarbonato ligands for the description of the structure and therefore allows changes from the overall planarity of the anion molecule. In figure 2.97, where the unit cell structure of $K_2[Pd(CS_3)_2] \cdot$ ethanol **36** is depicted, a clear bending of the anion is demonstrated, which is fashioned by a tilt of the trigonal-planar trithiocarbonato ligands out of the PdS_4-coordination plane. To figure the deviancy from the ideally planar geometry (D_{2h}: torsion = 180°), the torsion angles C1−S11−S21−C2, S12−C1−S11−Pd and S22−C2−S21−Pd can be considered. They value 167.2(2), 173.5(3) and 169.9(3)°, respectively. Still within the margin of accuracy the Pd^{2+} ion is in plane with the four sulfur donors. The clear bending of the complex plane may not only be a result of the lattice symmetry. Apparently, visualising the unit cell, the bending in the complex plane may be involved with the presence of a neutral ethanol molecule of crystallisation. The oxygen atom of the ethanol molecule occupies the mirror site 2e, resulting in a mirror disorder of the attached ethyl group and the hydroxy hydrogen atom (all occupying the regular site 4f). For the solution of the data the disorder was realised by a site occupation of 50 % for each atom in the ethanol molecule except oxygen, as it is not disordered. For clarity, only one orientation of each ethanol molecule site in the lattice is drawn in figure 2.97. The parallel view along the mirror plane depicted in the unit cell drawing in figure 2.98 visualises this disorder of the ethanol molecule.

From the square planar coordination of it can be derived that the d_z^2-orbital of the Pd^{2+} ion is occupied by non-bonding electrons, which may electrostatically interact with the dipole of the hydroxy group, resulting in the orientation of the O−H bond towards the nearest Pd^{2+}

centre. However, the distance of Pd···H1 is about 270 pm and too long for a sustained formulation of a hydrogen interaction. A close depiction elucidating the geometry of the anionic palladate(II) complex is given below in figure 2.99.

There is only one potassium site K1 occupying the regular 4f position. It connects the complex anions by ionic bonding with seven K−S interactions of 327.2 to 347.4 pm distance. A close electrostatic stabilisation K−O can be concluded from distance of only 281.3 pm between the potassium ions and the dipole of the ethanol molecule. This concludes the potassium ion with coordination number 8.

In the course of this work, the capricious incorporation of an ethanol molecule per formula unit could not be explained thoroughly.

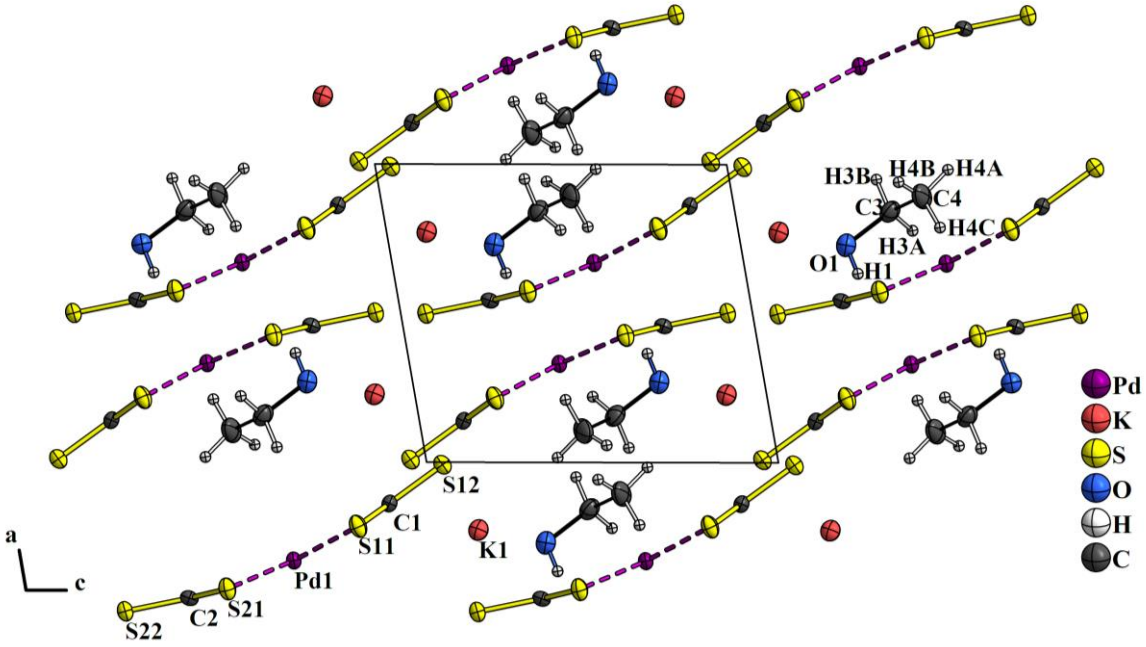

Figure 2.97: Extended unit cell display of $K_2[Pd(CS_3)_2] \cdot EtOH$ **36**. The view along the *b*-axis, perpendicular to the mirror plane, visualises the bending of complex anions.

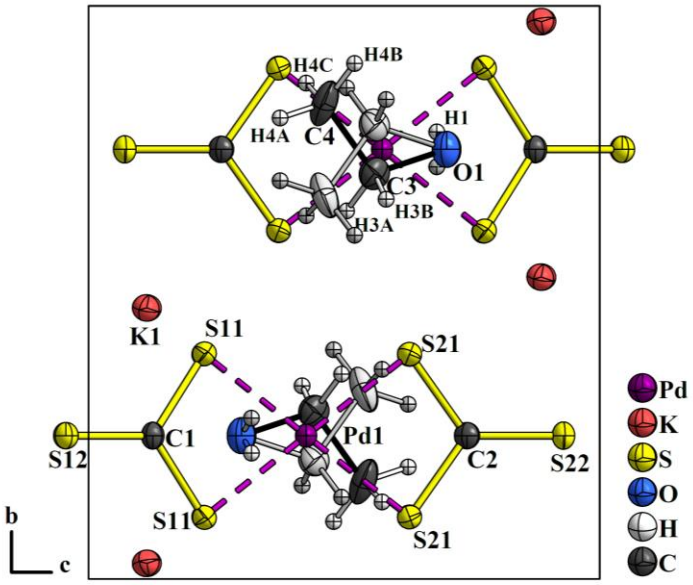

Figure 2.98: Display of the unit cell of $K_2[Pd(CS_3)_2] \cdot EtOH$ **36** along the *a*-axis, shows a view parallel with the mirror plane, which are occupied by the atoms S12, C1, Pd1, C2, S22 and O1. The latter is bound to the disordered ethyl group and the hydroxy hydrogen H1.

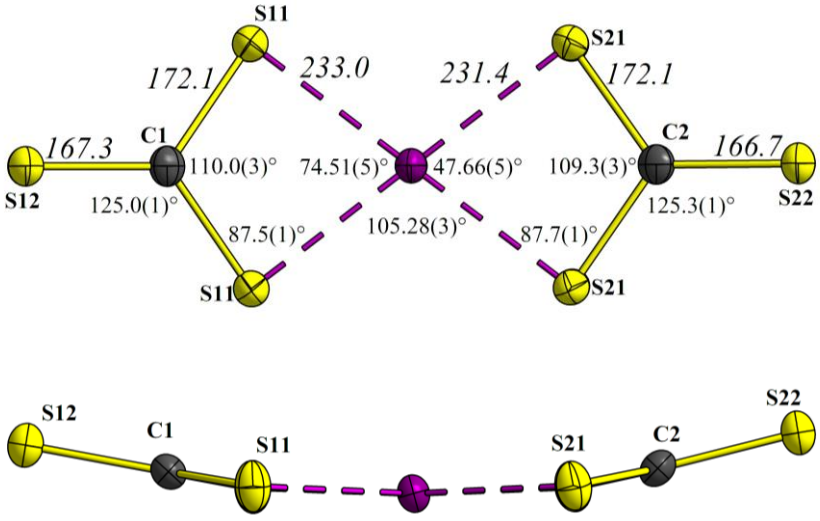

Figure 2.99: The complex $[Pd(CS_3)_2]^{2-}$ in the structure of **36** in top and side view. Numbers in the top view are bond lengths in pm (italic) and angles. From the side view a clear bending of the molecule is observed. All atomic displacement ellipsoids are drawn with 70 % probability.

Tetraphenyl phosphonium bis(trithiocarbonato) palladate(II)

Crystal structure model

The $[Pd(CS_3)_2]^{2-}$ complex anion was obtained in a second crystal structure, but with tetraphenyl phosphonium cations: $[Ph_4P]_2[Pd(CS_3)_2]$ **39**. The preparative route was adapted from MÜLLER, KRICKEMEYER et al., who were able to crystallise a series of homoleptic metal trithiocarbonato complexes with these large phase transfer catalytic cations (cf. preface of this chapter).[70] In this crystal structure, four formula units obey the space group $P2_1/c$ (No. 14) in the monoclinic lattice system, which is shown in . Noteworthy, the related $[Ph_4As]_2[Ni(CS_3)_2]$ structure is not isomorphous as it applies a *C*-centred monoclinic lattice ($C12/c1$).[121] In the structure of **39**, the complex anion shows no lattice site symmetry, i.e., all nine atoms in $[Pd(CS_3)_2]^{2-}$ possess a set of independent lattice coordinates. Thus, the complex can be geometrically evaluated free of site symmetry impact, which as described above was different in the potassium compounds.

It is visualised in figure 2.100, that the ideal planarity within the margins of accuracy, i.e., point group D_{2h}, is not obtained. In a strict view the accuracy allows to reduce the point symmetry to C_1, but for simplicity the complex anion can be called planar. In particular, the acute bending as observed in **36** is not seen here, highlighting, that the chemical environment around these known transition metal complexes can have significant influence the structure.

As expected, there are no $Pd^{2+}\cdots Pd^{2+}$ interaction observed either, in contrast to e.g., VAUQUELIN's salt $[Pd(NH_3)_4][PdCl_4]$. This is in accord with the structure of $[Ph_4P]_2[Ni(CS_3)_2]$ and similar bis(trithiocarbonato) compounds described earlier.[121,122]

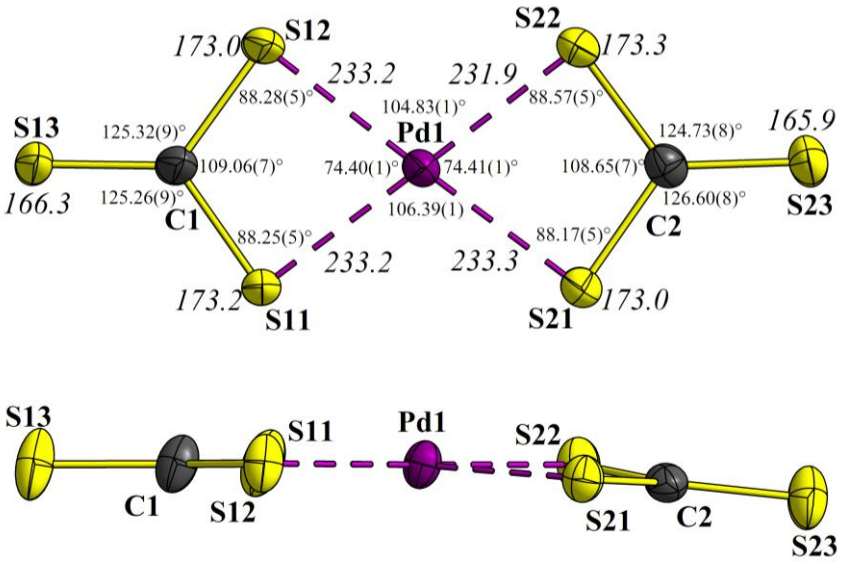

Figure 2.100: No atoms in $[Pd(CS_3)_2]^{2-}$ in the structure of **39** are symmetry equivalent. Numbers in the top view are bond lengths in pm (italic) and angles. All atomic displacement ellipsoids are drawn at 70 % probability.

Likewise in the complex compounds using potassium ions, the trithiocarbonato ligand geometry is anisotropically compared with the free anion. This may be a result of the lower ionic character of $(Ph_4P)_2[Pd(CS_3)_2]$ **39**, due to the screening of the positive charge at the phosphonium ion with bulky phenyl groups, The exocyclic C−S bonds are only 165.9 and 166.3 pm,. which is shorter than in the reported Ni^{2+} structure reported by McKechnie in 1967 (168 pm).[121]

Coordination aspects in nickel group bis(trithiocarbonato) complexes

According to the ligand field theory, the metal centre d-electrons are energetically altered from their degenerated level to allow the square-planar coordination by two bidentate trithiocarbonato ligands. This distribution is fashioned in the way, that the $d_{x^2-y^2}$ orbital of the metal centre remains unoccupied, as it lies in coordination plane, directed unfavourably towards the electron orbitals of the ligands. This allows the dative coordination with the negative charged sulfur atoms in the virtual *x*-*y*-plane centred by the transition metal ion. Accordingly, six d-electrons of the bivalent metal centres occupy the orbitals with a *z*-component, i.e., d_{z^2}, d_{xz}, d_{yz}, which are lowered in energy as they are not repulsive towards the ligands. The two remaining electrons fill the highest occupied orbital d_{xy}, which is less strongly affected by electrostatic repulsion than the $d_{x^2-y^2}$ orbital. One obtains a diamagnetic low-spin configurated d^8-complex. Depending on the metal centre, the d_{z^2} orbital can, but does not have to be the energetically lowest, i.e., energetically most favourable, orbital. It

was shown that the late transition metal ions like Ni^{2+}, Pd^{2+}, Pt^{2+} and Au^{3+} (d^8-ions) are prominent to form square-planar coordination compounds. But there are some other, more or less rarely found examples like d10 (Cd^{2+}), d9 (Cu^{2+}), d7 (Co^{2+}), d6 (Co^{3+}, Fe^{2+}) and d4 (Cr^{2+}), where square-planar coordination was observed.[16] Essentially, the four-fold coordination in a square-plane fashion, becomes more and more unfavourable the smaller the metal centre and the bigger, more room consuming the ligands are.[16] With increase of the size of the metal ion, the size of the ligands become less significant, thus for complexes with both Pd^{2+} and Pt^{2+}, (with few exceptions) coordination in the square-planar fashion, can be expected majorly. This was confirmed in the complex structures of **36**, **37** and **39** .

The situation is different for the 3d transition metals, that are generally smaller. More favourable for a four-fold coordination, is a tetrahedral arrangement of dative bonds towards a metal centre, because symmetrically the ligands are less repulsive towards each other. This includes a tetrahedral splitting of the d-orbital degeneracy and thus, a tendency to fill the $d_{x^2-y^2}$ orbital with electron density. Indeed, McKechnie et al., claimed a *tetrahedral buckling*, i.e., a non-planar coordination plane of the Ni^{2+} metal centre, which they quantified with a 5° angle between the planes spanned by Ni^{2+} and two sulfur atoms on either side.[121]

In the structure of **35** discussed above, as a consequence of an inversion symmetry centred by Ni^{2+} in the $[Ni(CS_3)_2]^{2-}$ anion, a perfectly planar arrangement of the sulfur donators is obtained. Thus, the coordination plane in **35** cannot be evaluated in this regard. Hence, only the structure of $[Pd(CS_3)_2]^{2-}$ in **39** can be analysed as it is free of special lattice sites. As stated, for Pd^{2+} a square-planar coordination should not be unfavourable. However, in consideration of such a tetrahedral tendency as stated by McKechnie et al., an angle between the S_2Pd planes in the square-planar coordination can be determined to a value of 3.9(2)° in **39**. Calling this a *tetrahedral buckling* after all appears exaggerated.

Furthermore, the earlier mentioned π-back bonding between the p-orbitals of the ligand and the d_z^2-orbital of the metal centre may be considered to compensate the anisotropic coordination in a square-plane compared to an octahedron. In short, the square-planar coordination can be understood as the result of an infinite stretching of the four-fold axis of an octahedral coordination.[16] This favours the population of the coaxial d_z^2-orbital with electrons. A suitable ligand may then attractively interact with the d_z^2-orbital, constituting the π-back bonding. This explains, why the square-planar coordination is less suitable for non-d^8 metal centres, because the d_z^2-orbital is left empty or only partially filled, decreasing the stabilisation effect. In this regard, the deficit of only four dative bonds in a square-planar

coordination compared to an octahedral six-fold coordination, which is prominent for Ni^{2+} with small ligands, is mitigated. Overall, the π-back bonding effect performed by trithiocarbonate ligands may be a useful way to explain the coordination of Ni^{2+}. X-ray structure data on the carbonate analogue i.e., $K_2[Ni(CO_3)_2(H_2O)_4]$ was published, showing monodentate CO_3^{2-} ligands and an octahedral coordination of the Ni^{2+} centre.[134]

Potassium tris(trithiocarbonato) cobaltate(III) trithiocarbonate

The green $K_5[Co(CS_3)_3]CS_3$ **38** complex was obtained from the solvothermal reaction of anhydrous $CoCl_2$ with K_2CS_3 **9** (cf. figure 2.91). The cobalt ion was thus not only coordinated by three trithiocarbonato ligands but oxidised about one electron under these conditions. Alongside with the green needles, an orange-yellow side product could be identified as a double anionic potassium salt, namely $K_7(CS_3)_3Cl \cdot H_2O$ **14**, which was described above in sub-section 2.1.2.

The unit cell of the transition metal complex compound is depicted in figure 2.101.

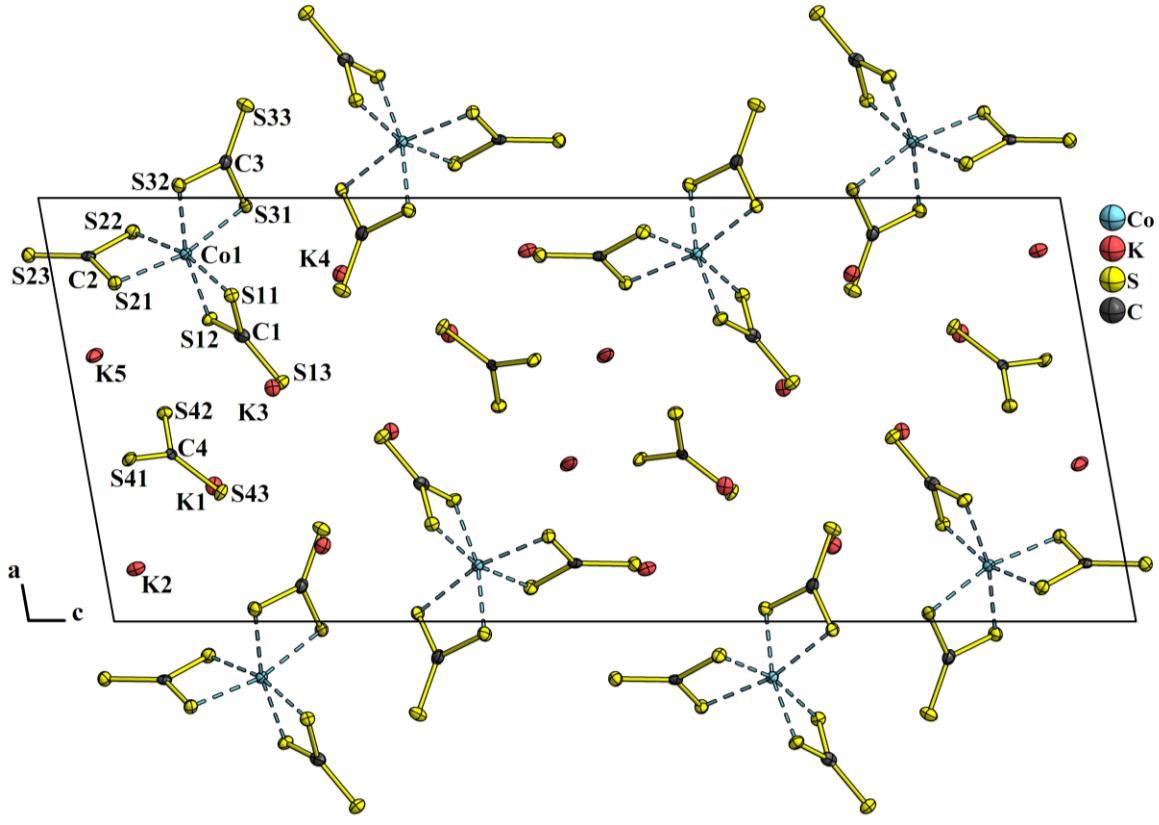

Figure 2.101: Unit cell depiction of $K_5[Co(CS_3)_3]CS_3$ **38**. All atomic displacement ellipsoids are drawn at 70 % probability.

All atoms in the structure of $K_5[Co(CS_3)_3]CS_3$ **38** occupy regular sites, describing one unique $[Co(CS_3)_3]^{3-}$ and one free trithiocarbonate anion, that are connected with five non-

equivalent potassium ions *via* an ionic network. Four formula units are included in the monoclinic lattice obeying the space group $P2_1/c$ (no. 14). In figure 2.101 the eponymous two-fold screw axes are located at ¼ and ¾ *c* as well as in the virtual parallel line running through the centre horizontally.

The Co^{3+} complex anion is fashioned the same like described in the crystal structure of $[Co(NH_3)_6]_3[Co(CS_3)_3]_2 \cdot 6\ NH_3$, which is also a green compound.[94] This is that three individual trithiocarbonato ligands arrange trigonally around the transition metal centre in a pedal wheel like manner. The complex anion can be idealised with C_3 symmetry in isolation. Each ligand performs bidentate coordination *via* two sulfur atoms, setting up a distorted octahedron around Co^{3+}. In other words, the coordination features a set of three four-membered CS_2Co rings. The anion is drawn in figure 2.102 and angles between atomic distances are listed in table 2.16. Each four-membered ring represents the repulsive and attractive interplay between the cobalt centre and the ligand. To achieve coordination, the interaction must level out to a stabilising net energy. Alike in the bis(trithiocarbonato) complexes (cf. above), the endocyclic (coordinating) S−C−S angle is buckled to about 108° on all three ligands, although it could span up to 120° like in the ideal free trithiocarbonate anion. A larger angle could then decrease the level of distortion of the octahedral coordination polyhedron. However, this would bring the ligand closer to the metal centre, considering the C−S and S−Co distance to stay constant. The six non-bonding electrons of Co^{3+} occupying the d_{xy}, d_{xz} and d_{yz}-orbitals ($3d^6$, low spin) possess electron density probability oriented towards the carbon atoms, prohibiting them to draw nearer. In turn, the $d_{x^2-y^2}$ and d_{z^2}-orbitals are empty and offer to combine with the electron density of the charged sulfur donators. From these preliminary considerations the non-suitability of Co^{3+} to be coordinated in a square-planar arrangement like Ni^{2+} can be derived. The emptiness of the d_{z^2}-orbital results in a lack of stabilisation *via* π-back bonding with the p-orbitals of CS_3^{2-}. In turn, in the d_{z^2}-axis no repulsion occurs and the three ligands eventually perform the octahedral coordination.

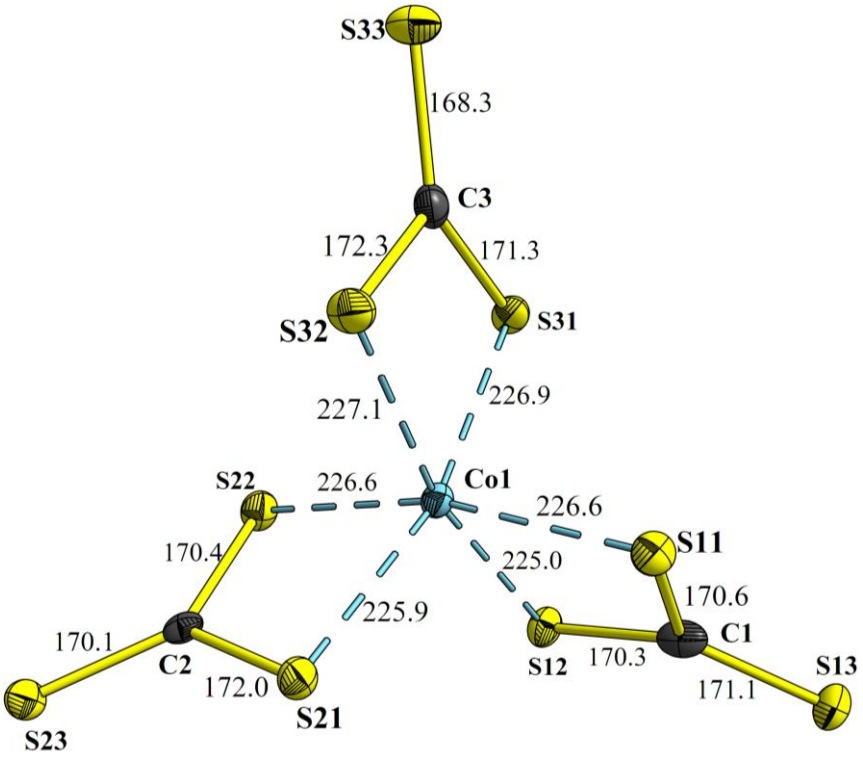

Figure 2.102: The tris(trithiocarbonato) coblatate(III) anion as found in the structure of $K_5[Co(CS_3)_3]CS_3$ **38**. The numbers on the connections give the atomic distance in pm. All atomic displacement ellipsoids are drawn at 70 % probability.

Although the octahedral coordination in $K_5[Co(CS_3)_3]CS_3$ **38** is distorted to some degree, in a series of mononuclear tris(trithiocarbonato) complexes of the trivalent pnictogen cations As^{3+}, Sb^{3+} and Bi^{3+}, the octahedral coordination was observed to distort much stronger. In the As^{3+} compound $(Ph_4P)_2[As(CS_3)_3]$ the trithiocarbonato ligands are forced to reorient, which results in one near and one far As−S coordination per ligand. This is because the pnictogen cations As^{3+} possess a lone pair, which is repulsing with the electrons of the ligand.[116] Very alike obtained in the Co^{3+} complex, shown in figure 2.102, in the Fe^{3+} complex all six coordinative distances approximately are of same value (228.6 – 232.3 pm), whereas for instance the As^{3+} complex comprises three shorter (~230 pm) and three longer (~300 pm) dative As−S bonds. Calculations of the As^{3+} complex however yielded even larger differences, with the longer coordination to approximate to 360 pm, rising from the lone pair repulsion of the ligands. To explain this, the cation environment was considered. In the publication, it was concluded, that the anions could be described as guests inside a matrix of $(Ph_4P)^+$ ions, only offering anion sites of limited volume. The final molecule shape of the As^{3+} complex anions was thus explained to stem from squeezing into the cation framework even under increased repulsive interaction with the lone pair of the

cation. Increasing the size of the latter ion, by substitution with Sb^{3+} or Bi^{3+}, does apparently not suffice to fit in the anion sites of the matrix and demands reformation. Consistently a different crystal metric is obtained for the Sb^{3+} and Bi^{3+} centred complexes, still describing one longer and one shorter dative bond per ligand.[70,116] Cancellation of the bulky cation matrix could probably allow the octahedral anion structure to even more distort as predicted from calculation. It remains open for future work as the respective pnictogen trithiocarbonato complexes have not been prepared apart from such a cation matrix. The solvothermal route presented here may allow access to these complexes in this concern.

Table 2.16: Angles between the atomic distances in the $[Co(CS_3)_3]^{3-}$ anion. All S−Co−S angles with sulfur atoms from different ligands range between 92.84(8) and 97.87(8)°.

		angle / °			angle / °
endocyclic	S11−Co1−S12	75.72(8)	endocyclic	S11−C1−S12	108.8(5)
endocyclic	S21−Co1−S22	75.96(8)	endocyclic	S11−C1−S13	126.3(5)
exocyclic	S31−Co1−S32	75.66(8)	exocyclic	S12−C1−S13	124.7(5)
endocyclic	S21−C2−S22	108.8(4)	endocyclic	S31−C3−S32	108.3(5)
endocyclic	S21−C2−S23	125.6(5)	endocyclic	S32−C3−S33	124.7(5)
exocyclic	S22−C2−S23	125.5(5)	exocyclic	S31−C3−S33	127.0(5)

Consistently with the evolution of dative bonds between sulfur and cobalt, the exocyclic C−S bond of the ligands that are not involved in coordination, should be shorter, compared to the coordinating ones. However, the significant decrease in the bond length that was obtained from the structures of the bis(trithiocarbonato) complexes is here relatively low and in the case of the C1 ligand even turned upside down. Indeed, the atomic distance, given as a number for the assignment of the C−S single or C=S double bond, or at least the favoured characteristics to one or the other, cannot be used unambiguously in this case.

As potassium connect with the complex moiety by ionic interaction with the sulfur atoms, not all negative charge can be distributed towards the coordination of Co^{3+}. Three negative charges must therefore be neutralised by the surrounding cations and are thus localised outward the coordination sphere, which may explain the increased exocyclic covalent C−S bond length. In this, apparently the three-fold coordination of Co^{3+} allows maintenance of a delocalised π-electron system on the ligands.

The trithiocarbonato ligands are close to planar, because within the limits of measurement accuracy, the carbon atom centres C1, C2 and C3 are 3.5(8), 1.5(8) and 1.9(8) pm distant from the trigonal plane spanned by the three attached sulfur atoms, respectively. In contrast, the additional free trithiocarbonate anion in the structure is perfectly planar and the C4−S

bonds could be measured with 172.6(9) (S41), 169.5(8) (S42) and 174.6(9) pm, featuring the typical shortening of one of the bonds with increased probability of the C=S double bond to be located in.

Overall, the structure of $K_5[Co(CS_3)_3]CS_3$ **38** comprises a K_2CS_3 network, connecting the complex anions individually. Omitting the ligand cation interaction for clarity, the complex anions are represented by octahedrons arranging in channels parallel to the crystallographic *b*-axis in figure 2.103.

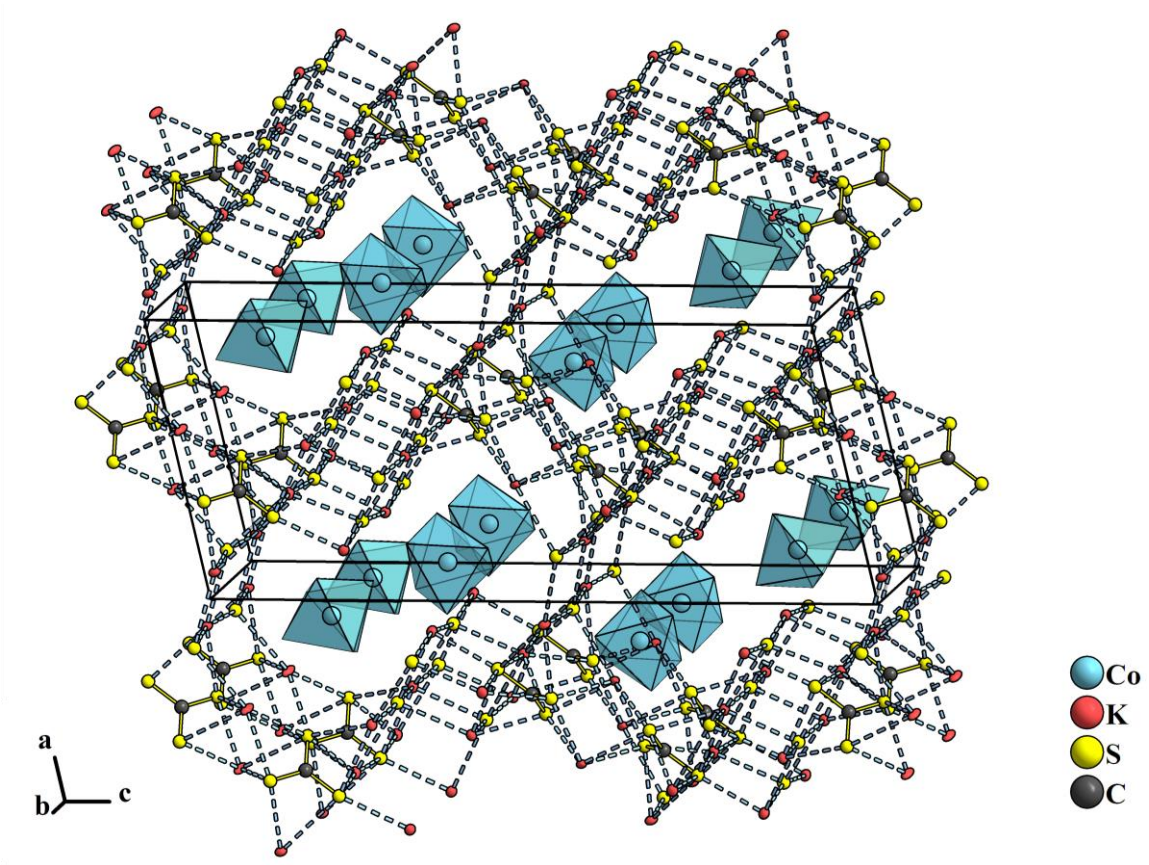

Figure 2.103: Extended drawing of the crystal structure model of $K_5[Co(CS_3)_3]CS_3$ **38**. The trithiocarbonato ligands are omitted for clarity, depicting the complex anion as blue octahedrons. Each complex anion is however ionically attached to the surrounding K_2CS_3 network.

Formation of the trivalent metal centre from the divalent, i.e., the oxidative species in the reaction, is unknown. BENZ, who used $CoCl_2 \cdot 6\,H_2O$ as a starting material in aqueous ammonia, suggested the formation of hydrogen. Gas evolution under the solvothermal conditions in sealed ampoules is doubtful, however, the presence of water in the solvothermal reaction cannot be denied as it crystallises in the side product **14**. The amount of water impurity should be low in absolute ethanol used as a solvent. Moreover, the introduced $CoCl_2$ was taken from stock stored under argon and was coloured with the

characteristic blue of the anhydrate. Maybe K_2CS_3 **9** could have introduced water due to its hygroscopic nature and might have contained some impurities acting as oxidants. For instance, sulfur or thiosulfate could be incorporated, offering alternative species that might have been reduced by Co^{2+} in the reaction mixture. After all, the ampoule carried a confusing variety of products of which two crystalline species could be investigated. The key to understand the red-ox reaction might be hidden in the residuals of the reaction mass. Earlier reported preparations of the tris(trithiocarbonato) cobaltate(III) used the metal in its trivalent state already from the starting material.[70] Therefore, not much is known on the formation mechanics of the complex.

RAMAN spectroscopy of trithiocarbonato complexes

It was possible to measure a none-destructive µRAMAN spectrum on the compounds $K_2[Pd(CS_3)_2] \cdot EtOH$ **36**, $K_2[Pt(CS_3)_2]$ **37**, $[Ph_4P]_2[Pd(CS_3)_2]$ **39** and $K_5[Co(CS_3)_3]CS_3$ **38**. ATR-IR spectra were recorded but not used. The sensitive products weathered very soon after they were collected from the ampoule and could not be transferred to the ATR-IR table without destruction. The only exception was $(Ph_4P)_2[Pd(CS_3)_2]$ **39**, which is stable in ambient atmosphere and the IR absorption curve is added in the respective diagram in figure 2.104, with the RAMAN spectra that are drawn for said complexes.

To help to assign the RAMAN signals, the shift frequencies were simulated from an optimised structure model of the transition metal complexes. The geometry optimisation routine within the *Turbomole* program package was based on the structures obtained through SC-XRD data. A calculation using the PBE0 hybrid functional applying the base function cc-pVTZ for C, S and LANLDZ2 Hay&Wad for M = Pd^{2+}, Pt^{2+} and Co^{3+}, respectively converged to a molecule structure with C_1, D_{2h} and *C3* symmetry, respectively. As seen in the crystal structure models of **36** and **39**, the design of the complex anion can be of significant difference. Starting the geometry calculation without symmetry, i.e., C_1 (c.f. $K_2[Pd(CS_3)_2] \cdot EtOH$ **36**), however converges to an almost D_{2h} symmetry, where atomic distances and angles differ from the high symmetry values in the decimal places only. This insignificant divergence from ideal D_{2h} symmetry is therefore neglected. From the calculated molecule structures, the RAMAN shift frequencies of the ground state could be simulated.

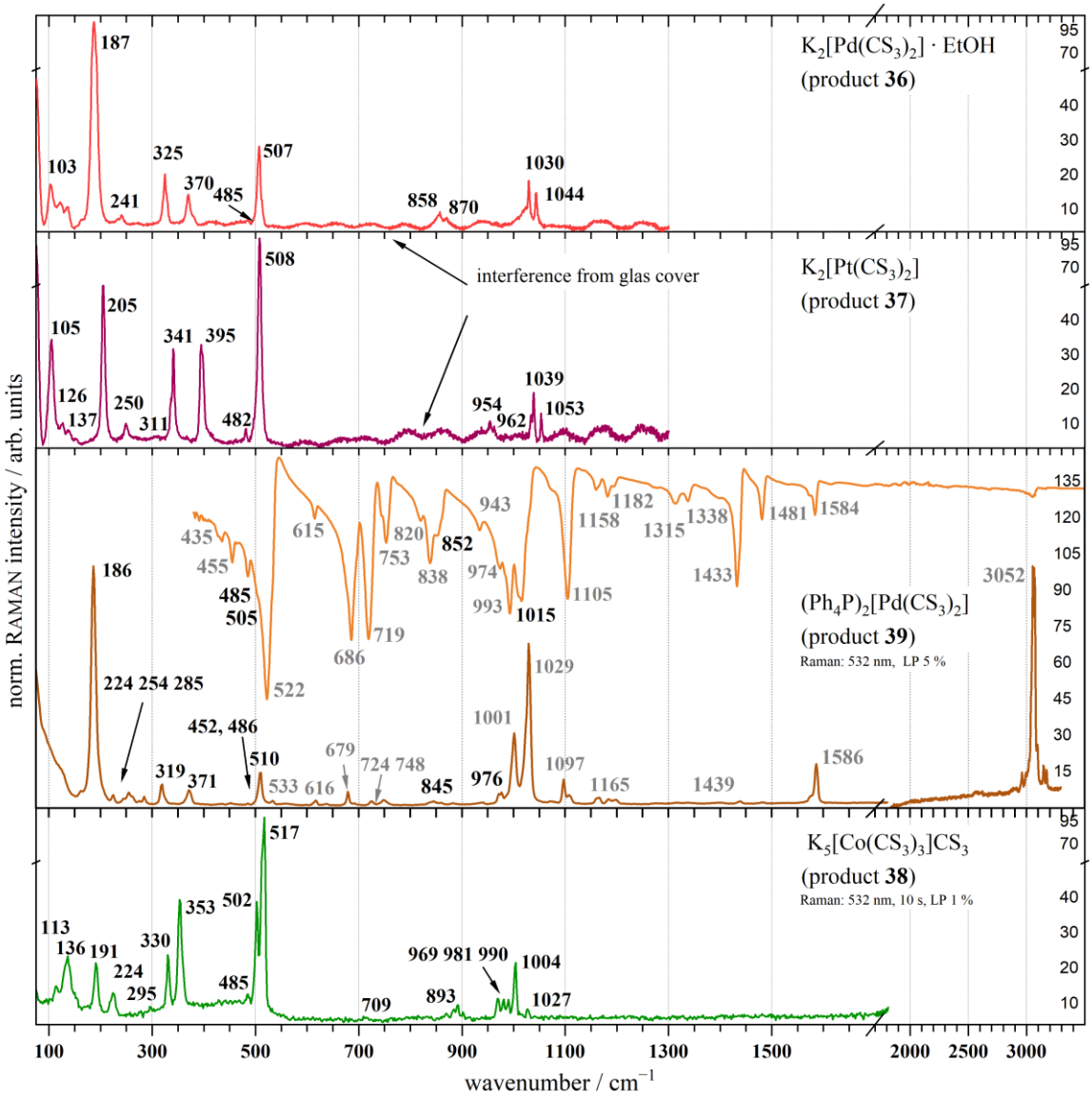

Figure 2.104: RAMAN spectra of $[M(CS_3)_2]^{2-}$ (M = Pd^{2+} **36**, **39**; Pt^{2+} **37**) and $[Co(CS_3)_3]^{3-}$ **38**. In the lower mid diagram additionally the IR spectrum of **39** is shown and all peak centres written in grey have their origin in the complex cation $(Ph_4P)^+$ or are non-fundamentals.[119] The numbers give the signal centre frequency in cm^{-1}.

In contrast, the divergence of the symmetry of the ligands from ideal D_{3h} in their free state is no more only marginally lowered by omnidirectional ionic interaction (cf. e.g., alkali salts), but by the formation of two dative bonds, directed towards the transition metal centre. The highest possible ligand symmetry is therefore C_{2v}, which as discussed earlier becomes evident by cancelation of the degenerate asymmetric C–S valence stretching and CS_3 deformation.

These fundamental ligand molecule vibrations are now coupled in the structure of the complex and can split up energetically. For instance, there occurs one strongly RAMAN

active total symmetric C−S stretching mode (ν_s(C−S)^{tot}) near 500 cm^{-1} signalising a collective synchronic motion in all ligands. With rising number of ligands, asynchronous versions of the same ligand fundamental vibration can be derived, e.g., the sulfur atoms of one CS_3^{2-} ligand oscillate symmetrically towards the carbon, while in the two other ligands the sulfur atoms move away. These combinations are degenerated and generally calculated to have slightly decreased wavenumbers.

As the X-ray structure models indicated, the C=S double bond of the CS_3^{2-} ligands should be favourably located at the terminal (non-coordinating) sulfur atom, in accordance with the bidentate coordination manner. But still there are no bands that clearly indicate a C=S double bond expected at ~1050 – 1200 cm^{-1}, thus a certain degree of delocalisation remains. This is in line with earlier reported variations of the C=S stretching frequency in 1,1-dithiolates over hundreds of cm^{-1} starting above 700 cm^{-1}.[122] All RAMAN spectra in figure 2.104 show the C=S stretching of the terminal sulfur atom in the 1000 – 1050 cm^{-1} region. There is an energy difference caused by the vibration to be totally symmetric or antisymmetric (cf. above). Scattering on the Co^{3+} complex yield a finely resolved triple band just below the strong peak at 1004 cm^{-1}, indicating an even more differentiated fashion of C=S stretching modes due to more combinations of vibrations of even three ligands.

However, next to that, in the wavenumber regime 800 to 1000 cm^{-1}, also the symmetric and antisymmetric fundamental valence stretching ν_{as}(C−S) of the coordinating sulfur atoms are found. These motions might intermix or even couple with the former C=S motions, which overall makes the spectral range not specific and a clear assignation impossible.[115] In the IR spectrum of $(Ph_4P)_2[Pd(CS_3)_2]$ **39** the group of IR and RAMAN intensities around 1000 cm^{-1} do not only include signals from the complex anion. In consideration of reference data, only the strong absorption band at 1015 cm^{-1} was assigned in this regard, whereas the intense shoulders were tentatively attributed to $(Ph_4P)^+$.[119] This also holds for the bands foreign to the complex anions towards lower wavenumbers.

Except for a weak signal of unknown origin at 709 cm^{-1} in the spectrum of **38** (overtone or probably a low frequent ν_{as}(C−S) of the free CS_3^{2-} ion), the next group of RAMAN intensities rising from the trithiocarbonato complex anions was expected near 500 cm^{-1}. Here the above mentioned total symmetric valence stretching ν_s(C−S) is observed represented in one relatively sharp signal. The DFT calculations yield a series of degenerated asynchronous combinations of the individual ligands near that wavenumber, which could not be resolved. Again, for **38** the additional free anion can be considered to exhibit the respective fundamental at 502 cm^{-1}, where a shoulder peak could be detected.

Other than the properties of the free trithiocarbonate anion, the out of plane deformation $\gamma_{op}(CS_3)$ was detected as a weaker RAMAN intensity on the left of $\nu_s(C{-}S)^{tot}$ at ~450 to 500 cm^{-1}. According to $\nu_s(C{-}S)$ the IR spectrum of **39** has the characteristic strong absorption 505 cm^{-1} hidden in the shoulder of the stronger cation mode at 522 cm^{-1}. Further assignment of the weak absorptions in this so-called fingerprint region are easily mistaken, because a variety of deformation modes of the phosphonium cations are intermixed.

Between 300 and 400 cm^{-1} the RAMAN intensities related with the transition metal vibrations are found, i.e., M−S valence stretching, where M = Pd^{2+}, Pt^{2+}. This was found in accordance with earlier publications of the trithiocarbonato complexes.[122] However, reference for RAMAN data of the tris(trithiocarbonato) cobaltate(III) anion was found limited to wavenumbers above the crucial range.[70] A mid-70s work of MÜLLER et al. was probably the first to identify the $[Co(CS_3)_3]^{3-}$ anion by ESR and IR vibration spectra.[115] In comparison, only one IR absorption at 344 cm^{-1} was discovered to stem from Co−S valence stretching, whereas in the RAMAN spectrum presented above, two signals (330 and 353 cm^{-1}) could be identified to result from the coordinative structure. The totally symmetric stretching of all six coordinating dative Co−S bonds was calculated at 350 cm^{-1}, perfectly agreeing with the experimental value. From the approximated ideal C_3 symmetry of the complex anion, it was derived that this collective motion is silent in the IR, explaining only one mode in the reference. Indeed, the calculations also yield a band at 344 cm^{-1} identical to the reference, which is IR active only. Because there are no strong RAMAN intensities expected from the free CS_3^{2-} ion in this area, and as the bis(trithiocarbonato) complexes also exhibit two M−S signals, the less intense but still sharp intensity at 330 cm^{-1} was also signed with Co−S vibration, which is thus a combination variation between the three ligands. Again, by the calculation of the vibrational spectrum of the isolated $[Co(CS_3)_3]^{3-}$ ion, three two-fold degenerate modes at 293, 329 and 341 cm^{-1} were obtained. Apparently, the ideal model, neglecting the crystal field effects, is too unprecise to describe the data at this particular mode.

The spectral region below 300 cm^{-1} is home to the in-plane deformation vibration of the free CS_3^{2-} anion and its ligand form.[122] The calculated spectrum accounts several degenerated deformation modes this region. But there is also community of another relatively strong RAMAN signal near 180 cm^{-1} observed in figure 2.104, which is foreign to the free ligand anion. It was found in agreement with the calculation, that it must be the symmetric bending motion of the ligands towards the metal centre $\delta_s(M{-}CS_3)$, explaining the significant signal in the RAMAN spectra, because the polarity of the complex anions

stays constant during this vibration. Consistently, only a weak absorption should be expected rising from that motion or probably even silence. Agreeing with MÜLLER et al., who measured IR as low as 50 cm^{-1} and discovered a weak signal at 185 cm^{-1}, clearly a lattice effect can be considered to cancel the motion to be exclusive to the RAMAN spectrum. The mode was called ring deformation, referring the four-membered CS_2M rings of coordination.[119]

Lower than $\delta_s(M{-}CS_3)$ were only bending motions δ(complex) throughout the structure of the complex molecule, involving all moieties and the bonds in between.

Although the Co^{3+} complex includes three trithiocarbonato ligands, the fundamental vibrations are comparable in their position with those measured on the bis(trithiocarbonato) complexes. It was moreover expected to discover the fundamental vibrations of the isolated CS_3^{2-} anion as well as manipulated versions of these, covering the individual degrees of freedom, as each complex anion includes more than one ligand. The resolution of said combinations was however not distinctively clear.

With exception of the switched position of $\gamma_{op}(CS_3)$ to be shifted to lower wavenumbers than $\nu_s(C{-}S)$, the assignment of the vibration characters to the detected modes could be transferred from the free CS_3^{2-} ion.

Including the significant M−S stretching all crucial vibration characters are briefly ordered to the respective band in table 2.17.

A trend of the M−S RAMAN modes to shift towards lower wavenumber with decreasing weight of the complex cation is observed. In $[Pt(CS_3)_2]^{2-}$ the high frequent $\nu_s(M{-}S)$ is at almost 400 cm^{-1}, while in the Co^{3+} complex the respective motion of three ligands occurs near 350 cm^{-1}. Both the RAMAN spectra of $[Pd(CS_3)_2]^{-2}$ show agreement with each other and align midway between those of the Co^{3+} and Pt^{2+} complex. Qualitatively, the values of the RAMAN frequencies for the palladate(II) and platinate(II) complex match the report of BURKE and FACKLER, JR, who published respective IR absorption spectra alongside. The authors noticed non-coincidence comparing IR and RAMAN spectra, with the former showing the expected shift to higher frequencies upon decreasing the weight of the metal centre, but like obtained here, an opposite trend in the latter. Without further explanation, the discrepancy was suggested to be indicative for interligand interaction, which is a term to describe energy transfer between the ligands. Conceptionally, the bond strength levels with the amount of orbital overlap, which (next to electrostatic interaction) is a crucial driving force for dative bonds. The smaller Co^{3+} ion ($3d^6$, CN = 6, low spin ~ 57.0 pm)[135] is surrounded by three CS_3^{2-}ions, which act repulsive on each other, equalised by the

attractive electrostatic interaction. In turn, only two ligands coordinate Pt^{2+} ($5d^8$, CN = 4, ~ 60.0 pm)[135], which is larger, decreasing the interligand repulsion while maintaining attractive overlap of orbitals to create square-planar coordination. It is thus suggested that the frequencies of the representative modes of M−S stretching are ranged proportionally with these repulsive and attractive energy mixes. An effect of the different coordination numbers is yet not addressed, but most probably must be taken into account. In this matter, it is unfortunate that the RAMAN spectra of $[Pn(CS_3)_3]^{3-}$, with *Pn* = As^{3+}, Sb^{3+}, Bi^{3+}, earlier published, do not display the spectrum lower than 450 cm^{-1}.[70] To gain more knowledge in this special spectral region, certainly additional data, probably employing metal- and ligand isotope substitution is needed.

Using potassium cations in the compounds leaves the spectrum above 1100 cm^{-1} free of RAMAN intensities, which is only not the case for the example with tetraphenyl phosphonium ions $(Ph_4P)^+$, which exhibit intense IR absorptions as well as low to high frequent RAMAN modes. For instance, the sharp absorption at 1433 cm^{-1} is due to P−C stretching, energetically home to this spectral region. Another example is the intense RAMAN signal beyond 3000 cm^{-1}, which - that high frequent - can only describe C−H stretching. The region of 1000 cm^{-1} is also overlapped with cation modes, interfering with ν(C=S) and ν_{as}(C−S) expected there.[70]

Table 2.17: Assignment of vibrational character to the observed RAMAN bands of $[M^x(CS_3)_x]^{x-}$ anions M = Pd^{2+}, Pt^{2+} and Co^{3+}.

vibration character	$[Pd(CS_3)_2]^{2-}$ **36**		$[Pd(CS_3)_2]^{2-}$ **39**	$[Pt(CS_3)_2]^{2-}$ **37**		$[Co(CS_3)_3]^{3-}$ **38**	
	exp.	calc.	exp.	exp.	calc.	exp.	calc.
ν(C=S)	1044 m 1030 m	1062 1055	1029(*) vs 1001(*) s 976? w	1053 m 1039 m	1071 1063	1027 vw 1004 m	1034 1026d
ν_{as}(C−S)	870 w 858 w	889 883	845 vw	962 vw 954 w	877d	990 – 893 w	921 916d
ν_{as}(C−S)tot ν_{as}(C−S)	507 s	526 (520)	510 m	508 vs	527 (523)	517 vs 502 s	530 (526d)
γ_{op}(CS_3)	485 vw	497	486 vw 452? w	482 w	490d	485 vw	501 (500d)
ν_s(M−S)	370 m	371	371 m	395 s	401	353 s	350
ν_{as}(M−S)	325 m	336	319 m	341 s	355	330 m	344 341d 329d
δ_{ip}(CS_2M) δ_{ip}(CS_3)	241 w	333 313 281 263 211	285 vw 254 w 224 vw	311 vw 250 w	330 328 263 251 222	295 vw 224 w	329d 293d 277 206d
δ_{sym}(M−CS_3)	187 vs	177	186 vs	205 s	200	191 m	173
δ(complex) (# modes)	103 m	158 – 35 (5)	not resolved shoulder	137 w 126 w 105 s	162 – 35 (5)	136 m 113 w	152 – 45 (7)

v very, w weak, m medium, s strong, ?uncertain; (*)cannot be distinguished from cation; ddegenerated: more than one mode with this wavenumber in calculation

2.6.2 Copper perthiocarbonate in a polymeric arrangement

Routes to prepare Cu^+ thiocarbonates were first reported in the literature at around the beginning of last century.[124,125,136] HOFMANN obtained metallic green *(CS₃)CuNH₄* from letting a solution of CuCl in aqueous concentrated ammonia stand on a volume of CS_2.[136] Benz followed these historical traditions and described the crystal structures of $ACuCS_3 \cdot x\ H_2O$, with $A = H_4N^+$, K^+, Rb^+, Cs^+.[94] In contrast, it was a surprise to obtain crystals that could be X-ray structure determined with $(H_4N)_2{}^1_\infty[Cu\{CS_2(S_2)\}]CS_2(S_2)$ **40** following these preliminary work. In figure 2.105 microscope photographs of the amber-red crystals found engulfed in a dark brown precipitate are shown.

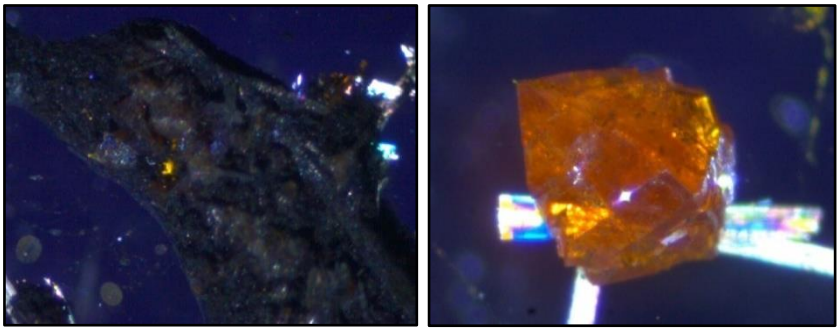

Figure 2.105: Amber-red crystals of $(H_4N)_2{}^1_\infty[Cu\{CS_2(S_2)\}]CS_2(S_2)$ **40**. On the left, with polarised light, the crystals show through the dark precipitate CuS precipitate.

In aqueous ammonia, Cu^+ may underwent disproportion and/or oxidation to form tetraamine copper(II), which was assumed from the blue colour of the solution (equation 2.5). After addition of CS_2, the blue colour disappeared and flakes of metallic gloss - probably copper - formed within one day. In aqueous ammonia the formation of trithiocarbonate was shown earlier, giving $(H_7N_2)_2CS_3$ (cf. sub-section 2.5.2). Either by oxidation or residual Cu^+ in solution, CS_3^{2-} could have been oxidised to give CS_2 and $CS_2(S_2)^{2-}$ (equation 2.6). The perthiocarbonate anion was eventually replacing the ammine ligands in favour of bidentate coordination (equation 2.7). Copper ions that were not included in the coordinative perthiocarbonato complex formed the stable CuS, which was confirmed the identity of the black product with PXRD (cf. figure 5.4). Ammonium ions are present during the whole process, which eventually compensate the negative charge of the free perthiocarbonate anions. Forming an ionic lattice then apparently realised the crystallisation of the polymeric perthiocarbonate copper(II) complex.[13]

$$2\ Cu^+ \xrightarrow{H_3N_{aq}} Cu + [Cu(H_3N)_4]^{2+} \qquad 2.5$$

$$2\ CS_3^{2-} \xrightarrow{Cu^+} CS_2(S_2)^{2-} + CS_2 \qquad 2.6$$

$$[Cu(H_3N)_4]^{2+} + CS_2(S_2)^{2-} \longrightarrow [Cu(CS_2(S_2)] + 4\ H_3N \qquad 2.7$$

Until 1970, Cu^{2+} dithiolate complexes were limited to dithiocarbamates. The compound $Cu[S_2C(NEt_2)]_2$ was determined to build axial S−Cu connections (≈ 285 pm) between two monomers, resulting in a five-fold coordination of the Cu^{2+} ion.[12] A trimeric setup of similar structure was realised in a series of cationic complexes $[Cu_3\{S_2C(N(n\text{-but})_2)\}_6][MBr_3]$ (M = Zn, Cd, Hg), where mixed valent Cu^{3+} and Cu^{2+} ions are present.[112]

Polymeric copper perthiocarbonate structures have been X-ray determined in alkyl ammonium salts of $[Cu(CS_2(S_2)]^-$, stressing the mono valency of copper in these compounds. In 1999, GUO and MAK, reported on the crystal structure of $[Me_3HN]^2_\infty[Cu\{CS_2(S_2)\}]$, including a two-dimensional anionic polymer network of $[Cu_2\{CS_2(S_2)\}_2]^{2-}$ units. These are designed in the way shown in figure 2.106.

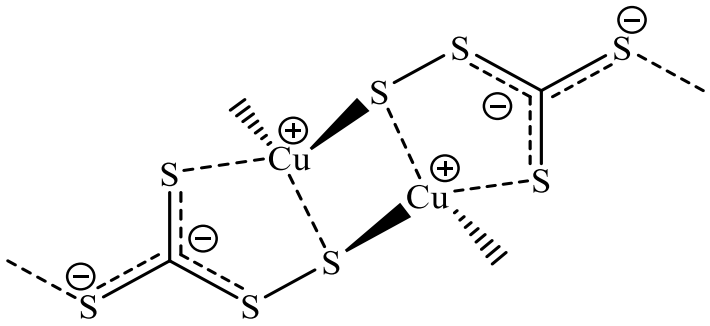

Figure 2.106: $[Cu_2\{CS_2(S_2)\}_2]^{2-}$ building units as found in $[Me_3HN]^2_\infty[Cu\{CS_2(S_2)\}]$. The two broken off bonds of the terminal sulfur atoms connect to the Cu^+ ion in the adjacent building unit, in a tetrahedral manner shown from the broken off bonds of the Cu^+ ions.[137]

Next to the chelate coordination of Cu^+ by $CS_2(S_2)^{2-}$ ions, it is peculiar, that the terminal exocyclic sulfur atoms are involved in coordination of the Cu^+ ion of the adjacent building unit (not shown in figure 2.106).[137] The same two-dimensional network, was X-ray determined in $[Me_4N]^2_\infty[Cu\{CS_2(S_2)\}]$ by TANG et al. in 2001, conducting tetranuclear copper cluster complexes in reaction with CS_2 and S. The paper could unfortunately not be found obtained for more details.[138]

Long before that, in 1969, the alkali salts $M_6[Cu_2(C_5S_{16})] \cdot x\ H_2O$ (with M = K, Rb, Cs) have been investigated and found to demonstrate the $[Cu_2(C_5S_{16})]^{6-}$ poly-perthiocarbonato

anions, by means of IR spectroscopy.[1] The original reference could not be assessed and these reviewed compounds have apparently never been investigated by means of structure determination methods. At least, no structure date of such a complex anion exists.
Crystal structures of copper ions with sulfur donors in polymeric arrangements are known. Among those, MÜLLER and co-workers were able to determine the crystal structure of an anionic trimer complex with CuS_4^--units and a dimer complex with neutral CuS_6-rings.[139] The latter are linked with a dianionic S_8^{2-}-ring, connected to the Cu^{2+} atoms of the CuS_6-rings. Thus, Cu^{2+} is in a trigonal-planar sulfur coordination. The crystallisation was realised with tetraphenyl phosphonium ions and the reddish-brown compound was moreover the first to describe a S_8^{2-} ion in a crystal structure.[139] Another (distorted) trigonal-planar sulfur coordination was found in the crystal structure of $[Ph_4As]_2[(S_3N)Cu(S_2O_3)Cu(S_3N)]$, where two mono valent copper ions are coordinated by one $S3N^-$ chelate ligand and bridged via the terminal sulfur atom of a thiosulfate anion.[140]

Ammonium perthiocarbonato copper(II) perthiocarbonate

Crystal structure model

All atoms in the X-ray crystal structure of $(H_4N)_2{}^1_\infty[Cu\{CS_2(S_2)\}]CS_2(S_2)$ **40** occupy regular 16b WYCKOFF position. Thus, sixteen furmula units are found in the unusual space group *Fdd*2 (No. 43) in the orthorhombic crystal system. Figure 2.107 shows the extenmded unit cell in view along the [101] direction.

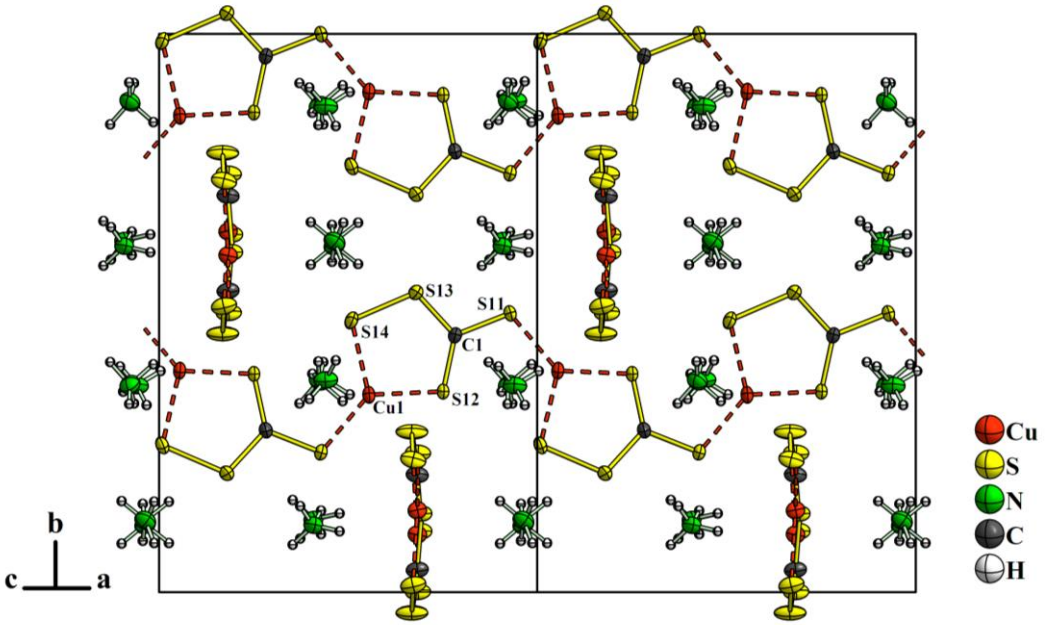

Figure 2.107: Unit cell of $(H_4N)_2{}^1_\infty[Cu\{CS_2(S_2)\}]CS_2(S_2)$ **40** in view along the [101] direction, parallel and perpendicular to the $[Cu\{CS_2(S_2)\}]$ polymer complex. The free perthiocarbonate anions are omitted for clarity, the ammonium cations are in rough alignment along [101] and form a primitive pattern in paper plane. All non-hydrogen atom displacement ellipsoids are drawn at 70 % probability.

Building units of $[Cu\{CS_2(S_2)\}]$ form one-dimensional chains and due to the lattice symmetry and a crosswise arrangement is obtained (cf. below). In between, the lattice is filled with ammonium and disordered free perthiocarbonate ions. Within the chain, the atoms are not perfectly meeting in one plane. However, like other structures above, they can be considered planar for simplicity. Written in numbers, the chain comprises with dihedral angles > 0°/< 180°: |S11−Cu1−S14−S13| = 177.83(4)°, |Cu1−S14−S13−C1| = 3.0(1)°, |S14−S13−C1−S11| = 178.2(1)° and |S13−C1−S11−Cu1| = 173.9(1)°. Figure 2.108 depicts a close up of the one-dimensional polymeric arrangement of the neutral $[Cu\{CS_2(S_2)\}]$ chain.

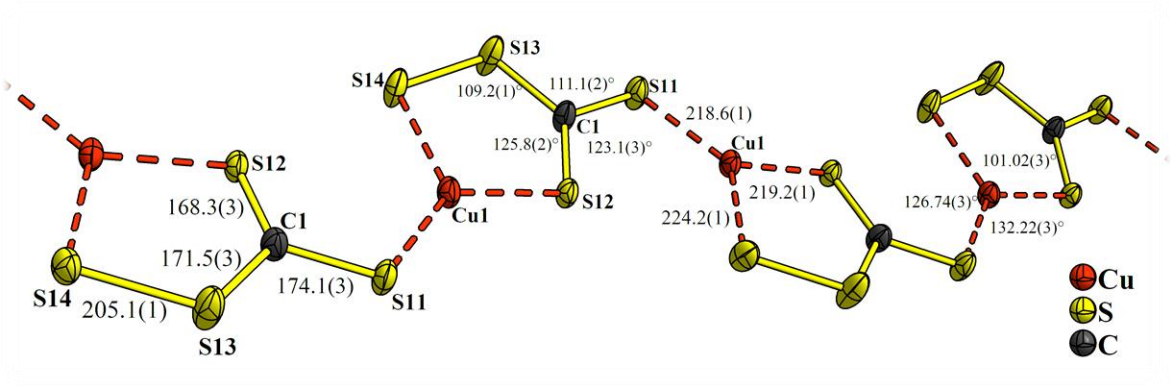

Figure 2.108: Fragment of the one-dimensional chains build up by [Cu{$CS_2(S_2)$}] units in the crystal structure of **40**. From left to right, the bond lengths and angles of the perthiocarbonate ligand and of the S−Cu coordination are given in pm and °, respectively. All atom displacement ellipsoids are drawn at 70 % probability.

Crossing of two neighboured chains is described with an angle between the chain planes of about 80°. The chains propagate along two distinct directions, namely [101] and [−101]. Thus, they have no component along the *b*-axis, which is the viewing direction in figure 2.109.

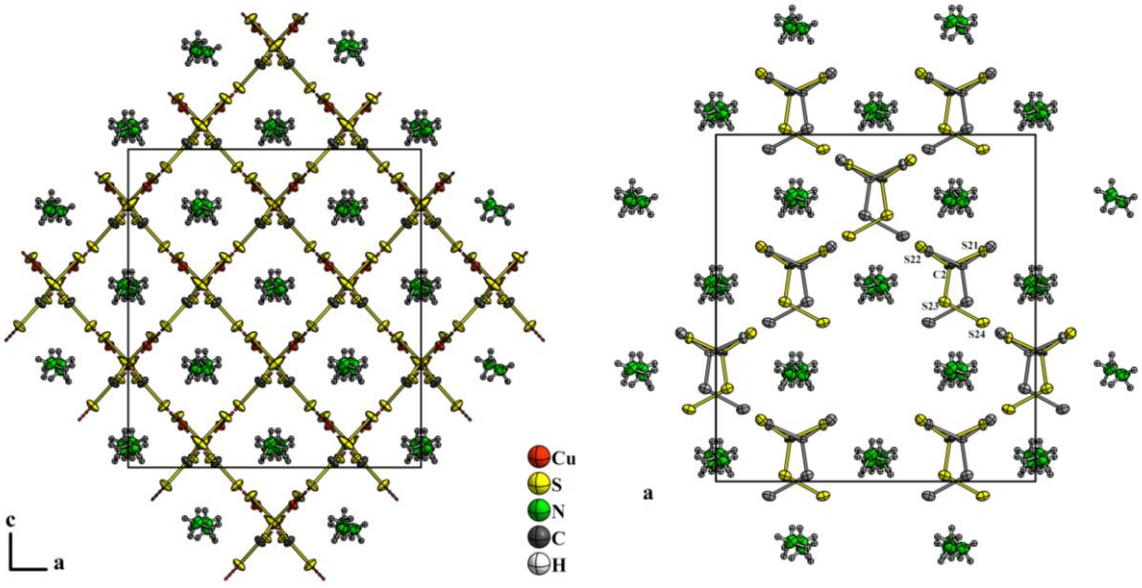

Figure 2.109: Extended display of unit cell of $(H_4N)_2{}^1_\infty$[Cu{$CS_2(S_2)$}]$CS_2(S_2)$ **40** in view along *b*-axis. The polymeric [Cu{$CS_2(S_2)$}] chains form a non-orthogonal checked pattern that is filled by the ammonium cations, lining up along the axis of viewing (left). Visualisation of the free perthiocarbonate anions, which are disordered due to the two-fold axis of symmetry (right). For clarity, they are omitted in the left display as they lie in the cross section of the chains. All non-hydrogen atom displacement ellipsoids are drawn at 70 % probability.

The image has been drawn in two parts, which means to visualise the disordered perthiocarbonate anion that lies in the crossing axes of the chains, and which is shown in figure 2.110. Like in the chain structure, it is close (but not ideally) planar with dihedral angles below 6° (cf. caption figure 2.110). Its plane is thereby oriented orthogonal with that of the chains intersecting in the virtual point next to the $CS_2(S_2)^{2-}$ ion. The disorder is due to the two-fold axis symmetry along the crystallographic *c*-axis. However, none of the atoms occupies the site symmetry properly and only a random orientation to that two-fold axis was observed.

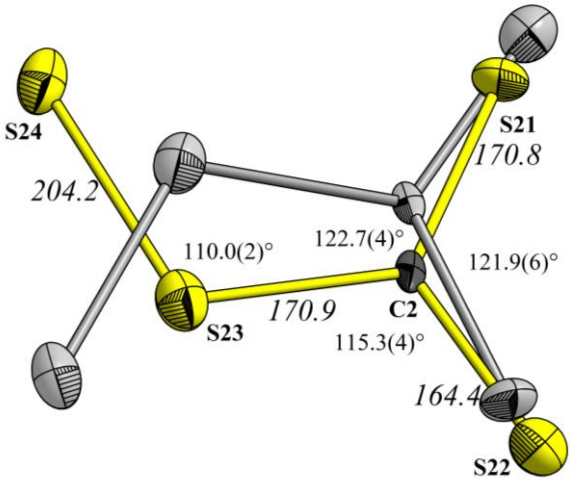

Figure 2.110: Close up of the disordered free perthiocarbonate anion in **40**. The two-fold axis runs horizontally along the virtual middle, thus none of the atoms occupy the site symmetry. Bond angles and lengths (numbers written in italics) in pm are given. The anion is close to but not ideally planar, with a torsion angle S24−S23−C2−S21 of 2.5(5)° and S24−S23−C2−S22 of 5.7(4)°. All atom displacement ellipsoids are drawn at 50 % probability.

For the structure solution, the atoms C2, S21, S22, S23 and S24 were accordingly refined with an occupancy of only 50 %, allowing the perthiocarbonate anion to be situated in either one of the two possible orientations regarding the two-fold axis.

Two crystallographically non-equivalent ammonium ions are posing the positive counter charge for the free perthiocarbonate dianions, as the chain building group is neutrally charged. The cations line up both along the chain propagation directions [101] and [−101] and the *b*-axis of the unit cell. In view of the latter (cf. figure 2.109), it is seen that the cations are occupying the rhombic loops of the chain pattern. Albeit the neutrality, both the perthiocarbonate and the complex units should perform attractive hydrogen interaction with the ammonium ions. From the connectivity list, it can be suggested that the N1 and N2

atoms have thirteen and eleven sulfur atoms in distance between 328.3(9) and 380.5(3) pm as well as eleven 323.3(3) and 390.5(4) pm to set up moderate to weakly dispersive N−H···S bonds.[38] The number of half occupied sulfur atoms was thereby counted half only.

2.6.3 Other compounds

Treatment of $Tl_2(SO_4)$ with $BaCS_3$

BENZ and BECK published the crystal structure of thallium trithiocarbonate, Tl_2CS_3, which they obtained from the treatment of PXRD data with a RIETVELD routine. They reported on several attempts to obtain single crystalline material, which all failed. The structure is included in the ICSD.[36,94]

Thallium(I) trithiocarbonate is probably the most stable inorganic trithiocarbonate salt. Uniting aqueous solutions of Na_2CS_3 and $TlNO_3$ immediately afford a brownish-red precipitate, which could not be dissolved or recrystallised. A photo of the powder is shown in figure 2.111. It could be identified with Tl_2CS_3 with the published structure as shown in the PXRD data plotted in figure 5.5.

In this work, among different other attempts, to obtain crystals of Tl_2CS_3, $BaCS_3$ **26** was treated with Tl_2SO_4 in aqueous ethanol in evacuated ampoules at elevated temperatures, trying to exploit the great stability of $BaSO_4$ to form as a side product. After the process, the ampoule was covered with yellow microcrystals on the inside. Presuming a recrystallisation of $BaCS_3$ similar to that used to obtain $BaCS_3$ crystals (cf. above). They were not investigated. At a closer look, as shown in figure 2.111, small brown crystals could be observed. Alongside, a lump of brownish-red material and huge colourless crystals (most likely $BaSO_4$) were obtained. Indeed, a red single crystal was found suitable for a SC-XRD measurement. It was identified as $Tl_2(S_5)$ **43**. The structure of $Tl_2(S_5)$ was published in the ICSD and thoroughly described earlier.[141] The obtained crystallographic data is given in the appendix. The formation of $Tl_2(S_5)$ is chemically interesting, considering the stability of Tl_2CS_3 observed for instance in water. It shall therefore not be excluded to form the desired Tl_2CS_3, as the mentioned lump of the red product was consisting of crystalline material only (cf. figure 2.111 (bottom right)). However, the obtained and determined crystal of $Tl_2(S_5)$ demanded both the dissolution of Tl_2SO_4 and the formation of sulfide ions in course of the solvothermal treatment.

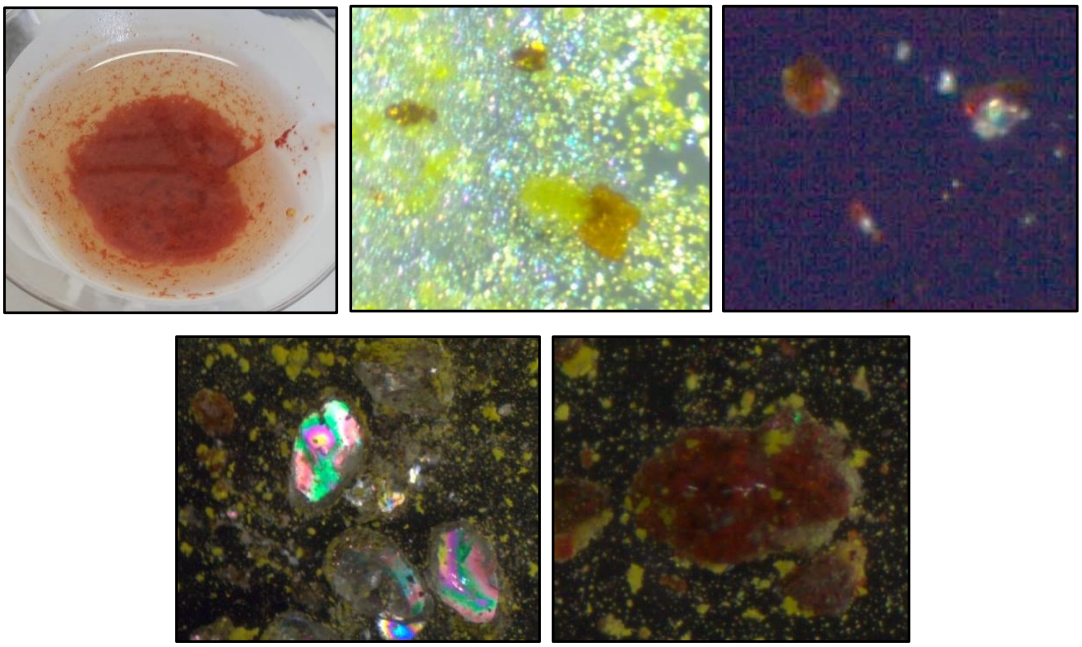

Figure 2.111: Photograph of brick red Tl_2CS_3 powder as obtained from an aqueous Tl^+ and CS_3^{2-} solution (top left). Photographs of the products obtained from the solvothermal treatment of Tl_2SO_4 with $BaCS_3$ **26**. Photo of yellow recrystallised $BaCS_3$ alongside with the brownish-red crystals as obtained on the ampoule wall (top middle). Red crystalline specimens (top right) obtained from a larger red lump (bottom right) are shown, which were found suitable for the SC-XRD data collection. Alongside, larger colourless crystals were obtained and may be considered to be residual educt or side produced SO_4^{2-} or $S_2O_3^{2-}$ salts (bottom left).

Thus, next to the guessed recrystallisation of $BaCS_3$ (yellow crystals), some CS_3^{2-} may have been decomposed to yield (poly)sulfide anions. For this, equation 2.8 and 2.9 describe the possible reaction pathways. An indication for the role of sulfate anions as reactants may be the reason for the colourless side product, i.e., formation of barium or thallium thiosulfate (cf. figure 2.111 (bottom left)).

$$CS_3^{2-} + SO_4^{2-} \xrightarrow[\text{sealed ampoule}]{\text{water/EtOH, 100 °C, 6d}} S^{2-} + S_2O_3^{2-} + COS \qquad 2.8$$

$$CS_3^{2-} \xrightarrow[\text{sealed ampoule}]{H_2O/\text{EtOH, 100 °C, 6d}} CS_2 + HS^- + HO^- \qquad 2.9$$

In the sealed ampoule a decent gas evolution is doubtful, but gaseous products may have formed intermediately in solution. The Tl^+ ion is a very soft cation, and in terms of HSAB it can be considered to readily form a stable salt if sulfide or hydrosulfide are offered.

Potassium tri(*μ*-acetato)hexaacetato dieuropiate(III) tris(trithiocarbonate)

So far, no reports exist on compounds that combine lanthanide elements with (tri)thiocarbonates. In the series of solvothermal reactions in glass ampoules, experiments involving trivalent europium, the most reactive lanthanide element,[128] were carried out. Europium(III) acetate was conducted to a solvothermal treatment with K_2CS_3 9. The complex $K_9[Eu_2(CH_3COO)_9](CS_3)_3$ **41**, was obtained as yellow hexagonal-shaped crystals, which are shown on the photograph in figure 2.112.

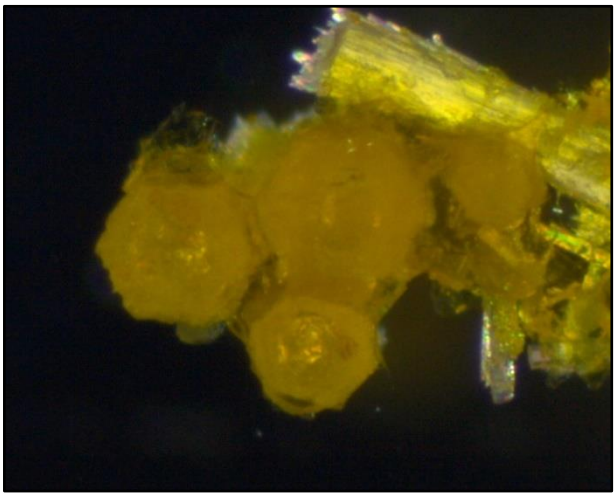

Figure 2.112: Photograph of the hexagonal-shaped crystals of $K_9[Eu_2(CH_3COO)_9](CS_3)_3$ **41** alongside with fibrous yellow crystals of unknown composition.

Crystal structure model

The X-ray single crystal data at 150 K, could be solved using the hexagonal crystal system. No interaction of Eu^{3+} with the trithiocarbonate ions occurs. In turn, potassium ions connect the different anionic species *via* ionic bonding and a binuclear europium(III) acetate complex, i.e., $[Eu_2(CH_3COO)_9]^{3-}$, is included. It comprises two $[EuO_9]$ monomers, as on each Eu^{3+} ion three bidentate and three monodentate (bridging) acetate ligands are coordinating. The unit cell contains two formula units which obey the space group $P6_3/m$ (No. 176). Figure 2.113 and 2.114 depict the unit cell in view along [110] and the *c*-axis, respectively, showing the lattice structure to be separated in a potassium trithiocarbonate and europium(III) acetate domain.

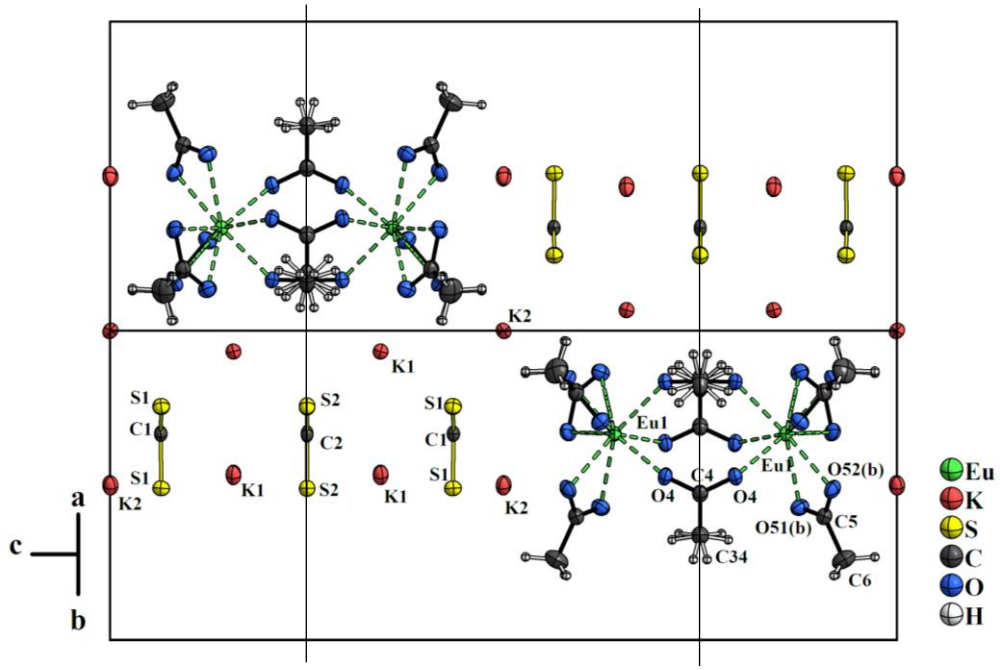

Figure 2.113: Unit cell of $K_9[Eu_2(CH_3COO)_9](CS_3)_3$ **41** in diagonal view along (110). The cell can be virtually divided along the vertical middle along the potassium ions. Focussing on one part of the unit cell, the two included sub-structures are further separated by a mirror plane (blue lines), inhabited by several atoms. In particular, this demands the binuclear fashion of the $[EuO_9]_2$ dimer. The disorder of acetate ligands is omitted for clarity. All non-hydrogen atom displacement ellipsoids are drawn at 50 % probability.

Two non-equivalent trithiocarbonate anions are included in the X-ray structure model of $K_9[Eu_2(CH_3COO)_9](CS_3)_3$ **41**. They are piled up parallelly along the three-fold axis of symmetry running perpendicularly through their trigonal plane centres, which are the carbon atoms. Sets of three trithiocarbonate anions ($C1(S1)_3^{2-}$, $C2(S2)_3^{2-}$, $C1(S1)_3^{2-}$) make one domain, which is translated along all three unit cell directions in alternation with the $[Eu_2(CH_3COO)_9]^{3-}$ complex, which for the sake of convenience shall be written as $[EuO_9]_2$. The carbon atoms (C1 and C2) thus inhabit special lattice sites, causing only one unique sulfur atom per carbon atom (S1 and S2). Due to that, the point symmetry the trithiocarbonate anions is the perfect D_{3h}, i.e., planar with S−C−S angles of 120°. The C1 atom occupies the three-fold-axis (WYCKOFF site 4f), equalising the three attached sulfur atoms (S1) on the regular site 12i. The C1−S1 bond measures 172.11(6) pm. The C1 trithiocarbonate anion is multiplied by the mirror planes, adding up four anions per unit cell (cf. figure 2.113). The C2 atom is located in the three-fold axis, too, but its trigonal plane additionally coincides with the mirror plane. (This means C2 occupies the WYCKOFF site 2d, which is equivalent to a six-fold and inversion point symmetry.) The

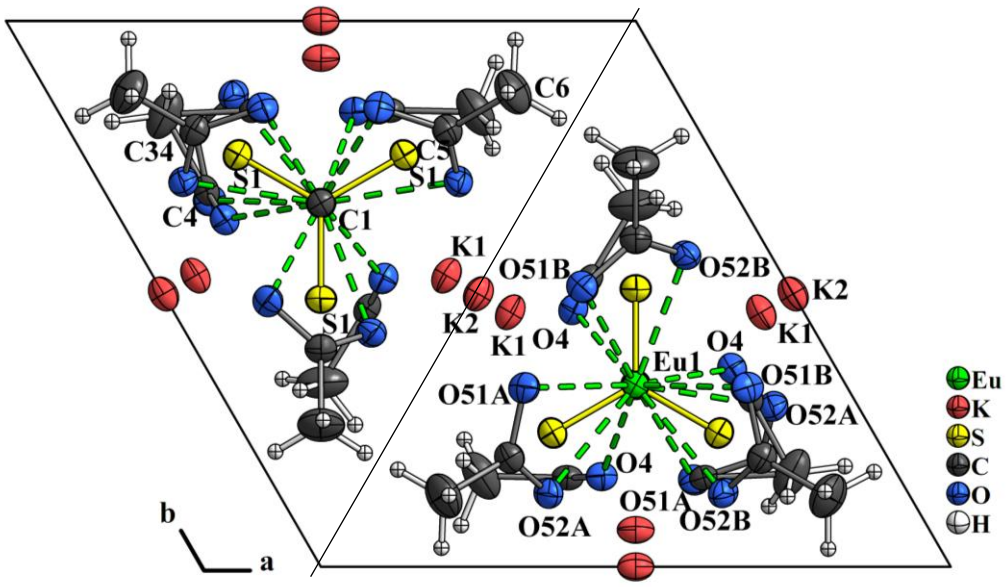

Figure 2.114: Unit cell of $K_9[Eu_2(CH_3COO)_9](CS_3)_3$ **41** in view along the c-axis. For the sake of clarity, the acetate disorders are arbitrarily omitted. The carbon atoms of the trithiocarbonate anions and the europium atoms occupy the centre of the two asymmetric regions, indicated by the separating line. No atoms occupy the unit cell corners (*c*-axis). By adding unit cells along the *a*-and *b*-axis, lipophilic channels along the c-axis form, as the methyl groups are directed towards their centre. All non-hydrogen atom displacement ellipsoids are drawn at 50 % probability.

C2−S2 bond values 172.29(9) pm. No tendency for an increased double bond character among the identical C−S bonds can be assigned for both non-equivalent CS_3^{2-} anions.

The mirror plane (indicated in figure 2.113) furthermore comprises the carbon atoms C3, C4 and C34 (WYCKOFF site 6h) that formulate one of the two non-equivalent, namely the equatorial (bridging) acetate anions. As seen in figure 2.115, the lattice site 2d, with the six-fold and inversion point symmetry, is vacant in the europium acetate unit. It is the centre of the virtual Eu···Eu line in the $[EuO_9]_2$ dimer unit coinciding with the three-fold axis of symmetry. The C−C bond of the equatorial acetate anion, lying in the mirror plane is affected by that symmetry centre at 2d. Thus, the equatorial acetate anion was solved with a 50 % disorder. Part (a) forms with the C34−C3 and part (b) with the C34−C4 ethyl backbone. (Note, both the anions share the terminal methyl group carbon C34 constrained to 100 % occupancy. However, the size of the ellipsoid of C34 is large compared to C3 or C4, indicating some degree of disorder at that position either) The hydrogen atoms are restrained to C34 with execution of the ADD H command within the X-ray data solution work-through.[142,143] They are arranged in two different orientations, according to the disorder of the molecule. For each of the two possible acetate orders, there is only one

unique oxygen atom (O3 or O4), residing in the regular lattice site 12i. As shown in figure 2.115, O3 (O4) is bound to C3 (C4) and by reflection about the mirror plane both the hydroxy and carbonyl group of the respective acetate anion is formed. Consequently, the geometries of the carboxy groups of the equatorial (bridging) acetate ligands are strongly affected by the point symmetry of C3 and C4, respectively. The bond distance of C3−O3 (C4−O4) is 125.9(6) pm (126.2(6) pm), which ranks only slightly above the value for a C=O double bond. For comparison, the C−O and C=O bond lengths have been reported to approximate to 143 and 123 pm, respectively.[13] Due to the symmetry condition the equatorial acetate ligand is obtained in the state of a free anion (middle position in scheme 3) having the negative charge equally distributed on both the oxygen atoms.

In contrast, the second of two non-equivalent acetate anions (axial), carries two non-equivalent oxygen atoms with anisotropic C−O bond lengths. Furthermore, C5 and C6 do not possess any site symmetry and the C5−C6 connection could be solved ordered. Nevertheless, again, a 50 % disorder was used for the orientation of the carboxy oxygen atoms, which as well can be understood with regard to the point of six-fold and inversion symmetry present in the centre of the $[EuO_9]_2$ unit. The plane through O52(a) C5 O51(a) spans an angle of 64.3(9)° between the plane of O52(b) C5 O51(b), which is a rotation of the carboxy group planes about the non-disordered ethyl C5−C6 axis. For part (a) and (b), a C5−O51 single bond length of 130.2(4) and 130.9(7) pm and a C5=O52 double bond length of 121.6(6) and 121.1(5) pm is determined, respectively.

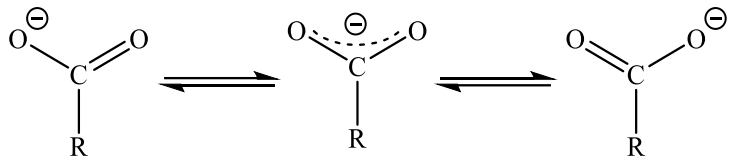

Scheme 3: Resonance formulas of the π-electron system of a carboxyl group. In the crystal structure of **41**, the equatorial acetate anion, bridging between the Eu^{3+} centres can be described as a free anion in consideration of the crystal symmetry and the determined atomic distances. The axial acetate anion exhibits different C−O lengths indicating polarisation of the carboxyl group.

Consistently, the coordination of the Eu^{3+} ion is fashioned by nine oxygen atoms ($CN(Eu^{3+})$ = 9), that each possess a 50 % disorder. The axial acetate ligands perform bidentate coordination, while the equatorial ligands are bridging between the Eu^{3+} centres.

Under similar reaction conditions, allowing to lower the water content in the structures, GOMEZ TORRES, PANTENBURG and MEYER prepared a series of europium(III) acetate hydrates. The X-ray crystal structures showed different numbers of ligands. Among them, $[Eu\{H(CH_3COO)_2\}_3](H_2O)$ displayed dimers of $[EuO_9]_2$ with Eu···Eu distance of 398.0 pm. The crystal formula should be better described as $[Eu_2(CH_3COO)_6(CH_3COOH)_2(H_2O)_2](CH_3COOH)_4$, thus presenting a mixed acetate and hydrate coordinating acetic acid adduct of europium acetate monohydrate. Mono, bi- and tridentate acetato ligands, as well as acetic acid and water offer the oxygen donors in the $[EuO_9]_2$ dimers.[144] Earlier, eight and nine-fold coordination of Eu^{3+} with acetate ligands have been observed, where chains are formed, if the bridging performance of the acetate ligands is not interrupted.[145,146]

Naturally neither aqua ligands nor acetic acid coordination of Eu^{3+} is present in **41** and a much larger Eu···Eu distance of 539.98(7) pm is found. From a qualitative point of view, the dimer stabilisation in **41** can be understood, as this is the smallest crystal fragment of europium(III) acetate. In other words, the bridging coordination is interrupted by the incorporation of trithiocarbonate anions and through the dimer formation, typically observed in crystal structures of lanthanide acetates, the Eu^{3+} coordination with acetates is stabilised.

Chemically, the coordination of Eu^{3+} by acetate ligands instead of trithiocarbonato ligands was expected. Trivalent lanthanide cations favour the *harder* electron donor, which is the carboxy oxygen atom, over the *softer* sulfur donors offered from trithiocarbonate. Indeed, the number of crystal structures with rare-earth−sulfur coordination is low compared to that where oxygen atoms coordinate.[xi]

However, it is remarkable, how the different species still engage to build up a new complex crystal instead of just recrystalising in their incident phases. Probably, by choice of potassium, in mid-position among the alkali ions, the attractive interaction with both the softer trithiocarbonate sulfur and the harder acetate oxygen donors was key to realise a new ionic network of both educts. Figure 2.115 displays the $[Eu_2(CH_3COO)_9]^{3-}$ complex in the unit cell, emphasising the dimeric fashion of the $[EuO_9]_2$ building units.

[xi] CCDC search: Number of crystal structures with any type of lanthanide−sulfur bond (without element compounds): 539. Number of crystal structures with any type of oxygen bond (without element compounds): > 35.000 (5th July 2021)

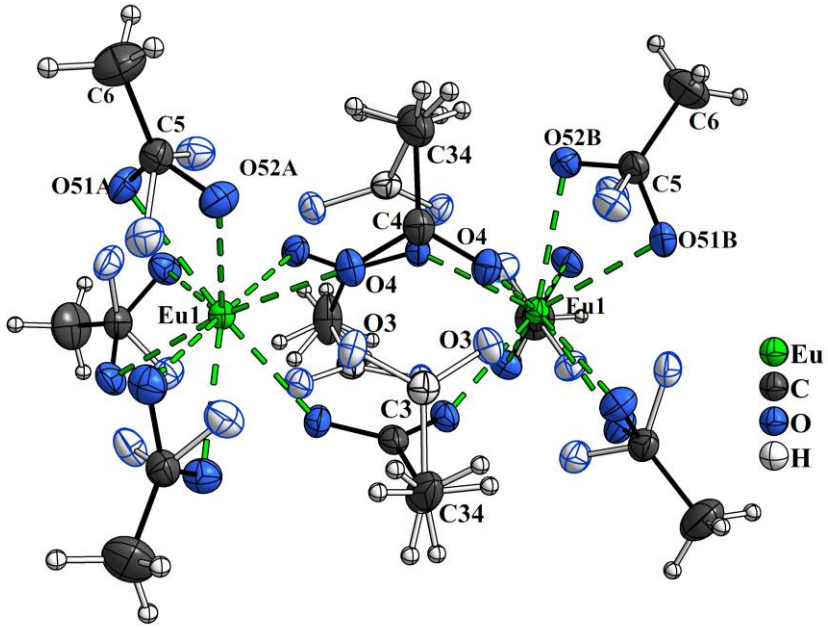

Figure 2.115: Close up of the $[Eu_2(CH_3COO)_9]^{3-}$ complex, which is found in the structure of **41** connected with a potassium trithiocarbonate network. The disorder of the acetate ligands is indicated by a colour-filled and a colourless model each. The left Eu^{3+} ion is drawn in coordination of axial acetato ligands with disorder type (a), the mirror-translated Eu^{3+} on the right is drawn in coordination with disorder type (b) (cf. paragraph and atom names). The bridging acetato ligands in the middle are arbitrarily drawn in orientation of C34−C4(O4)2 (cf. paragraph and atom names). All non-hydrogen atoms are drawn with displacement ellipsoids of 50 % probability.

Exchanging the possible Eu−O coordination in accordance with the disorder, the Eu^{3+} coordination polyhedron is best described with the shape of an irregular pentagonal bicapped bipyramid. In this, the Eu−O connections range between 236.6(4) and 252.8(5) pm, representing typical values of dative bond distances.[144,145]

The crystallographically equivalent europium atoms in the $[EuO_9]$ monomers occupy the lattice point 4f in alternation with two C1-trithiocarbonate anions along the three-fold axis as mentioned above.

There are two non-equivalent potassium ions present in the structure, where K1 occupies a general lattice position (12i) and K2 is residing in the inversion centres (6g), which can be visually derived from figure 2.113 (centre and cell edge middle). Their closest ionic interaction is depicted in figure 2.116 and 2.117 , respectively. Two closest bidentate trithiocarbonate anions (centred by C1 and C2) set up K−S distances of 322.72(8) and 325.6(1) pm, respectively. The values match the expectation learned by earlier discussed structures. The axial acetate ligand connection K1−O52(a) is of much shorter distance

amounting 265.0(3) pm, where the connection with O5(b) type is 265.4(5) pm. Considering an electrostatic repulsion, a coordination with both type (a) and (b) of neighbouring acetate anions is improbable. At the bottom right, the equatorial acetate coordination is drawn with O3 (K1−O3 265.2(4) pm) instead of O4, which points away in figure 2.116. Replacing the coordination with O4 gives a K1−O4 distance of 264.8(3) pm, but again only one of the neighbouring acetate anions can realise an ionic interaction. Depending on the disorder, the K1 site is coordinated by three oxygen donors. This all together adds up to a coordination number of seven for K1.

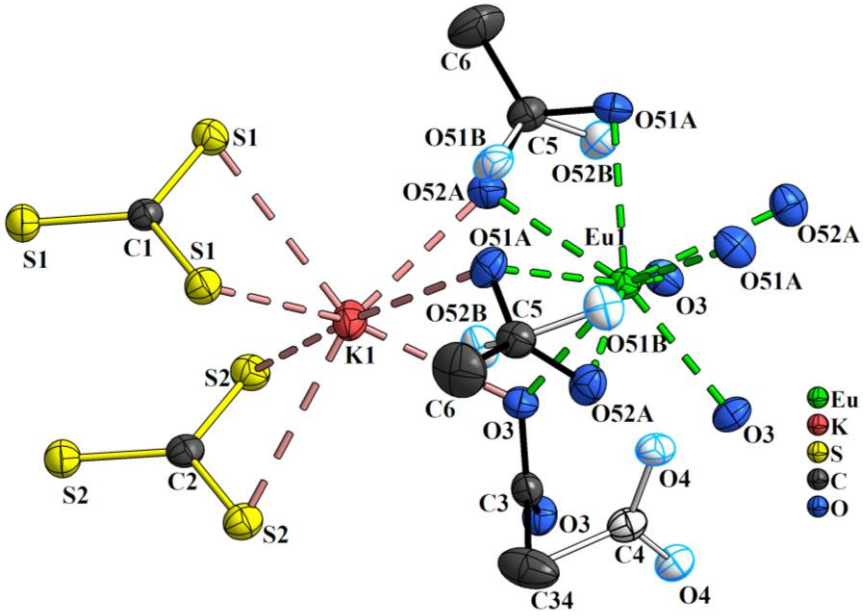

Figure 2.116: Coordination of K1 in the crystal structure of **41**. The potassium cation occupies regular lattice position 12i and connects the two different anion sub-structures *via* ionic interaction. The disorder is indicated by the empty and filled atomic ellipsoids. All atomic displacement ellipsoids are drawn at 50 % probability.

In figure 2.117, the axial acetate anions of the adjacent [EuO_9] unit on the left of K2 are drawn suggesting only one possible K−O interaction (here: with O51(b), 275.8(3) pm). In turn, by choice of the disorder, on the right-hand side two of the axial anions next to K2 are drawn *active* with O51B and O51A donors. Next to the symmetry equivalent distance to O51(b), the additional K2−O51(a) distance is 275.7(3) pm. However, the orientation of the involved acetate anions results in a short distance between O51(b)− O51(a) of 208.7(7) pm, which may be too close in consideration of repulsion. Consistently, the latter coordination circumstances may be assumed improbable, which makes the K2 ion to be six-fold coordinated. Two equivalent trithiocarbonate anions are coordinating in bidentate manner.

As K2 possesses inversion symmetry, all sulfur coordination distances amount the same value of 324.29(6) pm.

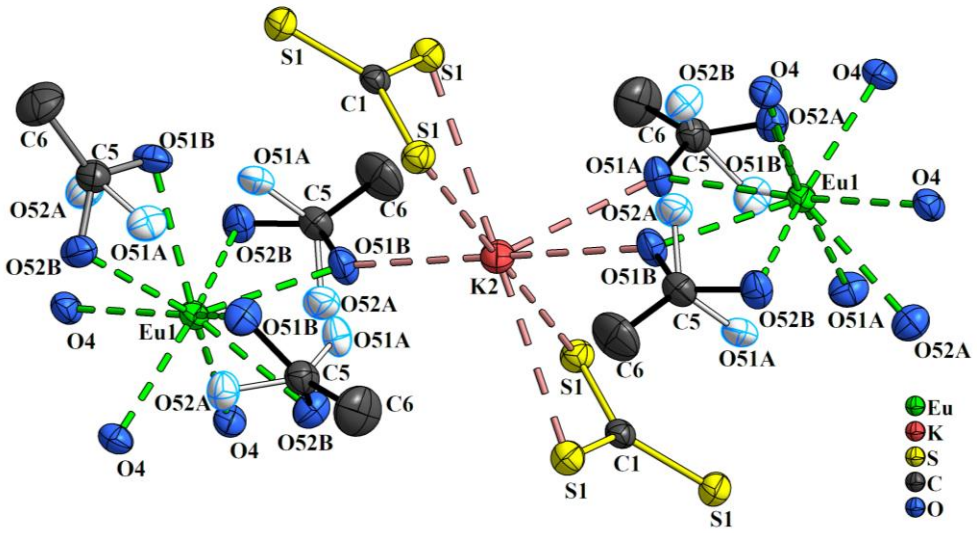

Figure 2.117: Coordination of K2 in the crystal structure of **41**. The potassium cation possesses point inversion symmetry, explaining the crosswise heterogenic coordination by oxygen and sulfur donors. The acetate disorder is drawn with filled and empty ellipsoids, respectively. All atomic displacement ellipsoids are drawn at 50 % probability.

As mentioned above, the $6_3/m$ axis of symmetry, located on the corners of the unit cell along *c*-direction is vacant and surrounded by the methyl groups of the acetate anions, directed towards the corners (cf. figure 2.114). This results in the formation of one-dimensional lipophilic channels along that high symmetry axis. The nearest methyl carbon atoms form an isosceles triangle of 439.0(7) pm edge length. No residual density inheriting the channel position was detected during the X-ray data solution.

To develop the chemistry of lanthanoids with thiocarbonate, exchange of the europium(III) acetate starting material should be considered. For instance, EuI_2 may be used, as iodide is a good leaving group and the material is readily available. This would provide europium in oxidation state +II, which could be preferred for coordination with trithiocarbonate, which is sensitive to oxidative species. Also, Eu^{2+} ions are softer, probably allowing a sulfur coordination more easily. As EuI_3 is unstable with respect to disproportionation under release of iodine, the neighbouring SmI_3 may be used as an alternative for a lanthanoid in their common oxidation state +III. Both the heavier and lighter elements in the 4f-block have not been incorporated in such structures. Application of the lanthanoid ions free of their favoured oxide coordination may allow CS_3^{2-} ligands or more generally 1,1-dithiolates to form lanthanoid complexes. From size considerations of the cation, europium, standing

in the middle of the lanthanoid series, opens the field to explore the chemistry towards both the left (larger) and right (smaller) of the 4f-metals in this regard. Further investigations on crystallisation in form of dimeric complexes in the neighbourhood of trithiocarbonate and substitution of acetate with other leaving groups like e.g., iodide could give new insights into the less explored system of sulfur and lanthanoids.

A route to access these compounds was described here and may be optimised to some degree. For instance, the solvothermal reaction conditions like max. temperature and cooling times could be altered and other solvents could be favoured over ethanol, which was used here. Indeed, a treatment of lanthanum(III) acetate hydrate in the same way as the europium(III) acetate yield crystalline specimen. However, crystal data collected from these were discarded as they could not be solved probably and were of too poor residuals. First attempts employing Eu^{2+} by use of $EuCl_2$ did not yield crystals and were discarded, as crystal data is inevitable to gain understanding in this chemistry.

Thus, in course of this work only the very beginning of this chemistry is covered, which and may lead to new interesting coordination motifs between lanthanoid and thiocarbonate.

3 Summary and outlook

This work discusses the synthesis and crystal structures of various ammonium and metal trithiocarbonates, alkali metal perthiocarbonates, 1,1-dithiolates, as well as selenodithiocarbonates. The compounds were synthesised from solution and solvothermal methods and characterised by means of powder X-ray diffraction (PXRD), thermal analysis and molecular vibrational spectroscopy using infrared (IR) and µRAMAN techniques, which were further supported by *density functional theory* (DFT) calculations.

Salts including the trithiocarbonate anion CS_3^{2-} of the alkali metals and barium were prepared using different synthetic routes. In particular, working under solvothermal conditions in glass ampoules sealed under reduced pressure was superior to traditional solution procedures and resulted frequently in crystals of suitable size for single crystal X-ray diffraction. In contrast to various well-known carbonates the chemistry of the heavier trithiocarbonates has not seen much attention since the 1960s, 70s and 80s. As part of this work, the known compounds $Na_2CS_3 \cdot 2\,H_2O$ and K_2CS_3 were re-investigated and crystallographically described for the first time by modern single crystal X-ray diffraction. It is highlighted that the structure of $BaCS_3$ could now for the first time be described accurately. It was found that the compound crystallises with a higher symmetry than reported nearly 60 years ago.

Furthermore, the solvate free crystal structures of the perthiocarbonates $Na_2[CS_2(S_2)]$ and $K_2[CS_2(S_2)]$ were elucidated for the first time. The crystals were obtained by exploring the solvothermal route starting from alkali metal polysulfides. Thanks to this approach, two caesium salts including mixed trithio-perthiocarbonate $Cs_5(CS_3)[CS_2(S_2)]_{1.5}$ and perthiodicarbonate $Cs_2(C_2S_6) \cdot CS_2$ were obtained and crystallographically described for the first time.

In order to investigate the influence of substitution of a sulfide for the heavier selenide anion under solvothermal conditions, single crystal data of the first ever perselenodithiocarbonate

anion $CS_2(Se_2)^{2-}$ could be obtained, which co-crystallised with CS_3^{2-} giving the sum formula $K_5[CS_2(Se_2)]_{1.5}(CS_3) \cdot H_2O$. The structure of the $[CS_2(Se)_2]^{2-}$ anion was found to be comparable to the perthiocarbonate anion with atomic distances ranging with those in related selenium compounds, like $(H_3C)_2Se_2$ or $Se_2(CN)_2$. µRAMAN spectroscopy was used to identify the nature of the molecular vibrational energies showing a significant energy shift of 200 cm^{-1} of the Se–Se stretching mode compared to that of S–S in perthiocarbonate anions. Further work in this regard should include the substitution of CS_2 with CSe_2, which could in scope of this work not be used but should allow the formation of $CSSe_2^{2-}$ and CSe_3^{2-}. Initial work may for instance be to attempt isolation of crystals of the known potassium and barium triselenocarbonates.

Attempts to isolate crystals and investigate the structures of the lighter Li_2CS_3 and heavier Rb_2CS_3 and Cs_2CS_3 were undertaken. Li_2S and CS_3 were treated solvothermally, but no solid products, not to mention crystals, were obtained. Moreover, contrarily to the heavier alkali metals, a solution of LiHS did not immediately yield trithiocarbonate upon addition of CS_2, which could stem from the lower solubility of the starting material LiOH. However the solution did react with CS_2, eventually giving crystals of $Li_4(CS_3)(SH)_2 \cdot 5\ H_2O$ in very low yield, which could be isolated and characterised. The crystals elucidated that the conversion from LiHS to Li_2CS_3 was apparently incomplete. An alternative route treating trithiocarbonic acid $(HS)_2CS$ with *n*-butyllithium yielded a solid amorphous product. Nevertheless, by means of molecular spectroscopy the formula Li_2CS_3 cannot describe the properties of the product in total. On routes given in the literature, $(HS)_2CS$ was prepared from K_2CS_3 and briefly characterised with IR spectroscopy, confirming the expected properties.

Crystal data of a small pink crystal grown from a solvothermal reaction mixture of amorphous rubidium (poly)sulfide with CS_2 was insufficient for a structure model. However, µRAMAN spectra of the species included all modes of CS_3^{2-} exclusively, indicating the potential formation of Rb_2CS_3. Since the small crystals only grew in very low yield and decomposed soon after recovery from the ampoule no further analyses could be carried out in course of this work.

Regarding caesium, the known hydrate $Cs_2CS_3 \cdot H_2O$ and two new compounds, namely the methanol solvate of $Cs_2CS_3 \cdot \frac{1}{6}$ MeOH and the mixed tithio- perthiocarbonate $Cs_5(CS_3)[CS_2(S_2)]_{1.5}$ were obtained and crystallographically described. The latter two recrystallised under solvothermal conditions, using the dried powder of $Cs_2CS_3 \cdot H_2O$ and

methanol as solvent. PXRD and molecular spectroscopy of the dried caesium salt indicated the potential identity of the anhydrous compound.

This thesis has explored the influence of different alkali metal cations on the formation of trithiocarbonates. While it was deduced that a formation with the small lithium ion was incomplete, the larger rubidium and caesium salts have formed readily from solutions, but a crystallographic description of the solvent free material could not be achieved, despite the fact that other analytical methods confirmed their successful formation.

In particular, the treatment of (poly)sulfides with CS_2 under solvothermal conditions adding only small amounts of solvent such as water or ethanol demonstrates a viable method to obtain crystalline thiocarbonates. These findings point out that a systematic investigation of trithiocarbonates across the periodic table is accessed to further elucidate the binding and stability of these salts. To overcome the integration of small quantities of solvents such as H_2O or MeOH, other media may be used or combined. However as these solvate molecules can stabilise the network of the desired target molecules in the solid state, they may be helpful in the crystallising processes. In this regard, it is mandatory to imply investigation of suitable temperature regimes, which was not covered extensively in this work. As most trithiocarbonates decompose upon exposure to moisture and oxidants, ongoing protocols should consider execution under inert conditions.

Substituting the alkali cation for H_4N^+ has resulted in a stabilised network by S···H–N hydrogen bridges. However, in the obtained crystals this did not lead to higher lattice order. The attempts to prepare ammonium trithiocarbonate using anhydrous concentrated alkaline solutions of $(H_4N)_2S$ and CS_2 failed, as the many coupled equilibria between NH_3, H_2S and CS_2, resulted, for the first time, in the isolation of $(H_4N)_5(CS_3)_2[S_2C(NH_2)]$, which includes both a trithiocarbonate and a 1,1-dithiocarbamate anion.

Furthermore, with the crystal structure of $(N_2H_7)_2CS_3$, the elusive $(N_2H_7)^+$ ion could be re-investigated. This is the ammonia version of the well-known $(O_2H_5)^+$ cation, and crystallographically $(N_2H_7)^+$ has so far only been determined in eight systems. Yet, only three of these comprise salts with a simple salt structure, namely $(N_2H_7)F$, $(N_2H_7)I$ and $(N_2H_7)CH_3COO$. Thus, $(N_2H_7)_2CS_3$ is the only binary compound presenting $(N_2H_7)^+$ in an exclusive sulfur interaction environment.

Of the ammonium related compounds IR and RAMAN data was collected, indicating molecular vibrations in the expected spectral regions, confirming their identity as determined by crystallography. Further investigation of the compounds calls for more powerful tools such as neutron diffraction, to determine the lattice positions of the hydrogen

atoms more precisely. This could then allow prediction of the energetic distribution of molecular vibrations more accurately and may help to better understand the nature of hydrogen bonding apart from oxygen donors and acceptors.

Additional work was done with respect to transition metal trithiocarbonates. Using the solvothermal route with ethanol as solvent, complexes of the nickel group metals and cobalt could be crystallised as $K_2[Ni(CS_3)_2]$, $K_2[Pd(CS_3)_2] \cdot EtOH$, $K_2[Pt(CS_3)_2]$ and $K_5[Co(CS_3)_3]CS_3$ and their structures elucidated. A novel route to obtain these transition metal trithiocarbonato complexes without bulky cations has thus been established. The nickel and platinum compounds crystallised isostructurally, which was not the case for the palladium complex, where an ethanol molecule was built into the lattice. The significant buckling of the $[Pd(CS_3)_2]^{2-}$ ion is remarkable, as this contrasts the bis(trithiocarbonato) complex anions of nickel and platinum which were found to be planar. This is likely due to the presence of the ethanol molecule, as the planarity could later also be proven for the palladium complex $(Ph_4P)_2[Pd(CS_3)_2]$, which was obtained from a solution of K_2CS_3 and $PdCl_2$ in DMSO with aqueous $(Ph_4P)Cl$. $(Ph_4P)_3[Bi(CS_3)_3]$ was obtained after analogous procedure but as it had been fully characterised in literature it was not further analysed.

An example for the coordination of transition metals with three trithiocarbonate anions is the cobalt compound $K_5[Co(CS_3)_3]CS_3$, which is unknown to crystallographic databases. However, the complex anion has been reported in earlier publications and described, amongst others, with IR spectroscopy. The structure comprises an octahedral coordination of the Co^{3+} in the $[Co(CS_3)_3]^{3-}$ anion. It is comparable with the Fe^{3+} complex, the only other mononuclear homoleptic trivalent transition metal complex previously reported. Contrary to the trivalent main group metal complexes As^{3+}, Sb^{3+} and Bi^{3+}, the metal−sulfur distances are of similar value, as on transition metals no electron lone pair acting repulsive towards the ligand is present. First attempts to include the heavier homologues of cobalt in trithiocarbonato complexes did not yield crystals for investigation of the coordination types that may be favoured in the respective rhodium and iridium trithiocarbonato complexes.

RAMAN spectroscopy amplified by microscope focussing allowed to measure spectra of the palladium, platinum and cobalt complexes. It can be highlighted that for the first time non-interfering potassium cations allowed recording of molecular vibration data of only the complex molecules, without disturbing modes of other species. Generally, RAMAN data on trithiocarbonato complexes are rare in the literature and here the metal−sulfur RAMAN bands are resolved and discussed.

First fundamental aspects regarding the chemistry of trithiocarbonates with regard to their reactivity towards lanthanoid compounds have been addressed. The oxophilic lanthanoids have never shown any crystal structures containing trithiocarbonate anions. In this work, an attempt was made towards a lanthanoid trithiocarbonate complex by treating $Eu(CH_3COO)_3$ with K_2CS_3 using ethanol as solvent under solvothermal conditions. This yielded yellow crystals of $K_9[Eu_2(CH_3COO)_9](CS_3)_3$, which include both starting materials in a sub-structural fashion. Even though the complex does not show a direct Eu−S interaction, a variation of the starting material may be useful to allow the formation of such a sulfur coordination.

In attempts to further this chemistry into other transition, p-block and 4f-metals a trial was made to convert $EuCl_2$, $La(CH_3COO)_3 \cdot 1.5\,H_2O$, $AuCl_3$, $Au(OH)_3$, $Au(CH_3COO)_3$, $Ag(CH_3COO)$, $FeCl_3$, $H_3[RhCl_6]$ $Hg(CH_3COO)_2$, $Ir(CH_3COO)_3$ and $In(CH_3COO)_3$ with K_2CS_3 as well as $Cu(SO_4) \cdot 5\,H_2O$ with $BaCS_3$ under solvothermal conditions. This did not yield products for crystallographic investigation and thus these experiments were discarded. However, changes in the treatments using other solvents and/or longer temperature regimes, with slower cooling phases, may be advisable to study these elements and their reactions with K_2CS_3 more systematically and may help to produce single crystals of adequate size. Moreover, experiments including large bulky phosphonium cations to prepare Au^{3+}, Hg^{2+}, Tl^{+}, Tl^{3+} and Ag^{+} trithiocarbonato complexes failed.

In contrast, Cu^{+} reacted with CS_2 in aqueous NH_3, giving $(H_4N)^1_{2\infty}[Cu\{CS_2(S_2)\}]CS_2(S_2)$. The compound consists of one-dimensional chains of neutral $Cu[CS_2(S_2)]$ units oriented crosswise, where in between ammonium ions and perthiocarbonate anions fill the voids. Thus, another multi molecular structure could be obtained, showing Cu^{2+} in a remarkable and yet rarely described polymeric arrangement. The oxidation of Cu^{+} in this experiment was discussed using different reactions to elapse parallel.

It was further attempted to isolate thallium(I) trithiocarbonate in form of single crystals. The published structure was already elucidated by means of RIETVELD refinement of PXRD data. Attempts to grow single crystals of this very stable salt under solvothermal conditions yielded crystals of Tl_2S_5 among other non-crystalline side products. It is yet unknown why the crystallisation of the pentasulfide salt was favoured over that of Tl_2CS_3, considering its stability. Powder of the desired compound forms readily from aqueous solutions but crystals could not be obtained. It may also be assumed that among the side products of the solvothermal treatment of $BaCS_3$ with Tl_2SO_4 some Tl_2CS_3 has formed as powder. It is suggested, that under the chosen conditions, trithiocarbonate anions may have been

decomposed and the stable pentasulfide formed with the soft Tl^+ ions. Methathesis reactions of thallium compounds under solvothermal conditions should therefore be investigated to a greater extent. In particular, the conditions to grow crystals should be reconsidered, and it may be advisable to change these to higher temperatures and longer growth times, concentrating the solvothermal reaction mixture. In order to clarify the formation of pentasulfide trial-and-error of the substitution of sulfate should be considered regarding the suggested decomposition of CS_3^{2-}.

Altogether, 27 compounds could be synthesised through solvothermal synthesis, solvothermal recrystallisation or techniques using saturated solutions and all of them were crystallographically elucidated successfully. Of these, eleven were re-investigated, as some have been described in long standing publications starting from the 1950s. The structures of these compounds could be unambiguously characterised for the first time, and further analyses confirmed the integrity of the material. Sixteen novel X-ray crystal structures were determined, including the series of alkali metals and barium to be crystallised with trithiocarbonate anions as well as solvent free sodium, potassium and caesium perthiocarbonates. For the first time the selenodithiocarbonate anion was obtained.

The compounds were analysed using various techniques, however, the PXRD in particular showed that the high sensitivity of the thiocarbonates towards moisture and air makes them prone to side reaction and leads to small amounts of unidentifiable impurities in the powdered samples.

The solvothermal reaction of alkali trithiocarbonate with transition metal salts was never reported before and allowed access to crystals of trithiocarbonato complexes with potassium cations for the first time. On the one hand, the earlier published complexes could be reinvestigated in an altered crystallographic environment, and on the other hand, a step towards a series of novel lanthanoid trithiocarbonato complexes was made. As such, the methods described herein may be useful for a further systematic investigation of thiocarbonates from across the periodic table and may lead to a variety of extraordinary bonding and coordination motifs.

4 Experimental and analytical methods

4.1 General preparative procedures

Unless otherwise stated, all proceedings were carried out in a fume hood of a workspace of approximately 120x80x200 cm^3. For reactions, where it was vital to keep out moisture, cleaned laboratory glassware was dried in an oven at 110 °C before use. During the setup of reaction vessels, the inside of the dried glass containers was flushed with argon or kept under dynamic argon flow as soon as possible and when still warm.

A SCHLENK apparatus, or vacuum inert gas manifold, consisting of a two-way glass distributor was applied to prevent atmosphere, i.e., oxygen, carbon dioxide, moisture and other unwanted species to enter reactions in laboratory glassware. Argon gas was dried by passing through a glass U-tube filled with silica gel and *Sicapent*® (phosphorous pentoxide on silica). Excess argon was vented through a bubbler filled with *Fomblin*® inert oil. With the gas manifold argon could be distributed on the laboratory glassware. On the side of reduced pressure of the SCHLENK line, the distributor tube was connected to a *Vacuubrand* rotary oil pump and for control of the pressure inside the evacuation path, a *Vacuubrand* digital manometer (p_{min} = 0.001 mbar) was attached. Moreover, a cold trap was integrated, forcing any volatiles in the evacuation path volume to condense in, prohibiting to enter the pump. Therefore, the trap was submerged in liquid nitrogen inside a DEWAR vessel. Between the described glassware and devices, rubber hoses were used for connecting the system.

Hydrogen sulfide gas, H_2S, was used straight from the gas cylinder without any further purification. The reactive and toxic gas was released through a pressure-reducing valve by simultaneously leading a safety current of nitrogen gas through it. In this way, the valve was cleaned from hydrogen sulfide after the release. The gas mix was directed through a glass distributor and a bubble counter filled with *Fomblin*®. As neither the exact volume, nor the composition of the mix could be monitored, all reactions involving H_2S were

performed with excess gas. Hydrogen sulfide was made use of in some preparative protocols given below, note, that never only pure hydrogen sulfide was added to the reactants, but the mix of nitrogen and hydrogen sulfide. After passing the reactor or the reaction solution, the excess nitrogen/hydrogen sulfide mix was disposed by venting it into a natural gas flame. Lithium, sodium and potassium were cleaned before use by cutting off the outer oxide/nitride layer while immersed in toluene.

List of purchased chemicals

Name	Cas-No.	Specifications	Supplier
Ammonia (aqueous)	1336-21-6	25 %	inhouse supply
Ammonia (gas)	231-635-3	technical grade, anhydrous	*Air Products*, Hattingen, Germany.
Barium hydroxide monohydrate	22326-55-2	95 %, crystalline	*Thermo Fisher Scientific*, *Alfa Aesar*, Massachusetts, USA
Caesium	7440-46-2	metallic, colour: gold	remainder of unknown origin
Caesium hydroxide monohydrate	12260-45-6	99.9 % (metals basis), crystalline	*Thermo Fisher Scientific*, *Alfa Aesar*, Massachusetts, USA
Carbon disulfide	75-15-0	99.9 %, extra pure, low in benzene content	*Thermo Fisher Scientific*, *Acros Organics*, Geel, Belgium
Cobalt(II)chloride	7646-79-9	anhydrous, colour: blue	remainder of unknown origin
Copper(I)chloride	7785-89-6	99 %	*Heraeus Chemicals*, Karlsruhe, Germany
Diethyl ether	60-29-7	extra dry over mole sieve, 99.5 %, stabilised	*Thermo Fisher Scientific*, *Acros Organics*, Geel, Belgium
Dimethyl sulfoxide	67-68-5	> 99.9 %, analytical reagent grade, 0.02 % H_2O	*Thermo Fisher Scientific*, *Acros Organics*, Geel, Belgium
Ethanol	64-17-5	absolute, 99.8 %, HPLC grade, < 0.02 % H_2O	*Thermo Fisher Scientific*, *Acros Organics*, Geel, Belgium
Europium(III)acetate hydrate	1184-63-0	99.999 %	*Sigma-Aldrich*, Steinheim, *Merck KGaA*, Darmstadt, Germany
Hydrochloric acid.	7647-01-0	analytical reagent grade, 37 %	*Thermo Fisher Scientific*, *Acros Organics*, Geel, Belgium
Hydrogen sulfide (gas)	04.06.7783	2.5 (99.5 %)	*Gerling Holz & Co. HGmbH*, Dormagen, Hamburg, Germany
Lithium	7439-93-2	in petrol ether	remainder of unknown origin
Lithium hydroxide	1310-65-2	98 %, reagent grade	*Sigma-Aldrich*, Steinheim, *Merck KGaA*, Darmstadt, Germany
n-buthyllithium	109-72-8	2.5 M, in hexane	*Thermo Fisher Scientific*, *Acros Organics*, Geel, Belgium
Nickel(II)acetate tetrahydrate	6018-89-9	99 %, extra pure	*Thermo Fisher Scientific*, *Acros Organics*, Geel, Belgium
Palladium(II)acetate	3375-31-3	47.5 % Pd	*Thermo Fisher Scientific*, *Acros Organics*, Geel, Belgium

Name	Cas-No.	Specifications	Supplier
Platinum(II)acetate - trimer		black	remainder of unknown origin
Potassium	07.09.7440	98 %, chunks in mineral oil	*Sigma-Aldrich*, Steinheim, *Merck KGaA*, Darmstadt, Germany
Potassium hydroxide	1310-58-3	pellets, analytical reagent grade, 0.28 % CO_3^{2-}	*Thermo Fisher Scientific*, *Acros Organics*, Geel, Belgium
Potassium polysulfide	37199-66-9	> 42 % K_2S basis	*Sigma-Aldrich*, Steinheim, *Merck KGaA*, Darmstadt, Germany
Potassium *tert*-butoxide	865-47-4	98+ %, pure	*Thermo Fisher Scientific*, *Acros Organics*, Geel, Belgium
Rubidium	7440-17-7	metallic, colourless	remainder of unknown origin
Selenium	7782-49-2	99.6 %, powder, 325 mesh	*ChemPur*, Karlsruhe, Germany
Sodium	7440-23-5		
Sodium hydroxide	1310-73-2	pellets, analytical reagent grade, < 1 % CO_3^{2-}	*Thermo Fisher Scientific*, *Acros Organics*, Geel, Belgium
Sodium sulfide nonahydrate	1313-84-4	98 %	*Thermo Fisher Scientific*, *Acros Organics*, Geel, Belgium
Sulfur	7704-34-9	reagent grade, powder, 100 mesh	*Sigma-Aldrich*, Steinheim, *Merck KGaA*, Darmstadt, Germany
Tert-butanol	75-65-0	99.5 %, extra pure	*Thermo Fisher Scientific*, *Acros Organics*, Geel, Belgium
Tetraphenyl phosphonium chloride	2001-45-8	98 %	*Thermo Fisher Scientific*, *Acros Organics*, Geel, Belgium
Thallium nitrate	10102-45-1	99.5 %, (metals basis)	*Thermo Fisher Scientific*, *Alfa Aesar*, Massachusetts, USA
Thallium sulfate	7446-18-6	99.5 %, (metals basis)	*Thermo Fisher Scientific*, *Alfa Aesar*, Massachusetts, USA
Toluene	108-88-3	HPLC grade, < 1 ppm H_2O	*Thermo Fisher Scientific*, *Acros Organics*, Geel, Belgium

4.2 Syntheses

Method A Precipitation from saturated solution

A feasible and long known route to obtain trithiocarbonates is based on the precipitation of the salts from a saturated ethanolic solution of alkali hydrogen sulfide by the addition of CS_2. The alkali metal can be introduced in its elemental state, which is denoted with **A.1**, below (equation 4.1). Upscaling of the reaction can be achieved by use of more abundant alkali hydroxides in exchange for the metals, denoted with **A.2** (equation 4.2). Water forms as a side product and may be dried off in a subsequent protocol. Other solvents or combinations with EtOH may be used for hydroxides of poor solubility.

A.1

$$M_{(s)} \xrightarrow[\text{2) + } H_2S_{(g)},\ T^{\uparrow}\ (\sim 60\ ^\circ C)\ \text{3) + } CS_{2(l)},\ T^{\downarrow}\ (RT)]{\text{1) + EtOH}} M_2CS_{3(s)}\downarrow \qquad (4.1)$$

A.2

$$MOH_{(s)} \xrightarrow[\text{2) + } H_2S_{(g)},\ T^{\uparrow}\ (\sim 60\ ^\circ C)\ \text{3) + } CS_{2(l)},\ T^{\downarrow}\ (RT)]{\text{1) + EtOH}} M_2CS_{3(s)}\downarrow + H_2O \qquad (4.2)$$

Method B Solvothermal reaction

The preparation route applied herein, which will be referred to as **B.1**, i.e., *solvothermal synthesis* below allows formation of alkali trithiocarbonate. Solid alkali sulfide was reacted with CS_2 (equation 4.3). Under these conditions, recrystallisation experiments have been carried out, where the trithiocarbonate salt was prepared beforehand. Thus, the crude powder was used to grow single crystal specimen by this method, summarised under **B.2**, i.e., *solvothermal recrystallisation* (equation 4.4). EtOH was added in only small amounts to act as a solvent.

B.1

$$M_2S_{(s)} + CS_{2(l)} \xrightarrow[\text{2) } T^{\rightarrow}\ \text{dwell (}\sim 1 - 2\ \text{d)}\ \text{3) } T^{\downarrow}\ RT\ (< 1\ K/h)]{+ \sim 10\ \text{drops EtOH}\ \text{1) } T^{\uparrow}\ \sim 100\ ^\circ C\ (5 - 10\ K/h)} M_2CS_{3(s)} \qquad (4.3)$$

B.2

$$\underset{\text{powder}}{M_2CS_{3(s)}} \xrightarrow[\text{2) } T^{\rightarrow}\ \text{dwell (}\sim 1 - 2\ \text{d)}\ \text{3) } T^{\downarrow}\ RT\ (< 1\ K/h)]{+ \sim 0.5 - 1\ \text{mL solvent}\ \text{1) } T^{\uparrow}\ \sim 100\ ^\circ C\ (5 - 10\ K/h)} \underset{\text{crystal}}{M_2CS_{3(s)}} \qquad (4.4)$$

The reaction vessels for method **B** were borosilica 3.3 glass ampoules of approximately 200 - 250 mm length, an outer diameter of 14 mm and an inner diameter of 12 mm. The ampoules were sealed with a natural gas/oxygen flame mix. For this purpose, they were connected with the vacuum system by a ground glass joint socket at the open end. The male cone at the vacuum apparatus was greased before connection.

The cleaned ampoules were stored in a drying oven at 110 °C before use. Adding reactants to the ampoule was done either maintaining a brisk counter flow of nitrogen gas or inside an argon glovebox, to assure oxygen, carbon dioxide and moist air kept out.

Proper evacuation of the ampoule volume was important for subsequent safe temperature treatment. The reactants at the bottom of the ampoule were frozen solid, immersing only the tip end of the ampoule into liquid nitrogen. Thereafter, the room above was evacuated. After the inner pressure decreased below 0.020 mbar the ampoule was sealed. During the sealing process, the lower tip of the ampoule was submerged in liquid nitrogen to prohibit evaporation of solvent or even reaction with the hot glassware.

The sealed ampoules were subjected to a temperature treatment to initiate the solution and reaction of the constituents. Therefore, a horizontal tube furnace was used. The ceramic tube had a diameter of 40 mm and a length of 400 mm and were stoppered with stone wool at both ends to prevent too much temperature gradient towards the furnace tube apertures. A thermocouple inside the tube allowed to set the desired temperature programme for the reaction. The temperature profile for the reactions was pre-set by manual adjustment on the digital power control device.

In the following descriptions, all treatments using sealed ampoules under *solvothermal conditions* are given in form of a table. (Note, the type at the top left in these tables determine whether a *synthesis* (**B.1**) or *recrystallisation* (**B.2**) was carried out.

4.2.1 Trithiocarbonic acid

Preparation of carbon sulfide di(hydrosulfide), $SC(SH)_2$ (also H_2CS_3) a.k.a. trithiocarbonic acid **1** was performed according to equation 4.5.

$$\underset{\mathbf{9}}{K_2CS_{3(aq)}} \xrightarrow{\sim 10\ \%\ HCl_{(aq)},\ 0\ ^\circ C} \underset{\mathbf{1}}{(HS)_2CS_{(l)}} \qquad 4.5$$

HCl (~37 %, analytical reagent grade) was diluted to get a solution of ~10 % and was cooled in a freezer. K_2CS_3 **9** (7.2 g, 38 mmol, 1 eq.) was suspended in 10 mL ice water and quickly dissolved by stirring. The red solution was added to the ice-cold hydrochloric acid in a glass beaker. The solution turned turbid and yellow, but soon became colourless. Red droplets of the desired product, formed at the same time and sank to the bottom of the beaker, where they agglomerated to form a second phase. The emulsion was transferred to a dropping funnel and separated from the hydrochloric acid solution (cf. photograph on page 95). The red oil-like product was quickly stirred with ice-cold water and separated again. It was subjected to reactions or analysis. It was refrained to store it over a longer period. Even, through a screw-top vial, proofed with a PTFE tape, the abhorrent odour could exit.

4.2.2 Lithium thiocarbonates

Treatment of $(HS)_2CS$ with *n*-butyllithium (2)

In a 250 mL round bottom flask, about 2 – 3 mL (~27 mmol) freshly $(HS)_2CS$ was added into 90 mL of toluene on mole sieve, cooled with a CO_2/isopropanol bath. The clear and colourless toluene became yellow and slightly turbid upon dissolution of the acid. While the solution was stirred, traces of water should have been captured in the mole sieve. The solution could warm up a little from the ambient and was pressed into a separate 250 mL round bottom flask. A solution of LiC_4H_9 in hexane (3 mL, 7.5 mmol, 1 eq.) was added. The reaction is given in equation 4.6.

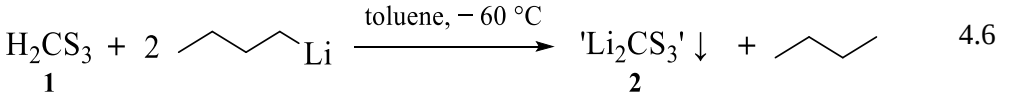

1 2 4.6

With the first drops of the slowly added LiC_4H_9 a yellow mass precipitated. The solid product was filtered from the liquid phase, washed with cold hexane, and dried in dynamic vacuum. The product released an unpleasant odour. It was stored in an argon glovebox inside a snap-cap vial, inside a screw-top flask. Powder residuals, that stuck to any tools almost immediately deliquesced to red droplets (cf. photograph on page 62).

A.1 Lithium trithiocarbonate - no solid product obtained

A piece of Li (0.61 g, 0.088 mol, 1 eq.) was cleaned from its dark lithium nitride layer with a toothbrush and rinsed with EtOH. With metallic appearance, it was then dissolved in a volume of 100 mL EtOH in a round bottom flask that carried a reflux condenser. The dissolution was accelerated by heating the mixture to 50 °C. A turbid solution of Li^+ and EtO^- was obtained, which was now saturated with H_2S gas for 30 minutes without heating. CS_2 (6 ml, 0.099 mol, 1.13 eq.) was added during heating of the solution to 60 °C. The clear and colourless solution immediately turned orange upon addition. Six portions of 5 mL of Et_2O were added to achieve precipitation of the desired product. Eventually, the heater was switched off and the solution left to cool overnight. On the next day, a slight amount of yellow solid had formed on the solution surface at the wall of the flask. However, it dissolved when the solution was moved. The solution was concentrated to about 50 mL upon which it turned turbid. It was left in the fridge in order to crystallise the desired Li_2CS_3, but no solid species formed.

A.2 $Li_4(CS_3)(SH)_2 \cdot 5\ H_2O$ (3)

LiOH (5 g, 0.21 mol, 1 eq.) was added into a 250 mL round bottom flask and dissolved in the a final volume of 145 mL EtOH, which was added stepwise to achieve solution of the complete amount of the hydroxide. After 125 mL had been added, H_2S gas was introduced with the usual precautions to maybe catalyse the dissolution by formation of HS^- and H_2O. For one hour the solution was fed with H_2S gas. Complete dissolution was only achieved by addition of portions of EtOH. The solution was then pale lime yellow and turbid. It was warmed with a water bath that was brought to 60 °C and a solution of CS_2 (40 mL, 0.66 mol, 3.1 eq.) and 20 mL EtOH was added. Immediately the colour of the reaction solution changed to dark red. Under reflux, Et_2O was added through a syringe and the solution allowed to cool down. On the next day, no solid phase had formed overnight. 10 – 20 mL of the solution was passed dropwise to a round bottom flask filled with 50 mL Et_2O. Immediately a yellow solid formed, which appeared to dissolve again by further transfer of the red solution. The process was stopped. In a water bath, the Et_2O solution was cooked under reflux and under argon atmosphere. After reflux was observed for 10 minutes, the heater was switched off and with cooling down a few microscopic yellow crystals grew on

the wall of the flask. They could be identified with $Li_4(CS_3)(SH)_2 \cdot 5\ H_2O$, confirmed by SC-XRD.

The large volume of the red mother liquor was concentrated by use of a rotary evaporator. A jelly orange mass was obtained and was discarded for any further investigation.

B.1 Treatment of Li_2S with CS_2

type	B.1 (cf. p. 198)		internal ID CJ_A_67
reactants	Li_2S* (30 mg, 0.65 mmol, 1 eq.)	CS_2 (0.8 mL, 0.013 mol, 20 eq.)	10 drops of EtOH
1st furnace programme	heating	dwelling	cooling
	100 °C, rate 8 K/h	48 hours	RT, 0.8 K/h
product	the ampoule carried no solid product		
2nd furnace programme	110 °C	24 hours	80 °C, 0.5 K/h, dwelling 5 hours, RT, 3.4 K/h
product	no solids, yellow solution + reddish amorphous mass (cf. photograph left)		
3rd furnace programme	150 °C, rate 8 K/h	24 hours	RT, 1.7 K/h
product	dark brown solution + dark brown amorphous mass (cf. photograph right)		
note	*anhydrous Li_2S purchased and stored in Ar-glovebox		

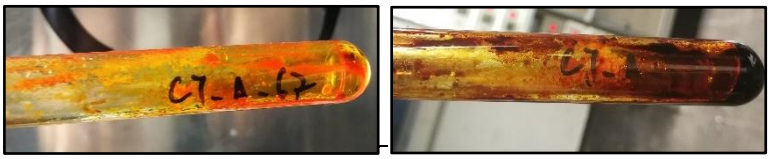

Figure 4.1: Photographs of the ampoule after solvothermal treatment. On the left after the 2nd, on the right after the 3rd furnace programme treatment.

B.2 Attempt of recrystallisation of 'Li_2CS_3'

type	B.2 (cf. p. 198)		internal ID CJ_A_73
reactants	'Li_2CS_3' **2** (100 mg)		~0.8 mL EtOH
furnace programme	heating	dwelling	cooling
	100 °C, rate 7.5 K/h	24 hours	RT, rate 0.75 K/h
product	dark brown mix of a liquid similar looking as shown in Figure 4.1 on the right		

4.2.3 Sodium trithiocarbonates

A.1 Na_2CS_3 (4)

In a dried round bottom flask fit with a reflux condenser and a glass tube for gas inlet, Na (3.3 g, 0.14 mol, 1 eq.) was dissolved in 100 mL dry EtOH. A slow argon gas flow was purged over the reaction solution to prevent oxygen and moist atmosphere to interfere. After the metal has dissolved completely, hydrogen sulfide was passed gently into the solution until a faint turbidity indicated saturation with sodium hydrosulfide. The H_2S flow was stopped, and the solution was heated to, CS_2 (0.08 mol, 4.8 mL, 0.57 eq.) was added to the reaction solution using a syringe. A magnetic stirrer bar helped to quickly mix the reactants. Upon addition of CS_2 the solution was no more turbid and was coloured in deep orange, indicating the reaction of CS_2 with hydrogen sulfide anions. The solution was warmed up and hold for 30 minutes at 60°C while stirring observing reflux of CS_2. Letting the solution cool down slowly, Et_2O was added to a point that the orange solution turned slightly turbid indicating the begin of precipitation of the product. At minimum stirring speed, the solution was left to cool down completely, where the precipitation of a yellowish orange solid was observed. The orange solution was pressed off from the solid product by argon overpressure, that was put on the glass apparatus. Therefore, a long syringe equipped with a piece of filter paper was placed in the reaction mixture. The obtained orange product was washed with dry Et_2O dried with a flow of argon at 60 °C for ~2 hours. The colour of the **powder** changes to a darker more saturated orange as the temperature was rising above 45 °C.

A.2 $Na_2CS_3 \cdot 2\ H_2O$ (5)

NaOH pellets (11g, 0,28 mol, 1 eq.) were washed with an aqueous mix of EtOH and Et_2O and quickly transferred to a round bottom flask. Under inert gas, NaOH was dissolved in 170 mL of absolute EtOH. The solution was then saturated with H_2S by gently running the gas through the solution with a glass tube at moderate stirring speed. After 15 minutes the solution turned turbid and the H_2S gas inlet was removed from the reactor. Afterwards, CS_2 (8.3 mL, 0.14 mol, 0.5 eq.) was added by a syringe while keeping the inner reactor volume above the solution free of oxygen by gently running argon through the glass setup. After a few drops of CS_2 being added, the solution turned bright orange, darkening with the rising amount of CS_2. The solution was heated up to 60 °C and 45 mL Et_2O was added observing reflux of CS_2. The solution was left to cool down. During the cooling process yellow

crystals of $Na_2CS_3 \cdot 2\ H_2O$ precipitated and filtered off from the mother liquor, washed with Et_2O and dried in a current of argon.

B.1 Na_2CS_3 (6)

type	B.1 (cf. p. 198)		internal ID CJ_A_5
reactants	Na_2S **44** (0.07 g, 0.9 mol, 1 eq.)	CS_2 (1.1 mL, 0.018 mol, 20 eq.)	~0.3 mL EtOH
furnace programme	heating	dwelling	cooling
	100 °C, rate 3 K/h	40 hours	RT, rate 0.75 K/h
product	red **crystalline** Na_2CS_3 **6**		

A.1 $Na(S_2COEt) \cdot 2\ H_2O$ (7)

Na (2 g, 87 mmol, 1 eq.) was dissolved in 125 mL EtOH. In an attempt to saturate the solution with H_2S, a KIPP's apparatus was used.[xii] FeS was therefore added to a three neck round bottom flask, carrying a dropping funnel filled with concentrated hydrochloric. H_2S was released from FeS by reaction with aqueous HCl. The flask had a greased stopcock attached, that directed the evolved gas through a deposit of $CaCl_2$ in order to catch water vapour from the exothermic reaction. The gas was supported by a gentle argon gas flow and thus introduced into the solution of Na^+ and EtO^-. After the reaction in the KIPP flask declined, CS_2 (4 mL, 66 mmol, 0.76 eq.) was added to the Na^+ solution turning yellow and stirred for an hour. The solution was heated to 60 °C by use of an oil bath and subsequently left to cool down. Passing 37 °C, a light-yellow crystalline powder precipitated. It was filtered and left to dry in ambient atmosphere. A crystallite was used for single X-ray diffraction and was thus identified to be $Na(S_2COEt) \cdot 2\ H_2O$. However, the data was not used herein as it was of too poor residuals. Apparently, the H_2S evolution from the KIPP's apparatus was insufficient to transform EtO^- to HS^- before CS_2 was added. By that, EtO^- (a very strong base) reacted with CS_2 to form ethylxanthate $(S_2COEt)^-$. Equation 4.7 shows the reaction. Note, that the introduction of H_2O molecules into the structure is not included as it should originate from the drying under ambient atmosphere.

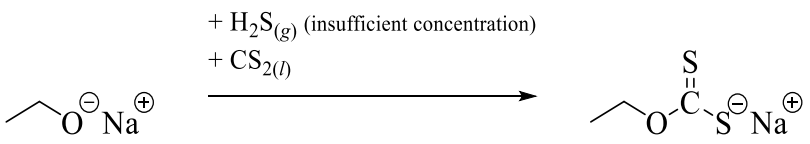

4.7

[xii] A gas cylinder containing H_2S was not at hand in the beginning of the work, thus evolution of H_2S was attempted by set up of a KIPP's apparatus.

4.2.4 Potassium trithiocarbonates and related compounds

A.1 K_2CS_3 (8)

K (1 g, 0.025 mol, 1 eq.) was dissolved in 100 mL of absolute EtOH applying the same precautions as mentioned above. Moreover, the solution was kept cool using a bath of dry ice and isopropanol, preventing the exothermic reaction to ignite the EtOH. For about 15 minutes H_2S was passed into the solution after K had completely dissolved. As a slight turbidity indicated saturation, CS_2 (0.91 mL, 0.015 mol, 0.6 eq.) was added to the solution of K^+ and HS^-. Immediately, orange solid precipitated and the liquid phase took a deep orange colour. The dispersion was heated to 60 °C and subsequently was allowed to cool down to RT as not all the precipitate was dissolved again. The solid product was left to wash twice with Et_2O after the mother liquor had been pressed off through a filter-equipped syringe. The powder was dried in a current of argon. The obtained **powder** could not be confirmed free of impurities and was not used any further. Moreover, the method was impractically after finding superior results using KOH instead of K.

A.2 K_2CS_3 (9) from $K_2CS_3 \cdot H_2O$ (10)

In a 500 mL three-neck-round bottom flask, KOH (50 g, 0.89 mol, 1 eq.) was dissolved in 200 mL EtOH. H_2S was passed through the solution for 15 minutes upon cooling the solution with a water bath. Immediate turbidity was observed, as H_2S was slowly introduced. A solution of CS_2 (100 mL, 1.7 mol, 1.9 eq.) in 200 mL EtOH was added over 20 minutes using a dropping funnel, yielding an orange red solution. Shortly after that, an orange precipitate was formed, which after adding the CS_2 solution was stirred for another 20 minutes upon water bath cooling. The mother liquor was disposed from the powder by use of a syringe, which had a filter paper attached to it. The solid product was washed by stirring the solid with 100 mL EtOH for ten minutes and after disposal of the washing solution it was rinsed twice with 75 mL Et_2O. Residual solvent was evacuated during the drying process in dynamic vacuum under gentle warming with the water bath. Upon that, the **powder** slowly turned pink.

It was found through drying the anhydrous compound was obtained. A **mixed powder** of K_2CS_3 and $K_2CS_3 \cdot H_2O$ **11** was obtained at an earlier experiment, where drying was not performed long enough, which was confirmed by SC-XRD of a crystallite form one of these first prepared batches.

K_2CS_3 was transferred to a screw-topped plastic bottle. This **powder** was used as a starting material carrying CS_3^{2-}.

B.1 K_2CS_3 12

type	B.1 (cf. p. 198)		internal ID CJIZ_10
reactants	K_2S **47** (0.05 g, 0.45 mol, 1 eq.)	CS_2 (0.27 mL, 4.5 mmol, 10 eq.)	~0.5 mL EtOH
furnace programme	heating	dwelling	cooling
	100 °C, rate 15 K/h	48 hours	RT, rate 0.9 K/h
product	pink **crystals** of K_2CS_3 **12** enclosed in yellow microcrystalline powder		

B.2 K_2CS_3 13

K_2CS_3 **9** was used as a precursor reagent, which is explained in detail at the respective passage. It shall nevertheless be noted here that the excess K_2CS_3 in these reactions recrystallises in EtOH under solvothermal conditions, affording large pink intergrown **crystals**, that could be separated under the microscope and were suitable for SC-XRD data collection. The crystal structure was determined and found identical with K_2CS_3 **12**.

$K_7(CS_3)_3Cl \cdot H_2O$ (14)

Orange rhombohedral **crystals** were obtained alongside with side product of the solvothermal reaction of K_2CS_3 9 with $CoCl_2$ (cf. section 4.2.11).

B.1 $K_5[CS_2(Se_2)]_{1.5}CS_3 \cdot ½\ H_2O$ (15)

Method B was used for experiments with potassium selenide attempting the following reaction.

$$K_2Se_{(s)} + CS_{2(l)} \xrightarrow[\text{solvothermal treatment}]{\text{+ 5 drops of EtOH}} K_2CS_2Se_{(s)}$$

type	B.1 (cf. p. 198)	internal ID	CJ_A_61
reactants	K_2Se **50*** (47 mg, 3 mmol, 1 eq.)	CS_2 (0.5 mL, 8 mmol, 2.67 eq.)	five drops EtOH
furnace programme	heating	dwelling	cooling
	100 °C, rate 7.5 K/h	48 hours	RT , rate 0.8 K/h
product	dark red crystals of $K_4(CS_3)(CS_2Se_2) \cdot H_2O$ **15** enclosed in undefined crust		
note	*Two batches of K_2Se were prepared for this experiment. Although the second batch showed improved purity in the PXRD, both were used as starting material and afforded red crystals as described. It was nevertheless infeasible to measure a sample of the obtained specimen from all of these experiments with SC-XRD.		

4.2.5 Rubidium trithiocarbonates

A.1 Rb_2CS_3 (16)

Rb (0.91 g, 0.01 mol, 1 eq.) was weighed into a large SCHLENK glass tube (diameter 40 mm) inside an argon glovebox. The metal did not suffer any oxidation before it was allowed to dissolve in 25 mL absolute EtOH at approx. −40 °C, applying an acetone/liquid N_2 cooling bath, the SCHLENK tube was immersed in. With a gas inlet tube, H_2S was passed into the solution after Rb completely dissolved and the cooling bath was removed. The solution was warmed up to 60 °C. The feeding with H_2S was stopped and CS_2 (0.9 mL, 0.015 mol, 1.5 eq.) was added into the hot solution in order to form Rb_2CS_3. The solution turned red and quickly after addition of CS_2, a salmon-red **powder** was obtained. After cooling to RT, the mother solvent was transferred into a different flask. The salmon-red product at the bottom of the SCHLENK tube was washed with three portions of Et_2O. After disposal of the washing solvent, the product was dried for a short time in dynamic vacuum using a water bath at 70°C.

B.1 Treatment of Rb_2S with CS_2 (17)

type	B.1 (cf. p. 198)		internal ID CJ_A_64
reactants	Rb_2S **48** (17 mg, 0.8 mmol, 1 eq.)	CS_2 (0.5 mL, 8 mmol, 10 eq.)	ten drops EtOH
furnace programme	heating	dwelling	cooling
	100 °C, rate 7.5 K/h	48 hours	RT, rate 0.71 K/h
product	pink **crystals 17*** shrouded in yellow mass		
note	*The single crystal data could not be solved properly. But CS_3^{2-} anions were determined to be part of the structure. µ-RAMAN spectroscopy was conducted to the single crystals.		

B.2 Recrystallisation of Rb_2CS_3 (18)

type	B.2 (cf. p. 198)		internal ID CJ_A_39
reactants	Rb_2CS_3 **16** (50 mg, 0.18 mmol)		0.6 mL EtOH
furnace programme	heating	dwelling	cooling
	100 °C, rate 7.5 K/h	40 hours	85 °C, rate 0.23 K/h RT, rate 0.6 K/h
product	pink **crystals 18***		
note	*the intergrown crystals could not be identified with SC-XRD		

4.2.6 Caesium thiocarbonates

A.1 Cs_2CS_3 powder (19)

In an argon glovebox, Cs (0.1 g, 0.75 mmol, 1 eq.) was weighed in into a small glass cup (5 mm diameter), that could subsequently be transferred to a 50 mL round bottom flask, where the reaction was to be executed in. The glass flask was cooled with a dry ice/isopropanol bath, while 50 mL of absolute EtOH was added, the magnetic stirrer bar set to moderate speed. In this way, Cs dissolved in EtOH and using a glass tube, H_2S gas was introduced for 15 minutes, thus, forming a solution of Cs^+ and HS^-. After that, CS_2 (1 mL, 0.017 mol, 22.7 eq.) was added to the solution, turning orange and immediately yielding an orange precipitate. The **powder** was filtered off, washed with dry Et_2O, and left to dry under dynamic argon atmosphere.

A.2 $Cs_2CS_3 \cdot H_2O$ (20)

Precipitation

In 20 mL of absolute EtOH, $CsOH \cdot H_2O$ (6 g, 0.036 mol, 1 eq.) was dissolved. Under introduction of H_2S gas through a glass tube, undissolved amounts of CsOH dissolved. The solution was clear and had a faint yellow colour. Upon warming the solution using a water bath, a mix of 10 mL absolute EtOH and CS_2 (10 mL, 0.166 mol, 4.6 eq.) was added with a dropping funnel so that after 5 minutes the CS_2 mix was completely added. With the first drop, a pink solid was obtained. For 30 minutes, the water bath kept the reaction mixture at 40 °C and the magnetic stirrer bar rotated at gentle speed. Thereafter, the pink **powder** was separated by pressing off the mother liquor through a long syringe equipped with a filter. The product was washed twice with small portions of Et_2O. Then the water bath was set to

55 °C and a brisk argon current enabled drying of the product. After a while, small residual amounts of solvent were dried by dynamic reduction of pressure on the round bottom flask, which was held at 40 °C. Water of crystallisation was however not completely removed.

Recrystallisation

Additionally, to recrystallisation under solvothermal conditions (cf. below), the obtained $Cs_2CS_3 \cdot H_2O$ powder **20** was treated in an EtOH-water mix for solvent. The poor solubility of the obtained powder was mediated with adding water dropwise to the mixture stirred with a magnetic bar. Approximately 3 ml of degassed water were added to yield a slight yellow orange colouration of the ethanolic dispersion carrying 400 mg of **20** in 10 mL of absolute EtOH. For two days, the mixture was left to its own devices. After that, irregular pink **crystallites** were discovered on the flask wall that could be investigated with SC-XRD. They were identified with $Cs_2CS_3 \cdot H_2O$ **21** by indexing.

The same compound was crystallised in the shape of needles. **20** was transferred to a reaction vial with PTFE screw top lid. The inside was flushed with argon before closing the lid and the tip of the vial buried in a sand bath. Then, the solution was heated up to 100 °C for 60 minutes, followed by a cool down, manually set by steps of 10 K every hour and switching off the heater at 50 °C, keeping the tip in the sand bath. Pink needle shaped crystals of several mm length were obtained and identified with $Cs_2CS_3 \cdot H_2O$ **22** by crystal indexing.

B.2 Recrystallisation of $Cs_2CS_3 \cdot H_2O$ (23)

type	B.2 (cf. p. 198)		internal ID CJ_A_66
reactants	$Cs_2CS_3 \cdot H_2O$ **20** (100 mg)		0.55 mL EtOH
furnace programme	heating	dwelling	cooling
	100 °C, rate 7.5 K/h	48 hours	RT, rate 0.7 K/h
product	pink intergrown crystals of $Cs_2CS_3 \cdot H_2O$ **23***		
note	*The intergrown crystals were identified after indexing and comparison with the ICSD. Nevertheless, a new set of crystal data was collected.		

B.2 $Cs_2CS_3 \cdot \frac{1}{6} H_3COH$ (24) and $Cs_5(CS_3)[CS_2(S_2)]_{1.5}$ (25)

$Cs_2CS_3 \cdot H_2O$ powder **20** was treated at 200 °C for 4 h under reduced pressure in a second attempt, to withdraw water of crystallisation. The reconditioned powder was slightly changed in colour shown in figure 4.2 and was subjected to a recrystallisation experiment in a sealed ampoule with methanol used as the solvent.

Figure 4.2: Photograph of pink $Cs_2CS_3 \cdot H_2O$ **20** as precipitated (left) and after thermal treatment at 200 °C under dynamic vacuum **20t** (right).

type	B.2 (cf. p. 198)		internal ID CJ_A_72
reactants	Cs_2CS_3 **20t** (**20** treated at 200 °C, 100 mg)		0.5 mL MeOH
furnace programme	heating	dwelling	cooling
	100 °C, rate 7.5 K/h	48 hours	RT, rate 0.75 K/h
product	orange red **crystals** of $Cs_2CS_3 \cdot$ ⅙ MeOH **24*** and yellow **crystals** of $Cs_5(CS_3)[CS_2(S_2)]$ **25**		
note	*main product		

4.2.7 Barium trithiocarbonate

A.2 $BaCS_3$ (26)

$Ba(OH)_2 \cdot H_2O$ (5.37g, 0.03 mol, 1 eq.) was dissolved in 50 mL degassed demineralised H_2O at 70°C. H_2S was passed through the solution, after $Ba(OH)_2$ had completely dissolved. After ~15 minutes the solution was slightly turbid and had a pale greenish yellow colour. The round bottom flask carrying the solution was kept inside the warm heating bath when CS_2 (10 mL, 0.17 mol, 5.7 eq.) was added within a couple of minutes. The solution turned yellow and then orange upon CS_2 addition. The flask was equipped with a reflux condenser and after CS_2 was completely added, reflux was observed at approximately 50 °C. The solution was kept at elevated temperature for 20 minutes. Then, allowing the solution to cool down slowly, the formation of a bright yellow solid was observed. To favour further precipitation, 25 mL EtOH was added to the mixture. The bright yellow **powder** was washed with EtOH after the mother liquor was disposed and eventually dried under reduced pressure in a desiccator over P_4O_{10}.

B.2 Recrystallisation of $BaCS_3$ (27)

type	B.2 (cf. p. 198)		internal ID CJ_A_42
reactants	$BaCS_3$ **26** (50 mg)		0.8 mL EtOH + ten drops of water
1st furnace programme	heating	dwelling	cooling
	100 °C, rate 7.5 K/h	101 hours	RT, rate 1.5 K/h
product	no crystals were obtained		
2nd furnace programme	115 °C, 8.5 K/h	10 hours	RT, 2.3 K/h
products	intergrown bright yellow **crystals** of BaCS3 **27**		

4.2.8 Sodium and potassium perthiocarbonate

Treatment of alkali polysulfides with CS_2 in evacuated ampoules was performed like explained in the general remarks (cf. page 198). As simplified with equation 4.8, sodium and potassium perthiocarbonate could be obtained on this route.

$$M_2S_{x(s)} \xrightarrow[\text{solvothermal treatment}]{+\ CS_{2(l)},\ +\sim 10\text{ drops EtOH}} M_2[CS_2(S_2)]_{(s)} \qquad 4.8$$

M = Na, K

B.1 $Na_2[CS_2(S_2)]$ (28)

type	B.1 (cf. p. 198)		internal ID CJRZ_Na2S4_2
reactants	'Na_2S_4' **45*** (50 mg)	CS_2 (0.9 mL, 15 mmol)	0.15 mL EtOH
furnace programme	heating	dwelling	cooling
	100 °C, rate 7.5 K/h	48 hours	RT, rate 0.75 K/h
product	yellow **crystals** of $Na_2[CS_2(S_2)]$ **28**		
note	*Not phase pure.		

B.1 $K_2[CS_2(S_2)]$ (29)

type	B.1 (cf. p. 198)		internal ID CJ_A_18
reactants	K_2S_x * (100 mg)	CS_2 (1 mL, 16,7 mmol)	~ ten drops of EtOH
furnace programme	heating	dwelling	cooling
	100 °C, rate 3 K/h	40 hours	RT, rate 0.75 K/h
product	orange **crystals** of $K_2[CS_2(S_2)]$ **29**		
note	*Commercially available, contains > 42 % K_2S among polysulfide and impurities of sulfate.		

4.2.9 Treatment of NH_3 with CS_2

$(H_7N_2)_2CS_3$ (30)

At RT CS_2 was covered with concentrated aqueous NH_3 in a 1:1 ratio of volume. The liquid phases were immiscible. Soon, the aqueous phase turned yellow and darkens to saturated orange, indicating reaction and the formation of CS_3^{2-} anions. With inert gas, the volume above the heterogeneous mix was purged to drive off oxygen and carbon dioxide and a screw top lid was used to seal the vessel. It was then placed in the freezer at −20 °C which allowed yellow block-shaped **crystals** to grow at the interface of the liquids. Their handling at that early stage of growth was difficult, as they deliquesce immediately on touching with tools. A crystal for investigation with SC-XRD was picked in a cold N_2 gas stream below freezing point.

$(H_4N)_5(CS_3)_2[S_2C(NH_2)]$ (31) and $(H_4N)[S_2C(NH_2)]$ (32)

A solution of 45 mL of NH_3 in EtOH was saturated with H_2S for 30 minutes in a round bottom flask, which was submerged in an ice bath. Abundantly, colourless crystals of $(H_4N)_2S$ (and/or $(H_4N)HS$) precipitated. The liquid phase was disposed through a syringe as it carried residual NH_3 and the colourless crystalline intermediate was washed with 10 mL of Et_2O. After removal of Et_2O, CS_2 (50 mL, 0.83 mol) was added with a glass funnel under counterflow of inert gas. A yellow solution was obtained that went turbid and darkened to orange within 30 minutes and an orange powder formed. The crude product was washed with cold Et_2O after it was filtered off from the mother liquor. Residual solvent was removed by very slow evaporation and trapping volatiles in a liquid N_2 cold bath, connected to the reaction vessel. The obtained **micro crystalline powder** was stored in a snap-cap vial in an argon glovebox. Under the microscope one could observe that at least two different

crystalline phases were obtained. On the one hand there was orange $(H_4N)_5(CS_3)_2[S_2C(NH_2)]$ **31** identified by SC-XRD, which **crystallised** with carrot like shape and the pale-yellow micro crystalline **powder** was later identified with $(H_4N)[S_2C(NH_2)]$.

In another reaction, using the same starting materials, the solution carrying NH_3 was not removed intermediately before addition of CS_2. Large yellow rhomboid **crystals** of $(H_4N)[S_2C(NH_2)]$ **32**. were obtained instead.

4.2.10 Perthiodicarbonates

B.1 $Cs_2(C_2S_6) \cdot CS_2$ (33)

From the treatment of a previously prepared powder of Cs_2S_3 (low Cs_2S_2 impurities) with CS_2 under solvothermal conditions, **crystals** of $Cs_2(C_2S_6) \cdot CS_2$ were obtained as simplified by equation 4.9.

$$Cs_2S_{3(s)} \xrightarrow[+\ \sim 10\ \text{drops EtOH}]{+\ CS_{2(l)}\ \text{solvothermal treatment}} Cs_2(C_2S_6) \cdot CS_{2(s)} \qquad 4.9$$

type	B.1 (cf. p. 198)		internal ID CJ_A_25
reactants	Cs_2S_3 (40 mg, 0.11 - 0.12 mmol, 1 eq.)	CS_2 (0.5 mL, 8.6 mmol, ~70 eq.)	12 drops of EtOH
1st furnace programme	heating	dwelling	cooling
	100 °C, rate 2.5 K/h	60 hours	RT, rate 0.25 K/h
product	No useful crystals observed		
2nd furnace programme	110 °C, rate 15 K/h	52 hours	RT, rate 0.7 K/h
product	brownish yellow crystals of $Cs_2(C_2S_6) \cdot CS_2$ **33**		

$[(C_6H_5)_4P]_2(C_2S_6)$ (34)

In the attempt to crystallise the unknown $[Al(CS_3)_3]^{3-}$ anion, $Al(CH_3COO)(OH)_2$ (204 mg, 1.7 mmol, 0.40 eq) was introduced to a solution of K_2CS_3 9 (800 mg, 4.3 mmol, 1 eq.) in 25 mL DMSO. An aqueous solution of $[(C_6H_5)_4P]Cl$ (800 mg, 2.1 mmol, 0.49 eq.) was added, upon which a yellow precipitate was formed. It was filtered and washed with EtOH

and water and doing this it is likely that the Al^{3+} salt was washed away unnoticed. The intermediate was re-dissolved in DMSO with water added to avoid solidification, as the mix was left in the fridge at 6 °C for three days. After that, yellow **crystals** had formed, that did not include the desired anion. From SC-XRD it was obtained, that tetraphenyl phosphonium perthiodicarbonate $(Ph_4P)_2(C_2S_6)$ **34** had formed.

4.2.11 Transition metal thiocarbonato complexes

$K_2[Ni(CS_3)_2]$ (35)

reactants	$Ni(CH_3COO)_2 \cdot 4\ H_2O$ (30 mg, 0.1 mmol, 1 eq.)	K_2CS_3 **9** (100 mg, 0.5 mmol, 5 eq.)	0.8 mL EtOH
furnace programme	heating	dwelling	cooling
	100 °C, rate 8 K/h	40 hours	89 °C, rate 0.2 K/h
		10 h	RT, rate 0.6 K/h
product	red **crystals** of $K_2[Ni(CS_3)_2]$ **35**		
note	A variety of crystals were obtained on the ampoule wall. Amongst other unidentified species was recrystallised K_2CS_3. A dark monolith was found to be of dark red colour separated in smaller crystallites, which were subjected to SC-XRD.		

$K_2[Pd(CS_3)_2] \cdot H_5C_2OH$ (36)

reactants	$Pd(CH_3COO)_2$ (15 mg, 67 µmol, 1eq.)	K_2CS_3 **9** (100 mg, 0.5 mmol, 7 eq.)	0.8 mL EtOH
furnace programme	heating	dwelling	cooling
	100 °C, rate 5 K/h	48 hours	RT, rate 0.7 K/h
product	yellow **crystals** of $K_2[Pd(CS_3)_2] \cdot EtOH$ **36**		
note	K_2CS_3 recrystallised amongst other unidentified solid side products.		

$K_2[Pt(CS_3)_2]$ (37)

reactants	$Pt(CH_3COO)_2$* (25 mg, 80 µmol, 1 eq.)	K_2CS_3 **9** (50 mg, 0.27 mmol, 3.4 eq.)	1 mL EtOH
furnace programme	heating	dwelling	cooling
	100 °C, rate 8 K/h	60 hours	RT, rate 0.5 K/h
product	orange red **crystals** of $K_2[Pt(CS_3)_2]$ **37**		
note	*formula for simplicity		

$K_5[Co(CS_3)_3]CS_3$ (38)

reactants	$CoCl_2$ (22 mg, 0.17 µmol, 1 eq.)	K_2CS_3 **9** (150 mg, 0.8 mmol, 4.8 eq.)	0.8 mL EtOH
furnace programme	heating	dwelling	cooling
	100 °C, rate 8 K/h	27 hours	RT, rate 0.7 K/h
		10 h	RT, rate 0.6 K/h
product	green **crystals** of $K_5[Co(CS_3)_3]CS_3$ **38** and orange crystals of $K_7(CS_3)_3Cl$ **14**		

$[(C_6H_5)_4P]_2[Pd(CS_3)_2]$ (39)

In a glass beaker, $PdCl_2$ (88.7 mg, 0.5 mmol, 1eq.) was dissolved in 12.5 mL DMSO. K_2CS_3 9 (400mg, 2.1 mmol, 4.2 eq.) was added to the solution, which became brownish red. In a second beaker an aqueous solution of $[(C_6H_5)_4P]Cl$ (403 mg, 1.07 mmol, 2.1 eq.) was prepared and added to the DMSO solution, while stirring. Immediately, a brownish orange precipitate formed, and the solution was cooled with a water bath at freeze point. The solid compound was separated from the solution through a glass frit and washed with degassed water, *i*-propanol and diethyl ether. Then the product was re-dissolved in 12.5 mL DMSO and 5 mL of degassed H_2O was added. The solution was quickly stirred and placed in the fridge at 6 °C. In the following weeks, no crystalline material was formed. The solution was left in the fridge to its own devices, until after one year, when the measurement of the yellow-orange **crystals** that meanwhile had formed was carried out.

$(H_4N)_2{}^1_\infty[Cu\{CS_2(S_2)\}]CS_2(S_2)$ (40)

Aqueous concentrated NH_3 (25 %, 3 mL) was used to dissolve colourless CuCl (0.3 g, 3 mmol, 1 eq.). To the blue solution carbon disulfide (4 mL, 66 mmol, 22 eq.) was added. The appearance of the solution changed rapidly both in colour and in homogeneity. A metallic brown coating formed on the surface of the solution and on the walls of the snap-cap vial. Furthermore, the solution slowly turned brownish red. The vial was closed left on its own devices. Three days later the solution had turned red, and a dark precipitate had formed, which was later identified with CuS. On the inside of the snap-cap, a yellow coating had formed. The vial was transferred to the fridge and left there for one week at 6 °C. Amber red **crystals** of $(H_4N)_2{}^1_\infty[Cu\{CS_2(S_2)\}]CS_2(S_2)$ **40** were obtained as identified by means of SC-XRD.

Attempted solvothermal reactions

Several transition metal compounds were treated with K_2CS_3 **9** under solvothermal conditions. After the cool down, the ampoules contained various products, and some are depicted on the photographs in figure 4.3 - 4.6. In this explorative work, not all products could be investigated thoroughly, and priority was laid on collecting single crystal data. Thus, ampoules which carried no suitable products were discarded. Occasionally, single crystals were obtained, but when their cell metrics were found already published, a time-consuming collection of data was abandoned.

Solvothermal treatments

reactants	$AuCl_3$ (13 mg, 40 µmol, 1 eq.)	K_2CS_3 **9** (100 mg, 0.5 mmol, 12 eq.)	0.7 mL EtOH
furnace programme	heating	dwelling	cooling
	100 °C, rate 8 K/h	48 hours	RT, rate 0.7 K/h
product	no crystals were obtained, dark brown mass and turbid solution		

reactants	$Au(OH)_3$ (30 mg, 0.12 mmol, 1 eq.)	K_2CS_3 **9** (100 mg, 0.54 mmol, 4 eq.)	0.7 mL EtOH
furnace programme	heating	dwelling	cooling
	100 °C, rate 8 K/h	48 hours	RT, rate 0.7 K/h
product	a lump of brown mass and pink crystals of **9**		

reactants	$Au(CH_3COO)_3$ (20 mg, 0.05 mmol, 1 eq.)	K_2CS_3 **9** (50 mg, 0.27 mmol, 5 eq.)	1 mL EtOH
furnace programme	heating	dwelling	cooling
	100 °C, rate 8 K/h	60 hours	80°C, rate 0.25 K/h
		10 h	RT, rate 1 K/h
product	Yellow crystals (cf. figure 4.3 (left)), which by crystal data collection, were identified to be a mixed potassium trithio- perthiocarbonate salt.		

reactants	$In(CH_3COO)_3$ (73 mg, 0.25 mmol, 1 eq.)	K_2CS_3 **9** (84 mg, 0.45 mmol, 2.1 eq.)	1 mL EtOH
furnace programme	heating	dwelling	cooling
	100 °C, rate 5 K/h	48 hours	RT, rate 0.7 K/h
product	Yellow powder (cf. figure 4.3 (middle)) which was discarded from further investigation.		

reactants	$La(CH_3COO)_3 \cdot 1.5\ H_2O$ (86 mg, 0.25 mmol, 1 eq.)	K_2CS_3 **9** (84 mg, 0.45 mmol, 2.1 eq.)	1 mL EtOH
furnace programme	heating	dwelling	cooling
	100 °C, rate 5 K/h	48 hours	RT, rate 0.7 K/h
product	Yellow and pink crystals (cf. figure 4.3 (right)) which were investigated with SC-XRD. No data could be soulved with a crystal structure properly.		

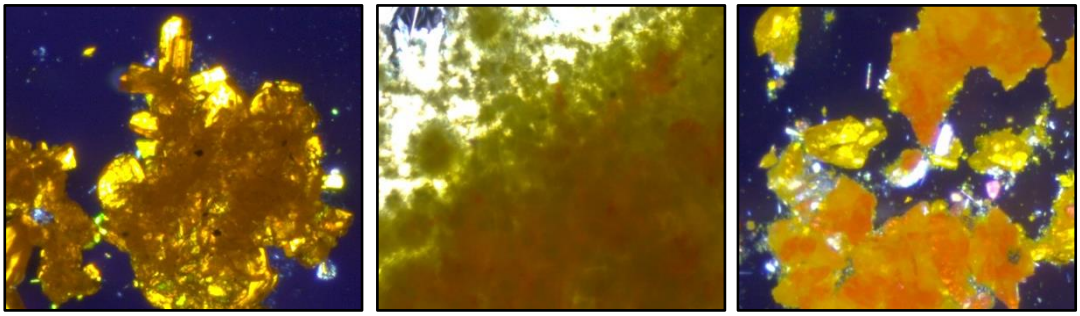

Figure 4.3: Products of attempts to react K_2CS_3 in EtOH with gold(III) acetate, indium(III) acetate (middle) and lanthanum(III) acetate hydrate (right). The yellow crystals on the left were identified free of any gold ions.

reactants	$Ag(CH_3COO)$ (30 mg, 0.02 mmol, 1 eq.)	K_2CS_3 **9** (50 mg, 0.27 mmol, 14 eq.)	1 mL EtOH
furnace programme	heating	dwelling	cooling
	100 °C, rate 8 K/h	60 hours	80°C, rate 0.25 K/h
		10 h	RT, rate 1 K/h
product	Black powder, and fibrous residuals of $Ag(CH_3COO)$ (cf. figure 4.3figure 4.4 (left)), which was discarded from further investigation. Alongside, large pink recrystallised K_2CS_3 was obtained.		

reactants	$Hg(CH_3COO)_2$ (30 mg, 56 µmol, 1 eq.)	K_2CS_3 **9** (50 mg, 0.27 mmol, 5 eq.)	1 mL EtOH
furnace programme	heating	dwelling	cooling
	100 °C, rate 8 K/h	60 hours	80°C, rate 0.25 K/h
		10 h	RT, rate 1 K/h
product	Black needles and orange powder (cf. figure 4.3figure 4.4 (middle)), which was discarded from further investigation.		

reactants	*$H_3[RhCl_6]$*	K_2CS_3 **9**	1 mL EtOH
furnace programme	heating	dwelling	cooling
	100 °C, rate 8 K/h	60 hours	80°C, rate 0.25 K/h
		10 h	RT, rate 1 K/h
product	Yellow crystalline product (cf. figure 4.3figure 4.4 (right)), which did not diffract properly and was discarded in favour of other crystals.		

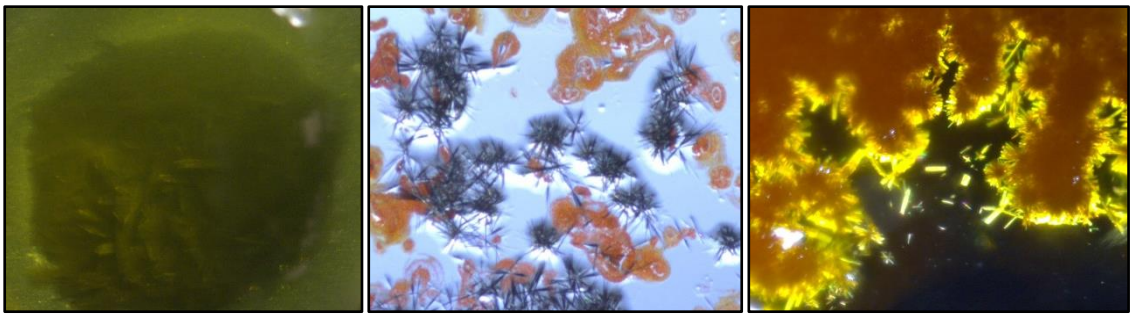

Figure 4.4: Products of attempts to react K_2CS_3 in EtOH with silver(I) acetate (left), mercury(II) acetate (middle) and a hexachloro rhodate(III) complex (right) under solvothermal conditions.

reactants	$Ir(CH_3COO)_3$ (15 mg, 0.04 mmol, 1 eq.)	K_2CS_3 **9** (50 mg, 0.27 mmol, 6 eq.)	1 mL EtOH
furnace programme	heating	dwelling	cooling
	100 °C, rate 8 K/h	60 hours	80°C, rate 0.25 K/h
		10 h	RT, rate 1 K/h
product	Red solution and turbid crystals (cf. figure 4.5 (left)), which were discarded as they did not obliterate light by use of the polarisation of the microscope.		

reactants	$FeCl_2$ (22 mg, 0.17 mmol, 1 eq.)	K_2CS_3 **9** (100 mg, 0.54 mmol, 3 eq.)	0.8 mL EtOH
furnace programme	heating	dwelling	cooling
	100 °C, rate 8 K/h	27 hours	RT, rate 0.7 K/h
before treatment	Adding the reactants immediately formed a dark mass. The formation of FeS may be assumed.		
product	The pink crystals should be recrystallised K_2CS_3 **9**. Alongside, a fibrous brownish yellow product was obtained (cf. figure 4.5 (middle)), which was not investigated.		

reactants	$EuCl_2$ (22 mg, 0.1 mmol, 1 eq.)	K_2CS_3 **9** (100 mg, 0.54 mmol, 3 eq.)	0.8 mL EtOH
furnace programme	heating 100 °C, rate 8 K/h	dwelling 27 hours	cooling RT, rate 0.7 K/h
before treatment	No reaction.		
product	The reaction mixture was converted to a reddish brown powder with some colourless side product (cf. figure 4.5 (right)). No crystals were obtained, and the attempt was discarded. The powder showed no luminescence under illumination with a blue laser pointer.		

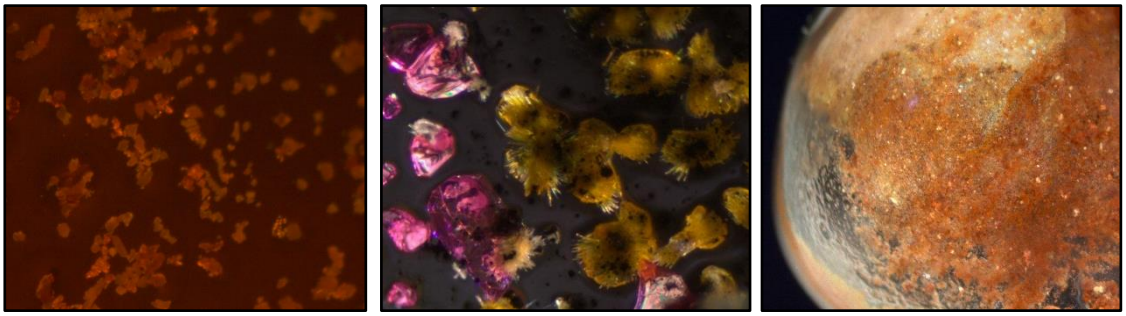

Figure 4.5: Products of attempts to react K_2CS_3 in EtOH with iridium(III) acetate (left), iron(II) chloride (middle) and europium(II) chloride under solvothermal conditions.

reactants	$Cu(SO_4) \cdot 6\ H_2O$ (22 mg, 0.1 mmol, 1 eq.)	$BaCS_3$ **26** (100 mg, 0.54 mmol, 3 eq.)	0.8 mL EtOH
furnace programme	heating 100 °C, rate 8 K/h	dwelling 24 hours 15 h	cooling 90 °C, rate 0.14 K/h RT, rate 1.6 K/h
product	A turbid greyish green dispersion was obtained that contained powder of the same colour (cf. figure 4.6). No crystalline species was discovered, and the attempt was discarded. The colour change may indicate the formation of a copper−sulfur interaction.		

Figure 4.6: Product of attempt to react $BaCS_3$ in EtOH with $Cu(SO_4) \cdot 6\ H_2O$

4.2.12 Other compounds

$K_9[Eu_2(CH_3COO)_9](CS_3)_3$ (41)

In a solvothermal reaction of potassium trithiocarbonate and europium(III) acetate in EtOH, the cocrystals of both educts were obtained as yellow hexagonal blocks. Following the general workflow described for solvothermal syntheses on page 198, the prepared ampoule containing the reactants was heated to 100 °C within 15 h and resided at that temperature for two days. After a crystallisation segment with a cooling rate of 0.8 K/h the **crystals** were obtained aside other yellow and colourless needle shaped crystallites.

reactants	$Eu(CH_3COO)_3$ (83 mg, 0.25 mmol, 1 eq.)	K_2CS_3 **9** (84 mg, 0.56 mmol, 0.4 eq.)	1 mL EtOH
furnace programme	heating	dwelling	cooling
	100 °C, rate 5 K/h	48 hours	RT, rate 0.8 K/h
product	yellow **crystals** of $K_9[Eu_2(CH_3COO)_9](CS_3)_3$		

Tl_2CS_3 (42)

Two solutions of aqueous $TlNO_2$ (~500 mg) and Na_2CS_3 (~250 mg) were prepared using ~10 mL degassed and demineralised water. The colourless solution of Tl^+ was reacted with the bright red CS_3^{2-} solution. Immediately, a brick-red **powder** formed. It was filtered of with a glass funnel and filter paper and left to dry in the ambient atmosphere. Without further purification, a PXRD curve confirmed the formation of Tl_2CS_3.

$Tl_2(S_5)$ (43)

reactants	$Eu(CH_3COO)_3$ (83 mg, 0.25 mmol, 1 eq.)	K_2CS_3 **9** (84 mg, 0.56 mmol, 0.4 eq.)	1 mL EtOH
1^{st} furnace programme	heating	dwelling	cooling
	100 °C, rate 8 K/h	24 hours	90 °C, rate 0.14 K/h
		15 h	RT, rate 1.6 K/h
product	red **crystals** of $Tl_2(S_5)$		

4.2.13 Preparation of starting compounds

Phase pure sulfides and polysulfides cannot be purchased. This holds in particular for the potassium-, rubidium- and caesium salts. In the framework of conversion of alkali sulfides and polysulfides with CS_2 under solvothermal condition, the preparation of these precursors was an objective to pursue.

Dehydration of $Na_2S \cdot 9\ H_2O$ (44)

A portion of approx. 3.6 g $Na_2S \cdot 9\ H_2O$ (greyish damp mass) was placed in a closed wide SCHLENK tube. The tube was evacuated, and the hydrate was heated inside, stepwise increasing the temperature. Water of crystallisation was thus removed from the solid compound kept under dynamic vacuum. A bench top tube furnace was operated. Step 1 was heating to 100 °C and holding for 100 minutes. After initial rise, the pressure decreased again successively. Step 2 was heating to 300 °C. Passing 290 °C, the manometer displayed an increased pressure of the order of 0.5 mbar. Within 45 minutes the pressure decreased to 0.0025 mbar. For another 100 minutes, reaching 514 °C at last, the as purchased $Na_2S \cdot 9\ H_2O$ was dehydrated. The mass had become a colourless and **dry powder**. A PXRD measurement, shown in figure 4.7, confirmed the desired Na_2S phase. The prepared precursor was transferred into a snap-cap vial and stored inside an argon glovebox.

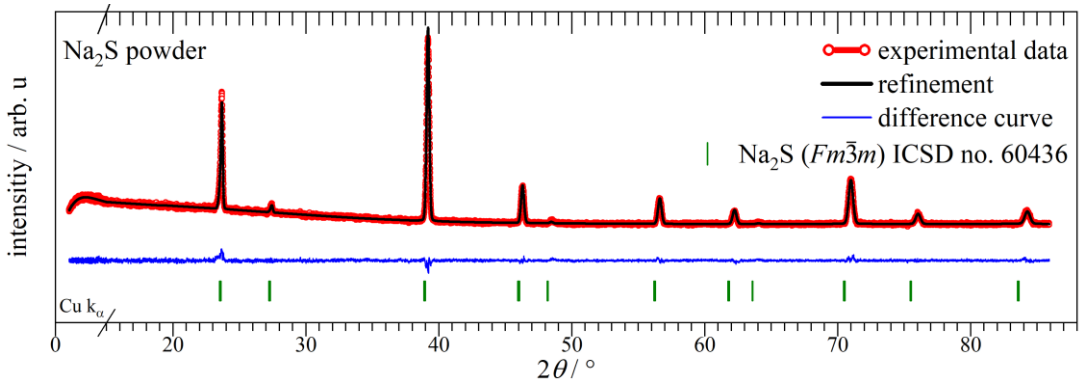

Figure 4.7: Simple RIETVELD refinement of the obtained PXRD data of the dehydrated $Na_2S \cdot 9\ H_2O$. Anhydrous Na_2S was successfully prepared because the phase info for Na_2S perfectly fits the experimental data.

Na_2S_x

For the preparation of *Na_2S_4* **45**, Na (2.15 g, 0.094 mol, 1 eq.) was dissolved in 50 mL EtOH and the solution was saturated with H_2S for 15 minutes. S_8 (0.56 g, 17.5 mmol, 0.19 eq.) was added and the colourless clear solution became dark red. It was cooked for an hour until

the solvent was concentrated under reduced pressure at about 40 °C. A **yellow powder** was obtained. On the next day, the residual solvent was disposed with a long syringe equipped with a filter paper. The yellow powder was then subjected to dry over P_4O_{10} in an evacuated desiccator. In wide accordance, Na_2S_5 **46** and *Na_2S_3* were prepared likewise.

Only Na_2S_5 was obtained in decent phase purity, which was confirmed by refinement of the PXRD data (cf. figure 4.8). Most likely, the introduction time of H_2S to the Na^+EtO^- solution was not lasting long enough for complete conversion to HS^-. Consequently, addition of S_8 to the incompletely converted solution then yielded a mixture of different sodium polysulfides.

The PXRD curve of *Na_2S_3* showed a mixed phase pattern mostly consisting of reflections belonging to crystal phases of Na_2S, Na_2S_4, $Na_2(S_2O_3)$ as well as unidentified impurities. The product was treated with CS_2, but no solid product was obtained.

The PXRD pattern of *Na_2S_4* **45** could only partially be identified with the orthorhombic phase of Na_2S_5. Other possible Na_2S_x phases as well as S_8 and $Na_2S_2O_3$ were not useful for the refinement analysis. After all, the subsequent treatment of *Na_2S_4* **45** with CS_2 under solvothermal conditions yielded $Na_2[CS_2(S_2)]$ **28**. All three PXRD curves are given in the appendix section 5.2.

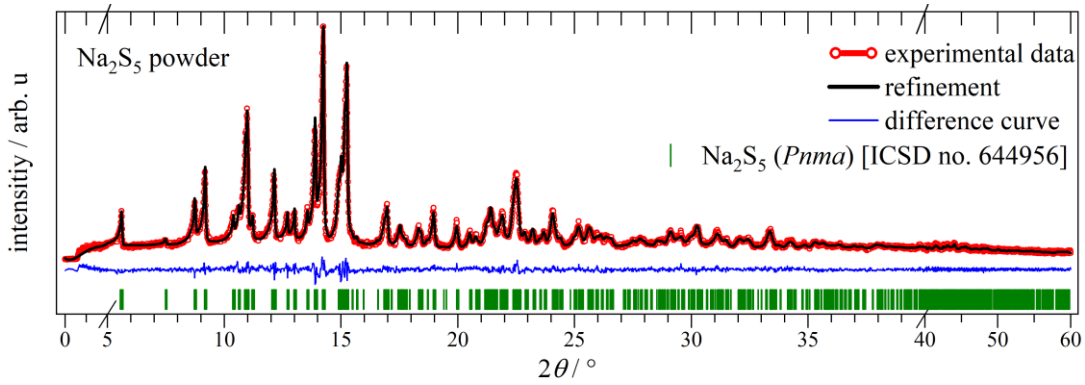

Figure 4.8: Graphical output of RIETVELD refinement of the measured PXRD data of Na_2S_5 **46**. The blue difference line indicates well agreement between the experimental data and the refinement, which was based on orthorhombic Na_2S_5.

K_2S (47), *Rb_2S_x* (48), Cs_2S_3 (49) and K_2Se (50)

The alkali metals were scaled and transferred into a SCHLENK tube in an argon glovebox. Beforehand, potassium was treated as usual (cf. section 4.1). Phases of alkali mono- or disulfide/selenide), i.e. $M_2(S/Se)_{1\text{-}2}$ were targeted to later carry out solvothermal treatment with CS_2.

To ensure complete conversion of the metal, slightly exceeded amounts (~ 1.1 eq.) of S or Se powder and a magnetic stirrer rod sealed in glass were added to the SCHLENK tube. With regard of the phase purity of the products it was found only at a later point in time that it was more useful to work with a little lack of sulfur (selenium).

The preparation was carried out with co-workers of a neighboured work group at the *Institute of Inorganic Chemistry* of the *University of Cologne*.

Stored under argon, the scaled heterogeneous mix in the SCHLENK flask was connected to a vacuum inert gas manifold, that had an ammonia gas cylinder attached. After proper evacuation, the metal and sulfur (selenium) mix was dissolved in dried liquid ammonia, which was condensed in the reaction tube. Indicating the dissolution of the metal, the liquid ammonia became coloured dark blue, which is shown in figure 4.9c. To achieve complete reaction the solution was stirred during the rising level of liquid ammonia.

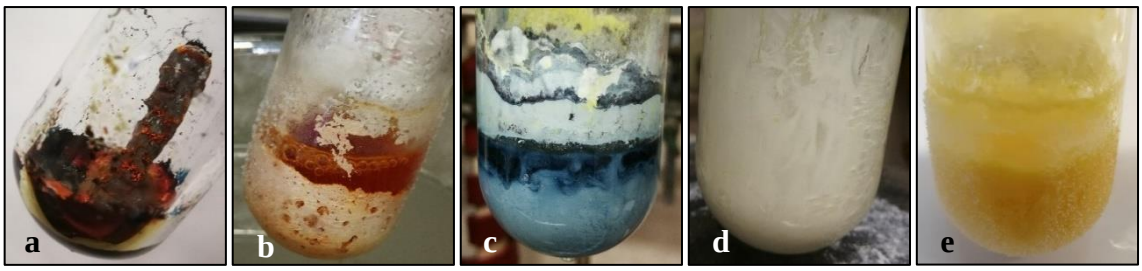

Figure 4.9: Photographs of alkali sulfide/selenide preparation in liquid NH_3. (a) Potassium becoming bright red coloured as NH_3 is condensed into the tube. (b) Colourless K_2Se **50** at bottom of tube. After the reaction, the solution became coloured red from dissolved K_2Se, indicating no solvated electrons are left. (c) Precipitation of colourless 'Rb_2S_x' **48** in liquid NH_3, solvated electrons (e_{solv}^-, dark blue colour). (d) Colourless 'Rb_2S_x' **48** as residual product after evaporation of NH_3. (e) Colourless liquid NH_3 after reaction of Cs with S. The yellow powder was identified with Cs_2S_3 **49**.

As soon as the blue colour had vanished and no metal residuals could be observed inside the glass tube, the cold bath was withdrawn, and the ammonia vented through the bubbler and the fume hood. Inside the glass tube, the obtained powders were heat-gunned dry under dynamic vacuum and as soon as possible stored in the argon glovebox. The PXRD data of the obtained starting materials for solvothermal reactions is given below in figure 4.10 - 4.14. From the treatment of the data with simple RIETVELD methods sometimes phase shifting from e.g., impurities with other phases, could be identified. The refinement residuals or figure-of-merits are found in the appendix section 5.2 for PXRD data.

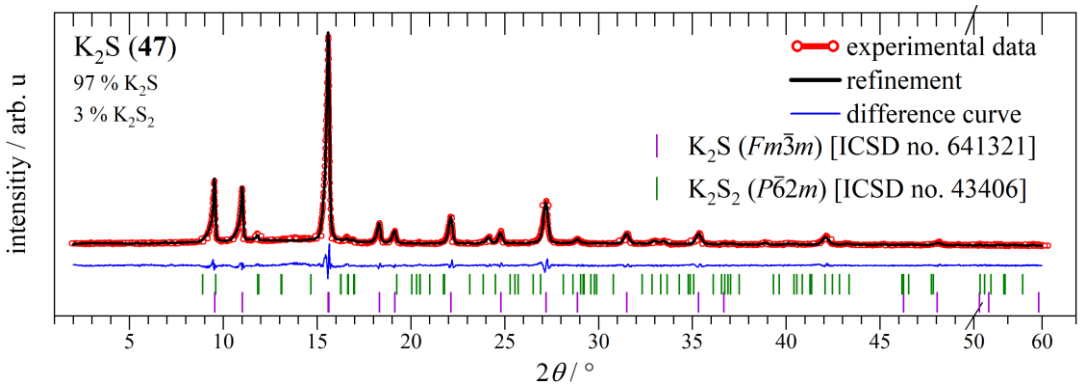

Figure 4.10: Graphical result of RIETVELD refinement of PXRD data of 'K_2S' **47**. Indeed, a slight impurity of K_2S_2 could be determined. Nevertheless, the obtained powder was used for reaction with CS_2 and proved reasonably pure to yield crystals of K_2CS_3 **12** (cf. page 206).

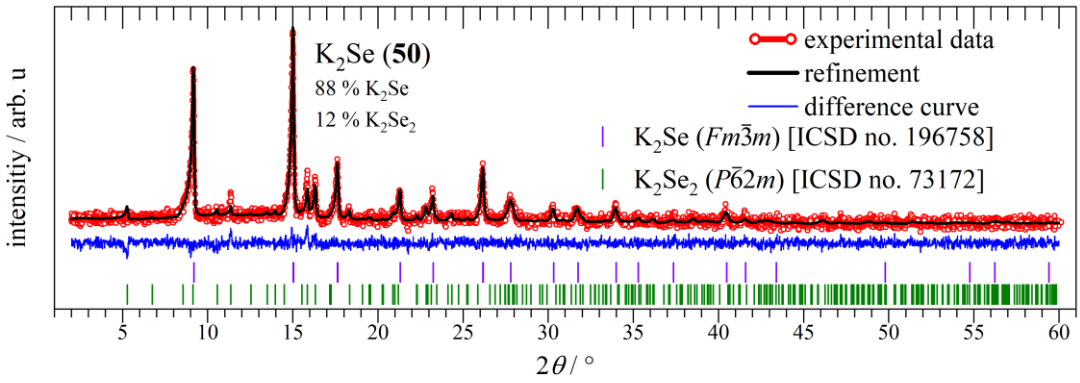

Figure 4.11: Graphical result of RIETVELD refinement of PXRD data of the first batch of 'K_2Se' **50**. Based on single crystal data of K_2Se and K_2Se_2, the experimental diffraction curve could be described well, as seen by the flat difference line (blue). The powder was used in the solvothermal preparation of $K_5(CS_3)[CS_2(Se_2)]_{1.5} \cdot H_2O$ **15**.

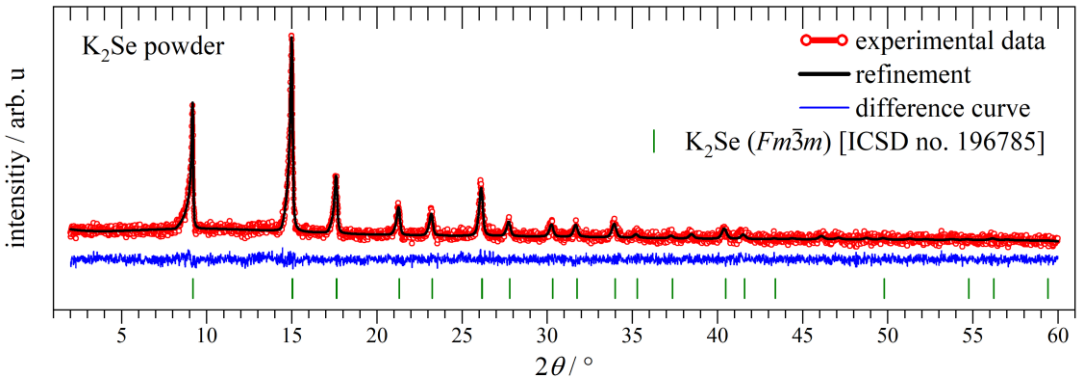

Figure 4.12: A second batch of K_2Se was prepared and from the analysis shown here, the K_2Se_2 impurities from the first batch (see above) could be eliminated. In this procedure, the selenium powder was added with a slight mass deficit. This powder was treated with CS_2 in evacuated ampoules as well affording crystals of the same colour as found with 'K_2Se' **50** from the first batch.

In the case of two prepared batches of Rb_2S_x (cf. figure 4.13) no refinement and phase identification was possible due to the poor crystallinity of the products. However, in the second batch (Rb_2S_x **48**) , the stoichiometric amount of sulfur was added with inert gas counter flow only after rubidium was completely dissolved in NH_3. In the PXRD patterns the weakly resolved intensities differ in their position compared to the curve of the first powder batch. It could thus be concluded that a *different* phase was obtained, probably including the targeted phase of Rb_2S_2.

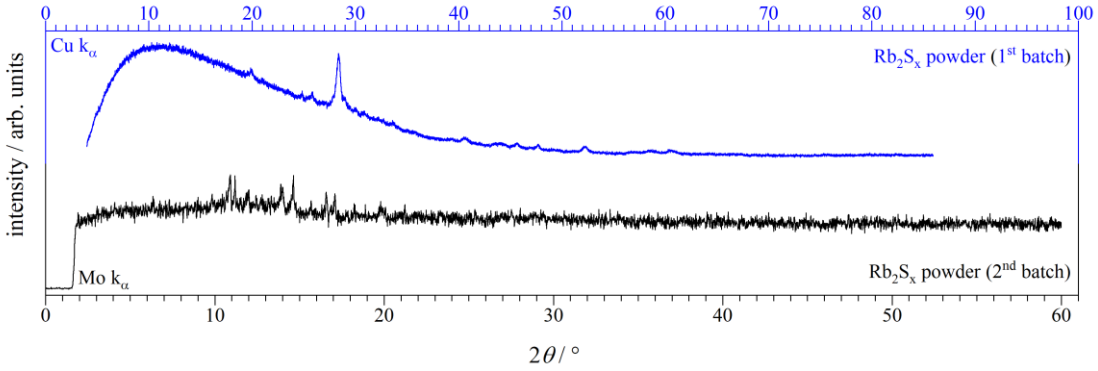

Figure 4.13: PXRD measurements of Rb_2S_x. Both diffractograms were unsuitable for refinement as they almost show no crystallinity. The weak intensities differ between the two batches. Both powders were applied in solvothermal reactions with CS_2, which by use of batch #2 yielded pink crystals of Rb_2CS_3 **17**.

A phase identified with Cs_2S_3 **49** (cf. figure 4.14) was obtained as a first batch attempting to prepare Cs_2S_2.

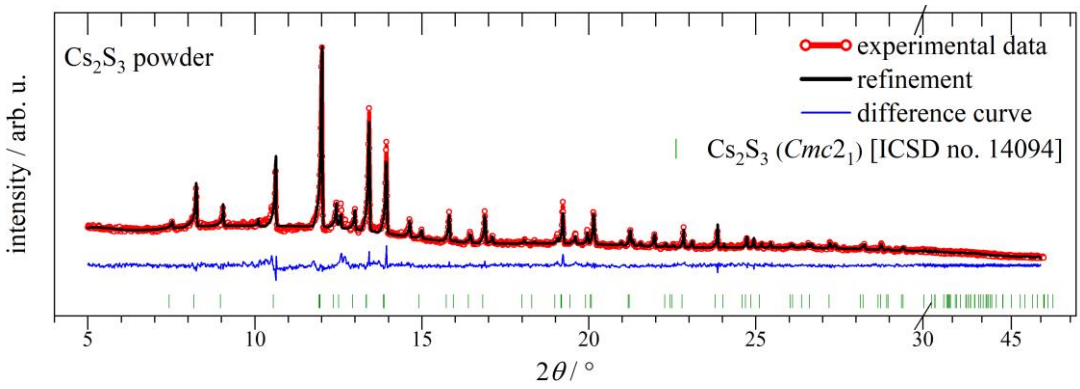

Figure 4.14: Graphical result of a RIETVELD fit of experimental PXRD data of the caesium sulfide starting material for solvothermal treatment with CS_2. The refinement was based on a crystal information file of Cs_2S_3, found in the ICSD. With some minor intensity differences (peaks in the blue line), the black line, showing the calculation, is decently matching the experimental data.

A second batch was prepared showing an altered PXRD reflection pattern. It was however not possible to refine it unambiguously among different possible Cs_2S_x phases found in the ICSD, where x = 1, 2, 3, 5 and 6. Eventually, the experimental data was matched with a mixed phase of 17.0 % Cs_2S, 17.9 % Cs_2S_3, 19.5 % Cs_2S_5 and 45.6 % Cs_2S_6, which is shown in figure 4.15. Not all, intensities (especially above 2θ = 15°) could be calculated properly. After all, the scaling of caesium and sulfur for this preparation was found too spiteful to meet at the exact stoichiometry, a third attempt to prepare Cs_2S was abandoned.

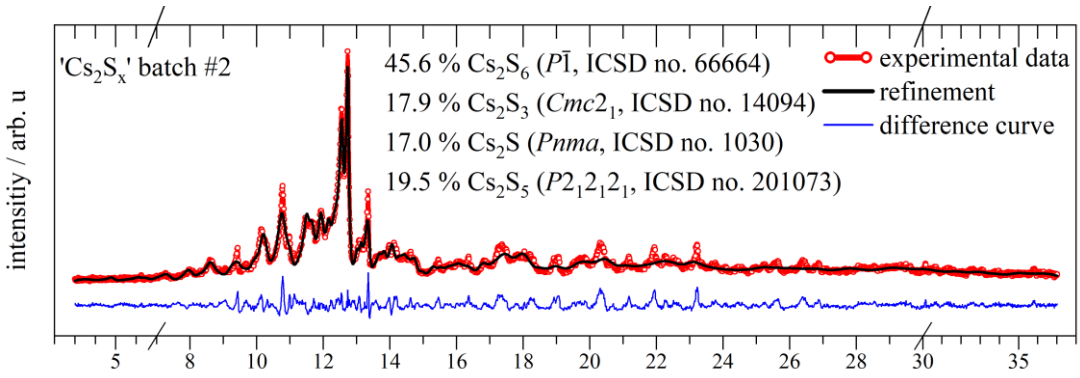

Figure 4.15: Refinement attempt of the powder data of batch #2 of caesium (poly)sulfide. The reflection curve could be roughly calculated using the single crystal phases of caesium mono-, tri-, penta- and hexasulfide.

Saturation of EtOH with NH_3

In a wide SCHLENK tube (diameter 5 cm) 100 mL of EtOH was degassed by alternating evacuation and purging with argon, and a magnetic stirrer bar was added. The column of EtOH was about 5 cm inside the tube. It was connected to a SCHLENK apparatus, that provided ammonia and inert gas in desired composition. The tube was cooled below −40°C inside a DEWAR vessel with a CO_2/*i*-propanol bath and it was provided, that the tube was completely cooled. With a gentle inert gas flow, dry NH_3 was condensed on top of the EtOH column. After about 1 hour, the column was grown to approximately 7 – 8 cm inside the tube and a faint interface was observed between the two colourless liquids, before the stirrer was switched on with moderate speed. The cold bath was lowered in steps of about 1 cm, so that the solution could warm up slowly. Thus, the solution was brought to RT preserving the ammonia to stay in solution rather than evaporate suddenly. The formation of very little gas bubbles indicated that some of the ammonia was evaporated on warming up. Eventually, the cold bath was removed, and the solution was left to warm up to RT, while still connected to the manifold allowing pressure balance. Estimated from the volume increase and the density of ammonia at boiling point, the as prepared ethanolic ammonia solution **51** was roughly estimated to 26 – 36 %. The maximum solubility of ammonia in EtOH at 0°C was reported to be 21 %, which raised confidence that saturation was accomplished.

4.3 Procedures for analytical methods

If not stated otherwise in chapter 2, the protocol of analytical methods has been carried out as written below.

4.3.1 X-ray powder diffraction (PXRD)

The standard method to gain intelligence on the identity and phase purity of solid products was X-ray diffraction of a powder sample.

The powder was either transferred into a 3.3 borosilicate glass capillary of 60 mm length and outer diameters of 0.3 or 0.5 mm, the glass wall thickness was given as 0.01 mm. This way provided the powder to be safe from ambient atmosphere, e.g., moisture, oxygen etc., during the measurement. Furthermore, this method was particularly useful for powder samples that were dry and able to trickle densely into the thin glass tube. The preparation was carried out inside under inert gas. The capillary was melted close after it was filled high enough. Therefore, hot a metal wire loop was used under inert gas.

The samples were attached upright in a piece of regular wax on a brass cylinder, that was then screw fixed on the goniometer[xiii], to perform the measurement in DEBYE-SCHERRER geometry. It was made sure that the sample was coinciding with the axis of rotation of the goniometer.

Another way for PXRD data collection was the measurement in transmission mode. The method proved useful for samples, that was either clumsy, damp, or unavailable in useful scale to fill a glass capillary. Samples were transferred onto adhesive *Scotch Magic Tape* with a spatula. Excess powder could be tapped of. The powder was sealed under a non-scattering foil (Co. *STOE & Cie GmbH*, Darmstadt, DE), which stuck to the free tape area. The prepared tape holding the sample sealed under the foil was trimmed to a suitable size, now fitting in the sample holder ring for the transmission mode goniometer. During the measurement, the horizontal radiation was directed through the tape, powder sample and foil layers. The ring was rotating parallel to the optical axes.

The diffractometer used for PXRD was a *STOE Stadi P* (Co. *STOE & Cie GmbH*, Darmstadt, DE). It was run with a molybdenum X-ray tube that was (usually) supplied with an amperage of 40 mA and a voltage of 50 kV. The $K_{\alpha 1}$ radiation was defined by a Ge

[xiii] Greek: *γωνια (gonía)* – angle, *μετρούν* (*metroún)* – measure

monochromator and collection of the diffracted X-ray was handled by use of a silicon-based position sensitive *Dectris Mythen 1K* (Co. *Dectris Ltd.*, Baden-Daettwil, CH) detector. Calibration was performed with a suitable standard sample of silicon powder.
The PXRD raw data was converted to a *.xyd*-file with the WinXPow software suite. The *.xyd*-file was compatible to *Origin* and *Topas* the majorly used program for data drawing and evaluation.

4.3.2 X-ray structural analysis (SC-XRD)

Data of diffraction of X-ray on single crystalline specimen are used to model a description of the atomic construction of the compound. To do that, it is mandatory to rotate the object of interest, that is believed to be a single crystalline domain[xiv], inside the X-ray radiation. On occasions of constructive interference of diffracted X-ray, the BRAGG condition is met, and an intense spot or reflection is detected. The number of counted reflections, each belonging to a special lattice plane *hkl*, usually range between $5 \cdot 10^2$ and 10^4, to yield a structure model. The *hkl* planes set up the three-dimensional reciprocal lattice of the crystal and by that the spatial intelligence to model a structure of the atomic lattice is obtained. This analytical method requires expert experience, which is represented in a division of crystallography in the *Department of Chemistry* at the *University of Cologne*.

Crystal sorting and selection

The crystals obtained from the experiments were quickly submerged in a drop of inert perfluoropolyether (*Fomblin Y®*) on a glass slide where they could be visually inspected and sorted under the microscope (*Stemi 508*, *CARL ZEISS Microscopy GmbH*, Jena, DE). A microscopy-camera (*AxioCam ERc 5s Rev.2*, *CARL ZEISS Microscopy GmbH*, Jena, DE) mounted on the microscope allowed to take photos of the crystals. Moreover, the microscope was equipped with a polarization filter, that allowed to extinguish the light from below. Single crystals often cancel out the polarisation of the filter and as a result, single crystalline specimen can be discovered easier. When a crystal was chosen, it was picked up from the oil with a non-scattering resin loop (sizes ~ 10^1 to 10^2 µm). The crystal was mounted on the goniometer head of the diffractometer, where it was frozen in a stream of

[xiv] Note, the term *single crystal* is used for convenience, but theoretically does not allow twinning, mosaicity, disorder, absorption etc., that naturally occur in a realistic sample. At an appropriate paragraph, these deviations will be introduced and discussed with reasonable scope.

evaporating liquid nitrogen. With a camera, the specimen could be brought into the beam focus.

Diffractometer device specifications

Until august 2020, all crystals were measured on a *STOE IPDS **2T*** manufactured by *STOE & Cie GmbH*, Darmstadt, DE. After that, a second, newly acquired single crystal diffractometer was available, which was a ***D8** Venture* by *Bruker AXS GmbH*, Karlsruhe, DE. Both devices used MoKα radiation, while the *Bruker* diffractometer was appointed with Kα radiation of a Ag X-ray-tube, too.[xv] The older *2T* diffractometer worked with three-circle geometry, with a rotating detector orientation in horizontal plane (θ-circle), a coaxially oriented ω-circle, that carried the goniometer, and an upright turning axes (φ-circle) at the centre of the goniometer, which met the sample holder pin axes. The *D8* device was equipped with a four-circle setup with *kappa*-geometry. In this, a fourth κ-circle is integrated at the intersection between the ω- and the φ-circle. Thereby, the coaxial orientation, that is fixed in the *2T* three-circle system, could be altered, allowing to meet all angles of the crystal, that are available in EULER geometry.[57] The extended degree of free moving, combined with a fast reflection collecting rate on the *D8*, amplified with a powerful measurement strategy management, arranged to collect data needed for the structure solution in less time than on the *2T*. The inferior three-circle set up was run in a standard programme of two runs, both[xvi] covering the ω-circle of 0 – 180° in steps of 2°. The φ-circle was fixed at 0° and 90° for the first and second run, respectively.

One of the many demands for a descent structure determination is a suitable number of reflections to describe the reciprocal lattice, which leads to the real-space structure. Albeit the identified differences of the goniometer geometries, both the *2T* and *D8* were used.

Before the actual measurement was commenced, assurance of the mounted crystal to show single crystal reflections was approached by running a fast scan, with lower exposure time and/or larger step size between the individual frames, which included all the reflections dependent of the beam angle. Usually, one could examine and evaluate the appropriateness of the crystal by looking at the frames of the fast scan. In principle, first the strength of the discrete point-shaped reflections and second their distribution over the complete image, and particularly towards the edges, were indicators for a well grown crystallite. In this case, based on the fast scan, the crystal reflections were indexed with one of the 14 BRAVAIS lattices, that matched the reflection pattern. In other words, the conditions for describing

[xv] The same device was already available earlier at the Institute of Organic Chemistry at the University of Cologne. There CuKα radiation was optional to use.

[xvi] As mentioned below, the second run was usually abort before the completion.

the majority of reflections with a reduced number of parameters was tested. This already gave the unit cell lattice parameters, which could be compared with the ICSD (inorganic crystal structure database) and/or CCDC (Cambridge crystallographic data centre). In case of a match, the need for the time-consuming experiment was renegotiated.

Detectors for single crystal X-ray diffraction

The *STOE IPDS 2T* used an imaging plate (Ø = 340 mm) working an europium(II)-based phosphor ($BaBrF:Eu^{2+}$) thin film, for the detection of the scattered radiation. The phosphor in the film is excited precisely at the position of an impact of diffracted X-ray photons. After the X-ray exposure, the excited discrete spots on the film remain locally trapped and a focussed red He-Ne-laser that performs a screening of the imaging film area, forces the recombination of the excited phosphor sites. The provoked fluorescence is captured by an optical system, running with a photomultiplier. Proportional to the collected reflection intensity, the crystal information is eventually digitalised into an image (so-called *frame*) mapping the reflections intensities on the film.[147] A halogen lamp erases all excited point intensities and resets the phosphor material for the next frame. The major drawback of this method was the large exposure time that could exceed 10 minutes for each frame. Consequently, the overall time for the measurement of a crystal with low symmetry was exceeding a regular workday. The trade-off was to stop the measurement at an earlier stage on the next day, but with enough frames collected to be able to completely describe the crystal theoretically. However, in practice, this still was sometimes problematic when the specimen poorly diffracted with a low signal-to-noise ratio of the collected reflections. Weak signals usually resulted in poor residuals of the final crystal structure.

A charge integrating pixel array detector (*Photon III C14, Bruker AXS GmbH.*, Karlsruhe, DE) with an active area of 140x100 mm^2 was used on the *Bruker* device that could collect the intensities in a much higher rate. In contrast to the imaging plate system, the digital detector counted every single diffracted X-ray photon, that hits the active area. Latest detectors are built up from an array structured complementary metal oxide semiconductor (CMOS) film, separated into microscopic pixels (area ~10^2 μm^2) handles the spatial detection of diffracted X-rays. Simply speaking, the diffracted X-ray photon separates charges[xvii] (electrons and holes) proportional to the light energy in a limited area on the detector. An electrical field perpendicular to the area of the structured silicon layer conducts

[xvii] The X-ray photon first is absorbed by a so-called *scintillator*, that transforms the energy of the incident energy to a proportional lower level in the ultraviolet or even visible wavelength regime. These photons are now converted to a current in the photodiode.

the charges in opposite directions to their respective electrode, where they are amplified and transformed to a digital signal. The signal is furthermore read out by an equally small-structured circuit array, that is connected to the lower electrode of the semiconducting film structure. As the charge separation does not diffuse liberally over the area of the pixel, a locally accurate detection is granted.[148]
Instead of counting each photon individually as described above, integration of the signals is performed.[149]

SC-XRD data evaluation

Both the diffractometer systems are computer controlled *via* a respective software package, running on *Microsoft Windows*. Measurements on the *STOE IPDS 2T* was managed with *X-Area* (*STOE & Cie GmbH*, Darmstadt, DE) and the *Venture D8* used *APEX 3* (*Bruker AXS GmbH*, Karlsruhe, DE). Details on the data evaluation work-through can be found in section 4.3.6 for *X-Area* and *APEX 3*, respectively.

4.3.3 Molecule spectroscopy

IR and RAMAN spectroscopy

Two similar, yet complementary methods to obtain information on vibrational energy of compounds is infrared (IR) and RAMAN spectroscopy. Simply speaking, vibrations that result in changes of the polarizability of a molecule are visible in a RAMAN spectrum. A change of the dipole moment of a molecule is IR active and invisible in RAMAN spectrum (selection rule). As a general rule, in a molecule that possesses a centre of symmetry, all vibrations that are constant with regard to that symmetry centre are IR inactive and RAMAN active.[84]
The (quantum) mechanics behind both the spectroscopy methods however diverge fundamentally.
In IR spectroscopy, the molecule absorbs energy of the light of the IR region, which typically excites atomic vibrations. From a ground state, the next higher vibrational level is occupied if the incident light is resonant with the energy difference of the two states. The absorbed intensity of light is measured.
In RAMAN spectroscopy the vibration is a result of inelastic scattering of incident photons, i.e., a part of the energy of the photons is transferred to occupy higher vibrational states, too. The mechanism is however different, and it is particularly not a resonance phenomenon.

As the photons hit the sample, high *virtual* vibrational levels are reached but actually cannot be occupied. Most excitations simply recombine with the ground state (RAYLEIGH scattering). Nevertheless, about 10^{-3} excitations result in an occupation of a higher energy level above the ground state, which declares an energy loss due to the interaction of light with matter (RAMAN effect). Because of that energy change, in RAMAN spectroscopy the abscissa of the graphical output often carries the title *RAMAN shift*, indicating inelastic scattering. Usually, the incident light frequency (energy) is decreased, which is called STOKES-shift. (The anti-STOKES shift can be observed, if for instance the excitation does not commence from the ground state but from an already excited state. Then there is a chance to increase in energy of the phonon after the scattering event.) The ratio between inelastic and elastic RAMAN scattering events deviates by three to four orders of magnitude, which makes high intensity monochromatic light sources – a LASER, to be precise – necessary.[84]

Fundamental molecular vibrations are often classified either IR or RAMAN active and the number of normal modes of both physical interactions is equal to $3N - 6$ or $3N - 5$, for non-linear or linear molecules, respectively, where N is the number of atoms in the molecule[xviii].[86] As molecular vibrations imply movement of atoms, a description of the molecule within the view of symmetry, the group theory was invented. Each molecule can be assigned to a point group, that mathematically contains all possible symmetry operations giving an indistinguishable state from the original molecule. There are different classes of symmetry operations defined: identity E, rotation C_n (with n-fold rotation axes, i.e., 360°/n rotation), reflection σ and inversion i. Furthermore, each point group and its respective classes formulate a unique *character table*. The character table contains the different irreducible representations (or *symmetry species*) and its symmetry or none-symmetry towards the classes. In this way, it is possible to raise rules for nomenclature and assignment of molecular vibrations, which thus can be compared and categorised in course of scientific exchange. Not least, from the inspection of the character table, RAMAN or IR activity can be predicted.

To understand vibrational spectra of specimen of solid state two noteworthy effects should be mentioned:[84]

1. The measurement yields a superimposed spectrum cumulating the vibration of the molecule(s) of interest, but possibly with intermolecular interaction modulation.

[xviii] There are examples, where silent modes, neither RAMAN nor IR active, occur.

This usually reduces the symmetry of the molecule compared to their state in isolation and combinations of fundamental vibrations bands can be observed.

2. At lower frequencies around ~300 cm^{-1}, due to lattice vibrations of different moving types (e.g., rocking or rotation), other than the stretching and bending, the interpretation of the spectrum must be careful.

Infrared spectroscopy (ATR-IR)

A standard method to earn intelligence of the vibrational properties of molecular compounds, is the excitation with infrared radiation. Measurements of the first and foremost solid compounds were executed with attenuated total reflection (ATR) infrared (IR) spectroscopy. This method was helpful to either identify a product and/or to collect data on vibration energies of compounds, that were characterised with SC-XRD or PXRD beforehand. In contrast to regular IR spectroscopy in transition mode, where the intensity of the probe light, that transmits a sample, is detected, and compared with the incident intensity (LAMBERT-BEER law), in ATR-IR spectroscopy, evanescence at total reflection affords interaction with the material. More detailed, the incident light beam is lead towards and into an optical material, the ATR-element. With a critical angle, the light reflected totally and does not transmit the ATR-element under refraction. In some devices, the ATR-element is designed to internally direct the beam towards the boundary for multiple times, where each node is reflected totally. At each reflection, a spatially concentrated evanescent field builds up that is a consequence of the exclusion of an electromagnetic beam to be discontinuous at a boundary (even at a critical angle, i.e., total reflection). The evanescent waves intensity decreases exponentially, but they penetrate the solid or liquid sample, that is pressed tightly on the ATR-element. The information on chemical bonding types and vibration energies is captured in the modulation of the reflected probe beam, which runs through the ATR-element and towards the detector electronics. Simply speaking, the penetration depth is essentially proportional to the information one can collect and multiple total reflections are key, as the standing evanescent waves do only impact with a fraction of λ into the sample.[150]

With this type of IR spectroscopy, there is only a low amount of material needed that is used straight on the device. This particularly, makes ATR-IR very effective for the investigation of crystalline material, that was not available in high yield (e.g., solvothermal grown crystals).

The ATR-IR signal is FOURIER-transformed to a respective transmission spectrum. Finally, the data was qualitatively useful and could be compared with literature data. The advantage that no solvent or KBr pellet making is required, makes ATR-IR a powerful tool for solid and liquid specimen that are prone to deteriorate or reactive towards the solvent demanded in a classic IR measurement.

Two different devices were used for analysis of the products with ATR-IR spectroscopy. In ambient atmosphere, a *Spectrum Two FTIR-Spektrometer* equipped with the *Universal ATR Sampling Accessory* from the company *Perkin Elmer LAS*, Rodgau-Jügesheim, DE, was operated. A device from *Bruker Optik GmbH*, Ettlingen, DE, was used inside the argon glovebox. The *ALPHA* FT-IR-spectrometer was equipped with the *QuickSnap*-module *Platinum-ATR*. Both devices used a diamond ATR-element, which covers applicability over a wide range of both solid and liquid samples, and they both had a mechanical stamp arm attached, that was used to press the sample material firmly onto the diamond.

After a background spectrum with no sample material was recorded, measurements of the samples were carried out over the range of 450 – 4000 cm^{-1}. The lower limit was 400 cm^{-1} in some spectra. The collected spectra were transformed to ASCII format, which made further evaluation in *Origin* possible.

µRaman spectroscopy

RAMAN spectra were recorded with an i*nVia Qontor confocal RAMAN microscope* by *Renishaw GmbH*, Pliezhausen, DE) equipped with 10x, 50x and 100x magnification lenses. Two different LASERs were used, a red (786 nm, 50 mW) or a green (532 nm, 100 mW) with beams of a lateral size of the order of 10^{-1} µm. The sample stage was moved electrically, to allow focus of the sample and to move the focus around the sample sites of interest. The samples could be measured just how they were obtained, for example analysis of crystals through the glass ampoule wall was possible. Detection and transformation of the scattered laser beam was performed with a front- and back-illuminated charge coupled device (CCD) detector. The spectra were obtained after tuning the LASER power and the exposure time to values that resulted in high mode signals preventing to exceed the limit of the detector. Furthermore, with use of a live microscope camera, the samples were inspected after the laser exposure for any burning signs from too high LASER intensity.

UV-Vis spectroscopy

Investigation of electronic transitions in molecules provoked by illumination with the visible and near UV spectrum of light were carried out using a *Cary 5E UV-Vis NIR spectrophotometer* (*Varian*, Porto Alto, Ca., USA). In a 100:1 ratio, KBr and the sample powder were mixed in a stainless-steel ball mill container. At low rotation speed, the mixture was ball milled for 10 minutes and a finely ground composite was obtained. In a uniaxial hand press about half a gram of this material was consolidated at a tonnage of 10 t (not calibrated) in a stainless-steel mould. The pellets obtained in this routine had an opaque glassy look and were attached to a holder, which was put into the spectrophotometer. UV-Vis spectra between 200 and 800 nm were recorded and using a pristine KBr pellet of the same mass, the reference signal of KBr was levelled out.

4.3.4 Thermal analysis

Some products were conducted to thermal analysis. Different devices were available, which were 1) a *Netzsch DTA 404 C Pegasus Thermal analyzer* by *Netzsch Gerätebau GmbH*, Selb, DE, 2) a *Mettler Toledo TGA/DSC 1 Star^e* by *Mettler Toledo* inc., Greifensee, CH and 3) a *Simultaneous Thermal Analyzer STA 6000* by *Perkin Elmer LAS*, Rodgau-Jügesheim, DE. In this context, TGA means thermogravimetric analysis, DTA means differential thermal analysis and DSC means differential scanning calorimetry.

The *DTA 404* only offered DTA analyses, while both the other devices 2 and 3 measured TGA simultaneously with DSC or DTA, respectively. The samples were weighed into corundum crucibles, that were heat-dried beforehand. In the machines the samples were heated together with an empty reference crucible. On increasing the temperature, both the crucibles warmed up and eventually chemical or physical changes in the sample were induced. These changes can be of exo- or endothermic type, which results in an increase or decrease of the temperature of the sample in comparison to the reference. The devices, that had a TGA system running simultaneously, recorded sample weight depending on the temperature. Combination of TGA and DTA/DSC was valuable for evaluation of the heat signals and allowed a less ambiguous assignment.

4.3.5 Computational methods

The geometry of some molecules that were determined by experimental crystal structure models, was optimised by means of density functional theory (DFT) calculations.[79] The calculation programme was *Turbomole*, which was run *via* the user interface *TMoleX* v.4.2.[151] After optimisation of the molecular structure, IR and RAMAN vibration frequencies could be calculated to support experimental data. To increase the reliability of the DFT level calculation, some structures were optimised using MP2 level methods.

4.3.6 Software

Evaluation and reduction of SC-XRD data

As described above in section 4.3.2, single crystals were exposed with X-ray radiation and the diffraction intensities were collected in an image format, displaying the point-shaped reciprocal lattice of the crystal. To evaluate these data, the programs *APEX 3* (*Bruker AXS GmbH*, Karlsruhe, DE)[152] and *X-Area* (*STOE & Cie GmbH*, Darmstadt, DE)[153] were used. All frames were imported to the user interface, in both software packages. The intensities were approved or left out by the I/σ-parameter, which is simply speaking the signal-to-noise ratio,. Occasionally, I/σ was chosen low (e.g., $6 < I/\sigma < 15$) in order to accept weak reflections, too. In the next step the indexing of the reflections with a lattice was performed. This means that the reciprocal axes were defined, resulting in an orientation matrix for the collected intensities. With *APEX 3*, this step was fully automatic, and a reduced unit cell was output. In *X-Area* the display of the reciprocal space was alternatively plotted using difference vectors and the cell axes were found manually in this representation of all reciprocal lattice points. Occasionally, that a third axis could not be found in this routine and thus indexing of the point lattice failed.

Next, both user interfaces offered implemented programs to refine the reduced unit cell and to assign it to one of the 14 three-dimensional BRAVAIS lattices. Handling of the data was from this point deviating in the different software suits and differed for each sample. In general, after assignment of the BRAVAIS lattice metrics, the reduction of data could commence, which was to recount the intensities, but this time subtracting all reflections that did not meet the geometrical limits for the assigned lattice type. This step is called *integration* and it automatically runs through all enabled frames. Again, using a defined I/σ-

parameter and settings for the tolerance of improper crystal properties could be implemented here.

It is natural, that in real crystals, the atoms, ions, or molecules do not perfectly obey the theoretical periodicity. However, over the volume of smaller domains ideal periodicity is obtained. These domains are slightly tilted towards each other and thus, imperfect regarding the over-all periodicity. This so-called mosaicity results in the appearance of diffraction reflections under a certain range of angles, instead of only one unique one. In well grown crystals, the tilt is in the range of about tenths of degrees. Yet, it can exceed and result in smearing of the intensities, which consistently decrease the quality and correctness of all further evaluation steps. Another problem during the integration was occasional overlapping of reflections that can severely damage the quality of the data set. This may be handled by adjusting the tolerance intensity limit, that neglects those overlapping reflections for integration, which are out of limit range.[57]

Both user programs offered powerful background algorithms to observe crucial parameters during the integration step. A rule of thumb was to observe the deviation of the indexed unit cell volume, which should stay at low single-digit percentage. The output of the integration is the *.hkl* file, which contains all reflections with their *hkl* index based on the confirmed lattice. Furthermore, the file contains the integrated intensity and a set of six direction cosines for each *hkl* reflection. They contained geometrical information of the in- and outgoing X-ray with regard to that *hkl* reflection for a number of volume increments and enabled a numerical absorption correction at the end, as a final step of data evaluation.

Without derivation, X-ray interacts with solid material in a variety of physical processes. It is not only diffracted on the crystal lattice but can be scattered both elastically and inelastically (RAYLEIGH and COMPTON scattering) as well as it can induce the photoelectric effect. These absorption effects depend the wavelength of the X-ray and on the atomic number of the elements in the crystal.

In an absorption correction, which was partially auto-applied by *X-Area* and *APEX 3* by use of tabulated mass attenuation coefficients, the actual crystal shape becomes relevant when its shape is anisotropic (e.g., plate- or needle-shaped). It appears logical to imagine the alteration of absorption of the X-ray when upon rotation, it passes through thicker and thinner layers of the crystal.[57]

In *X-Area*, the crystal shape was recalculated based on these *hkl*-direction cosines and with the implemented program *X-SHAPE*, the crystal shape calculation was carried out. Therefore, a generic dodecahedron shape of a width, height and depth of each 0.1 mm was

chosen as a base shape, which was automatically converging the *real* shape by use of the information written in the *.hkl* file. Although, this method did prove useful in many cases, occasionally the resulting shape was odd compared with the kind the real crystals actually did look like. Where inapplicable, a numerical absorption correction for these data sets was abandoned.

Measurements on the *D8* always had a video running simultaneously and the real crystal shape could be used for the numerical absorption correction. Furthermore, *APEX 3* provided an absorption correction with the *multi-scan* method, which was performed by implementation of SADABS[154].

Coming back to the point, where the integration was completed, next the examination of the terms of obliteration was scheduled. This was to find the correct LAUE and point group, affecting the actual orientation and positions of atoms, ions and molecules in the unit cell. In *X-Area*, this was done with the sub-programme *X-Red 32*. After the space group (BRAVAIS lattice and point group) was finally chosen, an instruction (*.ins*) file was written, containing the cell parameters, the chemical formula, the X-ray wavelength, the BRAVAIS type, the essential point group symmetry coordinates, the structure factors of atoms and their positions within the unit cell. Virtually, in *APEX 3* the same was performed with the programme implementation *X-Prep*, which could be run individually, dissociated from the *APEX 3* interface, affording the opportunity to reinvestigate any *.hkl* reflection file regardless of the used diffractometer.

The *.ins* and *.hkl* file was therewith providing all information needed for the structure solution within the *ShelX* programme suite, which was run *via* the general user interface (GUI) programme *Olex²*.

Olex²

In *Olex²*[155] the structure solution program package *ShelX* was implemented. The structure solution was performed with *ShelXT*.[143] Changes in the obtained solution, i.e., the solution refinement, was executed with *ShelXL*.[142] Therein different constraints or restraints in *ShelX* four-digit-commands could be performed.

The crucial refinement values were displayed within a tool bar on the right. Eventually, the solution model for the data set was written into a *.cif*, a crystallographic information file, which is the finalised document to be published. *Olex²* (v.1.3, *OlexSys Ltd*, Durham, UK) offered a *CIF-Check*, which uploaded the current solution to a server of the *International Union of Crystallography* (*IUCr*). This tool provided additional control over the solution as

the response of *IUCr* was downloaded in form of a list of alerts. The alerts contained short notes on the issue and for most likely serious and potentially serious problems they were denoted as A and B alert, respectively. Those were to be eliminated on occurrence by improvement of the refinement of the structure model. C alerts were categorised with lower importance but were also eliminated wherever possible.

Diamond

The illustrations of the three-dimensional structure models were prepared in the graphic program *Diamond* (*Crystal Impact GbR,* Bonn, DE).[156] Next to rendering the illustration of the structure in a suitable quality, the program offered quantitative insights in the structure, too. Atomic distances, bond and torsion angles could be prompted. Moreover, where applicable, polyhedrons could be added, using the connectivity list given by the *.cif* file, i.e., the solution and refinement of actual data.

OriginPro 2019b

OriginPro (*Origin Lab Corporation*, Northampton, Ma, US) is a column oriented graphical user interface that allows powerful data evaluation in a spreadsheet organisation. The major advantage, which is offered with *Origin* is that complex data structures can be fit and plotted for graphical export.

WinX^{Pow}

The powder X-ray diffractometer was operated with the *WinX^{POW}*[157] (*STOE & Cie GmbH*). Plotting and evaluation within *WinX^{POW}* was optional with a couple of applications. A frequently used tool was the *Theoretical Pattern* command, which transformed single crystal *.cif*-files into simulation of a powder diffraction curve. In this way a fast and simple comparison of the experimental PXRD data of products with published and own crystal structures was possible.

Topas

To perform a RIETVELD or PAWLEY fitting of PXRD data *Topas-Academic* (v. 6) was used.[158] The programming text editor *jEdit* (v. 5.5.0) was used with pre-set commands (*macros*) that were used by the *Topas* suite for the actual refinement.

For a simple RIETVELD refinement, basically, the PXRD data and the device information had to be given, alongside the number of background Chebychev-parameters[xix]. A sub-template was integrated using the *.cif*-file(s) downloaded from the CSD or used from own single crystal results. Now, lattice parameters and atomic sites could be refined in a stepwise manner, to fit the PXRD data switching between *Topas* and *jEdit*. Care had to be taken for atomic site parameters that were connected to special sites. These values were left unchanged.

Where a *.cif*-file for a specific phase was not accessible, an alternative approach was to perform a PAWLEY fit within *Topas*. Here, only the background, the cell parameters and a space group were given for the refinement. The crucial phase information were obtained either from publications, reviews, the PDF-2 database or results of an indexing routine.

For both the RIETVELD and PAWLEY method, an output file was generated, giving the experimental data curve, the calculated curve, i.e., the refinement, based on the implemented phase information, and the difference curve, allowing to see the agreement of the calculation with the data. Indeed, the qualitative examination of the difference curve shows best if a calculation met with the experimental data.[159,160] As the methods base on minimising the square errors between the observed and calculated intensity, the numerical quantification are expressed by some residual, namely R_p, R_{wp}, R_{exp} and the goodness-of-fit, R_{wp}/R_{eyp}. The statistically expected residual R_{exp}, gives a number for the quality of the measurement. For a *good* refinement the goodness-of-fit approaches somewhat larger than unity.[159] R_{wp} is the only residual, that is statistically relevant and thus the most important residual.

[xix] The term Chebychev originates in the name of the mathematician P. L. TSCHEBYSCHOW.

5 Appendix of experimental data

5.1 Crystallographic reports

Table 5.1

Compound name (**No.**)	Lithium hydrosulfide trithiocarbonate hydrate (**3**)	Sodium trithiocarbonate dihydrate (**5**)	Sodium trithiocarbonate (**6**)
Empirical formula	H12 C Li4 O5 S5	C H4 Na2 O2 S3	C Na2 S3
Sum formula	$Li_4(CS_3)(HS)_2 \cdot 5\ H_2O$	$Na_2CS_3 \cdot 2\ H_2O$	Na_2CS_3
Formula weight [g·mol^{-1}]	292.17	190.20	154.17
Temperature [K]	100(2)	100(2)	150(2)
Crystal system	orthorhombic	orthorhombic	monoclinic
Space group	*Fmm*2	*Cmce*	*C*2/*c*
a, *b*, *c* [pm]	1535.38(9), 798.18(4), 1033.41(5)	2017.21(15), 835.24(5), 829.43(6)	998.5(1), 628.86(6), 846.42(8)
α, β, γ [°]	90	90	90, 107.955(7), 90
V [nm^3]	1.2665(1)	1.39747(17)	0.50562(9)
Z	4	8	4
ρ_{calc} [g·cm^{-3}]	1.532	1.808	2.025
Absorption coef. μ [mm^{-1}]	0.900	1.092	1.455
Crystal size [mm^3]	0.204 × 0.179 × 0.114	0.14 × 0.07 × 0.06	0.12 × 0.07 × 0.05
X-radiation [nm]	MoKα1 (λ = 0.071073)	MoKα1 (λ = 0.071073)	MoKα1 (λ = 0.071073)
Diffractometer	*Bruker Venture D8*	*Bruker Venture D8*	*STOE IPDS 2T*
2θ range [°]	5.306 − 66.39	4.038 − 56.632	7.772 − 52.96
Index ranges	-20 ≤ *h* ≤ 22, -11 ≤ *k* ≤ 12, -14 ≤ *l* ≤ 15	-26 ≤ *h* ≤ 26, -11 ≤ *k* ≤ 11, -11 ≤ *l* ≤ 10	-12 ≤ *h* ≤ 12, -7 ≤ *k* ≤ 7, -10 ≤ *l* ≤ 10
Reflections collected	6484	7778	2594
Independent reflections [R_{int}, R_σ]	1124 [0.0283, 0.0225]	895 [0.0325, 0.0195]	529 [0.0666, 0.0373]
restraints / parameters	1/59	0/42	0/29
Goodness-of-fit on F^2	1.106	1.069	1.105
R_1, wR_2 indexes [$I \geq 2\sigma(I)$]	0.0188, 0.0355	0.0193, 0.0495	0.0257, 0.0624
R_1, wR_2 indexes [all data]	0.0205, 0.0362	0.0226, 0.0514	0.0283, 0.0633
Residual electron density peak/hole [e Å^{-3}]	0.35/0.32	0.29/-0.36	0.58/-0.54
Flack parameter	0.00(4)		
Absorption correction type	numerical	multi-scan	none
CSD no.	2112961	2112963	published earlier

Table 5.2

Compound name (**No.**)	Potassium trithiocarbonate hydrate (**10**)	Potassium trithiocarbonate (**12**)	Potassium trithiocarbonate (**13**)
Empirical formula	C H2 K2 O S3	C K2 S3	C K2 S3
Sum formula	$K_2CS_3 \cdot H_2O$	K_2CS_3	K_2CS_3
Formula weight [g·mol^{-1}]	204.41	186.39	186.39
Temperature [K]	150(2)	150(2)	150(2)
Crystal system	monoclinic	orthorhombic	orthorhombic
Space group	$P2_1/n$	$Cmc2_1$	$Cmc2_1$
a, *b*, *c* [pm]	637.8(1), 1689.7(3), 673.5(1)	999.7(2), 1565.0(3), 1208.9(2)	999.4(1), 1564.9(1), 1209.50(9)
α, β, γ [°]	90, 95.09(1), 90	90	90
V [nm^3]	0.7229(2)	1.8916(7)	1.8917(3)
Z	4	12	12
ρ_{calc} [g·cm^{-3}]	1.878	1.964	1.963
Absorption coef. μ [mm^{-1}]	2.070	2.352	2.352
Crystal size [mm^3]	0.16 × 0.15 × 0.12	0.054 × 0.053 × 0.052	0.06 × 0.07 × 0.08
X-radiation [nm]	MoKα (λ = 0.71073)	MoKα1 (λ = 0.071073)	MoKα1 (λ = 0.071073)
Diffractometer	STOE IPDS 2T	*STOE IPDS 2T*	*STOE IPDS 2T*
2θ range [°]	4.822 − 58.472	4.834 − 57.956	4.836 − 58.306
Index ranges	$-8 \le h \le 8$, $-22 \le k \le 22$, $-8 \le l \le 9$	$-13 \le h \le 13$, $-21 \le k \le 21$, $-16 \le l \le 16$	$-13 \le h \le 13$, $-21 \le k \le 21$, $-16 \le l \le 16$
Reflections collected	9702	16452	17924
Independent reflections [R_{int}, R_σ]	1945 [0.0508, 0.0295]	2660 [0.0562, 0.0271]	2690 [0.0475, 0.0209]
restraints / parameters	0/73	1/97	1/97
Goodness-of-fit on F^2	1.100	1.037	1.052
R_1, wR_2 indexes [$I \ge 2\sigma(I)$]	0.0289, 0.0570	0.0184, 0.0384	0.0156, 0.0380
R_1, wR_2 indexes [all data]	0.0372, 0.0595	0.0209, 0.0393	0.0162, 0.0382
Residual electron density. peak/hole / [e Å^{-3}]	0.36/-0.32	0.37/-0.28	0.33/-0.29
Flack parameter		0.02(3)	-0.05(3)
Absorption correction type	numerical	numerical	numerical
CSD no.	published earlier	1988072	

Table 5.3

Compound name (**No.**)	Potassium trithiocarbonate chloride hydrate (**14**)	Potassium trithiocarbonate dithiodiselenocarbonate hydrate (**15**)	Caesium trithiocarbonate hydrate (**20c**)
Empirical formula	C3 H2 K7 O Cl S9	C5 H2 K10 O S12 Se6	C H2 Cs2 O S3
Sum formula	$K_7(CS_3)_3Cl \cdot H_2O$	$K_5[CS_2(Se_2)]_{1.5}(CS_3) \cdot H_2O$	$Cs_2CS_3 \cdot H_2O$
Formula weight [g·mol^{-1}]	324.86	1327.55	392.03
Temperature [K]	150(2)	100(2)	100(2)
Crystal system	orthorhombic	monoclinic	orthorhombic
Space group (No.)	*Pmmn*	*C*2/*c*	$P2_12_12_1$
a, *b*, *c* [pm]	1584.22(5), 1050.57(3), 641.41(2)	1973.0(1), 644.89(4), 2812.2(2)	703.59(10), 1011.38(13), 1159.07(14)
α, β, γ [°]	90	90, 96.849(3), 90	90
V [nm^3]	1.06752(6)	3.5526(4)	0.82479(19)
Z	2	4	4
ρ_{calc} [g·cm^{-3}]	2.021	2.482	3.157
Absorption coef. μ [mm^{-1}]	2.414	8.066	9.506
Crystal size [mm^3]	0.14 × 0.12 × 0.12	0.31×0.31×0.04	0.3 × 0.15 × 0.14
X-radiation [nm]	MoKα (λ = 0.071073)	MoKα1 (λ = 0.071073)	MoKα (λ = 0.071073)
Diffractometer	*STOE IPDS 2T*	*Bruker Venture D8*	*Bruker Venture D8*
2θ range [°]	4.652 − 52.97	4.786 − 67.998	5.346 − 61.258
Index ranges	-19 ≤ *h* ≤ 18, -13 ≤ *k* ≤ 13, -8 ≤ *l* ≤ 8	-30 ≤ *h* ≤ 30, -10 ≤ *k* ≤ 10, -44 ≤ *l* ≤ 44	-7 ≤ *h* ≤ 10, -14 ≤ *k* ≤ 14, -16 ≤ *l* ≤ 16
Reflections collected	7677	103715	17118
Independent reflections [R_{int}, R_σ]	1205 [0.0661, 0.0311]	7237 [0.0490, 0.0213]	2388 [0.0388, 0.0238]
restraints / parameters	0/75	6/177	0/74
Goodness-of-fit on F^2	1.057	1.105	1.359
R_1, wR_2 indexes [$I \geq 2\sigma(I)$]	0.0276, 0.0509	0.0550, 0.1477	0.0195, 0.0458
R_1, wR_2 indexes [all data]	0.0419, 0.0545	0.0595, 0.1513	0.0195, 0.0458
Residual electron density. peak/hole / [e Å^{-3}]	0.70/-0.29	3.14/-2.53	0.66/-0.97
Flack parameter			0.45(3)
Absorption correction type	multi-scan	numerical	numerical
CSD no.	2112979	2112972	published earlier

* Later corrected with a different crystal to be lower by an order of magnitude in agreement with μ of compounds of similar constitution.

Table 5.4

Compound name (**No.**)	Caesium trithiocarbonate methanol (**24**)	Caesium trithiocarbonate perthiocarbonate (**25**)	Barium trithiocarbonate (**27**)
Empirical formula	C7 H4 Cs12 O S18	C2.5 Cs5 S9	Ba C S3
Sum formula	$Cs_2CS_3 \cdot \frac{1}{6} H_3COH$	$Cs_5(CS_3)[CS_2(S_2)]_{1.5}$	$BaCS_3$
Formula weight [g·mol^{-1}]	2276.10	983.12	245.53
Temperature [K]	100(2)	100(2)	150(2)
Crystal system	monoclinic	triclinic	hexagonal
Space group (No.)	$P2_1/n$	$P\bar{1}$	$P6_122$
a, *b*, *c* [pm]	1613.91(18), 1157.78(13), 2597.7(3)	689.73(6), 1072.44(9), 1469.24(13)	651.79(9), 651.79(9), 1969.7(3)
α, β, γ [°]	90, 103.925(3), 90	99.011(3), 102.130(3), 103.312(3)	90, 90, 120
V [nm^3]	4.7114(9)	1.0097(2)	0.7247(2)
Z	4	2	6
ρ_{calc} [g·cm^{-3}]	3.209	3.234	3.376
Absorption coef. μ [mm^{-1}]	9.972	9.848	9.321
Crystal size [mm^3]	0.187 × 0.151 × 0.04	0.14×0.07×0.02	0.08x0.08.0.08
X-radiation [nm]	MoKα1 (λ = 0.071073)	MoKα1 (λ = 0.071073)	MoKα1 (λ = 0.071073)
Diffractometer	*Bruker Venture D8*	*Bruker Venture D8*	*STOE IPDS 2T*
2θ range [°]	3.872 − 80	3.996 − 59.998	7.218 − 52.898
Index ranges	$-29 \le h \le 29$, $-20 \le k \le 20$, $-46 \le l \le 46$	$-9 \le h \le 9$, $-15 \le k \le 15$, $-20 \le l \le 20$	$-7 \le h \le 8$, $-8 \le k \le 7$, $-24 \le l \le 24$
Reflections collected	354314	94892	6988
Independent reflections [R_{int}, R_σ]	29165 [0.0574, 0.0240]	5877 [0.0457, 0.0187]	504 [0.0672, 0.0200]
restraints / parameters	20/370	12/168	0/25
Goodness-of-fit on F^2	1.300	1.420	1.336
R_1, wR_2 indexes [$I \ge 2\sigma(I)$]	0.0341, 0.0586	0.0244, 0.0594	0.0307, 0.0587
R_1, wR_2 indexes [all data]	0.0381, 0.0596	0.0245, 0.0594	0.0318, 0.0590
Residual electron density. peak/hole / [e Å^{-3}]	1.71/-1.13	2.42/-1.65	0.97/-1.12
Flack parameter			-0.01(3)
Absorption correction type	numerical	numerical	numerical
CSD no.	2112968	2112962	2112959

Table 5.5

Compound name (**No.**)	Sodium perthiocarbonate **(28)**	Potassium perthiocarbonate (**29**)	Diamine hydrogen trithiocarbonate (**30**)
Empirical formula	C Na2 S4	C K2 S4	C H14 N4 S3
Sum formula	$Na_2[CS_2(S_2)]$	$K_2C[CS_2(S_2)]$	$(H_7N_2)_2CS_3$
Formula weight [g·mol^{-1}]	186.23	546.12	178.34
Temperature [K]	100(2)	100(2)	100(2)
Crystal system	orthorhombic	monoclinic	monoclinic
Space group	*Pmna*	$P2_1/n$	$C2/c$
a, *b*, *c* [pm]	747.63(8), 726.35(7), 1147.6(1)	1219.9(1), 826.39(8), 1823.6(2)	928.60(7), 977.62(7), 1029.37(7)
α, β, γ [°]	90	90, 104.320(2), 90	90, 97.189(3), 90
V [nm^3]	0.6232(1)	1.7813(3)	0.9271(1)
Z	4	4	4
ρ_{calc} [g·cm^{-3}]	1.985	2.036	1.278
Absorption coef. μ [mm^{-1}]	14.282	21.765*	0.731
Crystal size [mm^3]	0.6×0.5×0.17	0.2 × 0.15 × 0.03	0.2 × 0.125 × 0.114
X-radiation [nm]	MoKα1 (λ = 0.071073)	CuKα (λ = 1.54178)	MoKα (λ = 0.071073)
Diffractometer	*Bruker Venture D8*	*Bruker Venture D8*	*Bruker Venture D8*
2θ range [°]	12.184 − 144.396	7.904 − 144.616	6.076 − 58.264
Index ranges	$-9 \le h \le 8$, $-8 \le k \le 8$, $-14 \le l \le 14$	$-15 \le h \le 15$, $-9 \le k \le 10$, $-22 \le l \le 22$	$-12 \le h \le 12$, $-13 \le k \le 13$, $-12 \le l \le 14$
Reflections collected	12773	42480	9129
Independent reflections [R_{int}, R_σ]	664 [0.0346, 0.0156]	3509 [0.0560, 0.0228]	1254 [0.0475, 0.0277]
restraints / parameters	0/42	0/173	0/66
Goodness-of-fit on F^2	1.148	1.061	1.113
R_1, wR_2 indexes [$I \ge 2\sigma(I)$]	0.0155, 0.0367	0.0261, 0.0699	0.0214, 0.0475
R_1, wR_2 indexes [all data]	0.0159, 0.0367	0.0274, 0.0707	0.0255, 0.0487
Residual electron density. peak/hole / [e Å^{-3}]	0.35/-0.30	0.85/-0.43	0.27/-0.20
Absorption correction type	multi-scan	multi-scan	multi-scan
CSD no.	2112964	1857465	2034257

Table 5.6

Compound name (**No.**)	Ammonium trithiocarbonate dithiocarbamate (**31**)	Ammonium dithiocarbamate (**32**)	Caesium perthiodicarbonate carbon disulfide (**33**)
Empirical formula	C3 H22 N6 S8	C H5 N2 S2	C3 Cs2 S8
Sum formula	$(H_4N)_5(CS_3)_2[S_2C(NH_2)]$	$(H_4N)[S_2C(NH_2)]$	$Cs_2(C_2S_6) \cdot CS_2$
Formula weight [g·mol^{-1}]	398.74	108.97	526.27
Temperature [K]	100(2)	150(2)	100(2)
Crystal system	trigonal	orthorhombic	monoclinic
Space group	$P3_1$	$Pca2_1$	$P2_1/c$
a, *b*, *c* [pm]	866.47(2), 866.47(2), 2059.05(8)	819.75(3), 560.78(2), 1062.82(3)	727.99(5), 1459.6(1), 1297.88(9)
α, β, γ [°]	90, 90, 120	90	90, 98.152(3), 90
V [nm^3]	1.33877(8)	0.48858(3)	1.3651(2)
Z	3	4	4
ρ_{calc} [g·cm^{-3}]	1.484	1.481	2.561
Absorption coef. μ [mm^{-1}]	0.991	0.915	51.295*
Crystal size [mm^3]	0.094 × 0.079 × 0.075	0.266 × 0.046 × 0.024	0.1 × 0.02 × 0.01
X-radiation [nm]	MoKα (λ = 0.071073)	MoKα (λ = 0.071073)	CuKα (λ = 0.0154178)
Diffractometer	*Bruker Venture D8*	*STOE IPDS 2T*	*Bruker Venture D8*
2θ range [°]	5.428 − 55.002	7.266 − 57.908	12.128 to 135.954
Index ranges	$-11 \le h \le 11$, $-11 \le k \le 11$, $-26 \le l \le 26$	$-11 \le h \le 11$, $-7 \le k \le 7$, $-13 \le l \le 14$	$-6 \le h \le 8$, $-17 \le k \le 17$, $-15 \le l \le 15$
Reflections collected	28479	12703	15822
Independent reflections [R_{int}, R_σ]	4073 [0.0238, 0.0139]	1265 [0.0484, 0.0185]	2488 [0.0719, 0.0492]
restraints / parameters	1/235	1/77	0/118
Goodness-of-fit on F^2	1.100	1.169	1.159
R_1, wR_2 indexes [$I \ge 2\sigma(I)$]	0.0128, 0.0311	0.0192, 0.0407	0.0508, 0.1478
R_1, wR_2 indexes [all data]	0.0129, 0.0311	0.0196, 0.0412	0.0530, 0.1488
Residual electron density. peak/hole / [e Å^{-3}]	0.22/-0.12	0.37/-0.56	1.50/-1.09
Flack parameter	0.277(17)	0.03(4)	
Absorption correction type	numerical	numerical	multi-scan
CSD no.	2112965	published earlier	2113131

* Later corrected with a different crystal to be lower by an order of magnitude in agreement with μ of compounds of similar constitution.

Table 5.7

Compound name (**No.**)	Tetraphenyl phosphonium perthiodicarbonate (**34**)	Potassium bis(trithiocarbonato) nickelate(II) (**35**)	Potassium bis(trithiocarbonato) palladate(II) EtOH (**36**)
Empirical formula	C50 H40 P2 S6	C2 K2 Ni S6	C4 H6 K2 Pd O S6
Sum formula	$[(C_6H_5)_4P]_2(C_2S_6)$	$K_2[Ni(CS_3)_2]$	$K_2[Pd(CS_3)_2] \cdot H_3C_2OH$
Formula weight [g·mol^{-1}]	895.12	353.29	447.05
Temperature [K]	150(2)	100(2)	150(2)
Crystal system	monoclinic	monoclinic	monoclinic
Space group	$P2_1/c$	$P2_1/c$	$P2_1/m$
a, *b*, *c* [pm]	1659.9(2), 1418.4(2), 1850.6(2)	812.80(8), 1617.1(2), 802.33(7)	770.59(4), 989.15(6), 898.6(5)
α, β, γ [°]	90, 94.06(1), 90	90, 102.749(3), 90	90, 99.946(4), 90
V [nm^3]	4.3462(9)	1.0286(2)	0.67334(7)
Z	4	4	2
ρ_{calc} [g·cm^{-3}]	1.368	2.281	2.205
Absorption coef. μ [mm^{-1}]	0.424	1.968	2.891
Crystal size [mm^3]	0.40 × 0.11 × 0.10	0.487 × 0.386 × 0.352	0.14 × 0.12 × 0.12
X-radiation [nm]	MoKα (λ = 0.071073)	AgKα (λ = 0.056086)	MoKα (λ = 0.071073)
Diffractometer	*STOE IPDS 2T*	*Bruker Venture D8*	*STOE IPDS 2T*
2θ range [°]	2.46 − 53.534	4.054 − 60	4.612 − 55.988
Index ranges	$-20 \le h \le 20$, $-17 \le k \le 17$, $-23 \le l \le 22$	$-14 \le h \le 14$, $-28 \le k \le 28$, $-13 \le l \le 14$	$-10 \le h \le 10$, $-13 \le k \le 13$, $-11 \le l \le 11$
Reflections collected	42469	87226	5807
Independent reflections [R_{int}, R_σ]	9191 [0.1535,0.1632]	6084 [0.0430, 0.0198]	1697 [0.0609, 0.0603]
restraints / parameters	0/679	0/103	0/85
Goodness-of-fit on F^2	0.983	1.248	0.966
R_1, wR_2 indexes [$I \ge 2\sigma(I)$]	0.0784, 0.0734	0.0253, 0.0493	0.0349, 0.0549
R_1, wR_2 indexes [all data]	0.1675, 0.0919	0.0268, 0.0498	0.0592, 0.0592
Residual electron density. peak/hole / [e Å^{-3}]	0.30/-0.31	0.94/-0.53	0.57/-0.75
Absorption correction type	numerical	numerical	numerical
CSD no.	published earlier	2031931	1988420

Table 5.8

Compound name (**No.**)	Potassium bis(trithiocarbonato) platinate(II) (**37**)	Potassium tris(trithiocarbonato) cobaltate(III) trithiocarbonate (**38**)	Tetraphenyl phosphonium bis(trithiocarbonato) palladate(II) (**39**)
Empirical formula	C2 K2 Pt S6	C4 K5 Co S12	C50 H40 P2 Pd S3
Sum formula	$K_2[Pt(CS_3)_2]$	$K_5[Co(CS_3)_3]CS_3$	$[(C_6H_5)_4P]_2[Pd(CS_3)_2]$
Formula weight [g·mol^{-1}]	489.67	687.19	1001.52
Temperature [K]	150(2)	102(2)	110(2)
Crystal system	monoclinic	monoclinic	monoclinic
Space group	$P2_1/c$ (14)	$P2_1/c$	$P2_1/c$
a, *b*, *c* [pm]	816.2(2), 1641.1(4), 808.6(2)	1198.9(2), 646.2(1), 2847.9(5)	1434.3(1), 1938.9(1), 1718.0(1)
α, β, γ [°]	90, 104.13(2), 90	90, 100.166(9), 90	90,111.586(2), 90
V [nm^3]	1.0504(4)	2.1717(7)	4.4425(5)
Z	4	4	4
ρ_{calc} [g·cm^{-3}]	3.097	2.102	1.497
Absorption coef. μ [mm^{-1}]	15.277	2.890	0.808
Crystal size [mm^3]	0.024 × 0.016 × 0.016	0.219 × 0.058 × 0.055	0.199 × 0.183 × 0.112
X-radiation [nm]	MoKα (λ = 0.071073)	MoKα (λ = 0.071073)	MoKα (λ = 0.071073)
Diffractometer	*STOE IPDS 2T*	*Bruker Venture D8*	*Bruker Venture D8*
2θ range [°]	4.964 − 52.988	4.89 − 53.998	3.706 − 59.998
Index ranges	$-10 \le h \le 10$, $-20 \le k \le 20$, $-10 \le l \le 10$	$-15 \le h \le 15$ $-7 \le k \le 8$, $-29 \le l \le 36$	$-20 \le h \le 20$, $-27 \le k \le 27$, $-24 \le l \le 24$
Reflections collected	9784	14787	232070
Independent reflections [R_{int}, R_σ]	2172 [0.0726, 0.0483]	4670 [0.0620, 0.0708]	12947 [0.0470, 0.0155]
restraints / parameters	0/104	0/199	0/692
Goodness-of-fit on F^2	0.953	1.172	1.090
R_1, wR_2 indexes [$I \ge 2\sigma(I)$]	0.0359, 0.0568	0.0663, 0.1326	0.0247, 0.0581
R_1, wR_2 indexes [all data]	0.0703, 0.0644	0.0874, 0.1388	0.0281, 0.0596
Residual electron density. peak/hole / [e Å^{-3}]	0.96/-1.65	0.79/-0.82	0.42/-0.37
Absorption correction type	numerical	numerical	numerical
CSD no.	2031934	2112967	2112966

Table 5.9

Compound name (**No.**)	Ammonium perthiocarbonate copper(II) perthiocarbonate (**40**)	Potassium tri(μ-acetato) hexaacetato di europiate(III) tris(trithiocarbonate) (**41**)	Thallium(I) pentasulfide (**43**)
Empirical formula	C1.5 H8 Cu N2 S6	C21 H36 Eu2 K9 O18 S9	Tl2 S5
Sum formula	$(H_4N)_2[Cu\{CS_2(S_2)\}]CS_2(S_2)$	$K_9[Eu_2(CH_3COO)_9](CS_3)_3$	Tl_2S_5
Formula weight [g·mol^{-1}]	310.00	1520.86	569.04
Temperature [K]	100(2)	150(2)	100(2)
Crystal system	orthorhombic	hexagonal	orthorhombic
Space group	*Fdd*2	$P6_3/m$	$P2_12_12_1$
a, *b*, *c* [pm]	1502.8(1), 1629.6(1), 1630.7(1)	1127.02(3), 1127.02(3), 2479.91(7)	649.96(6), 662.24(6), 1651.9(2)
α, *β*, *γ* [°]	90	90, 90, 120	90
V [nm^3]	3.9936(5)	2.7279(2)	0.7110(1)
Z	16	2	4
ρ_{calc} [g·cm^{-3}]	2.062	1.852	5.316
Absorption coef. μ [mm^{-1}]	3.379	3.364	46.616
Crystal size [mm^3]	0.123 × 0.104 × 0.096	0.13 × 0.11 × 0.11	0.060 × 0.056 × 0.035
X-radiation [nm]	MoKα (λ = 0.071073)	MoKα (λ = 0.071073)	MoKα (λ = 0.071073)
Diffractometer	*Bruker Venture D8*	*STOE IPDS 2T*	*Bruker Venture D8*
2θ range [°]	4.454 − 79.972	3.284 − 53.834	4.932 − 49.998
Index ranges	$-27 \le h \le 27$, $-28 \le k \le 29$, $-29 \le l \le 29$	$-14 \le h \le 14$, $-14 \le k \le 14$, $-31 \le l \le 31$	$-7 \le h \le 7$, $-7 \le k \le 7$, $-19 \le l \le 19$
Reflections collected	57844	37435	5801
Independent reflections [R_{int}, R_σ]	6178 [0.0624, 0.0397]	2002 [0.0654, 0.0178]	1245 [0.0579, 0.0455]
restraints / parameters	19/151	0/130	0/64
Goodness-of-fit on F^2	1.056	1.061	1.068
R_1, wR_2 indexes [$I \ge 2\sigma(I)$]	0.0342, 0.0748	0.0201, 0.0525	0.0354, 0.0837
R_1, wR_2 indexes [all data]	0.0454, 0.0817	0.0257,0.0548	0.0375, 0.0846
Residual electron density. peak/hole / [e Å^{-3}]	1.79/-0.70	0.83/-0.75	1.45/-2.47
Flack parameter	0.015(5)		0.00(2)
Absorption correction type	numerical	numerical	numerical
CSD no.	2112960	1988072	published earlier

5.2 Powder XRD

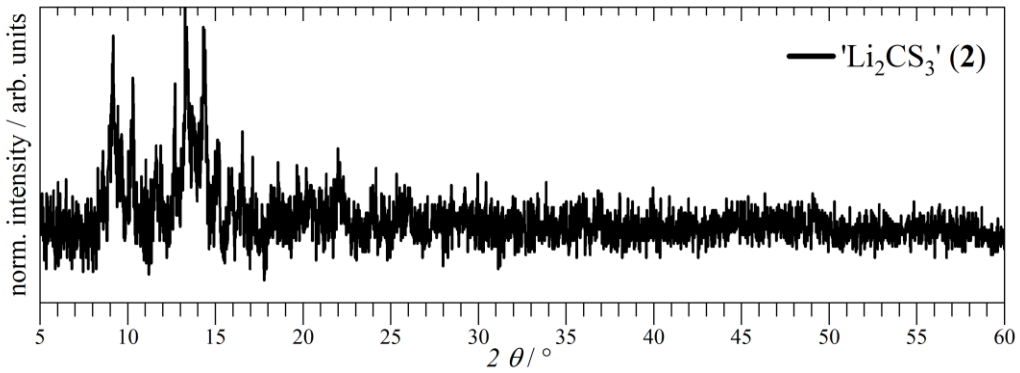

Figure 5.1: PXRD curve (black) of product **2**. Grey lines are the peaks obtained with the *WinXPow* software suite. No suitable entry in the PDF-2 matched the peak pattern.

Table 5.10: Rietveld refinement parameters

Figure	Phase(s) (**no.**) (ratio)	[a]background	[b]r_{exp} / %	[c]r_p / %	[d]r_{wp} / %	[e]gof
Figure 2.4	Na_2CS_3 **4** / $Na_2CS_3 \cdot 2\ H_2O$ (90/10)	9	12.42	14.69	18.99	1.53
Figure 2.8	$Na_2CS_3 \cdot 2\ H_2O$ **5** / Na_2CS_3 (35/65)	14	4.68	14.17	20.50	4.3
Figure 2.16	K_2CS_3 **9**	15	6.56	5.33	9.14	1.39
Figure 2.20	$K_2CS_3 \cdot H_2O$ **11** / K_2CS_3 (21/79)	10	2.92	6.43	8.62	2.95
Figure 2.39	$BaCS_3$ **26**	18	7.26	11.98	16.38	2.25
Figure 2.79	$(H_4N)_5(CS_3)_2[S_2C(NH_2)]$ **31** / $(H_4N)[S_2C(NH_2)]$ (75/25)	18	6.07	5.78	7.51	1.24
Figure 4.7	Na_2S **44**	5	3.71	2.72	3.65	0.98
Figure 4.8	Na_2S_5 **46**	17	7.28	6.01	8.96	1.23
Figure 4.10	K_2S **47** / K_2S_2 (97/3)	12	6.79	7.20	8.98	1.32
Figure 4.11	K_2Se **50** / K_2Se_2 (88/12)	13	3.85	2.66	3.40	0.88
Figure 4.12	K_2Se (batch #2)	10	5.28	3.56	4.46	0.85
Figure 4.14	Cs_2S_3 **49**	22	4.87	4.23	5.52	1.13

[a]no. of Chebychev background terms, [b]expected profile residual, [c] profile residual, [d]weighed profile residual, [e]goodness of fit (r_{wp}/r_{exp})

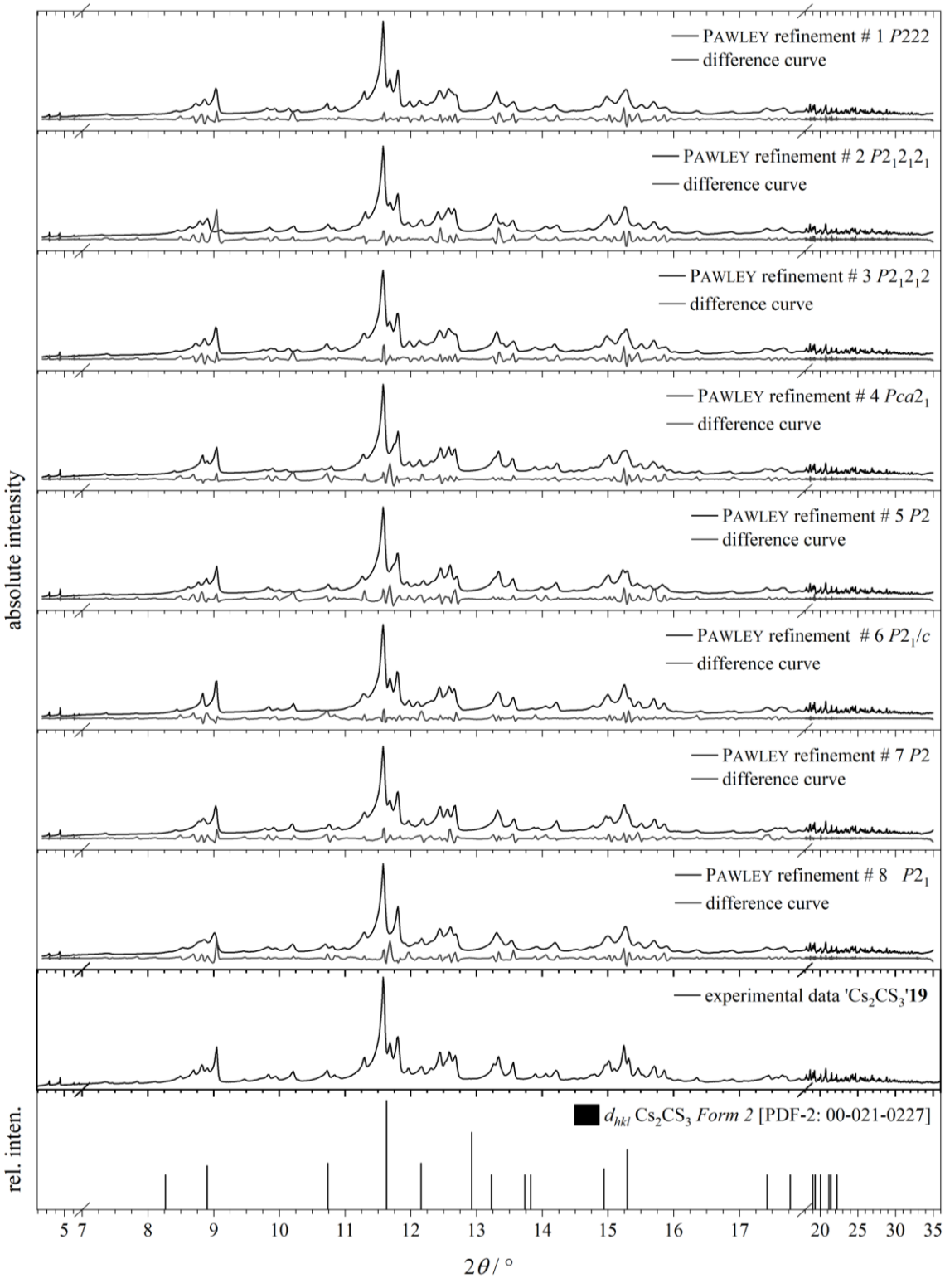

Figure 5.2: PAWLEY refinements after indexing of 'Cs_2CS_3' **19**. The refinements and difference curves correspond to the numbers (#) in table 2.6. At the bottom the PDF-2 entry, i.e., the d_{hkl} positions transferred to 2θ values are plotted. The intense reflections at 8.9, 11.5 or 15.2° in the experimental data fit the literature values, suggesting the product to contain partially Cs_2CS_3.

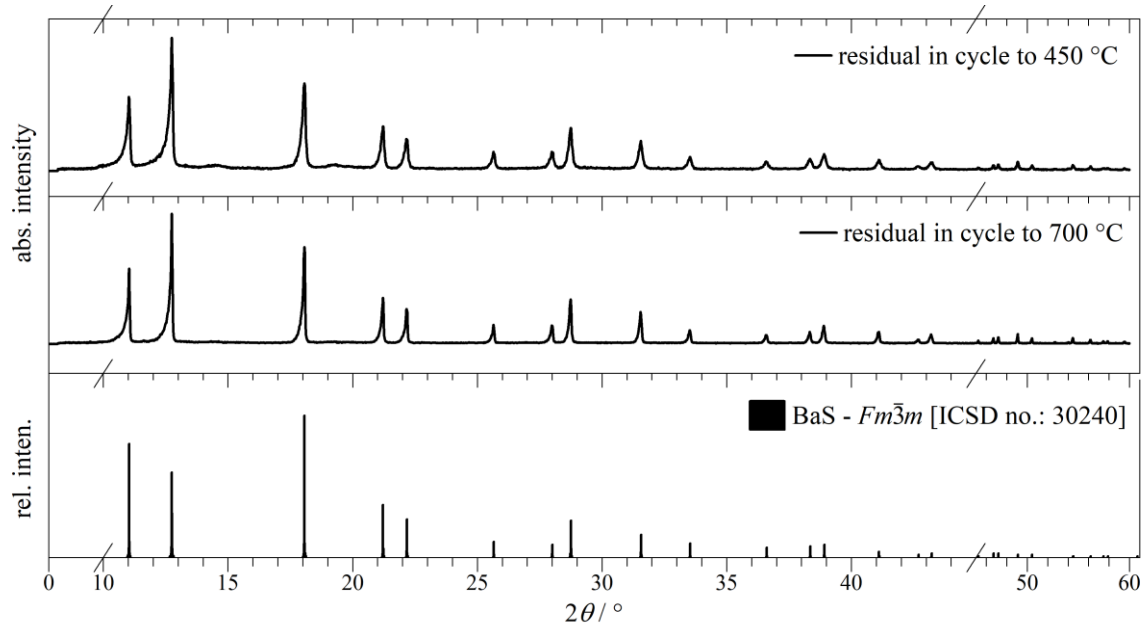

Figure 5.3: PXRD curves of DTA residuals of samples of $BaCS_3$. The top and mid data were obtained from different thermal analysis cycles to 450 and 700 °C, respectively. Reference data at the bottom shows perfect agreement with the cubic phase of BaS.

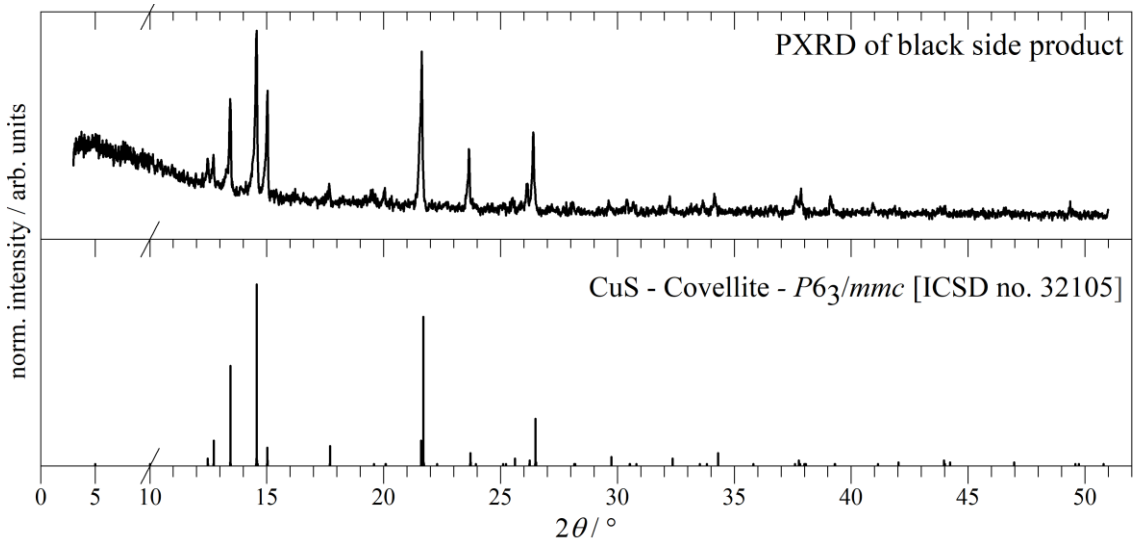

Figure 5.4: Identification of the black solid side product obtained next to $(H_4N)_2{}^1_\infty[Cu\{CS_2(S_2)\}]CS_2(S_2)$ **40**. CuS formed as a black precipitate.

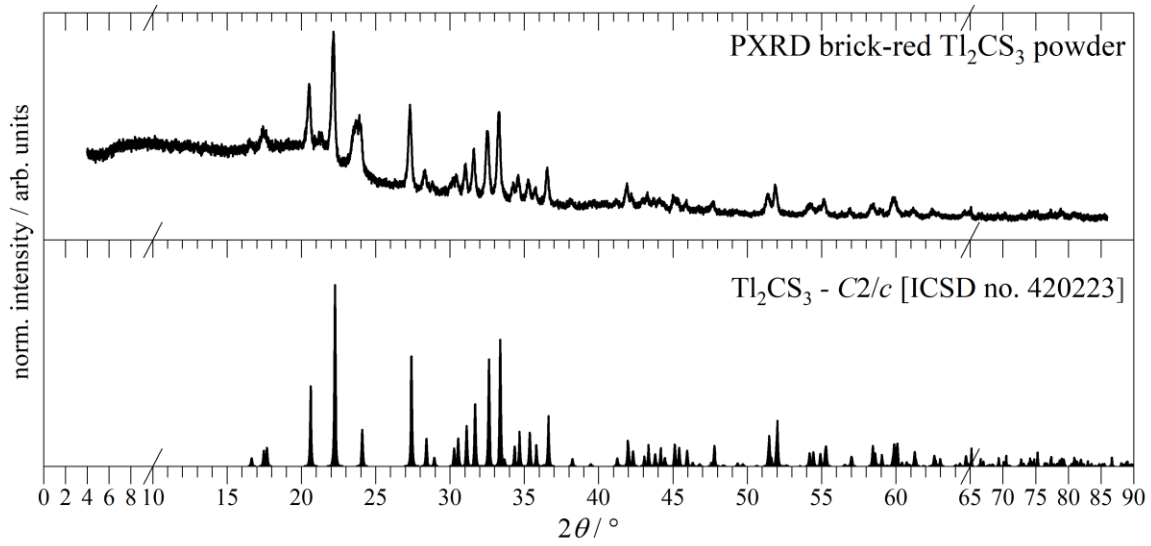

Figure 5.5: Comparison of the PXRD curve of brick-red Tl_2CS_3 powder **42** with the deposited crystal data.

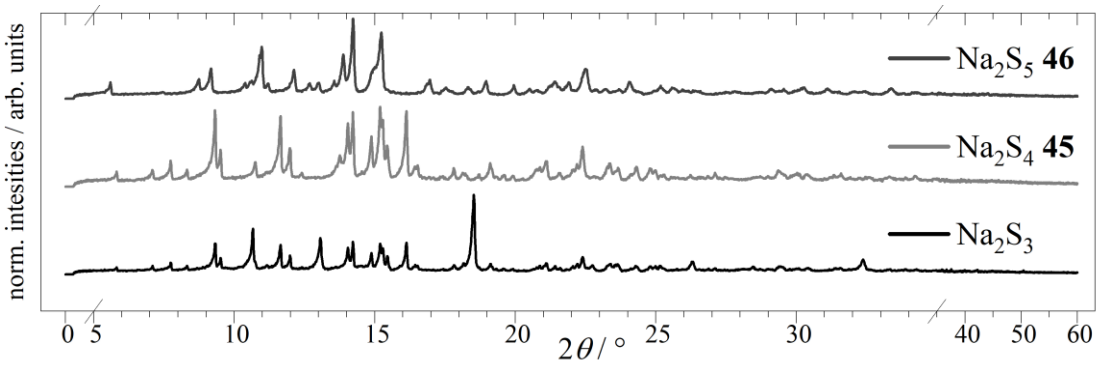

Figure 5.6: PXRD of the prepared sodium polysulphides.

5.3 Thermal analyses

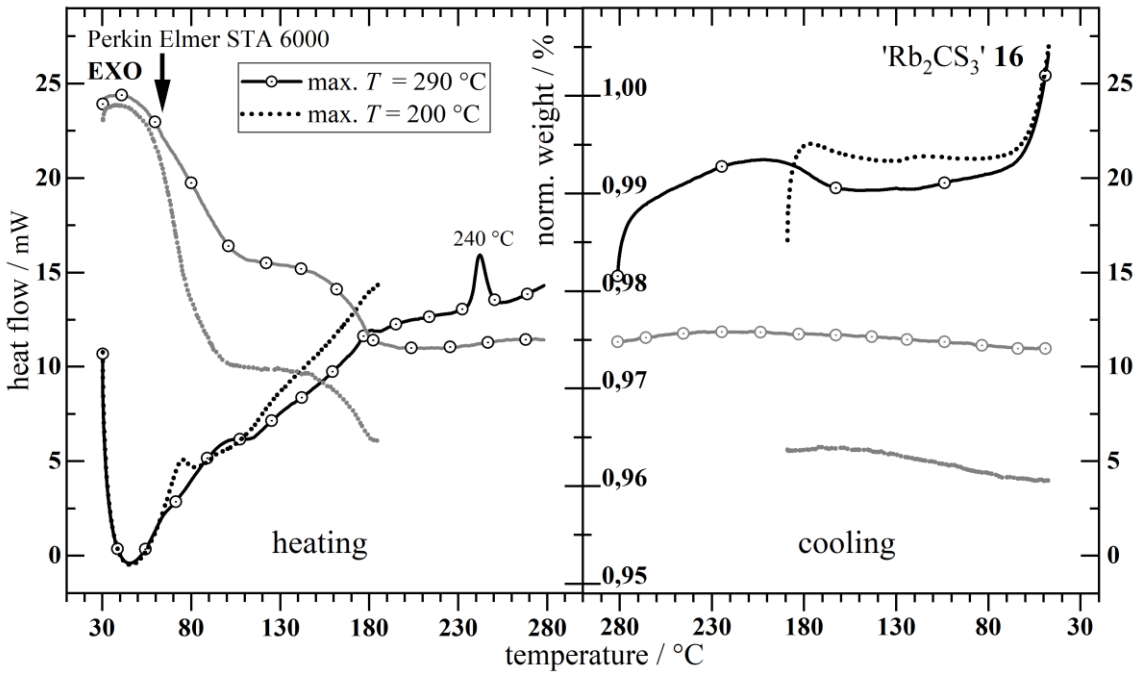

Figure 5.7: DTA-TG measurements of 'Rb_2CS_3' **16** with max. temperature of 200 °C and 290 °C. The black curves describe the heat flow, the grey curves describe the weight (axis in the centre). The dotted lines correspond to the measurement up to 200 °C, while the lines with open symbols are that of the run up to 290 °C. The endothermic signal at 240 °C was unaccompanied with a change in the sample weight. The residuals were investigated with PXRD and IR spectroscopy, which gave no rise for a crystallisation event at that temperature.

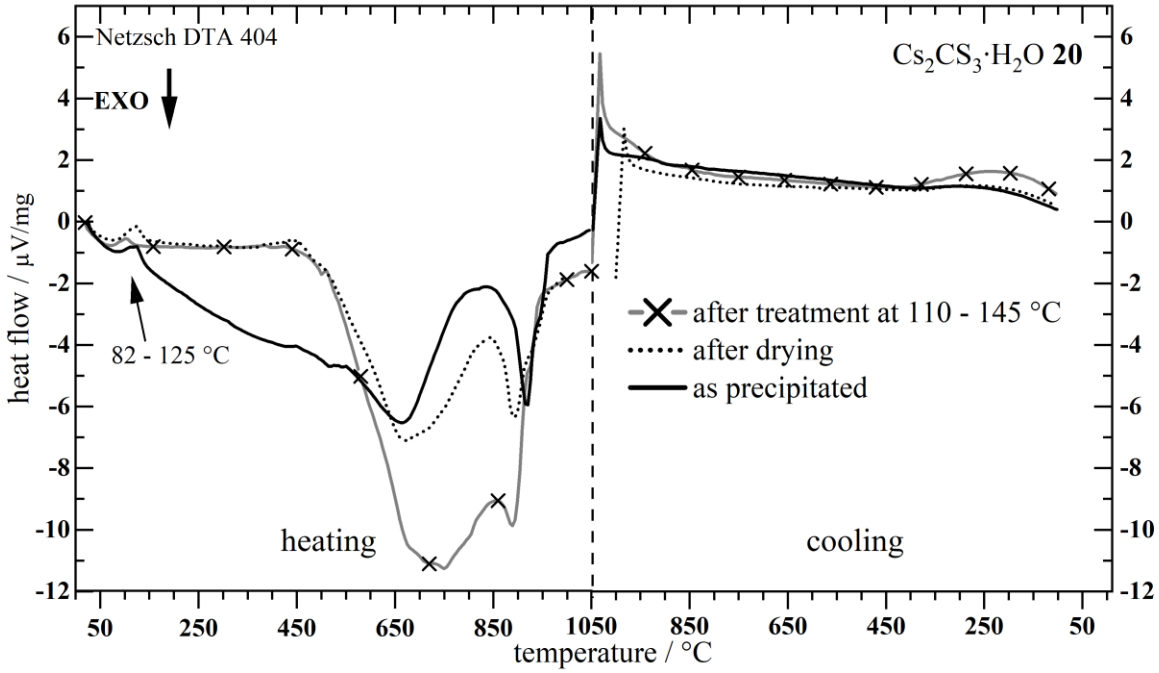

Figure 5.8: Preliminary analyses of $Cs_2CS_3 \cdot H_2O$ 20 with DTA. All curves show very similar features of the heat flow vs. temperature curvature in the heating (left) and cooling (right) phases. In particular, the endothermic signal at ca. 100 °C indicated the evaporation of water. Upon heating, the solid black line has a constant exothermic slope, which could have different origins, e.g., restructuration. The dotted line gives the data of the powder as precipitated but dried in a mild treatment, showing a stable line up to about 400 °C. Two exothermic signals above 650 °C suggest major deterioration of the compound, disregarding the steps carried out. Upon cooling, no signals are obtained. No residuals were obtained.

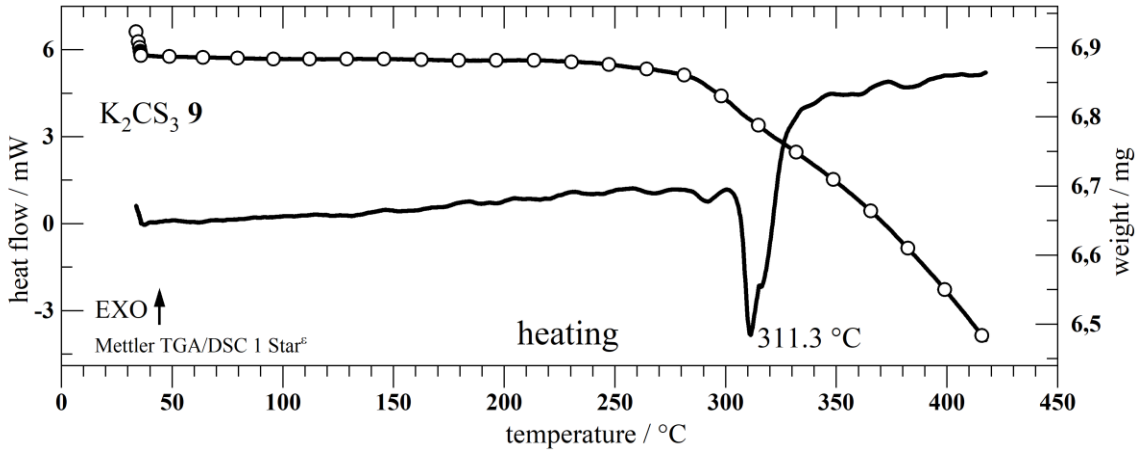

Figure 5.9: DSC-TG data heating up K_2CS_3 **9** to 415 °C. No volatiles escaped the material up to about 300 °C. The endothermic signal with peak at 311.3 °C indicates decomposition. The residual brown material was analysed with PXRD, denying to define it with only one known phase. A mixed phase of potassium polysulfides is guessed.

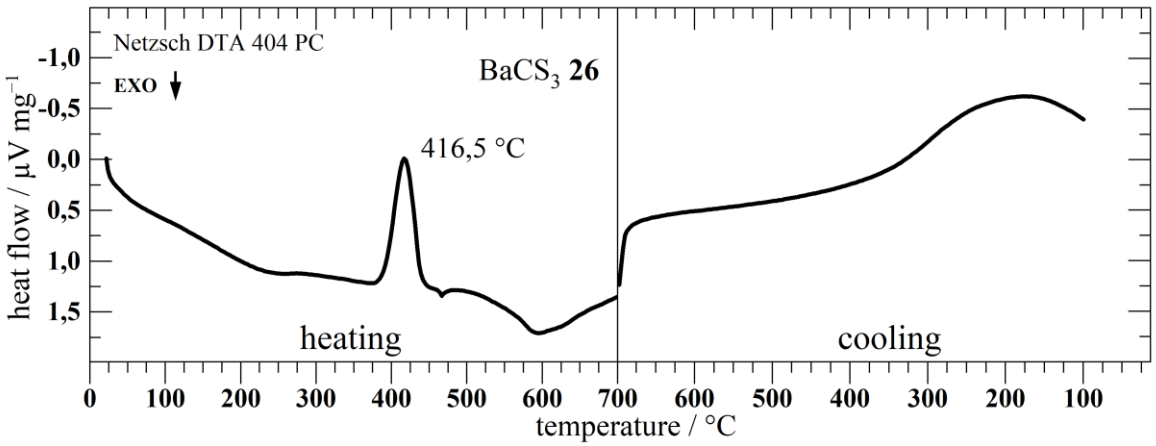

Figure 5.10: DTA data recorded from a sample of $BaCS_3$ powder **26** (6.4 mg). The endothermic signal at 416.5 °C should be due to decomposition (evaporation of CS_2). This is because the PXRD data of the residual could be assigned with BaS (cf. figure 5.3) even for thermal treatment up to only 450 °C (not shown).

5.4 Calculated structural values

Table 5.11: Geometry optimisation for $SC(SH)_2$ using an isolated molecule taken from the *.cif* published on α-H_2CS_3 by KREBS et al. All values are given in pm.

C=S		atomic base sets for optimisation			
level	hybrid functionals	6−31G*	cc−pVDZ	cc−pVTZ	α-H_2CS_3 KREBS et al.[33]
DFT	B3LYP	164.2	164.5	163.4	
DFT	PBE0	163.5	163.8	162.8	1.649*
MP2		163.1	164.0	162.6	
C−SH		6−31G*	cc−pVDZ	cc−pVTZ	α-H_2CS_3 KREBS et al.[33]
DFT	B3LYP	177.8	178.2	176.9	
DFT	PBE0	176.1	176.4	175.2	172.7*
MP2		176.3	177.6	175.4	

* (mean value for four non-equivalent molecules determined in the solid state)

Table 5.12: Results from geometry optimisation routine on the SC-XRD structure model of a CS_3^{2-} anion as found on the C2 site in $Cs_2CS_3 \cdot$ ⅙ MeOH **24** (structural details in the right column). The calculation was carried out at DFT and MP2 level applying D_{3h} symmetry. All numbers are given in pm.

C−S		atomic base sets for optimisation			CS_3^{2-} anion structure (symmetry C_1)
level	hybrid functional	6-31G*	cc-pVTZ	cc-pVDZ	
DFT	PBE0	178.8	**173.6**	174.8	C−S22 170.9(2), C−S21 172.3(3), C−S23172.9(3);
DFT	B3-LYP	175.8	175.0	176.3	
MP2		175.8	**173.2**	175.1	

Table 5.13: Results from geometry optimisation routine on the SC-XRD structure model of a $CS_2(S_2)^{2-}$ anion as found on the C1 site in $K_2[CS_2(S_2)]$ **29** (experimental structure details in the left column). The calculation was carried out at DFT level with PBE0 functional applying *C1* symmetry. All distances are given in pm.

$CS_2(S_2)^{2-}$ anion structure (symmetry *C1*) / pm		calculated optimisation (cc-pVTZ)
C−S11	169.2(2)	168.6
C−S12	171.8(2)	172.7
C−S13	173.3(2)	176.1
S13−S14	203.5(7)	205.8
dihedral angle / ° (S12−C1−S13−S14)	176.09(8)	179.945

Table 5.14: Results from geometry optimisation routine on the SC-XRD structure model of a $CS_2(Se_2)^{2-}$ anion as found on the C1 site in $K_5[CS_2(Se_2)]_{1.5}(CS_3) \cdot H_2O$ **15** (experimental structure details in the left column). The calculation was carried out at DFT and MP2 level applying *C1* symmetry. All distances are given in pm.

$CS_2(Se_2)^{2-}$ anion structure (symmetry *C1*) / pm		calculated optimisation	
		(PBE0 cc-pVTZ)	MP2 (cc-pVTZ)
C−S21	171.9(4)	171.0	170.3
C−S22	168.5(4)	167.2	165.4
C−Se21	189.3(4)	193.9	193.6
Se21−Se22	230.5(1)	234.9	236.2
dihedral angle / ° (S21−C2−Se21−Se22)	178.2(1)	179.931	180.0

Table 5.15: Results from geometry optimisation routine on the SC-XRD structure model of the $S_2C(NH_2)^-$ anion as found on the C3 site in **31** (experimental structure details in the left column). The calculation was carried out at DFT and MP2 level applying C_1 symmetry. All distances are given in pm.

$S_2C(NH_2)^{2-}$ anion structure (symmetry C_2) / pm		calculated optimisation (PBE0 cc-pVTZ)	MP2 (cc-pVTZ)
C3−S31	172.3(2)	170.3	170.1
C3−S32	171.8(2)	170.3	170.1
C3−N1	132.4(4)	136.1	137.1
N1−H	88.0(2)	100.3	100.3
angles / °			
(S31−C3−S32)	121.6(1)	128.3	128.5
(N1−C3−S32)	119.1(2)	115.9	115.7
(N1−C3−S31)	119.3(2)	115.9	115.7

Table 5.16: Results from geometry optimisation routine on the SC-XRD structure model of the trithiocarbonato complex anions $[M^{x+}(CS_3)_x]^{x-}$ The calculations were carried out at DFT level. PBE0 hybrid functional was used with atomic base set cc-pVTZ for C and S and LANLD2Z for M, with ECP (Hay&Wad) values of 10 (Co), 28 (Pd), 60 (Pt).

connection	$M = Pd^{2+}$	$M = Pd^{2+}$	$M = Pt^{2+}$	$M = Co^{3+}$
S^{term}–C /pm	167.24	167.3	167.1	169.5
C–S^{coord} /pm	172.95	172.9	173.3	171.2
S–M / pm	236.03 / 236.04	236.0	234.5	229.4
S^{term}–C–S^{ccord} / °	125.678 / 125.679	125.7	126.5	126.0
S^{coord}–C–S^{coord} / °	108.642 / 108.644	108.7	107.1	108.0
C–S^{coord}–M / °	89.450 / 89.151	89.1	90.0	88.7
molecule symmetry	C_1*	D_{2h}	D_{2h}	D_3

*C_1 could be considered D_{2h} after rounding of the calculated values. The low symmetry only applies using the exact values as written in the first column.

6 References

[1] G. Gattow, W. Behrendt, *Carbon Sulfides and Their Inorganic and Complex Chemistry*, Thieme, Stuttgart, **1977**.

[2] J. J. Berzelius, *Ann. Phys. Chem.* **1826**, 444-458.

[3] H. Mills, P. C. Robinson, *J. Chem. Soc. (London)* **1928**, 2326.

[4] J. G. O'Donoghue, Z. Kahan, *J. Chem. Soc. (London)* **1906**, 1812.

[5] E. W. Yeoman, *J. Chem. Soc. (London)* **1921**, 38.

[6] G. Gattow, B. Krebs, *Angew. Chem.* **1962**, *74*, 29.

[7] M. Dräger, G. Gattow, *Angew. Chem.* **1968**, *80*, 954.

[8] W. C. Zeise in *Journal für Chemie und Physik*, **1824**, S. 98–115.

[9] a) W. C. Zeise in *Journal für Chemie und Physik*, **1824**, S. 170–182; b) W. C. Zeise in *Journal für Physik und Chemie*, **1822**, S. 1–67.

[10] W. C. Zeise in *Annalen der Physik und Chemie*, **1834**, S. 369–431.

[11] S. R. Ramadas, P. S. Srinivasan, J. Ramachandran, V. V. S. K. Sastry, *Synthesis* **1983**, *1983*, 605.

[12] D. Coucouvanis in *Progress in Inorganic Chemistry*, *Vol. 11*, John Wiley & Sons, Inc.; Wiley, New York, **1970**, S. 233–371.

[13] A. F. Holleman, N. Wiberg, M. Krieger-Hauwede, J.-H. Chang, *Grundlagen und Hauptgruppenelemente*. *Band 1: Grundlagen und Hauptgruppenelemente,* 103. Aufl., de Gruyter, Berlin/Boston, **2016**.

[14] A. L. Allred, E. G. Rochow, *J. Inorg. Nucl. Chem.* **1958**, *5*, 264.

[15] G. N. Lewis, *Valence and the Structure of Atoms and Molecules*, Chemical Catalog Company, Incorporated, **1923**.

[16] J. E. Huheey, E. A. Keiter, R. L. Keiter, *Anorganische Chemie*. *Prinzipien von Struktur und Reaktivität*, 4. Aufl., de Gruyter, Berlin, **2012**.

[17] M. Nič, J. Jirát, B. Košata, A. Jenkins, A. McNaught *IUPAC Compendium of Chemical Terminology*, IUPAC, Research Triagle Park, NC, **2009**.

[18] R. G. Pearson, *J. Chem. Educ.* **1968**, *45*, 581.

[19] G. Gattow, *Sulfur Rep.* **1993**, *14*, 1.

[20] a) US2010/152081, A1. W. Hierse, N. Ignatyev, M. Seidel, E. Montenegro, P. Kirsch, A. Bathe, **2010**; b) Merck & Co., Inc., US5369125, A. G. D. Berger, J. D. Bergstrom, T. Biftu, R. L. Bugianesi, Burk, R. M., et al., **1994**.

[21] a) K. Kato, *Acta Crystallogr B Struct Sci* **1972**, *28*, 606; b) W. G. Perdok, P. Terpstra, *Rec. J. R. Neth. Chem. Soc.* **1946**, *65*, 493.

[22] G. Gattow, B. Krebs, *Z. anorg. allg. Chem.* **1963**, *325*, 15.

[23] M. Bögemann, *Angew. Chem.* **1938**, *51*, 113.

[24] M. Bögemann in *Handbuch der Katalyse*. *Katalyse in der Organischen Chemie*. Zweite Hälfte, Springer Vienna, Vienna, **1943**, S. 569–584.

[25] S. Mostoni, P. Milana, B. Di Credico, M. D'Arienzo, R. Scotti, *Catalysts* **2019**, *9*, 664.

[26] R. L. Baron in *Handbook of pesticide toxicology*. *Classes of pesticides*, Academic Press, San Diego, **1991**, S. 1125–1176.

[27] T. R. Roberts, D. H. Hutson, P. W. Lee, P. H. Nicholls, J. R. Plimmer, *Insecticides and fungicides*, Royal Society of Chemistry, Cambridge, **1999**.

[28] G. Moad, J. Chiefari, Y. K. Chong, J. Krstina, R. T. A. Mayadunne, A. Postma, E. Rizzardo, S. H. Thang, *Polym. Int.* **2000**, *49*, 993.

[29] A. D. Jenkins, R. G. Jones, G. Moad, *Pure Appl. Chem.* **2009**, *82*, 483.

[30] S. Perrier, *Macromolecules* **2017**, *50*, 7433.

[31] a) F. Dehmel, T. Ciossek, T. Maier, S. Weinbrenner, B. Schmidt, M. Zoche, T. Beckers, *Bioorg. Med. Chem. Lett.* **2007**, *17*, 4746; b) M. F. Ali, S. Abbas, *Fuel Process. Technol.* **2006**, *87*, 573; c) H. Yekeler, M. Yekeler, *Appl. Surf. Sci.* **2004**, *236*, 435; d) US4504384. R. M. Parlman, J. B. Kimble, **1982**; e) N. Singh, R. Khare,

K. Srivastava, *Asian J. Chem.* **2019**, *31*, 1989; f) M. Fallah-Mehrjardi, *Monatsh. Chem.* **2018**, *149*, 1931.

[32] P. Silber, D. Zins, M. Robineau, M. C. Brianso-Perucaud, *Rev. Chim. Miner.* **1975**, *12*, 347.

[33] B. Krebs, G. Henkel, H.-J. Dinglinger, G. Stehmeier, *Z. Kristallogr. – Cryst. Mater.* **1980**, *153*, 285.

[34] B. Krebs, G. Henkel, *Z. Kristallogr. – Cryst. Mater.* **1987**, *179*, 373.

[35] U. Henseler, M. Jansen, *Z. anorg. allg. Chem.* **1993**, 1203.

[36] J. Beck, S. Benz, *Z. anorg. allg. Chem.* **2009**, *635*, 962.

[37] E. Philippot, M. Ribes, *C. R. Acad. Sci. Ser. C* **1969**, 1371.

[38] T. Steiner, *Angew. Chem. Int. Ed.* **2002**, *41*, 48.

[39] P. Silber, S. Pelloux, *C. R. Acad. Sci. Ser. C* **1966**, *262*, 1006.

[40] S. Pelloux, *Rev. Chim. Miner.* **1970**, *7*, 133.

[41] J. Vogt, S. Alvarez, *Inorg. Chem.* **2014**, *53*, 9260.

[42] E. Philippot, O. Lindqvist, *Acta. Cryst. B* **1970**, 877.

[43] M. Abrouk, *Rev. Chim. Miner.* **1974**, *11*, 726.

[44] a) T. A. Stephenson, E. S. Switkes, P. W. Armit, *J. Chem. Soc., Dalton Trans.* **1974**, 1134; b) Cole-Hamilton, D. J., Stephenson, T.A, *Dalton trans.* **1974**, 1818.

[45] H. Ott, *Z. Kristallogr.* **1926**, *63*, 222.

[46] A. Müller, N. Mohan, P. Christophliemk, I. Tossidis, M. Dräger, *Spectrochim. Acta, Part A* **1973**, *29*, 1345.

[47] G. Gattow, M. Dräger, *Z. Anorg. Chem.* **1967**, *349*, 202.

[48] G. Gattow, M. Dräger, *Z. Anorg. Chem.* **1966**, *348*, 229.

[49] H. Seidel, *Naturwissenschaften* **1965**, *52*, 539.

[50] O. Mundt, G. Becker, J. Baumgarten, H. Riffel, A. Simon, *Z. Anorg. Chem.* **2006**, *632*, 1687.

[51] C. J. Burchell, P. Kilian, A. M. Z. Slawin, J. D. Woollins, K. Tersago, C. van Alsenoy, F. Blockhuys, *Inorg. Chem.* **2006**, *45*, 710.

[52] D. R. Lide *Handbook of Chemistry and Physics*, CRC Press, Boca Raton, Florida, **2004**.

[53] P. Cherin, P. Unger, *Acta Crystallogr., Sect. B: Struct. Crystallogr. Cryst. Chem.* **1972**, *28*, 313.

[54] E. Zintl, A. Herder, B. Dauth, *Z. Elektrochem. Angew. Phys. Chem.* **1934**, *40*, 588.

[55] B. Krebs, G. Gattow, A. Müller, *Z. anorg. allg. Chem.* **1965**, *337*, 279.

[56] E. Philippot, M. Maurin, *C. R. Acad. Sci. Ser. C* **1968**, *266*, 1290.

[57] W. Massa, *Kristallstrukturbestimmung*, 5. Aufl., Teubner, Wiesbaden, **2007**.

[58] H. Seidel, R. Meyn, *Z. Naturforsch. B* **1971**, *26*, 1192.

[59] W. Buehrer, F. Altorfer, J. Mesot, H. Bill, P. Carron, H. G. Smith, *J. Phys.: Condens. Matter* **1991**, *3*, 1055.

[60] M. Fugel, L. A. Malaspina, R. Pal, S. P. Thomas, M. W. Shi, M. A. Spackman, K. Sugimoto, S. Grabowsky, *Chemistry* **2019**, *25*, 6523.

[61] E. Philippot, *Rev. Chim. Miner.* **1967**, *4*, 643.

[62] E. Philippot, M. Ribes, M. Maurin, *C. R. Acad. Sci. Ser. C* **1969**, *268*, 612.

[63] W. Biltz, E. Wilke-Dörfurt, *Z. Anorg. Chem.* **1905**, *48*, 297.

[64] E. Philippot, O. Lindqvist, *Rev. Chim. Miner.* **1971**, *8*, 491.

[65] a) V. Cirpus, J. Wittrock, A. Adam, *Z. anorg. allg. Chem.* **2001**, *627*, 533; b) P. Boettcher, G. Trampe, *Z. Naturforsch. B* **1985**, *40*, 321.

[66] A. Müller, B. Krebs, *Z. anorg. allg. Chem.* **1966**, *347*, 261.

[67] R. D. Shannon, *Acta Cryst A* **1976**, *32*, 751.

[68] P. Silber, M. Robineau, D. Zins, M. C. Brianso-Perucaud, *C. R. Acad. Sci. Ser. C* **1975**, *280*, 1517.

[69] P. Jeroschewski, B. Strübing, H. Berge, *Z. Chem.* **1980**, *20*, 102.

[70] A. Müller, E. Krickemeyer, F. El-Katri, D. Rehder, A. Stammler, H. Bögge, F. Hellweg, *Z. anorg. allg. Chem.* **1995**, *621*, 1160.

[71] E. Bernhardt, *Z. Anorg. Chem.* **2021**, *647*, 777.

[72] US005288753. J. A. Green, D. C. Young, **1994**.

[73] R. E. Dinnebier, S. Vensky, P. W. Stephens, M. Jansen, *Angew. Chem. Int. Ed. Engl.* **2002**, *41*, 1922.

[74] R. E. Dinnebier, S. Vensky, M. Jansen, *Chemistry* **2003**, *9*, 4391.

[75] G. Gattow, B. Krebs, *Z. anorg. allg. Chem.* **1963**, *321*, 143.

[76] a) G. Gattow, B. Krebs, *Z. anorg. allg. Chem.* **1963**, *323*, 260; b) G. Gattow, B. Krebs, *Z. anorg. allg. Chem.* **1963**, *323*, 13.

[77] G. Gattow, B. Krebs, *Z. anorg. allg. Chem.* **1963**, *322*, 113.

[78] A. Müller, B. Krebs, G. Gattow, *Z. Anorg. Chem.* **1967**, *349*, 74.

[79] C. Adamo, V. Barone, *J. Chem. Phys.* **1999**, *110*, 6158.

[80] a) T. H. Dunning, *J. Chem. Phys.* **1989**, *90*, 1007; b) D. E. Woon, T. H. Dunning, *J. Chem. Phys.* **1993**, *98*, 1358.

[81] D. O. Kashinski, G. M. Chase, R. G. Nelson, O. E. Di Nallo, A. N. Scales, D. L. VanderLey, E. F. C. Byrd, *J. phys. chem. A* **2017**, *121*, 2265.

[82] J. Horn, W. Sterzel, *Z. anorg. allg. Chem.* **1973**, 211.

[83] B. Krebs, A. Müller, G. Gattow, *Z. Naturforsch., B* **1965**, *20*, 1017.

[84] K. Nakamoto, *Infrared and Raman spectra of inorganic and coordination compounds*, 4. Aufl., John Wiley & Sons, New York, **1986**.

[85] H. Seidel, *Naturwissenschaften* **1965**, *52*, 257.

[86] M. Hesse, H. Meier, B. Zeeh, S. Bienz, L. Bigler, T. Fox, *Spektroskopische Methoden in der organischen Chemie*, 8. Aufl., Georg Thieme Verlag, Stuttgart, New York, **2012**.

[87] W. A. Bueno, A. Lautie, C. Sourisseau, D. Zins, M. Robineau, *J. Chem. Soc., Perkin Trans. 2* **1978**, 1011.

[88] D. Wang, K. Mittauer, N. Reynolds, *American Journal of Physics* **2009**, *77*, 1130.

[89] H. Seidel, *Naturwissenschaften* **1969**, *56*, 212.

[90] G. Gattow, V. Hahnkamm, *Z. anorg. allg. Chem.* **1969**, *364*, 161.

[91] C. L. Teske, W. Bensch, *Z. anorg. allg. Chem.* **2010**, *636*, 356.

[92] V. Hahnkamm, G. Kiel, G. Gattow, *Naturwissenschaften* **1968**, *55*, 80.

[93] D. Coucouvanis, J. P. Fackler Jr., *Inorg. Chem.* **1967**, *6*, 2047.

[94] S. Benz, *Trithiocarbonate. Synthese und Strukturaufklärung anorganischer Salze des Anions der Trithiokohlensäure*, Dissertation, Bonn, **2010**.

[95] I. Nahringbauer, S. E. Rasmussen, G. O. Steen, U. Schwieter, J. Paasivirta, *Acta Chem. Scand.* **1968**, *22*, 1141.

[96] H. J. Berthold, W. Preibsch, E. Vonholdt, *Angew. Chem.* **1988**, *100*, 1581.

[97] S. Scheiner, L. B. Harding, *J. Am. Chem. Soc.* **1981**, *103*, 2169.

[98] J. L. Atwood, L. J. Barbour, A. Jerga, *J. Am. Chem. Soc.* **2002**, *124*, 2122.

[99] K. Pfisterer, N. Korber, *Z. anorg. allg. Chem.* **2002**, *628*, 762.

[100] T. Roßmeier, M. Reil, N. Korber, *Inorg. Chem.* **2004**, *43*, 2206.

[101] F. Kraus, S. A. Baer, M. B. Fichtl, *Eur. J. Inorg. Chem.* **2009**, *2009*, 441.

[102] F. Kraus, S. A. Baer, *Chemistry* **2009**, *15*, 8269.

[103] P. J. Malinowski, T. Jaroń, M. Domańska, J. M. Slattery, M. Schmitt, I. Krossing, *Dalton trans.* **2020**, *49*, 7766.

[104] J. B. Grinderslev, Y.-S. Lee, M. Paskevicius, K. T. Møller, Y. Yan, Y. W. Cho, T. R. Jensen, *Inorg. Chem.* **2020**, *59*, 11449.

[105] T. Roßmeier, N. Korber, *Z. anorg. allg. Chem.* **2004**, *630*, 2665.

[106] T. Roßmeier, N. Korber, *Z. Naturforsch. B* **2003**, *58*, 672.

[107] R. S. Krishnan, *Proc. Indian Acad. Sci.* **1947**, *26*.

[108] T. Birchall, I. Drummond, *J. Chem. Soc. A* **1970**, 1859.

[109] J. Knoeck, J. Witt, *Spectrochim. Acta, Part A* **1976**, *32*, 149.

[110] V. Hahnkamm, G. Kiel, G. Gattow, *Z. anorg. allg. Chem.* **1969**, *368*, 127.

[111] a) D. Coucouvanis, P. R. Patil, M. G. Kanatzidis, B. Detering, N. C. Baenziger, *Inorg. Chem.* **1985**, *24*, 24; b) J. P. Fackler Jr., D. Coucouvanis, *Chem. Commun. (London)* **1965**, 556.

[112] D. Coucouvanis in *Progress in Inorganic Chemistry, Vol. 26*, John Wiley & Sons, Inc, Hoboken, NJ, USA, **1979**, S. 301–469.

[113] D. Coucouvanis, J. P. Fackler Jr., *J. Am. Chem. Soc.* **1966**, *88*, 3913.

[114] D. Coucouvanis, J. P. Fackler Jr., *J. Am. Chem. Soc.* **1967**, *89*, 1346.

[115] A. Müller, P. Christophliemk, I. Tossidis, C. K. Jrgensen, *Z. anorg. allg. Chem.* **1973**, *401*, 274.

[116] A. Müller, E. Diemann, E. Krickemeyer, H. Bögge, C. Menke, C. Kuhlmann, *Monatsh. Chem.* **1996**, *127*, 43.

[117] J. Vicente, M.-T. Chicote, P. González-Herrero, P. G. Jones, *Inorg. Chem.* **1997**, *36*, 5735.

[118] J. Vicente, M.-T. Chicote, P. González-Herrero, P. G. Jones, *J. Chem. Soc., Chem. Commun.* **1995**, *0*, 745.

[119] A. Cormier, K. Nakamoto, P. Christophliemk, A. Müller, *Spectrochim. Acta, Part A* **1974**, *30*, 1059.

[120] A. Bruhn, H. Seidel, *Z. Naturforsch. B* **1974**, *29*, 123.

[121] J. S. McKechnie, S. L. Miesel, L. C. Paul, *Chem. Commun. (London)* **1967**, 152.

[122] J. M. Burke, J. P. Fackler Jr., *Inorg. Chem.* **1972**, *11*, 2744.

[123] G. de Boer, H. Seidel, *Z. Naturforsch. B* **1972**, *27*, 1105.

[124] O. F. Wiede, K. A. Hofmann, *Z. anorg. allg. Chem.* **1896**, *11*, 379.

[125] K. A. Hofmann, *Z. Anorg. Chem.* **1897**, *14*, 263.

[126] M. Makosza, *Pure Appl. Chem.* **2000**, *72*, 1399.

[127] Johri, K. N., Kaushik, N. K., *Curr. Sci.* **1968**, *37*, 433.

[128] A. F. Holleman, J.-H. Chang, M. Krieger-Hauwede, N. Wiberg, *Nebengruppenelemente, Lanthanoide, Actinoide, Transactinoide*, 103. Aufl., de Gruyter, Berlin, Boston, **2016**.

[129] J. Bremi, D. Brovelli, W. Caseri, G. Hähner, P. Smith, T. Tervoort, *Chem. Mater.* **1999**, *11*, 977.

[130] M. Atoji, J. W. Richardson, R. E. Rundle, *J. Am. Chem. Soc.* **1957**, *79*, 3017.

[131] T. W. Thomas, A. E. Underhill, *Chem. Soc. Rev.* **1972**, *1*, 99.

[132] B. E. G. Lucier, K. E. Johnston, W. Xu, J. C. Hanson, S. D. Senanayake, S. Yao, M. W. Bourassa, M. Srebro, J. Autschbach, R. W. Schurko, *J. Am. Chem. Soc.* **2014**, *136*, 1333.

[133] E. Riedel, C. Janiak, *Anorganische Chemie*, 9. Aufl., de Gruyter, Berlin, Boston, **2015**.

[134] Y. Q. Zheng, A. Adam, *Acta. Cryst. C* **1994**, *50*, 1422.

[135] R. D. Shannon in *Structure and Bonding in Crystals II*, Academic Press, New York, London, Toronto, Sydney, San Francisco, **1981**, S. 53–70.

[136] K. A. Hofmann, F. Höchtlen, *Chem. Ber.* **1903**, *36*, 1146.

[137] G.-C. Guo, T. C. W. Mak, *Chem. Commun.* **1999**, 377.

[138] Tang K., Jin X., Y. Long, P. Cui, Y. Tang, *Chem. J. Chin. Univ.* **2001**, *22*, 717.

[139] A. Müller, F.-W. Baumann, H. Bögge, M. Römer, E. Krickemeyer, K. Schmitz, *Angew. Chem. Int. Ed. Engl.* **1984**, *23*, 632.

[140] J. Weiss, *Z. Anorg. Chem.* **1986**, *532*, 184.

[141] B. Leclerc, T. S. Kabré, *Acta Crystallogr., Sect. B: Struct. Crystallogr. Cryst. Chem.* **1975**, *31*, 1675.

[142] G. M. Sheldrick, *Acta. Cryst. C* **2015**, *71*, 3.

[143] G. M. Sheldrick, *Acta. Cryst. A* **2015**, *71*, 3.

[144] S. Gomez Torres, I. Pantenburg, G. Meyer, *Z. Anorg. Chem.* **2006**, *632*, 1989.

[145] S. Ganapathy, V. P. Chacko, R. G. Bryant, M. C. Etter, *J. Am. Chem. Soc.* **1986**, *108*, 3159.

[146] A. Lossin, G. Meyer, *Z. Naturforsch., B* **1992**, *47*, 1602.

[147] M. Ermrich, F. Hahn, E. R. Wölfel, *Textures Microstruct.* **1997**, *29*, 89.

[148] P. Allé, E. Wenger, S. Dahaoui, D. Schaniel, C. Lecomte, *Phys. Scr.* **2016**, *91*, 63001.

[149] a) "SCD PHOTON III. Photon counting with mixed mode detection", bruker.com/photonIII. 16/04/2021, **2019**; b) R. Durst, *Pixel Array Detectors: Counting and Integrating*. *The quest for a perfect detector.* Lecture at:. ANF-2016 RÉCIPROCS, Fréjus, **2016**.

[150] a) N. J. Harrick, *Phys. Rev. Lett.* **1960**, *4*, 224; b) N. J. Harrick, *J. Phys. Chem.* **1960**, *64*, 1110.

[151] a) University of Karlsruhe, Forschungszentrum Karslruhe 1989-2007, *TURBOMOLE v. 7.4.1. Program Package for ab initio Electronic Structure Calculations*, TURBOMOLE GmbH, **2019**; b) C. Steffen, K. Thomas, U. Huniar, A. Hellweg, O. Rubner, A. Schroer, *J. Comput. Chem.* **2010**, *31*, 2967.

[152] a) Bruker, *APEX 3*, Bruker AXS Inc., Madison, Wi, USA, **2019**; b) Bruker, *SAINT. Data Integration and Scaling*, Bruker AXS Inc., **2012**.

[153] a) STOE & Cie, *X-RED 32*, STOE & Cie GmbH, Darmstadt, Germany, **2009**; b) STOE & Cie, *X-SHAPE*, STOE & Cie GmbH, Darmstadt, Germany, **2009**; c) STOE & Cie, *X-AREA*, STOE & Cie GmbH, Darmstadt, Germany, **2009**.

[154] G. M. Sheldrick, *SADABS*, University of Göttingen, Göttingen, DE, **1997**.

[155] Dolomanov O. V., Bourhis L. J., Gildea R. J., Howard J. A. K., Puschmann H., *J. Appl. Cryst.* **2009**, *42*, 229.

[156] K. Brandenburg, *DIAMOND*, Crystal Impact GbR, Bonn, Germany, **1999**.

[157] STOE & Cie, *WinXPOW. Powder Diffraction Software*, STOE & Cie GmbH, Darmstadt, Germany, **2008**.

[158] A. A. Coelho, *J. Appl. Cryst.* **2018**, *51*, 210.

[159] L. B. McCusker, R. B. von Dreele, D. E. Cox, D. Louër, P. Scardi, *J. Appl. Crystallogr.* **1999**, *32*, 36.

[160] R. B. von Dreele in *Powder Diffraction*, Royal Society of Chemistry, Cambridge, **2008**, S. 266–281.

7 Acknowledgements

The accomplishment of this work required the support of many, to whom, I, the author, would like to express my acknowledgements at this point. First, I am very grateful to my first reviewer and doctoral supervisor, Prof. Dr. Mathias Wickleder, who made it possible for me to study chemistry for a doctorate not only through his trust. His acceptance of Chair at the Institute for Inorganic Chemistry at the University of Cologne also enabled my personal development by moving there from Justus-Liebig-University Gießen. At the new location in Cologne, I am grateful to have been able to participate in new challenging tasks involved in rebuilding the research group of Prof. Wickleder. With the commissioning of this work, I felt honoured, and I am happy today, to have been able to lay a first milestone of a new exciting topic in this working group.

I thank Prof. Dr. Sanjay Mathur of the Institute for Inorganic Chemistry for kindly accepting the second review of this thesis. The encounters with him were always friendly and gave me confidence in my work. I would like to thank Prof. Dr. Sandro Jahn of the Institute of Geology and Mineralogy of the University of Cologne for his immediate commitment to take over the chairmanship of the examination committee.

Former members of the research group of Prof. Dr. Wickleder are warmly thanked for their positive influence on the shaping of my scientific career. Here, I would particularly like to mention, Dr. Alexander Weiz, Dr. Daniel Werner, Dr. Jan Peilstöcker, Dr. Anne Schulze and Dr. Friederike Machka.

Many of the results of this work would not have been possible without the active and unconditional support of Dr. David van Gerven in the evaluation of crystal data. I am deeply grateful for this and the professional knowledge that I have learned from him. From a professional and personal point of view, a big thank you goes to Dr. Christian Logemann, who helped me with his positive assessment of me in opting for a doctorate. Besides, he gave some additional help with X-ray data. In this regard, I also would like to thank the members of the division for X-ray structure analysis for the interest in my work and the

stamina to stand the frequent odour nuisance emitted from the investigated specimens during the hunt for crystals. Silke Kremer and Dr. Ingo Pantenburg shall therefore be acknowledged. I owe the opportunity to measure X-ray powder diffractograms in this division to Daniel Moog.

I would like to thank the active members of the reasearch group Wickleder for almost five years of good cooperation, new friendship, joy and solidarity in everyday university business and, last but not least, a lot of fun both in- and outside of chemistry. I have to take this opportunity to thank my long-term colleague Laura Straub in particular, for her personal support. Special thanks are also addressed to Dr. Annabelle Mattern, Alisha Mertens and Stefan Sutorius. In finalising this work a big thank you goes to Dr. Markus Zegke, for reviewing and professional advice. Dr. David van Gerven, Dr. Christian Logemann and Dr. Bertold Rasche are not less gratefully acknowledged in these regards.

Some long-term former and active fellows from the neighbouring research groups Mathur, Klein and Ruschewitz must be acknowledged. I thank Dr. Daniel Stadler, Dr. Alexander Haseloer, Markus Krüger, Christian Tobek, Dr. Melanie Werker, Dr. Daniel Smets and Marc Hetzert for sharing professional skills and good cooperation within the institute and on a personal level.

I would like to thank the people without whom research would not be possible in the everyday life of the institute and the departement. In this, I personally acknowledge Thomas Dautert, Franz Röttgen, Robert Hempel and Mustafa ‘Johnny’ Demirbilek, as well as many more people in the chemical dispensing, disposing, workshop and glass blowing divisions. I thank Dr. Corinna Hegemann for her will to take on as assessor in the thesis defense committee and for her introduction to the institute in the very beginning.

For supporting the experimental work, I would like to say thanks to Wolfram Goetz, Iuliia Zagidullina, Atakan Baskan, Richard Ziegler and most notably Ben Lasse Mink, whose research internships made this dissertation possible in the first place.

Finally, I would like to thank the people in my life, who have supported me personally and unconditionally beyond the time of my doctorate. They made me the person who I am today, and I am forever indebted to them. Above all, I have to thank my family for their great love and solidarity, no matter what. Not less, I also received much support to accomplish my doctorate from my long-standing friends, which I am highly thankful for.

8 Declaration

Hiermit versichere ich an Eides statt, dass ich die vorliegende Dissertation selbstständig und ohne die Benutzung anderer als der angegebenen Hilfsmittel und Literatur angefertigt habe. Alle Stellen, die wörtlich oder sinngemäß aus veröffentlichten und nicht veröffentlichten Werken dem Wortlaut oder dem Sinn nach entnommen wurden, sind als solche kenntlich gemacht. Ich versichere an Eides statt, dass diese Dissertation noch in keiner anderen Fakultät oder Universität zur Prüfung vorgelegen hat; dass sie – abgesehen von unten angegebenen Teilpublikationen und eingebundenen Artikeln und Manuskripten – noch nicht veröffentlicht worden ist sowie, dass ich eine Veröffentlichung der Dissertation vor Abschluss der Promotion nicht ohne Genehmigung des Promotionsausschusses vornehmen werde. Die Bestimmungen dieser Ordnung sind mir bekannt. Darüber hinaus erkläre ich hiermit, dass ich die Ordnung zur Sicherung guter wissenschaftlicher Praxis und zum Umgang mit wissenschaftlichem Fehlverhalten der Universität zu Köln gelesen und sie bei der Durchführung der Dissertation zugrundeliegenden Arbeiten und der schriftlich verfassten Dissertation beachtet habe und verpflichte mich hiermit, die dort genannten Vorgaben bei allen wissenschaftlichen Tätigkeiten zu beachten und umzusetzen. Ich versichere, dass die eingereichte elektronische Fassung der der eingereichten Druckfassung vollständig entspricht.

Teilpublikationen

Christopher M. James, Mathias S. Wickleder, *The bis(trithiocarbonato) complexes* $[M(CS_3)_2]^{2-}$ *(M = Ni, Pd, Pt), in submission*

Köln, 04.10.2021

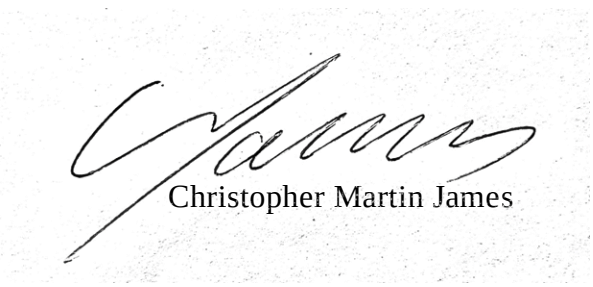

Christopher Martin James